CROSSFLOW MICROFILTRATION OF SUSPENSIONS CONTAINING LACTALBUMIN PARTICLES

A thesis presented in partial fulfilment of the requirements for the degree of

Doctor of Philosophy

in

Process and Environmental Technology

at Massey University, Palmerston North, New Zealand.

Harit Kantichandra Vyas

1999

ABSTRACT

Crossflow microfiltration (CFMF) is a very important membrane separation process with many applications in different fields including the dairy and other food industries. Often these applications involve processing of particulate suspensions. Many reports on the CFMF of particulate suspensions are found in the literature. However, these reports often deal with uniform sized and/or shaped rigid model particles and often contain contradictory and unexplained results. There is a need to develop further understanding of the CFMF of particulate suspensions, particularly of biological origin with a wide particle size distribution (PSD). This work was carried out to investigate the effects of the operating and feed conditions, and membrane configurations on the CFMF of particulate suspensions using tubular ceramic membrane modules that are commonly used in the food and other similar industries. Lactalbumin particles were selected as the feed material for their irregular shape, wide PSD, and food origin. Experiments were carried out in both constant transmembrane pressure and constant flux modes and all important parameters: internal and surface fouling, and cake mass, height, porosity and PSD were estimated to provide a more complete understanding of the process than has been attempted before. Simple methods were developed and used for the estimation of cake height and porosity.

Although many unforeseen effects of the studied parameters were obtained, the results of the study explained some observations and contradictory results reported in the literature. Mathematical models based on resistance in series and force balance mechanisms were developed and successfully used to describe the results of this study. This was achieved by extending these models to include the wide PSD and compressibility of the lactalbumin particles. The developed force balance model was further successfully used to achieve separation of desired feed particle sizes by CFMF under the constant flux mode.

A process was developed based on the observed effects of the operating parameters on the CFMF performance that enables operation at very low internal fouling and high flux for as long as 160 min. The developed process has the potential to become commercial if coupled with backflushing.

ACKNOWLEDGEMENTS

I would like to thank Dr. A.J.Mawson, Chief Supervisor, and Mr. R.J.Bennett, Co-Supervisor, both at the Institute of Food, Nutrition and Human Health, Massey University; and Dr. A.D.Marshall, Co-Supervisor, at the New Zealand Dairy Research Institute, for advice and assistance during the course of this project.

John Alger, Bruce Collins and Don McLean, Institute of Technology and Engineering, thank you all very much for your assistance in design, manufacture and modification of many experimental devices. Dr. G.J.Manderson, at the same institute, thank you for your suggestions on micro-photography.

I would like to acknowledge the New Zealand Dairy Board for funding this project, and the New Zealand Dairy Research Institute for making available the Malvern Mastersizer and the single-channel membrane module used in this work.

Special thanks to Dr. John Bronlund, Institute of Technology and Engineering, Massey University, for the valuable discussions and for your friendship. Prof. Donald Cleland, Institute of Technology and Engineering, Massey University, thank you very much for your efforts as a Coordinator of Post Graduate Studies.

A big thank you to my parents, my wife Jigisha and son Ankit for their love, support and patience. Now we all can breath a sigh of relief.

CONTENTS

CHAPTER 3
MATERIALS AND METHODS

CHAPTER 4
CHARACTERIZATION OF LACTALBUMIN

CHAPTER 5
CFMF OF LACTALBUMIN UNDER CONSTANT TMP MODE

CHAPTER 6
DEVELOPMENT AND APPLICATION OF MATHEMATICAL MODEL

CHAPTER 7
CFMF OF LACTALBUMIN UNDER CONSTANT FLUX MODE

LIST OF FIGURES

LIST OF TABLES

1. INTRODUCTION

Microfiltration in its cross flow mode is a very important membrane filtration process with many applications in the dairy and other food industries. The most significant application of crossflow microfiltration (CFMF) in the dairy industry is in removing micro-organisms from milk or whey. However, more recently attention has focused on the separation of milk proteins using CFMF process. Recoveries of soluble as well as precipitated proteins using CFMF are attempted. Recovery of soluble proteins requires small pore sized membranes and hence higher applied pressure compared to the recovery of the precipitated proteins. However, the native structure of the protein is altered by precipitation. Methods like alkali treatment (in preparation of the caseinates) or enzymatic hydrolysis (in preparation of hydrolysed lactalbumin) can be used to improve the solubility of the precipitated proteins. There are only a few reports on the CFMF of precipitated milk proteins and these describe denaturation of some of the whey proteins before CFMF of whey to achieve the protein fractionation. However, attempts to recover precipitated soya proteins using CFMF were made during the mid eighties. A lot more understanding about the CFMF of the particulate suspensions has been developed since then, particularly during recent years. The recovery of the particles (e.g. protein precipitates) from the feed suspensions is generally achieved better with CFMF compared to that achieved with centrifugation. This is mainly because the immiscibility of, and the density difference between, the phases to be separated are absolute requirements for centrifugation and not for the CFMF. The very little density difference between the precipitated proteins and the mother liquor gives CFMF the edge over centrifugation as a method of recovery.

The major limitation to the application of CFMF is the membrane fouling problem. The fouling reduces the permeation rates, modifies the rejection properties and increases the cleaning cost of the membrane. The feed components larger than the membrane pores foul the membrane externally by forming a cake layer on the membrane surface. Feed components smaller than the membrane pores either permeate through the membrane or foul the membrane internally. However, they may get retained by the cake layer formed on the membrane surface by the large feed components. Systematic studies have been carried out to understand the

membrane fouling phenomena. Although it is not possible to totally avoid fouling, many methods have been suggested to reduce the fouling problems. Several reports on the effect of the membrane configurations, feed properties and operating parameters on the performance of the CFMF of particulate suspensions are found in the literature. The reported studies on the CFMF of the particulate suspensions however, generally involve rigid model particles with uniform size and/or shape (e.g. polystyrene, latex, yeast, $CaCO_3$ etc.). Actual filtration often involves particles which have far different properties than such model particles. The knowledge of the properties of the cake formed on the membrane surface is very important for the cake often governs the filtration process for most of the filtration time. Several mathematical models have been developed to explain the CFMF performance, particularly to predict the permeate flux. Different approaches to the mathematical modelling of the CFMF process mainly include - the blocking laws, resistance in series models, particle back transport models, and models based on flowing cake theory.

Lactalbumin is a product obtained by drying the heat precipitated acid whey proteins. The particles of lactalbumin are highly irregular in shape and widely size distributed.

The aim of this project was to investigate the effects of membrane configurations, feed conditions and operating parameters on the performance of the CFMF of particulate suspensions. The types of fouling of the membrane and properties of the cake - height, mass, porosity and particle size distribution, were of particular interest. Lactalbumin particles were chosen for this study due to their configuration and the distributed size which put them in the class of the particles encountered in the actual filtration rather than in the class of the model particles. Also considered was the fact that by nature they are protein particles. This offers the prospect of applying the results of this study to the separation of the protein precipitates and other food particles through CFMF. Another objective was to develop a mathematical model to explain the observed effects of different parameters on the process performance.

2. LITERATURE REVIEW

2.1 Overview of membrane filtration

Microfiltration (MF), ultrafiltration (UF) and reverse osmosis (RO) are the three major membrane filtration processes. Membrane filtration describes the pressure-driven separation (Fig. 2.1) of the components of a fluid mixture by selective permeation through an interface (the membrane) separating the retentate stream from the permeate stream (Gutman 1987). Separation is achieved because the membrane has the ability to transport one component of the feed mixture more readily than any other component(s).

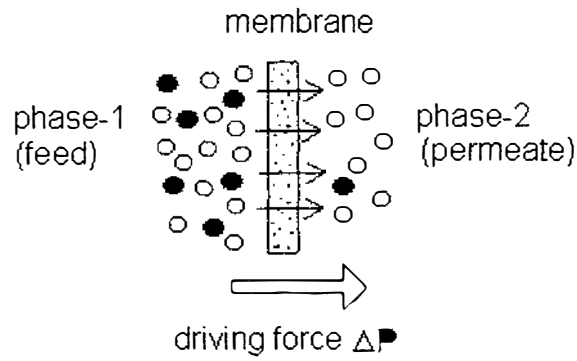

Fig. 2.1 Schematic of pressure-driven separation (Mulder 1991)

There are two basic modes of membrane filtration - dead-end and crossflow (Fig. 2.2), which differ in retention behaviour, filter geometry and complexity of operation. In dead-end filtration, pressure drives the entire feed through the porous membrane. The suspended solids are either retained or pass through the membrane into the permeate. When the membrane is plugged with retained solids, flow stops or declines to uneconomic level and the membrane must be cleaned or replaced. Dead-end filtration is suitable only for suspensions with very low solids (Michaels 1989, Rautenbach and Albrecht 1989). In crossflow filtration (CFF), pressure drives only part of the feed through the membrane. The remaining feed flows tangentially to the membrane surface, continually sweeping particles from the membrane surface back into the feed. CFF can therefore be used to process fluids with much higher solids concentration but should still be viewed as a means of concentrating the feed rather than yielding a solid cake.

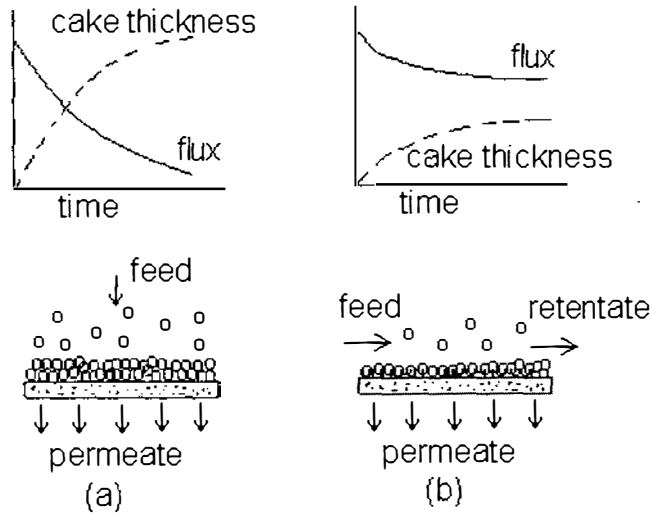

Fig. 2.2 Types of membrane filtration - (a) dead-end (b) crossflow (Davis 1996[a])

Out of many methods employed for separation, crossflow membrane filtration is a relatively new method but has rapidly gained commercial importance over the last thirty years (Mulder 1991). The major membrane filtration processes cover a wide separation range (Fig. 2.3). Centrifugation encompasses the MF size range. However, immiscibility of, and density difference between, the phases to be separated are the absolute requirements for centrifugation, but not for the membrane processes.

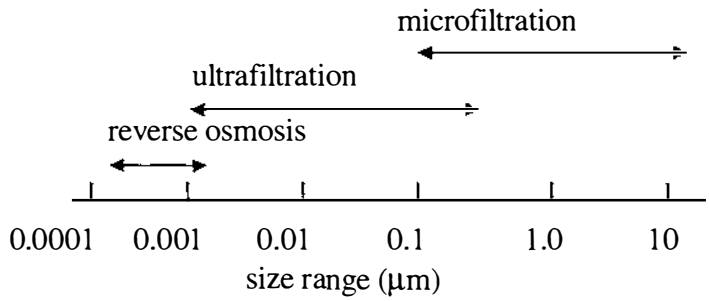

Fig. 2.3 Membrane processes and their separation ranges (Mulder 1991)

MF, UF and RO are distinguished on the basis of the retained particle size which is a consequence of difference in the membrane structure and the applied pressure. The latter is usually expressed as transmembrane pressure difference (TMP) which is the difference between the average pressure on feed side and the pressure on the permeate side of the membrane. The three processes are schematically represented in Fig. 2.4 and their general characteristics are compared in Table 2.1.

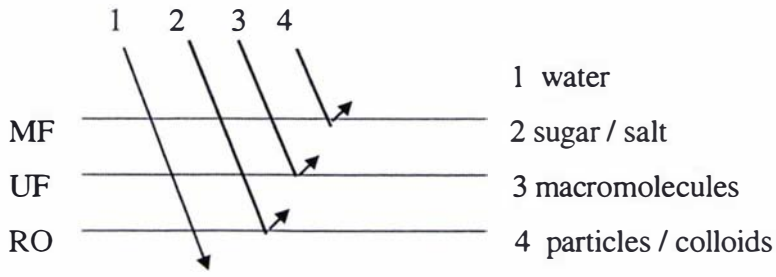

Fig. 2.4 Schematic of the three membrane processes (Cheryan 1991)

Table 2.1 General characteristics of the major membrane separation processes (Mulder 1991)

microfiltration	ultrafiltration	reverse osmosis
separation of particles	separation of macromolecules	separation of low MW solutes
osmotic pressure negligible	osmotic pressure negligible	osmotic pressure high (500-2500 kPa)
applied pressure low (<200 kPa)	applied pressure low (100-1000 kPa)	applied pressure high (1000-6000 kPa)
symmetric membrane (not always)	asymmetric membrane	asymmetric membrane
thickness of separating layer:10-150 μm	thickness of actual separating layer:0.1-1.0 μm	thickness of actual separating layer:0.1-1.0 μm
pore size: 0.05 - 10 μm	pore size: 0.001 - 0.1 μm	pore size:< 0.002 μm
separation based on particle size	separation based on particle size	separation based on differences in solubility and diffusivity

2.2 Microfiltration

2.2.1 Introduction

MF is a method for separating colloidal and suspended particles with a size above about 0.1 μm from the feed stream. MF is the oldest of the membrane technologies. It was first developed in 1920 in Germany as a technical membrane process and subsequently

commercially developed by Sartorious-Werke, Germany, in 1929 (Mulder 1991, Pedersen 1993). After initial use for research, it was later adapted for bacteriological analysis of water supplies during world war II (Merin and Daufin, 1990). The very first microfilters were of depth type, not suitable for industrial application. Later true surface type microfilters, symmetric or slightly asymmetric were developed. A further development was the implementation of the CFMF concept in 1981 (Van der Horst and Hanemaaijer 1990).

2.2.2 Microfiltration membranes

The membrane is at the heart of a membrane process and can be defined as a selective barrier between two phases (Mulder, 1991). The performance or the efficiency of a membrane is determined by its selectivity and flux (permeation rate).

MF membranes are porous and can be classified as symmetric or asymmetric on the basis of the pore structure (Fig. 2.5). Symmetric membranes have almost uniform pore size throughout the pore channel. Asymmetric membranes are made of a thin surface layer with the rated pore size that is supported by thick layer with a much larger pore size.

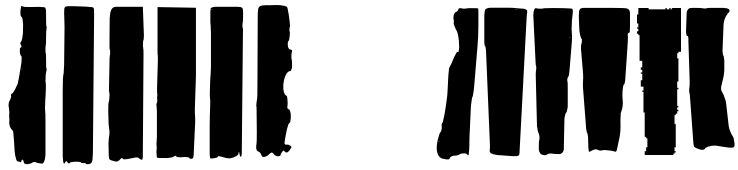

Fig. 2. 5 (a) symmetric membrane, (b) asymmetric membrane

MF membranes may be prepared from either organic materials (polymers) or inorganic materials (ceramics, metals, glasses). Table 2.2 lists materials used for MF membranes.

Table 2.2 Different types of MF membranes and their materials (Mulder 1991)

1.hydrophobic polymeric membranes	polytetrafluoroethylene (PTFE, teflon) polyvinylidene fluoride (PVDF) polypropylene (PP)
2.hydrophillic polymeric membranes	cellulose esters polycarbonate (PC) poly sulfone/polyether sulfon (PSf/PES) polyimide/polyether imide (PI/PEI) (aliphatic)polyamide (PA)
3.ceramic membranes	alumina (Al_2O) , zirconia (ZrO)
4.glass membranes	glass (SiO)
5.metal membranes	palladium, tungsten, silver, stainless steel

Polymeric MF membranes can be prepared by various techniques like sintering, stretching, track-etching, phase inversion. Sintering may be used in glass and other ceramic membranes, while sol/gel process and anodic oxidation can also be used to prepare ceramic membranes (Mulder 1991).

The key points to be considered in selecting MF membranes are: (1) pore size, (2) pore structure, (3) flow-channel dimensions, (4) chemical compatibility, (5) cleanability, (6) service life, (7) flux through the membrane, (8) mechanical stability at the operating range of temperature, pressure and pH, and (9) cost (Michaels 1989).

Particular advantages of ceramic membranes are their thermal, mechanical and chemical stability that allows the operation at high pressure and temperature, steam sterilisation, and the use of corrosive chemicals for cleaning and sterilisation. Another advantage is the significantly longer service life of these membranes. A major draw back of ceramic membranes is their high cost (Mir *et al.* 1996).

2.2.3 Microfiltration membrane modules

In practice membranes can be produced in a variety of forms, such as sheets, hollow fibres, tubes. These individual membrane elements are then assembled into a membrane module (Fig. 2.6).

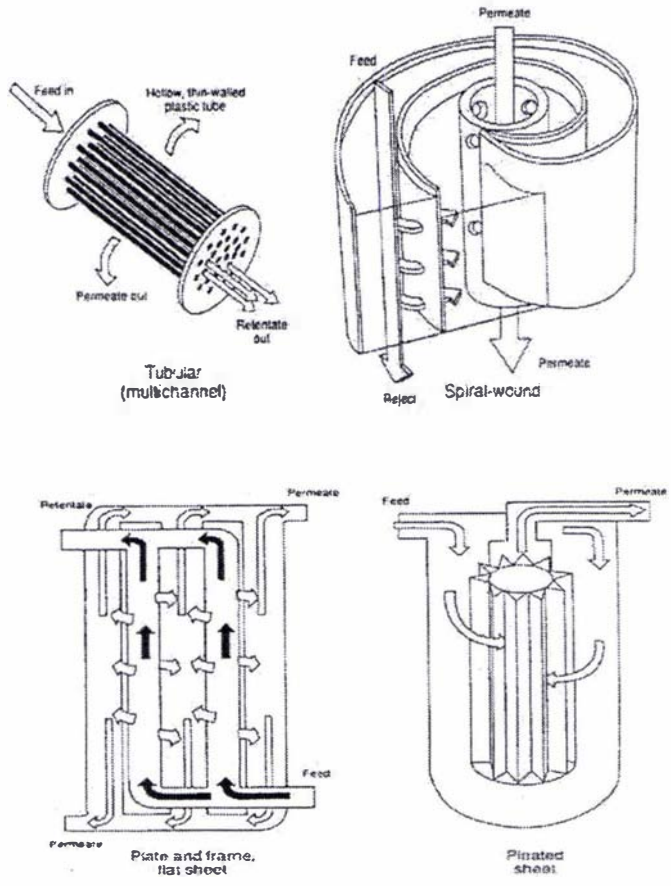

Fig. 2.6 Common MF modules (Mir *et al.* 1996)

The flat sheet module was one of the earliest configurations in the market (Cheryan, 1986). The membrane is cast on a fine 'scrim' or woven support layer. Flat sheet microfilters normally are assembled in plate-and-frame devices. But the filter can also be wrapped around a central collection pipe (spiral wound module) to obtain a greater packing density (100-400 m^2/m^3) or folded to form the pleated membrane that can be arranged around a central core (pleated sheet). Pleated sheet is typically used in dead-end operations with low solids loadings, e.g. for sterile filtration of beverages and pharmaceutical products. However, they can be adapted for crossflow mode. It is possible to achieve high crossflow velocities on these modules (Michaels 1989). In all these three module types the space between assembled membranes range from 0.25 to 2.50 mm.

Hollow fibre module contains large number of small hollow fibres (available in the range of 0.25 to 1.00 mm inner diameter), in a shell-and-tube arrangement. These modules have a high area:volume ratio, however the fibres are susceptible to plugging. In the tubular

module the membrane is cast on or supported by perforated tubes. Generally, the module consists of several tubes arranged in a shell-and-tube configuration. Tubular modules for MF are available with from 7 to 3000 tubes, 0.3 to 1.0 m long, generally 2.5 to 25 mm in diameter and total membrane area from 0.05 to 5.0 m^2. Advantages of this module include possibility of operating under high crossflow and tolerance of fouling streams due to the larger bore. Thus tubular modules are best for CFMF of large particulate (up to 800 μm) feed (Michaels 1989).

In rotating filter modules like rotating disc and annular rotating module, turbulence at the filter surface is generated by the rotation of the filter, rather than by pumping the feed across the membrane. These modules give enhanced fluxes, but are only suitable for small scale operations.

2.2.4 Modes of CFMF operation

The mode of the CFMF operation depends on the purpose of the operation. There are five basic modes of operation as shown in Fig. 2.7.

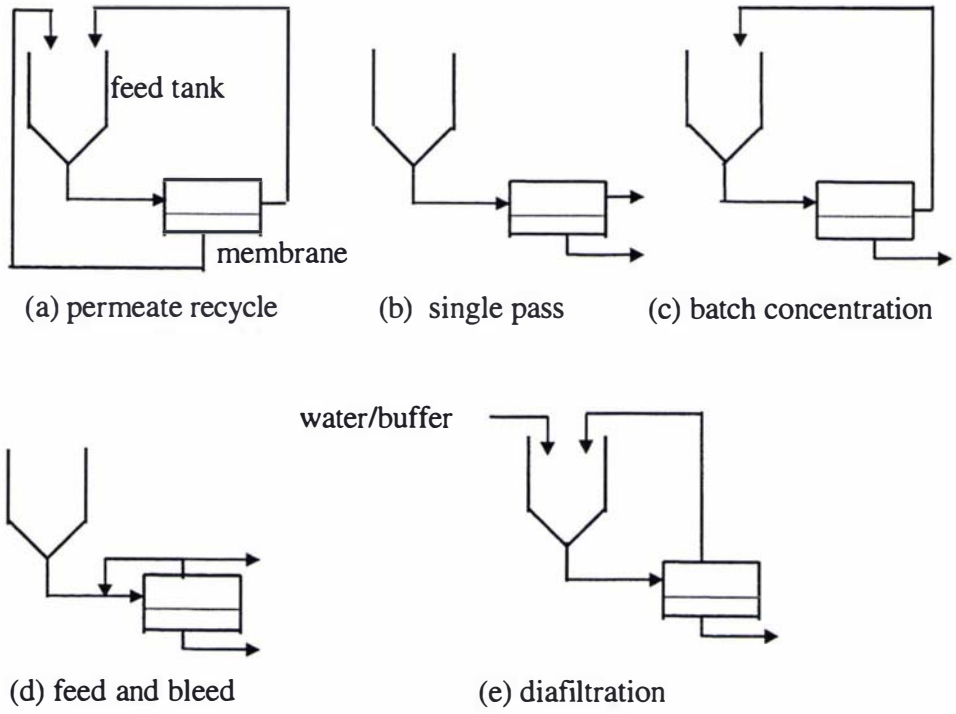

(a) permeate recycle (b) single pass (c) batch concentration

(d) feed and bleed (e) diafiltration

Fig. 2.7 Basic modes of CFMF

Permeate recycle

If both the retentate and permeate are returned to the feed tank, the system should, ideally, run at steady state. This mode is useful for experimental work, where the purpose may be investigating the performance of the membrane and module under defined conditions. This mode is not suitable for processing the feed.

Single pass concentration

In this mode, the feed is split into the two final product streams, retentate and permeate, in a single pass through the module. For MF this mode is only practical in rotating modules, which can run at very low feed rates.

Batch concentration

For small scale concentration or clarification operations, all the retentate is recycled and processing continues until the desired concentration level is achieved or until the flux becomes too low to economically continue. Recycling of the retentate helps maintain the required crossflow velocity along the membrane surface for non-rotating modules.

Feed and bleed

The recirculation loop of this mode contains only some of the process fluid. Once that fluid reaches the desired concentration, some retentate is bled off and feed is added to match the bleed rate. This mode is useful for large scale operation using single or multistage system.

Diafiltration

It is a washing process where washing liquid (wash water/buffer) is continuously or discontinuously added to dilute the retentate as permeate is removed. Diafiltration increases the removal of permeating components.

2.2.5 Concentration polarisation and membrane fouling

During CFMF operations, besides the membrane itself, concentration polarisation and membrane fouling offer resistance to the permeate flux (Fig. 2.8). Concentration polarization can be described as a build up of concentration of the feed component(s) rejected by the membrane in the vicinity of the membrane. The high concentration layer exerts a hydrodynamic resistance to the permeate flow. Fouling refers to the deposition of the retained feed component(s) on or in the membrane. This can impair the permeation flux and modify the rejection properties of the membrane. Feed components larger than the membrane pores foul the membrane externally by forming a surface cake layer. Components smaller than membrane pores penetrate the pores and may foul the membrane internally or may be retained on the membrane surface by the cake layer. The concentration polarization is easily reversible but the fouling is not so easily reversible and hence requires cleaning of the membrane.

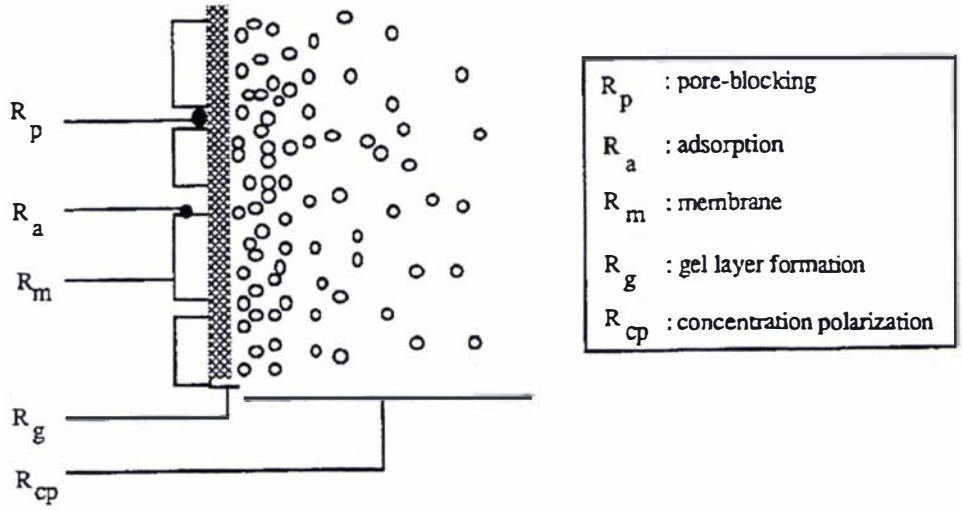

Fig. 2.8 Various types of resistance to the permeate flux (Mulder 1991)

2.2.6 Cleaning of microfilters

Generally, the objective of cleaning of any food processing equipment is to obtain a hygienically acceptable surface. However, the primary objective of membrane cleaning is to restore plant performance (i.e. normal capacity and characteristics). Different methods of membrane cleaning can be broadly classified as mechanical cleaning, electrical cleaning and chemical cleaning.

Mechanical cleaning

Mechanical cleaning can be effected by introducing a high shear rate at the membrane surface. Periodic backflushing also can be used with some types of modules. The use of foam balls for removing deposits from tubular membrane is another mechanical cleaning method (Michaels 1989). But this is only suitable for large bore membranes which can be intermittently opened.

Electrical cleaning

Electrical cleaning can be done by making use of the surface electrical charge acquired either by the membrane (electro-osmotic dewatering) or by the dispersed materials (electrofiltration), when brought in contact with polar medium. A limitation is the high power requirement (typically 10-100 kWh/m^3 of permeate) although the use of a pulsed field can reduce this. Another way is to dislodge the foulant out by the micro-bubbles formed at the electrically conducting membrane surface due to the applied voltage pulse (Bowen *et al.* 1989).

Chemical cleaning

Mechanical or electrical cleaning is generally effective only on the surface fouling. Chemical cleaning is very effective on both surface and internal fouling and hence, a most common method of membrane cleaning. It involves a heterogeneous reaction between chemical solution and the foulant layer. A chemical cleaning cycle generally includes (1) product removal by rinsing with water, (2) cleaning with chemical(s), (3) rinsing, (4) disinfection. The chemicals used should (1) loosen and dissolve the fouling, (2) keep the foulant in dispersion and solution, (3) avoid new fouling, (4) not attack the membrane or rest of the system, (5) disinfect all wetted surfaces (Trägårdh 1989). The ease of rinsing, stability, safety and cost of the chemicals are also important factors. Good chemical and microbiological quality of the water used and high pH and temperature resistance of the membrane are desirable for better, easier cleaning (Michaels 1989). Major types of cleaning solutions are reviewed in Table 2.3.

Table 2.3 Application of major cleaning solutions (Michaels 1989)

Type of solution	Type of soil removed
Acidic	Inorganic scale
Alkaline	Proteins and other biological deposits
Oxidising	Oxidisable organic deposits
Detergent	Insoluble particulates, colloids and emulsions
Organic solvent	Organic-chemical deposits that are insoluble in aqueous solutions

2.2.7 General applications of microfiltration

Microfiltration has many applications in different fields. Major applications are listed below (Mulder 1991):

- production of ultrapure water (semiconductors)
- polishing filtration of electronic grade chemicals
- clarifying whey, juice and alcoholic beverages
- recovery of precipitated heavy metals or other precipitates and nutrients from waste water
- removal of bacteria for cell recovery in cell culture or for sterilisation of liquids
- concentration of pigment slurry, crude oil (in product water), fermentation broth, crystals (during crystallisation)
- protein and enzyme recovery and recovery of finely divided catalyst
- removal of water from latex or solvent water emulsion
- plasmapheresis (medical)

2.3 Applications of CFMF in the dairy industry

2.3.1 Introduction

CFMF is an important concentration/separation unit operation with many applications in dairy and food processing. The introduction of inorganic membranes has widened its application for dairy processing (see 2.2.2). The limitations to more rapid development are mainly the high cost of these membranes and the fouling problems. However, these limitations have not prevented the membranes from being used. The main applications of CFMF in dairy industry are bacterial removal to prolong shelf-life, fat separation, and concentration and fractionation of proteins (Cheryan 1991, Pouliot *et al.* 1994, Zydney 1998). There are several other applications of MF in the dairy industry including treatment of dairy waste (Merin and Daufin 1990), extraction of lactoferrin and α-lactalbumin from human milk, manufacture of thickening ingredients for low fat cream from butter milk concentrate (Pouliot *et al.* 1994).

2.3.2 Removal of micro-organisms

This is the most significant emerging application of CFMF in the dairy industry. Replacing conventional methods like pasteurisation and sterilisation with CFMF can avoid heat induced changes in milk constituents and save energy required for heating and cooling of milk. The first pilot studies on MF of whole milk were reported by Piot *et al.*(1987). They achieved a bacterial reduction of two orders of magnitude with no apparent rejection of proteins using a 1.8 μm pore size inorganic alumina membrane.

As the largest casein micelles have a diameter of around 0.6 μm, a membrane pore size of 0.6 to 0.7 μm is recommended in order to obtain no or very low non fat solids retention and the highest bacteria removal (Pedersen 1993). Because the fat globules and common bacteria in milk are of similar size, it is necessary to separate the fat from milk before MF. For MF of milk, 50°C is the recommended temperature for obtaining optimal flux without irreversible changes in the protein or mineral balance (Pedersen 1993).

A microfiltration process, the 'Bactocatch' system patented by Alfa-Laval, can reduce total bacterial count by approximately 99.7% (Valming 1988). In this process, after raw milk separation, skim milk is microfiltered. The retentate and cream are mixed and given high temperature treatment (115-130°C/4-6 s). This is then mixed with skim milk filtrate. The mixture might be heat treated or pasteurised, which reportedly has no significant effect on the bacteriological quality of the milk (Olesen & Jensen 1989). The first full scale prototype 'Bactocatch' plant was installed at Skanemejerier's Lunnarp factory, Sweden. This process became commercial in 1988-89. It could be very useful in tropical countries, where inadequate refrigeration and transportation facilities result in high microbial loads in the raw milk (Cheryan 1992). Powder and cheese can be made straight from raw milk with help of the bactocatch process (Solberge 1991, Zoon and Hup 1993, Schuck *et al.* 1994, Bouton and Grappin 1995). The CFMF can be used to remove bacteria from whey or cheese brine since unlike other methods of whey or brine sanitation, it is safe on heat-sensitive whey proteins and does not change the native composition of brine (Mucchetti and Taglietti 1993, Pedersen 1993).

2.3.3 Removal of fat and clarification

The objective of defatting and clarification of whey is to improve the whey protein concentration process and to obtain better functional properties of the resultant WPCs (Van der Hoarst and Hanemaaijer 1990, Merin and Daufin 1990). The first reports on the use of CFMF in the dairy industry dealt with defatting and clarifying sweet whey (Tanny *et al.* 1982) and cheese brine (Merin *et al.* 1983). Centrifugal separation does not completely remove the fat and casein fines from whey. In addition MF also removes noncentrifugable phospholipoproteins, precipitated salts, foam depressants - which deteriorate the UF flux and the functional properties of WPC, and bacteria (Maubois *et al.* 1987, Daufin *et al.* 1993, 1994, Hawks *et al.* 1993). Hence microfiltered whey have 25-30 % higher UF fluxes compared with centrifuged whey (Merin & Daufin 1990). The initial cleanliness of membrane, the path to reach operating conditions and feed temperature all have a significant effect on the performance (Gesan *et al,* 1993, 1994). Clarification of cooker/stretcher water used in mozzarella cheese plant using CFMF is reported to increase milk solids and salt recovery and decrease effluent discharge load (Anon 1993).

2.3.4 Concentration of proteins

MF is also used either for fractionation of milk proteins or to obtain protein rich product without changing the native state of the proteins.

Milk contains about 3 to 3.5 % (w) proteins. Milk proteins as a whole have a specific gravity of 1.346 (Davies 1939). The major milk proteins are grouped as caseins and whey proteins. The other proteins in milk are milk fat globule membrane (MFGM) proteins and the minor proteins like lactoferrin, serum transferrin (Evans 1984).

2.3.4.1 Concentration of casein

CFMF of skim milk using 0.2 μm pore size membrane, allows concentration of micellar casein. The filtrate has a composition close to that of a sweet whey (Maubois and Ollivier 1993). On spray drying the retentate can easily compete with the calcium caseinates and its rennetability on reconstitution, is much better than that of raw milk (Pierre *et al.* 1992). However, enrichment of milk for powder making with casein by CFMF gives the powder with low solubility and dispersibility (Schuck *et al.* 1994). Loh (1990) reported preparation of lactic acid casein from both retentate and permeate of microfiltered skim milk. A continuous casein washing process developed by the Pillet Company, France based on diafiltration, is described by Laimay (1991). This process reduces water usage, washing time, and effluent. It is less subject to bacterial contamination and facilitates process control.

The dissociation of a certain proportion of β-casein from the casein micelle when skim milk held at approximately 4 °C can be successfully exploited by means of MF to produce a β-casein enriched product (Le Berre and Daufin 1994). Such a product is suitable for modifying the β-casein/α-casein ratio of cheese milks and consequently texture and flavour of resulting product. The β-casein enriched product is also an important substrate for producing numerous peptides thought to have physiological activities (Maubois and Ollivier 1993).

2.3.4.2 Concentration of whey proteins

The role of CFMF in concentration and fractionation of whey proteins has been reported recently. It mainly involves selective precipitation of whey protein(s) coupled with CFMF of the whey. Uchida *et al.* (1992) and Uchida *et al.* (1993) described a process to produce a fraction with high α-lactalbumin content. The process involves heat treating and subsequently or simultaneously CF-microfiltering the milk or heating the pH adjusted whey and then subjecting it to MF. The product so obtained is useful as a substitute for human milk and/or in other nutritional composition. Jensen and Larsen, (1993) have described a method to obtain high quality protein products from whey. In this process, the whey and retentate are circulated on one side of the membrane, while the permeate is circulated on the other side of the membrane during CFMF at constant TMP (<80 kPa). In this way it is claimed that fractionation of the whey proteins occurs, so that denatured whey proteins and fat are retained and undenatured whey protein permeates through. It is claimed that a low fat, whey protein product rich in α-lactalbumin and β-lactglobulin may be obtained. Another process involves removal of caseins from the milk by CFMF and subsequent reduction of β-lactglobulin from the permeate to about 4% through pH adjustment and NaCl addition. Thus the modification of bovine milk to simulate human milk protein composition could be achieved (Woychick 1992). A process combining affinity chromatography with MF can be used to isolate lactoferrin and immunoglobulin G from cheese whey. The process involves three steps - affinity binding, washing, and dissociation. Lactoferrin with 95% purity and 92% iron-binding capacity and immunoglobulin G with 90% purity and 86% activity can be obtained with reasonable yields (Chen & Wang 1991).

2.4 Application of CFMF in other fields involving recovery of particles

There are several other areas where CFMF is applied to remove or recover small particles present in the feed as a result of either the nature of the feed, or deliberate precipitation, or unaimed precipitation of feed component(s). CFMF is preferred because it has certain advantage(s) over the other methods of particle removal. Such applications are mainly in food, biotech, and chemical processing.

The uses of CFMF in food processing are similar to that in the dairy industry. CFMF is used for microbial stabilization, precipitate recovery, clarification of products and process water, and product refining in food processing (Gekas and Hallström 1990, Cheryan 1992). Devereux and Hoare (1986) and Bentham *et al.* (1988) have reported studies on the recovery of soya protein precipitates by CFMF with the membranes in the range of 0.2 to 1.2 μm nominal pore size. Based on their results it can be concluded that high flux rates, and high level of soluble protein transmission or minimum residual soluble protein in the feed are required for the efficient use of CFMF for this purpose. They obtained high soluble protein transmission by using the large pore size (1.2 μm) membrane. But pore penetration by fine particles caused a major flux problem.

CFMF is also used for clarification of juices, beverages, gelatin, sweeteners, and meat process water. Use of ceramic membranes for this purpose despite their high cost appears to be advantageous due to their high resistance to high temperature, pressure, abrasion and chemicals (Padilla-Zakour and McLellan 1993). Systematic studies on the fouling control by backflushing and flow pulsation, and the effect of membrane properties and operating parameters on the clarification of juice by CFMF have been reported (Ben Amar et al. 1990, Padilla-Zakour and McLellan 1993). In the production of beer, besides microbial stabilization, CFMF is used to recover beer by removing yeast and precipitates of haze-forming material from the fermentation and maturation tank bottoms respectively. These tank bottoms contain 90 and 99 % beer respectively (Le 1987, Gan *et al.* 1997). No adverse effect of CFMF on the taste of the product has been reported. CFMF of gelatin prior to concentration to remove dirt, coagulated proteins, fat and other insoluble particles is carried out. Sugar and other sweeteners are also refined using CFMF (Short and Skelton 1991).

The application of CFMF in bio-processing mainly includes bacterial and yeast cell harvesting and removal of cell debris. The specific advantage of CFMF is the high purity of the filtrate and the processing in the closed space without contact with the environment. CFMF can also be advantageously applied to separation of active biomass in a reactor in an anaerobic digestion process (Murkes and Carlsson 1988).

In the chemical processing industry CFMF is mainly applied for removing heavy metals. Removal of different metal hydroxides from effluents of galvanic plants, sea water (magnesium hydroxide) and thixotropic suspension from ion exchangers (mainly nickle hydroxide) are discussed by Murkes and Carlsson (1988). In preparation of PVC latex, concentration of suspension containing 1 μm particles up to 40 – 60 % by CFMF can save energy in the subsequent spray drying.

Effluents from the manufacture of television tubes contain about 1 μm size crystals of fluorescent solids that can be concentrated up to 25 % by CFMF (Murkes and Carlsson 1988).

2.5 Methods of particle recovery

The suitability and selection of a recovery method depends on the type and nature of the particles as well as the nature of the fluid suspending the particles. In the case of the protein precipitates, the protein source and precipitation method are significant factors in determining the separation efficiency and in defining the type of the separation method to be used (Bell *et al.* 1983, Glatz 1990).

The methods used for recovery of particles are
(1) settling or floatation
(2) traditional and vacuum filtration
(3) centrifugation
(4) membrane filtration (UF or MF - mainly in a crossflow mode)

Settling or floatation is used for systems with high density differences between particles and the fluid carrying them. Settling is used to remove sediments during beer making and dissolved air floatation for the recovery of isoelectric casein is an example of foam/floatation separation. Traditional filtration is useful when the particles are large in size. For smaller particles with higher density than the fluid carrying them, centrifugation is used. It is the principal approach to the recovery of the protein precipitates. However, as stated earlier (section 2.1.2), immiscibility of, and density difference between, the phases to be separated are the absolute requirements for centrifugal

separation. The small density difference between protein precipitate and mother liquor results in low efficiency of the centrifuge. To minimize this problem high speed centrifuges are employed. But their initial and operating costs are very high and since more residence time for the feed is required, they operate at very low liquid throughput. Another problem with centrifugal separation is denaturation of proteins due to temperature rises on passing through the bowls. Use of cooled centrifuges can minimize this problem but again their operation is more expensive (Hoare 1882, Bell et al. 1983, Hoare and Dunnill 1984). Since the size difference between the phases to be separated is the only major requirement for the membrane filtration, it is a potential alternative to the centrifugation for recovery of precipitates. The membrane filtration processes cover a wide range of particle sizes. The use of dead-end MF and UF for the recovery of soya protein precipitates have been attempted by several workers (Hoare 1982, Hoare and Dunnill 1984, Devereux et al. 1985, Devereux and Hoare 1986). The flux was limited by the presence of dissolved proteins during UF. Use of MF, which allowed the passage of soluble proteins could over come this problem. However, the problem of high cake resistance in dead-end MF necessitated the use of the crossflow mode.

As discussed in section 2.3.3, whey clarification by CFMF has proved more efficient than that by centrifugation. Use of CFMF for beer clarification and recovery is also economically more attractive compared to traditional and vacuum filtration. Further, it does not require the disposal of used filter aid (Gan et al. 1997).

Particles often break due to their handling during the recovery. This can adversely affect the efficiency of the recovery process. Hoare *et al.* (1982) studied the effect of shear on the soya protein precipitates during pumping using different types of pump. Their results are shown in Fig. 2.9. They concluded that minimization of production of fines by minimal exposure to shear should be the objective during protein precipitate recovery. They recommended the use of peristaltic pumps for this purpose.

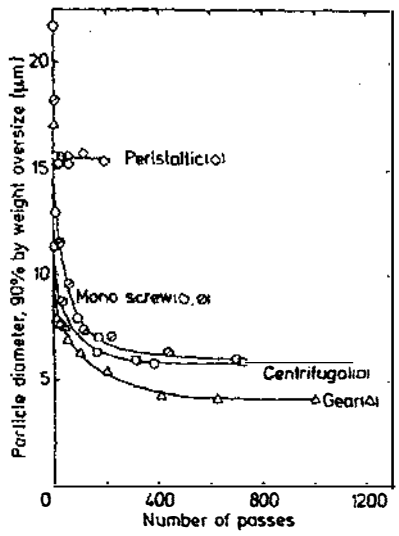

Fig. 2.9 Particle size change of Soya protein precipitates due to pumping. Total protein concentration = 2.5 % w (Hoare *et al.* 1982)

2.6 Models for CFMF

Generally, models for CFMF are developed with the aim of predicting the permeate flux. In that case a model should ideally take account of all factors which the flux is dependent on.

Zydney and Colton (1986) gave a formula for calculating the mean deviation between predicted and measured fluxes:

$$E = \exp\left[\frac{1}{N}\sum_{I=1}^{N}\left[\ln(J_{pr}) - \ln(J_{me})\right]\right] - 1 \qquad (2.1)$$

where,

E = deviation index
N = number of data pairs
J_{pr} = predicted flux
J_{me} = measured flux

However, values of E are not affected by the relative magnitudes of J_{pr} and J_{me}. Therefore, E =1 in the cases of $J_{pr} = J_{me}$, or $J_{pr} = 2\ J_{me}$, or $J_{pr} = 1/2\ J_{me}$.

2.6.1 Resistance models

Several resistance based models developed for dead-end filtration can be used to determine the extent of internal and external fouling. Sometimes they have been used to assess different resistances to the flux during CFF as well.

2.6.1.1 Standard blocking model (SBM)

In this model it is assumed that there is internal fouling only and the pore volume decreases proportionately to the filtrate volume (Hermia 1982). Hence it is applicable when particles are much smaller than the pores. The decrease in flux can be represented by

$$t/v = 1/J_o + K \cdot t/2 \qquad (2.2)$$

where,

t = filtration time (sec)
v = filtrate volume (m^3)
J_o = initial flux (m/s) and
K = filtration constant = $2 \cdot \varnothing_p / \delta_m \cdot A_o$
$\varnothing_p$ = volume of particles deposited per unit filtrate volume
δ_m = membrane thickness (m)
A_o = initial open pore area (m^2)

When this model holds , a plot of t/v versus t is linear. Several workers have observed the validity of this model for initial period of filtration (Matsumoto et al. 1987, Visvanathan and Ben Aïm 1989).

2.6.1.2 Cake filtration model (CFM)

This model assumes that there is only external fouling of the membrane. When particles are bigger than the pores or when the pores are sufficiently clogged so that particles are bigger than clogged pores, this model is applicable. Here the decrease in the flux can be described as

$$t/v = 1/J_o + K \cdot v/2 \qquad (2.3)$$

where,

$$\text{filtration constant } K = \frac{\alpha \cdot \rho_p \cdot s \cdot \eta}{A^2 \cdot \Delta P \cdot (1 - m \cdot s)}$$

where,

A = membrane surface area (m^2)
ΔP = TMP (Pa)
η = feed viscocity (Pa.s)
α = specific cake resistance
ρ_p = particle density (kg/m^3)
s = solid mass fraction in feed
m = mass ratio of wet to dry cake

When this model holds a plot of t/v versus v is linear. Visvanathan and Ben Aïm (1989) reported validity of CFM for rest of the run after the initial period of validity of SBM during CFMF of collidal suspension.

2.6.1.3 Constant flow rate blocking laws

The theory for these laws is based on following assumptions :

- The membrane is a bundle of parallel and straight pores with same radius and length
- The flow is laminar and flux is constant
- Each particle entering the membrane is captured

Complete and Standard blocking laws (CBL and SBL)

In CBL it is assumed that each particle coming in contact with the membrane plugs perfectly one pore and there is no superimposition of particles. The reduction in active surface area is thus proportional to the filtrate volume. The assumption in SBL is similar to that in case of SBM , but under assumed constant flux.

Intermediate law

Hermia (1982) developed the theoretical background of this law. The assumption here that each particle can deposit anywhere on the membrane surface is more realistic. However, it is also assumed that a depositing particle completely plugs the pore.

Combining the two basic resistance models - cake layer model and pore restriction models can give more realistic model (Persson and Nilsson 1991).

2.6.1.4 Resistance in series model

According to Darcy's law, at any instance during MF,

$$J = \frac{\Delta P}{\eta \cdot R_t} \qquad (2.4)$$

where,

J = permeate flux (m/s)
ΔP = TMP (Pa)
η = feed viscocity (Pa.s)
R_t = total resistance to the permeate flux (/m)

As noted in 2.2.5, the total resistance to the flux can be broken into resistances due to the membrane, fouling, and concentration polarisation (resistances in series):

$$R_t = R_m + R_f + R_{cp} \qquad (2.5)$$

R_f can be further broken down, into internal and external or reversible and irreversible or particle and colloidal fouling and so on. R_f can be substantially greater than the R_m (Deverux and Hoare, 1986, Vis vanathan and Ben Aïm, 1989). The resistance of the cake deposited on the membrane surface can be estimated using the Carman-Kozeny equation:

$$R_c = \frac{180 \cdot (1-\varepsilon)^2 \cdot h}{d_p^2 \cdot \varepsilon^3} \quad \text{for mono dispersed particles} \qquad (2.6)$$

Altmann and Ripperger (1997) considered

$$R_c = \frac{160 \cdot (1-\varepsilon)^2 \cdot h}{d_{pSauter}^2 \cdot \varepsilon^3} \quad \text{for size distributed particles} \qquad (2.7)$$

where,

R_c = cake resistance (/m)
d_p = particle diameter (m)
ε = cake porosity (void fraction)
h = height of the cake (m)
$d_{pSauter}$ = particle sauter mean diameter of a certain layer of the cake (m)
(But the meaning of 'certain layer' is not specified in the report)

$$\alpha = \frac{R_c}{\rho_p \cdot h} \qquad (2.8)$$

where,

α = specific cake resistance

ρ_p = particle density (kg/m^3)

The cake height can be estimated if porosity and mass of the cake are known

$$h = \frac{m}{\rho_p \cdot (1-\varepsilon)} \qquad (2.9)$$

where,

m = mass per unit area of cake (kg/m^2)

This resistance in series model has been found best suited for calculations (Persson *et al.* 1993[b]). Murkes and Carlsson (1988) developed a resistance in series model based on sedimentary pipe flow expression by replacing the gravity by applied pressure as a settling force acting on a particle during CFMF. They assumed the existence of a critical crossflow velocity below which particle starts to settle.

$$V = \frac{c \cdot (\Delta P / R_c)}{(a/V + b/V^{0.5} + 0.28)^{0.5}} \qquad (2.10)$$

where,

V = critical crossflow velocity (m/s)

$$a = \frac{21\,\eta}{dp \cdot \rho_L}, \quad b = 6\,(a/21)^{0.5}, \text{ and}$$

$$c = 2.4\, cv^{0.33} \cdot [2D/((1-\varepsilon) \cdot \rho_L)]^{0.5}$$

cv = volumetric solid concentration

ρ_L = density of liquid

solving for R_c we get

$$R_c = \frac{c^2 \cdot \Delta P}{(aV^3 + bV^{3.5} + 0.28\,V^4)^{0.5}} \qquad (2.11)$$

Further, Darcy's law can be used to express permeate flux using the eq. 2.11.

Ousman and Bennasar (1995) used the resistance in series model and Darcy's law to estimate different resistances to the permeate flux during CFMF of starch suspension. They used the pure water flux of clean membrane to estimate R_m and product flux to calculate R_t. They measured the pure water flux after rinsing the membrane at the end of the run to eliminate traces of solution and polarisation layer to estimate R_f and R_{cp}. The pure water flux again measured after removing the surface deposit using a brush was used to estimate internal fouling resistance R_i. However, most

of the reports neglect R_{cp} for CFMF of particulate suspensions while applying the resistance in series model (Persson and Nilsson 1991, Dharmappa *et al.* 1992, Chang *et al.* 1995, Piron *et al.* 1995, Altmann and Ripperger 1997).

2.6.2 Models based on particle back transport

2.6.2.1 Brownian diffusion

When the particles being filtered are very small or highly compressible, then a thin fouling layer quickly forms on the membrane surface. Due to a substantial resistance offered by this layer, a steady or quasi steady-state flux is quickly reached which is significantly lower than the clean membrane flux. The rate of the particles flowing toward the membrane surface is then balanced by back transport of particles away from the membrane and subsequent convection of those particles toward the membrane exit due to crossflow of feed.

The Brownian diffusion coefficient (D_{br}) for a spherical particle can be estimated by the Stokes-Einstein equation:

$$D_{br} = \frac{k \cdot T}{3\pi \cdot \eta_0 \cdot d_p} \qquad (2.12)$$

where,

k = Boltzmann's constant (1.38×10^{-6} g cm^2 / s^2 K)

T = absolute temperature (K)

η_0 = dynamic viscosity of particle free fluid (Pa.s)

Therefore, the Brownian diffusion motion V_{br} can be obtained as :

$$V_{br} = \frac{k \cdot T}{3\pi \cdot \eta \cdot r \cdot d_p} \qquad (2.13)$$

where,

r = clearance of crossflow channel (radius of tube) (m)

For non-spherical particles shape factor has to be included in these equations. Transport models based on back transport solely due to Brownian diffusion such as the traditional gel-polarization model (film theory) and other as reviewed by Belfort et al. (1994) and Davis (1996[b]), use in some form the following basic equation to predict the flux:

$$J = K \cdot \ln (\varnothing_w / \varnothing_b) \qquad (2.14)$$

where,

K = mass transfer coefficient which depends on D_b
$\varnothing_w$ = particle volume fraction at the edge of the cake
$\varnothing_b$ = particle volume fraction in the bulk suspension

Brownian diffusivity is inversely proportional to particle size, and therefore, it is important for submicron size (e.g. macromolecules). Unfortunately the Brownian diffusion as a sole mechanism of particle back diffusion grossly under predicts fluxes for micron sized particle suspensions. Green and Belfort (1980) termed this discrepancy as the 'flux paradox'.

2.6.2.2 Shear-induced diffusion

As a possible resolution to the flux paradox, Zydney and Colton (1986) proposed the replacement of the Brownian diffusivity by the shear-induced hydrodynamic diffusivity in the concentration polarisation model. Later Davis and Leighton (1987) also presented a theory based on the shear-induced transport of a particle layer along a porous wall and discussed its application to CFMF. Shear-induced diffusion is a result of particle-particle interactions in a shear field causing lateral migration of the particle from the instantaneous trajectories. Zydney and Colton (1986) used an approximate relationship for the shear-induced diffusion coefficient D_s given by Eckstein *et al.* (1977):

$$D_s = 0.3 \cdot \gamma \cdot r_p^2 \qquad (2.15)$$

where,

γ = shear rate (s^{-1})
r_p = particle radius (m)

Whereas, Davis and Sherwood (1990) and Sethi and Wiesner (1997) used the correlations established by Leighton and Acrivos (1987):

$$D_s = \gamma_l \cdot r_p^2 \cdot D_s'(\varnothing) \qquad (2.16)$$

where,

γ_l = local shear rate (/s)
$D_s'(\varnothing)$ = dimensionless function of the local particle volume fraction $\varnothing$, and
$= 0.33 \cdot \varnothing^2 \cdot (1+ 0.5e^{8.8\varnothing})$

The shear-induced velocity V_s can be obtained by:

$$V_s = \frac{V_{av} \cdot d_p^2}{20\, r^2} \qquad (2.17)$$

where,

V_{av} = average crossflow velocity (m/s)

The permeate flux (length averaged) as given by Belfort *et al.* (1994) can be obtained by :

$$J = 0.078\,\gamma \cdot (\varnothing_w\, r_p^4/\, \varnothing_b L)^{1/3} \ln(\varnothing_w/\, \varnothing_b) \quad \text{when } \varnothing_w - \varnothing_b << \varnothing_w \qquad (2.18)$$

$$J = 0.126\,\gamma \cdot (\varnothing_w\, r_p^4/\, \varnothing_b L)^{1/3} \quad \text{when } \varnothing_b << \varnothing_w \qquad (2.19)$$

The shear-induced diffusion dominates in typical CFMF applications involving micron sized and larger particles. This mechanism is based on the particle-particle interaction and hence can not be applied to situations of low particle concentration.

2.6.2.3 Inertial lift

The inertial lift theory is the primary alternative to the shear-induced model of CFMF. Inertial lift was the first mechanism to be widely accepted as an explanation for flux paradox of CFMF. An isolated, neutrally buoyant particle present in a duct under laminar flow conditions will migrate across the fluid stream lines due to the inertia resulting from interactions with the flow field and the duct wall. Belfort and co-workers extended this theory to porous channels and tubes (Green and Belfort 1980, Altena and Belfort 1984, and Drew *et al.* 1991). The strongest particle lift effect occurs when the sphere is much closer to one wall than the other. The inertial lift velocity V_l of a sphere in laminar flow conditions (Belfort *et al.* 1994):

$$V_l = \frac{b \cdot \rho \cdot \dot{\gamma}^2 \cdot r_p^3}{16 \cdot \eta} \qquad (2.20)$$

where,

b = dimensionless function of dimensionless distance from the wall

This equation is limited to dilute suspensions where particle-particle interactions are negligible. Drew et al. (1991) gave the value of b = 0.577 for maximum V_l ($V_{lmax.}$) under fast laminar flow conditions. Chang et al. (1995) and Sethi and Weisner (1997) later considered that value in their work. This value of 'b' is only strictly valid for two-dimensional channel, although this value is not expected to differ greatly for a tube (Davis 1996[b]).

The cake builds up until the permeate flux and inertial lift velocity are equal.

$$J_{ss} = V_l = \frac{V_{lmax.}}{(1-h')^m} \qquad (2.21)$$

where,

h' = dimensionless cake height = h/r

m = 4 (two dimensional channel) and 6 (tube)

The lift velocity is directly proportional to the cube of the particle size and square of the tangential shear rate or crossflow velocity, and so expected to be significant for large particles and high crossflow rates.

Fig. 2.10 shows the significance of the three back diffusion mechanisms with respect to the particle size. However, in situ observations of cake formation during CFF of particulate suspensions have not found any type of back diffusion (Mackley and Sherman 1992, Wakeman 1994).

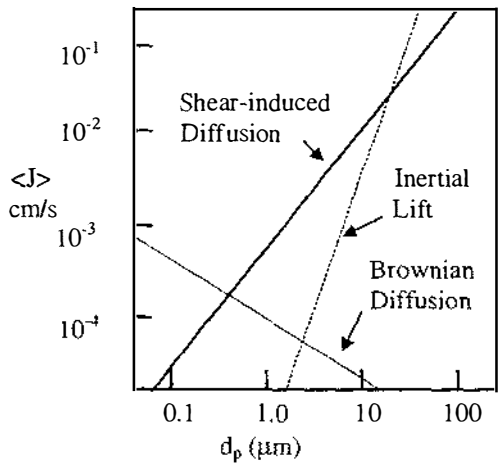

Fig. 2.10 Length averaged flux versus particle diameter according to the three back transport mechanisms under a certain operating condition (Belfort *et al.* 1994)

2.6.3 Flowing cakes and surface transport

As an alternative to back transport mechanisms, this theory assumes that particles carried to the membrane surface by the permeate flow roll or slide along the surface due to crossflow. Continuum and single-particle models have been developed to describe this possibility. In the continuum approach, the rejected particles are assumed to form a

flowing cake layer. The particles deposit into the cake and the cake flows toward the filter exit simultaneously. However, the prediction of the performance is difficult because particle concentration, viscosity and specific resistance of a flowing cake are not known in advance. In the single-particle models, the basic concept is to consider a spherical particle on the membrane surface or on the stagnant cake surface, and perform a force balance on the particle to determine whether it will adhere to the surface or not (Fig. 2.11).

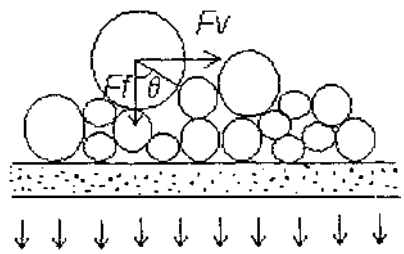

Fig. 2.11 Schematic of forces acting on a spherical particle on the cake surface (Belfort *et al.* 1994)

The drag forces F_v and F_f due to the crossflow velocity and the permeate flux respectively, can be estimated using Stokes equation:

$$F_v = 3 \cdot \pi \cdot \eta \cdot d_p \cdot V \qquad (2.22)$$

$$F_f = 3 \cdot \pi \cdot \eta \cdot d_p \cdot J \qquad (2.23)$$

Many workers have used a correction factor to the Stokes law due to the presence of the cake (C_t = 1.7009, the value given by O'Neill (1967)) in eq. 2.22 to calculate F_v (Lu and Ju 1989, Chang *et al.* 1995). This value of C_t is for a sphere resting on a smooth impermeable surface and it is expected to differ for rough cake surfaces. Similarly a correction factor to the Stokes law due to the presence of the cake (C_n) in eq. 2.23 is used to calculate the hydrodynamic forces acting normal to the membrane surface. The value of C_n as given by Goren (1979) can be determined by:

$$C_n = \{(R_m \cdot d_p/3) + (1.072)^2\}^{1/2} \qquad (2.24)$$

This eq. 2.24 used by Lu and Ju (1989) is restricted to porous membranes thinner than the sphere radius, or when flow is in direction normal to the membrane. Sherwood (1988) considered a porous medium thicker than the sphere radius which allows flow in any direction to yield the following equation for calculating C_n:

$$C_n = 0.36\,(k_p/r_p^2)^{-2/5} \qquad (2.25)$$

where,

k_p = permeability of the porous medium

Altmann and Ripperger (1997), based on the findings of Rubin (1977), have considered F_v in a linear wall-bounded shear flow to be 2.11 times higher than the calculated value by Stokes equation. However, they did not use any correction factors to the Stokes law due to presence of the cake.

Considering a simple situation in which all forces other than the drag force are negligible, the two components of the drag force F_v and F_f acting on a sphere in contact with a porous surface are balanced. When the net moment is equal zero,

$$F_f \sin\theta = F_v \cos\theta \qquad (2.26)$$

where,

θ = angle of repose (deg.)

To make this model applicable under actual situations, where other forces are significant, appropriate back diffusion mechanism(s), adhesive forces, friction forces, gravitational force etc. are also included in the force balancing exercise (Lu and Ju 1989, Schmitz *et al.* 1992, Chang *et al.* 1995, Altmann and Ripperger 1997, Sethi and Wiesner, 1997).

The back diffusion force F_b is calculated using the Stokes eq. by replacing flux (J) in eq. 2.23 by back diffusion velocity from eqs. 2.13, 2.17 and 2.20.

$$F_b = 3 \cdot \pi \cdot \eta \cdot d_p \cdot V_b \qquad (2.27)$$

where,

V_b = back diffusion velocity (m/s)

The gravitational force F_g is obtained by

$$F_g = \pi/6 \cdot d_p^3 \cdot (\rho_p - \rho_f) \cdot g \qquad (2.28)$$

where,

ρ_p = particle density (kg/m^3)

ρ_f = feed density (kg/m^3)

g = gravitational acceleration (9.81 m/s^2)

The adhesive forces are caused by Van der Waals forces and electrostatic interactions. The latter are very complicated to calculate and in general, negligible (Visser 1978). Therefore, generally only Van der Waals forces are considered for estimating adhesion forces (Schmitz et al. 1993, Altmann and Ripperger 1997).

One drawback of the single-particle models is that the filter or cake resistance and height are not determined and that they are also unable to specify the pressure-flux relationship (Schluep and Widmer 1996).

2.6.4 Combining different models

Some workers (Dharmappa *et al.* 1992, Piron *et al.* 1995, Schluep and Widmer 1996, Altmann and Ripperger 1997) have combined the back diffusion or the flowing cake mechanism with the resistance in series model to predict height and resistance of the cake. Shulz and Ripperger (1989) derived a model which connect the back transport with the filter theory.

2.6.5 Other models

A simple model to correlate the steady-state flux J_{ss} with the shear stress at the membrane wall (τ_w) for a given material is

$$J_{ss} = k_1 \cdot r_p \cdot \tau_w + k_0 \qquad (2.29)$$

where,

k_1 and k_0 = empirical constants

Holdich *et al.* (1995) included corrections in the calculation of τ_w to compensate for the effect of the cake height and pressure drop due to both flow before and after the filter and due to recirculation. They also replaced k_1 by another empirical constant k_2 to accommodate the wide particle size distribution of their feed stream.

Recently Hwang *et al.* (1998) developed a model involving a balance of compressive force due to permeate flux and inter-particle forces, Van der Waals force and electrostatic force. This model successfully estimated the values of average porosity and average specific filtration resistance under various electrolyte concentrations, crossflow

velocities and filtration pressures during CFMF of uniform submicron size spherical polymethyl methacrylate particles.

Blanpain *et al.* (1993) developed a model to describe the rebuilding of the cake layer after backflushes. This model incorporates hydrodynamically induced back transport effect and resistance theory.

2.7 Factors influencing the CFMF performance

2.7.1 Membrane properties

Since the membrane is always central to any membrane process, membrane related factors are very important for the process performance.

2.7.1.1 Membrane material

The membrane material plays an important role as it determines the chemical and pH stability, and temperature and pressure resistance of the membrane. The membrane material together with the pH of the feed, decides the charge on the membrane. Through interactions between solutes and the membrane, the membrane material has an important influence on flux, rejection and yield (Michaels 1989, Cheryan 1991).

Thus, for example, Tarleton and Wakeman (1994[b]) reported a significant difference in flux with different membrane materials for a low concentration suspension containing majority of particles larger ($d_{0.1}$, $d_{0.5}$, and $d_{0.9}$ = 11, 24.3 and 45.6 μm respectively) than the membrane pore size (0.2 μm). The sequence of performance was - mixed cellulose ester asymmetric microporous > cellulose nitrate cast homogeneous microporous > polycarbonate nuclear track etched = acrylic co-polymer homogeneous microporous > nylon 66 homogeneous membrane.

Hydrophobic membranes generally absorb more protein than hydrophilic membranes and may exhibit lower fluxes in applications involving soluble proteins (Persson *et al.* 1993[b]). However, when concentration polarisation and total protein deposition are high, the effect of hydrophobicity is masked by the effect of concentration polarisation. For

particulate suspensions, the effect of membrane hydrophobicity/hydrophilicity is short lived and not significant in determining long run fluxes (Persson *et al.* 1993[a], Tarleton and Wakeman 1994[b]).

The charge on a membrane depends on the membrane material, pH and ionic strength of the feed. Higher fluxes can be obtained for a feed containing solutes with similar charge to that of the membrane due to repulsion lowering the fouling. The charge on the membrane can also be used to assist separation of similar sized proteins (Marshall *et al.* 1993). However, with particulate suspensions e.g. anatase (Tarleton and Wakeman 1994[b]) membrane charge had very little effect on flux.

The effect of electric charge or hydrophobicity of the membrane can be reduced by modifying the membrane surface through the coating of polymers and surfactant of non-ionic or ionic origin (Akhtar *et al.* 1995, Van der Horst 1995).

2.7.1.2 Surface roughness

Surface roughness increases adhesiveness due to increased surface free energy. A rough surface may increase the protein adsorption (Marshall *et al.* 1993). In CFF, it is claimed that deposits are easily washed away if the membrane surface is smooth (Gatenholm *et al.* 1988). However, for the particulate suspensions the surface roughness has significance only for the cake layer adjacent to the membrane. Further, in most of the cases interparticle adhesive forces are far stronger than the adhesive forces between the particle and membrane surface.

2.7.1.3 Membrane pore size

Pore size and the pore size distribution are obviously of critical importance in determining the performance of MF membranes. Generally, for particulate suspensions membrane fouling is more severe with larger pore sizes. In many cases an optimum pore size is reported for highest flux where lower pore sizes give higher membrane and cake resistances and larger pore sizes give increased internal fouling. Devereux and Hoare (1986) observed greater flux decline with larger pore size membranes during recovery of soya protein precipitates. During CFMF of anatase suspensions, Tarleton

and Wakeman (1994[b]) reported a decrease in flux with increase in membrane pore size. But when the majority of the feed particles are significantly larger than the pore size, it has very little influence of pore size on flux or rejection. If the particles are too small compared with pores, flux improves but at the cost of good solids rejection. Thus, the pore size (d_m) / particle size (d_p) relationship is more important than solely pore size. Kawakatsu *et al.* (1993) found the situation where $d_m=d_p$ was optimum for maximum flux, particularly at lower TMPs for both compressible and incompressible particles. Wakeman (1994) using a high speed video camera observed low flux and thinner cake for condition $d_m \geq d_p$. In the case of $d_m<d_p$, cake layer at the surface controlled the filtration and there was no pore penetration by particles. For $d_m>d_p$ pore penetration was noticed.

The transmission of particles smaller than pore size is hindered by steric entrance effect, hydrodynamic drag, friction with other particles and pore wall. Further, it can be hindered through the changed membrane rejection properties due to the internal and/or surface fouling. Therefore, to obtain zero % retention, the ratio d_m/d_p has to be very large (Van der Horst and Hanemaaijer, 1990). Van der Horst and Hanemaaijer (1990) demonstrated this by calculating % of retention of different particle size with three imaginary membranes of same nominal pore size but different pore size distribution. This is shown in Fig. 2.12.

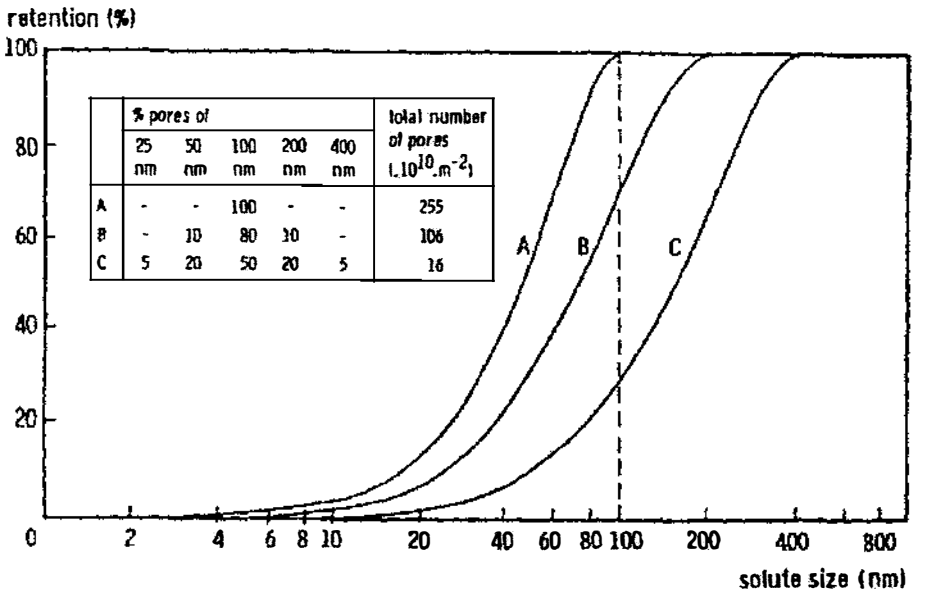

Fig. 2.12 Effect of pore size and size distribution on the retention of solutes (Van der Horst and Hanemaaijer 1990)

2.7.1.4 Porosity and Pore size distribution

MF membranes have a wide distribution of pore sizes. As shown in Fig. 2.12, membrane selectivity is poor when pore size distribution is poor. Fouling changes the pore size distribution. Flux is more sensitive to fouling of larger pores since the flow through larger pores has main contribution towards total flux.

MF membranes have higher porosity compared to the UF membranes. 'High' and uniform porosity is desirable. Porosity is adversely affected by fouling. The membranes with low porosity were fouled only externally where as high porosity membranes were fouled only internally during the studies on protein fouling of MF membranes carried out by Mueller and Davis (1996).

Variation in the pore size and pore size distribution among different batches of the same type of membrane as well as within the same membrane is not desirable since its affects the performance of the membrane.

2.7.1.5 Module design

The rotary modules described earlier (Section 2.2.3), can help reduce fouling due to high shear as a result of rotating part. Other similar approaches towards module design for local shear enhancement are the corrugated or dimpled membranes, vibrating membrane module, insertion of baffles, and induction of Dean or Taylor vortices (Finnigan and Howell 1989, Rappuoli and Unutmaz 1995, Mallubhotla *et al.* 1995). Cheryan (1992) described (1) the viscosity of feed, (2) particle size of suspension, (3) fouling potential of feed stream, (4) sanitary design and cleanability as the major criteria in selecting a module.

2.7.1.6 Cleaning and cleanability of filter

Efficient cleaning can restore the original flux by removing fouling. However, the cleanability of the membrane is essential. Generally, the greater the corrosion resistance of the microfilter, the easier is to find a suitable cleaning agent for it (Michaels 1989).

Bartlett *et al.* (1995) developed a qualitative model for membrane cleaning. They reported the use of an optimum cleaning agent concentration and temperature.

2.7.2 Effect of operating parameters

The operating parameters like time and temperature of filtration, transmembrane pressure, crossflow velocity are very important for the performance of the CFMF process as they affect the permeation rates and level as well as type of membrane fouling.

2.7.2.1 Time of filtration

An initial sharp decline in the flux,followed by a state of dynamic equilibrium,is typical of the behaviour in CFMF (as in many other membrane operations) and represents the effect of the time of filtration on the flux. The rate and mechanism of membrane fouling with time depend upon membrane configuration, feed conditions, and operating parameters. During CFMF of particles smaller than membrane pore size the initial fouling may be completely or dominantly the internal one. The rest of the filtration time is dominated by the surface fouling (Visvanathan and Ben Aïm 1989). This can be attributed to more availability of open pores in the beginning of filtration.

If a cake forms on the membrane surface with time during CFMF, at some stage this will start to govern the filtration process, i.e. the cake properties become more significant than the membrane properties with respect to filtration performance. The cake height is observed to increase with time and reaches a steady-state. But the flux continues to drop due to the penetration of smaller particles in the cake during this stage (Dharmappa *et al.* 1992, Schluep and Widmer 1996, Tien *et al.* 1997, Altmann and Ripperger 1997). The deposition of fines increases with time during CFMF and there is more penetration of these into the cake towards the end of the run. Jang (1987) observed an increase in the concentration of small particles (1.5 and 2.5 μm) and a decrease in large particles (4.5, 6.5, and 11 μm) in the cake with time during CFMF of kaolin clay suspension using 1.2 μm pore size membrane (Fig. 2.13).

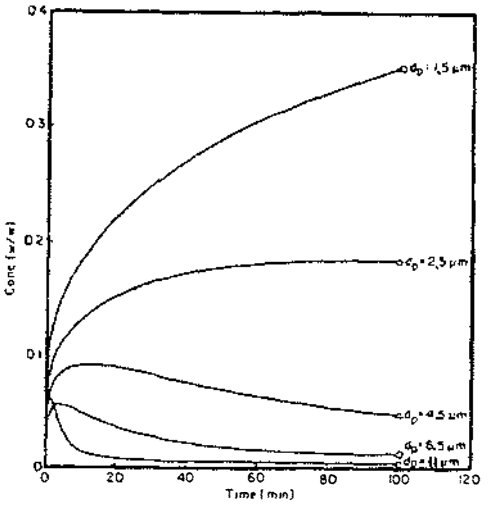

Fig. 2.13 Particle concentration in cake layer as a function of time (Dharmappa *et al.* 1992)

2.7.2.2 Temperature

Generally, increasing the temperature increases the permeate flux due to decrease in feed viscosity and increase in diffusivity. Thus the flow rate and dispersion of the polarised layer are improved. In the case of the particulate suspensions, the effect of temperature on the feed viscosity is of more significance. During CFMF of protein solutions, at higher temperatures, protein retention may decrease due to increased diffusivity to give higher flux (Michaels 1989). However, it can also increase due to increased protein denaturation and cause decrease in flux (Meireles *et al.* 1991). Precipitation of calcium as calcium phosphate at high temperatures has been reported by several workers to have reduced the flux during CFMF of model salt solution or cheese whey (Hanemaaijer *et al.* 1989, Piot *et al.* 1987).

2.7.2.3 Transmembrane pressure (TMP)

Considering Darcy's law (eq. 2.4), since TMP is the driving force in the process of CFMF, theoretically permeate flux should linearly increase with an increase in the TMP. This is observed for the pure water flux. For solutions and suspensions, temporary increases in permeate flux with increase in TMP are reported, but the increase in fouling is generally much higher and faster with increase in TMP (Persson *et*

al. 1993[a], Tarleton and Wakeman 1994[a], Russotti *et al.* 1995). Many reports show the existence of an optimum TMP, below which driving force limits the flux, and above which higher fouling results into lowering of flux (Fischer and Raasch 1986, Le 1987, Padilla-Zakour and Mclellan 1993, Van der Hoarst and Piersma 1993, Tarleton and Wakeman 1994[b], Wakeman 1994), or no further improvement in flux (Matsumoto *et al.*1988, Riesmeier *et al.* 1989, Taddei *et al.*1990). Marshall *et al.* (1993) stated that optimum pressure decreases with increasing membrane pore size.

The fouling (internal and/or surface) increases with increase in TMP. Faster and higher internal fouling of the membranes due to penetration of smaller particles or colloids, or internal adsorption of protein molecules with increase in TMP have been reported (Visvanathan and Ben Aïm 1989, Blanpain *et al.* 1993). Wakeman (1994) observed an increase in cake (particle layer) height directly proportional to increase in TMP. Increase in TMP is also thought to cause consolidation of the cake (Benkahla *et al.* 1995). Riesmeier *et al.* (1989) observed a linear increase in the cake resistance with increase in TMP during CFMF of the yeast suspension. They also reported a drop in the specific cake resistance with increase in TMP up to 0.7 bar (70 kPa) which they attributed to the smaller size deposition at lower TMP due to lower flux. However, the specific cake resistance increased above 0.7 bar, which they attributed to the compression of the particles. Increase in specific cake resistance with increase in TMP under dead-end MF is also reported (Kawakatsu *et al.* 1993, Foley 1994). However, there are no detailed reports on the effect of TMP on cake properties like compression, compaction and particle size distribution.

Attempts were made by Benkahla *et al.* (1995) to remove the cake formed during CFMF of $CaCO_3$ by decreasing TMP from 400 to 25 kPa at constant crossflow velocity to shift theforce balance in favour of back-diffusion or sweeping of particles. However, no change in cake resistance was observed due to cohesiveness of the cake.

2.7.2.4 Crossflow velocity (CFV)

CFV influences the CFMF performance mainly through its effect on the wall shear stress and particle size classification. Increasing crossflow velocity generally results in improved permeate flux due to reduced membrane fouling (particularly surface fouling)

and concentration polarisation. This is as a result of the thinner cake formation at a higher crossflow velocity due to high shear. Chang *et al.* (1995) observed an increase in steady-state flux with increasing wall shear rates during CFMF of polystyrene latex particles. Holdich *et al.* (1995) obtained a linear relationship between permeate flux and wall shear stress for CFMF of magnesium hydroxide slurries. Higher shear and turbulence, which generally reduce the fouling can, however, contribute to fouling. This could be due to protein denaturation during filtration of soluble proteins (Meireles *et al.* 1991) or through greater pore obstruction due to break up of precipitates during filtration of precipitated proteins (Devereux and Hoare 1986).

However, many workers have reported decrease in the flux with increase in the crossflow velocity (Fischer and Raasch 1985, Lu and Ju 1989, Wakeman and Tarleton 1991, Mackley and Sherman 1992, Tarleton and Wakeman 1994[a], Wakeman 1994). The common element in these studies was that the particulate suspensions used exhibited wide size distribution and the effect is attributed to the particle size classification. The cake formed under these effects contains smaller particles and offers higher resistance which results into lower flux. Fischer and Raasch (1985) and Lu and Ju (1989) analysed the cakes to study the effect of crossflow velocity on the cake PSD. Their results showed deposition of smaller size particles at higher crossflow velocities. Wakeman (1994) also (based on his *in situ* cake observations) reported more sweeping of cake and more deposition of fines compared to large particles at higher crossflow velocities. Foley *et al.* (1992) analysed the feed suspensions (of yeast cells) for their particle size distribution before and after the high crossflow velocity MF to reveal the preferential deposition of smaller particles. Mackley and Sherman (1992) observed that the cake of polyethylene particles (feed size 125-180 μm) deposited under crosflow had higher specific resistance than that under the static (dead-end) filtration. But Riesmeier *et al.* (1989) observed no difference in the specific cake resistance with change in CFV in the range of 1.0 to 4.0 m/s for the yeast cells.

2.7.2.5 Pressure and flow pulsation

Pressure and flow pulsations can reportedly improve the flux up to 45 % for apple juice (Gupta *et al.* 1992) and dramatically up to 268 % when combined with baffled systems for whey protein solution (Finnigan and Howell 1989). Mackley and Sherman (1993)

also observed marked improvements in flux using pressure switching, oscillatory crossflow and baffles during CFMF of polyethylene particles. They proposed that this was due to the erosion of surface fouling due to pulsations. However, a step change in TMP (from the operating levels of 400 to 25 kPa) did not alter the fouling during CFMF of a $CaCO_3$ suspension (Benkahla *et al.* 1995). Levesley and Bellhouse (1993) used oscillatory flow to generate high inertial lift forces on the polystyrene spheres and discs during CFF. This enabled them to retain the particles in the feed which otherwise would have passed through the membrane pores.

2.7.2.6 Backflushing

In backflushing, after a given period of time, the feed pressure is released and the direction of the permeate may be reversed in order to remove the fouling (internal or surface). There are three different ways of backflushing:

(1) Periodically stopping the feed pump

(2) Periodically applying external pressure using permeate and/or gas

(3) Periodically applying internal suction using permeate and/or gas

Applying external pressure using the permeate has been reported to give the best results (Matsumoto *et al.* 1988). The frequency and the strength of the backflush are important for the efficiency of cleaning. Wenten (1995) described a modified technique termed 'backshock', involving the application of external pressure using the permeate with high frequency for extremely short duration (0.1 sec). Ben Amar *et al.* (1990) and Gan *et al.* (1997) observed great improvement in permeate fluxes due to backflushing during clarification of apple juice and beer, respectively, by CFMF. However, Van der Horst and Hanemaaijer (1990) during defatting of whey and Padilla-Zakour and Mclellan (1993) during clarification of apple juice observed no significant effect of backflushing on the flux. In the case of protein fouling, backflushing is effective particularly on surface fouling, and only when the adsorption is not so strong (Marshall *et al.* 1993). Backflushing has been found less successful with CFUF compared to CFMF (Rappuoli and Unutmaz 1995).

2.7.2.7 Mode of operation

Apart from difference in the performance of different modes described in Section 2.2.4, the two different modes classified with respect to the TMP and flux - constant TMP and constant flux modes also perform differently. Membrane fouling causes a drop in the flux under the constant TMP mode and an increase in TMP under constant flux mode over the time of filtration. Hence, the force towards the membrane surface due to the flux is constant under constant flux mode and variable under constant TMP mode. Therefore, the two modes foul the membrane in different ways. The constant flux mode can be used to overcome the problems of interpretation of data due to flux variation in the constant TMP mode. However, constant flux mode would have its own problems of data interpretation due to TMP variation. It is possible to run the filtration with no fouling or negligible fouling when operated under constant flux mode at flux below the critical flux (Field *et al.* 1995). However, the concept of the constant flux is relatively new and less explored.

Turker and Hubble (1987) first reported the use of constant flux mode to investigate the fouling of a UF membrane. Aimar *et al.* (1989) proposed to maintain the flux constant so that the TMP become the dependent variable. Perrot *et al.* (1996) developed an automatic control using a fuzzy controller for the process of CFMF of raw sugar cane syrup. The controller simultaneously acts on and gradually increases the TMP and crossflow velocity to maintain the higher constant flux (double than that with the constant operating conditions). This performance was under the permeate recycle mode. Xu-Jiang *et al.* (1996) used constant flux mode for their dead-end MF experiments to develop a technique for study of membrane fouling. Kwon *et al.* (1996) also studied CFMF of polystyrene latex particles under constant flux mode.

2.7.3 Effect of feed properties

2.7.3.1 Feed concentration (C_{feed})

Generally an increase in the feed concentration results in a decline in the flux. This is due to higher fouling of the membrane in the presence of higher concentrations of foulants. However, the effect for particulate suspensions has been reported to depend on

the size of the particles (Wakeman and Tarleton 1991, Tarleton and Wakeman 1994[a], Wakeman 1994). These studies indicated a negligible effect of C_{feed} on the permeate flux for larger particles suspensions, such as calcite (25 μm mean size) and china clay (4.4 μm mean size). In contrast, for suspensions containing fine particles (e.g. ground calcite at 2.6 μm mean size, or anatase at 0.5 μm mean size), a drop in flux and increase in cake height with increasing C_{feed} were observed. The steady-state flux and the equilibrium cake height were reached faster at higher feed concentrations. The behaviour observed in the case of larger particles could be due to the increased inter-particle interaction and scouring action of rigid large particles on the deposits at higher C_{feed}. But in contrast to this, during CFMF of yeast cells (mean size ~ 7 μm), permeate flux decreased with increasing feed concentration (Redkar and Davis 1993). Riesmeier *et al.* (1989) reported an increase in the cake resistance with increasing feed concentration during CFMF of *E.coli.* Dropped flux during (bacterial) protein recovery (Parnham and Davis 1995) and increased protein (BSA) adsorption (McDonough *et al.* 1990) with increasing C_{feed} have been reported.

The process of estimation of the drag force acting on the particles in the feed, using Stoke s law (Section 2.6.3) is also C_{feed} dependant. Above certain C_{feed}, the effect of particle interaction needs to be accommodated through a correction coefficient (Fig. 2.14).

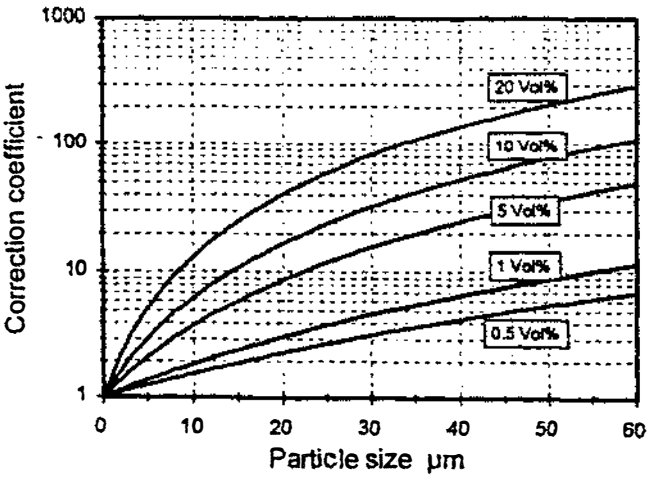

Fig. 2.14 Stokes correction versus C_{feed} and particle size for diatomaceous earth (Altmann and Ripperger 1997)

2.7.3.2 Particles in the feed

Particles in the feed have very significant but varying effects on permeate flux, fouling, and cake propeties. Particles may be present in the feed because of the nature of the feed or though precipitation of soluble feed component(s). The presence of particles as a result of denaturation or precipitation of feed solutes have been reported to reduce the permeate flux during CFMF of protein solutions (Kelly *et al.* 1993, Timmer *et al.* 1997). The particles can cause fouling through pore blocking, or pore narrowing, or cake formation. However, the use of 'scouring particles' which are at least 10 times larger than the feed particles can improve the CFUF performance by enhancing the local shear near the membrane surface. In CFMF, however, scouring particles may have the disadvantage of pushing the smaller particles on to the membrane surface (Dekker and Boom 1995).

Particle size

The size of the particle (which determines the pore size-particle size relationship) is important in deciding the permeate flux, and type and degree of fouling of the membrane. The resistance offered by a cake depends on the size of the particles present in it as described by the Carman-Kozeny equation (eq. 2.6).

Higher permate fluxes and cake thicknesses are obtained with larger particles (Wakeman 1994). Chang *et al.* (1995) observed higher steady-state flux with larger particles in the size range of 0.3 to 3.0 μm during CFMF of polystyrene latex. This effect was shear rate dependent. The difference in the steady state-flux was greater at higher shear rate in the range of 0.001 to 0.007 s^{-1}. This was attributed to the fact that, at high shear rates, tangential and lift forces are dominant and increase with increase in particle size, but at low shear rates, double layer repulsion forces are dominant and decrease with increase in particle size. It is thus the size of the particle that decides the mechanism of particle back-diffusion during CFMF as discussed earlier (Section 2.6.2). Larger particle size is one of the factors that inhibit deposition (Buffham and Cumming 1995).

Particle size distribution (PSD)

In actual filtration processes, the sizes of the feed particles often cover a wide range. The presence of fine as well as coarse particles results in a lower cake porosity as the fine particles can slide down between the large ones, filling the interstices. The porosity of a randomly packed bed of uniform spheres is 0.3 to 0.44 (Foust *et al.* 1980), whereas a mixture of widely size distributed spheres can give a porosity as low as 0.0384 (Dullien 1979). Benkahla *et al.* (1995) reported porosity of 0.17 - 0.18 for cake formed during CFMF of $CaCO_3$ in the size range of 1 - 17 μm (mean size 6 μm) at and above 150 kPa TMP. The cake resistance is inversely proportional to the cake porosity as per the Carman-Kozeny equation (eq. 2.6).

As discussed earlier (Section 2.7.2.1), there is more penetration of fines in the cake during the final phase of flux decline leading to the steady-state. The failure of the model by Mackley and Sherman (1992) in predicting the cake height accurately in the later stage of filtration seems to be due to not considering this effect. Dharmappa et al. (1992) considered this effect and successfully developed a semi-empirical equation to predict the permeate flux. Influence of PSD is most pronounced at low crossflow velocity and feed concentration where feeds containing higher proportion of fines give the lower flux. Tarleton and Wakeman (1993) suggested the use of the size fraction less than the 50% percentile (i.e. $d_{0.5}$) to characterise the feed as that is more indicative of the fouling potential of the feed. The range of the size distribution in the feed plays a major role in the selective deposition at high crossflows as discussed earlier (Section 2.7.2.4).

Particle shape

The shape of the particles is important in determining the porosity of the cake formed on the membrane surface. In general, the lower the particle sphericity, the greater is the porosity (Fig. 2.15). However, the platelet shaped particles form cakes with lower porosity than spheres (Dullien 1979).

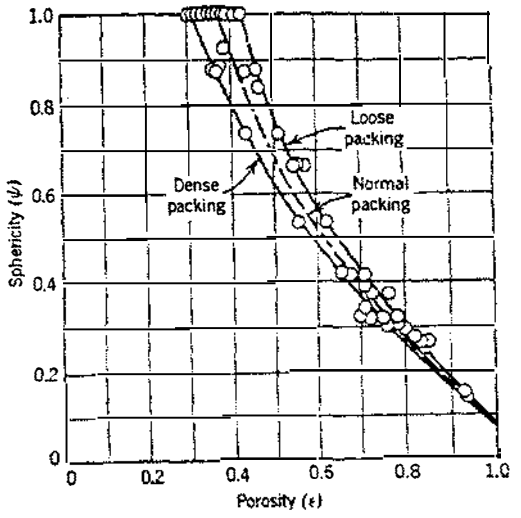

Fig. 2.15 Sphericity as a function of porosity for randomly packed uniform sized particles (Foust *et al.* 1980)

Tarleton and Wakeman (1994[a]) observed marked insensitivity of irregular (platelet) shaped china clay particles to applied pressure and feed concentration with respect to flux. They attributed this to the shape of the particles. They concluded that it was qualitatively and quantitatively difficult to predict the effect of particle shape.

2.7.3.3 pH, Ionic strength and surface charge

The pH and ionic strength of the feed affect (1) the charge on the membrane, (2) the charge on the particles, (3) conformation and stability of, and thereby adhesiveness of particles/molecules and (4) the effective size of the cake. Lower fluxes and higher hydraulic resistances at pI (iso-electric point where the net charge on a molecule is zero) are generally observed during CFMF of protein solutions (Bowen and Gan 1991, Hlavacek and Bouchet 1993, Pouliot *et al.* 1994). This is due to the greater potential for aggregation and deformation of proteins by shear, temperature and concentration at the pI. Greater adsorption on the membrane (Hanemaaijer *et al.* 1989) and slower back transport of protein molecules (Saksena and Zydney 1993) at pI are also reported. Bentham *et al.* (1987) observed a greater decline in flux during CFMF of soya protein precipitate suspension at its pI (pH 4.6) than at higher pH values. They attributed this to the precipitation of residual soluble proteins at pI. However, Wakeman (1994) observed maximum flux at pI during CFMF of anatase suspension. He explained it as a

consequence of more aggregation of particles at pI and hence formation of cake with less resistance than a cake made up of small particles.

Considering the charge effects, protein-membrane interactions are known to depend on the pH. Proteins are negatively charged at pH > pI and positively charged at pH < pI. The change in electric charge is more pronounced at pH below pI. The charge on the membrane at any particular pH will thus decide the level of protein adsorption (Micheals 1989). The presence of hydrophilic particles is also found to have a beneficial effect on the MF flux of protein solutions (Gekas and Hallström 1990).

2.8 Scope for the work and the present project

The CFMF is emerging as a very useful process for dairy and other food industries. More recently the work has focused on the separation and recovery of the milk proteins using CFMF. The recovery of the soluble proteins using a membrane process requires a smaller membrane pore size and a higher applied pressure compared to that required for precipitated proteins. However, the native state of the proteins is altered by precipitation. Since the recovery of particles is better achieved by CFMF than that by centrifugation, there is a scope to use it for recovery of casein fines from casein whey. Many workers attempted the recovery of precipitated soya proteins using membrane processes during the mid eighties. But more understanding about CFMF of particulate suspensions has been developed since then. However, most of the studies on the CFMF of particulate suspensions found in the literature are generally limited to rigid model particles of uniform shape and or size (polystyrene, latex, yeast, $CaCO_3$ etc.). Actual filtration often involves particles that have properties far different from the model particles. There is a need to further study the effects of different operating as well as membrane and feed related parameters particularly on the properties of the cake. Different methods of cake height measurement (laser triangulometer or high speed camera) used by several workers are limited to the flat sheet modules only.

Both the traditional constant TMP mode and the relatively new constant flux mode have their own advantages and limitations. However, combining the studies based on the two can be expected to develop the best understanding of the process performance. The flowing cake concept incorporating different forces on the feed particles with its own

limitations and resistances in series model are apparently the two most realistic approaches towards the modelling of the CFMF process.

Keeping the information needs in view, the following study is aimed at using lactalbumin particles (whey protein precipitates) in their natural configuration:

(1) Study on the effects of membrane configurations, feed conditions, and operating conditions on the fouling behaviour of the membrane under both constant TMP and constant flux modes. The parameters to study are mainly the steady-state flux, different types of membrane fouling, and cake properties - height, mass, porosity and PSD.

(2) Development of a force balance type model based on the flowing cake theory to describe these effects.

3. MATERIALS AND METHODS

3.1 Introduction

This chapter describes those materials and methods common to all investigations carried out. Specific information related to each experiment is reported in the appropriate chapters following.

3.2 Materials

3.2.1 Lactalbumin

Lactalbumin is an insoluble powder prepared by washing and drying the proteins precipitated from heat-treated whey (Robinson *et al.* 1976). A typical production process includes: (1) denaturation, coagulation and precipitation of proteins by heat treatment and pH adjustment; (2) separation of the lactalbumin from the whey by decantation, centrifugation or filtration; (3) spray, roller, ring or tunnel drying; and (4) grinding, blending and bagging.

Remilled lactalbumin powder was obtained in 1 kg packs with multi-layer packing (paper-polyethylene-foil) from the New Zealand Dairy Board.

3.2.2 Water

RO (reverse osmosis) water at room temperature was used to prepare the lactalbumin suspensions, to set the operating conditions, to measure the pure water flux, to rinse the membrane, and to prepare cleaning solution. RO water was obtained from the RO plant (Millipore, Milli-RO 30 plus, model 8000-791-246, USA).

3.2.3 Cleaning agent

The cleaning agent used for cleaning the membranes during this project was Ultrasil 2500 - a chlorinated alkali, supplied by Ecolab., Hamilton, New Zealand.

3.3 Equipment

3.3.1 Malvern Mastersizer

A Malvern Mastersizer (model E version1.1, Malvern Instruments, UK) with a reading range of 0.1-80 μm, located at the New Zealand Dairy Research Institute, Palmerston North, was used to determine the particle size distribution (PSD) of lactalbumin. This works on the principle of light scattering, a laser bulb is used as a source of light. Based on the light scattered by a lactalbumin particle in the suspension, the size of the particle is calculated. This is expressed in volume percent. It requires operation at least at 70 % laser power and feed at obscuration of about 20 %.

3.3.2 Membrane modules

Two different types of tubular alumina membrane module were used in this project. The first module (Ceraflow, Millipore Copr., Belford, USA) was 21 cm long, multi-channel type with 19 lumen, each of 2.5 mm inner diameter. Membranes with pore sizes- 0.2 μm and 1.0 μm were used in this module. The second module was 25 cm long, single-channel type with 6.8 mm inner diameter (Membralox, ITI-70, S.C.I., Bazet, France), obtained from the New Zealand Dairy Research Institute. Membranes with pore sizes 0.2 μm and 0.8 μm were used in this module.

3.3.3 Experimental set-up

The schematic diagram of the experimental set-up for constant TMP operation under permeate recycle mode is shown in the Fig. 3.1. The actual set-up is shown in Fig. 3.2.

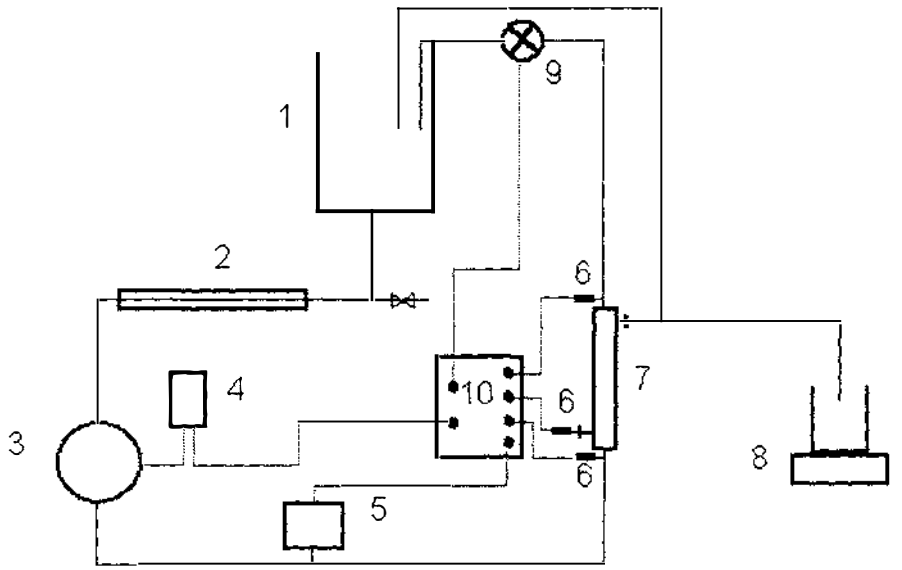

Fig. 3.1 Schematic of the experimental set-up for constant TMP operation - (1) jacketed feed tank, (2) heat exchanger, (3) rotary type positive displacement pump, (4) frequency inverter, (5) magnetic flowmeter, (6) pressure transducers each on inlet side, outlet side and permeate side of the membrane module, (7) membrane module, (8) weighing scale (9) electro-pneumatic valve and (10) control panel.

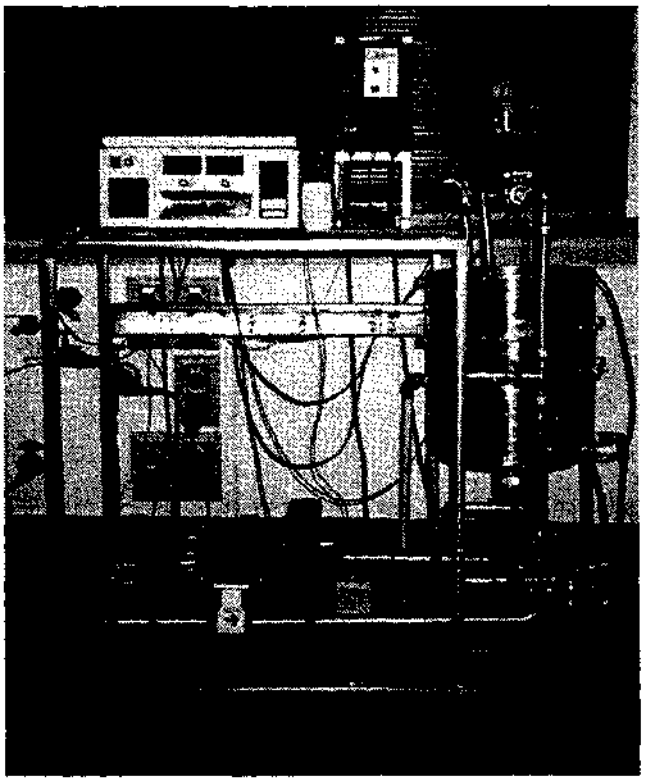

Fig. 3.2 Experimental set-up for CFMF

The feed tank was a 60 litre capacity stainless steel tank with a three compartment jacket. The bottom surface of the feed tank had a slope towards the central outlet to help avoid settling of the lactalbumin particles in the tank during operation and to facilitate complete draining at the end. A tubular heat exchanger was provided in the line. A twin lobe rotary positive displacement pump (model 55S, Flow Pump Ltd., UK) was used to pump the lactalbumin suspension. Selection of the pump was based on the results of the study on the effect of pumping on the lactalbumin particles (Chapter 4.3.2.2). The control panel comprised an automatic loop controller (Toshiba, model EC320, Japan) with two loops one each for controlling feed velocity through a frequency inverter (Zener, model MSC-M3, Australia) and for controlling TMP through an electro-pneumatic valve (Keyston, model IP6100, Australia). The control panel also housed a safety controller (Honeywell, model UDC200 Mini-Pro, USA) to protect the pump and rest of the system against high pressure by switching off the pump motor at a preset pressure. The frequency inverter was connected between the automatic loop controller and the rotary pump. Diaphragm type pressure transducers (Wika, Alexander Wiegand GmbH & Co., reading range 0-250 kPa, Germany) were placed at the inlet, at the outlet, and on the permeate side of the membrane. A magnetic flowmeter (Yokogawa, model AM202A, Japan) on the feed flow line and the three pressure transducers were connected to the controller. The membrane module was vertically placed in the line. The electro-pneumatic valve was placed on the exit side of the membrane module (Fig. 3.1). A weighing scale was provided to measure the permeate flux.

3.4 Methods

3.4.1 Setting the operating conditions

Operating conditions - TMP and CFV - were set by circulating RO water in the rig with a clean membrane in place. This was done prior to addition of the feed suspension. The required level of TMP was obtained by adjusting the electro-pneumatic valve position through the loop controller based on the readings from different pressure transducers. The required level of CFV was obtained by adjusting the pump speed with help of the frequency inverter through the loop controller based on the reading from the magnetic flowmeter. TMP was held constant by maintaining the permeate side pressure constant through keeping the permeate side open to the atmosphere.

3.4.2 Cleaning of the membrane

At the end of each run, after recovering the cake and measuring the pure water flux, the membrane was cleaned to re-establish the same initial clean water permeation rates. Thus all the experiments were conducted with a similar membrane condition.

The following cleaning procedure was found to give satisfactory results:

(1) Drain the suspension from the system by gravity.

(2) Replace the module after recovering the cake and circulate RO water at room temperature (about 18 °C) for 5 minutes.

(3) Circulation of hot RO water (50 °C) at 5.0 m/s CFV and no applied pressure for 10 minutes.

(4) Circulation of 1 % Ultrasil 2500 solution at 50 °C at 5.0 m/s crossflow velocity and no applied pressure for 20 minutes.

(5) Circulation of hot RO water (50 °C) at 5.0 m/s crossflow velocity and no applied pressure for 10 minutes.

(6) Circulation of RO water at room temperature for 10 minutes.

4. CHARACTERIZATION OF LACTALBUMIN

4.1 Introduction

The aim of this study was to investigate key physical properties of lactalbumin that might influence its behaviour during CFMF. The physical properties studied included: shape, particle size distribution (PSD), and particle and bulk density. Its behaviour was also studied under conditions of soaking, pumping, and under applied pressure similar to that encountered during the CFMF experiments.

4.2 Physical properties of lactalbumin

4.2.1 Methods

Lactalbumin powder was observed under 400x magnification using a microscope to study the shape of the lactalbumin particles.

The volume of known mass of the lactalbumin was measured using a volumetric cylinder to determine the bulk density. The volume of water displacement by a known mass of lactalbumin when added to a known volume of water was measured to determine the particle density.

PSD of the lactalbumin powder was determined by two methods - Microscopic analysis, and using the Malvern Mastersizer. In the former, a drop of RO water containing freshly suspended lactalbumin particles was placed on a haemocytometer and covered with a cover slide. The slide was observed under a calibrated microscope using 400x magnification. All measurements were carried out in triplicate and average results were expressed in number percent. Routine measurements were made using the Mastersizer which uses the principle of light scattering. A sample of freshly prepared lactalbumin suspension in RO water was fed to the Mastersizer after establishing the required laser power, and analyzed at required obscuration (as descried in Chapter 3.3.1) for its PSD. The PSD so obtained was expressed in volume % by the Mastersizer. This analysis was carried out in triplicate and mean values of the results were considered.

To provide an approximate comparison of the results of these two methods, the data from the microscopic analysis were converted to volume percent and similarly the results of Mastersizer were converted to number percent, assuming the particles to be spherical.

For the Mastersizer data,

$$\text{Number \%} = \frac{\text{(Volume \% / Volume of average size particle) for the range}}{\Sigma\text{ (Volume \% / Volume of average size particle) of all ranges}} \times 100$$

For Microscope,

$$\text{Volume \%} = \frac{\text{(Number \% x Volume of average size particle) for the range}}{\Sigma\text{ (Number \% x Volume of average size particle) of all ranges}} \times 100$$

4.2.2 Results and discussion

4.2.2.1 Appearance

Lactalbumin is a white amorphous powder of highly irregular particles (Fig. 4.1).

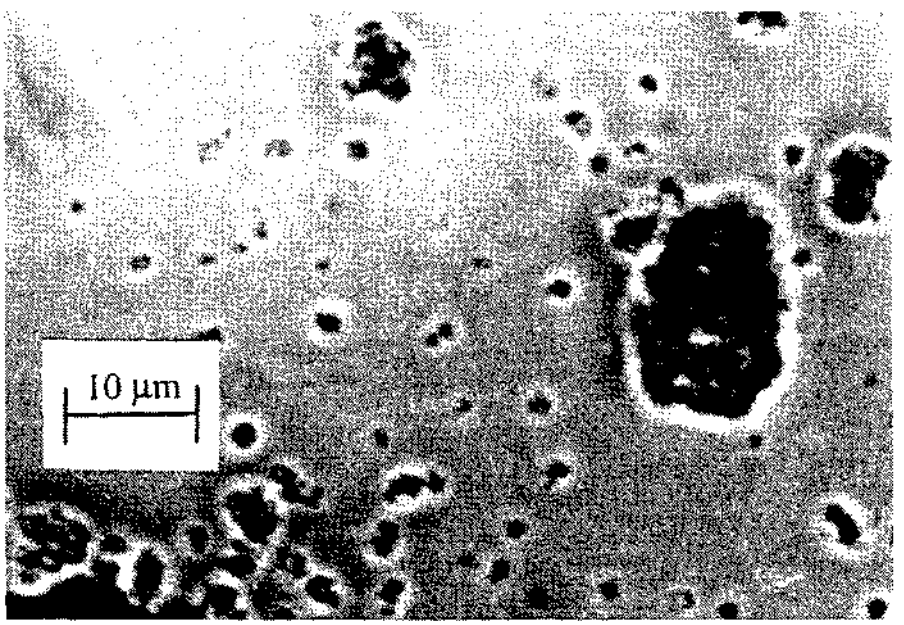

Fig. 4.1 Microphotograph of lactalbumin particles

4.2.2.2 Density of lactalbumin

The bulk and particle densities (ρ_b and ρ_p respectively) of the lactalbumin powder were found to be 488 kg/m^3 and 1200 kg/m^3 respectively. The value of the particle density was slightly lower than 1346 kg/m^3 - the reported solid density of the milk proteins as a whole (Davies 1939). This possibly reflects some internal voids within the lactalbumin particles.

4.2.2.3 Particle Size Distribution

The results of the microscopic study are shown in Fig. 4.2 and the results of the analysis of lactalbumin particles using Malvern Mastersizer are shown in Fig. 4.3. The parameters $d_{0.1}$, $d_{0.5}$ and $d_{0.9}$ in Fig. 4.3 means 10, 50 and 90 % of the particles in the sample, respectively, are smaller than or equal to these values. Lactalbumin particles were distributed in a wide size range of 0.1 μm to 80 μm.

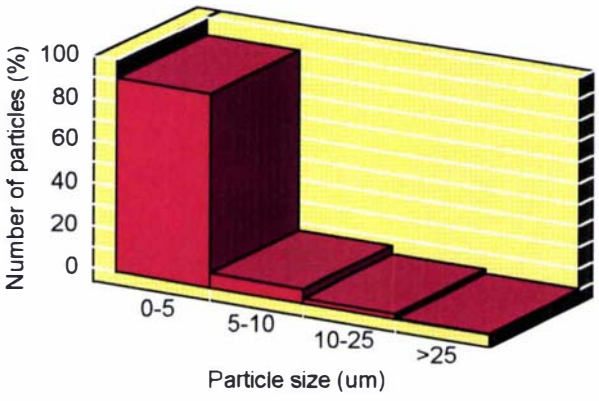

Fig. 4.2 PSD of lactalbumin based on microscopic observations

Version 1.1

Sat, 15 Mar 1997 04:26PM

Lact.feed fresh :Run Number 1

Fresh lact.feed from run 100-0.75
HaritVyas
PET, Massey.

Source: Analysed

Measured on: Sat, 15 Mar 1997 04:24PM

Presentation: (2NAD) 1.330, 1.456 + i 0.00000
Polydisperse model — Volume Result — Focus = 45 mm

Residual = 1.979 %
d (0.5) = 35.24 µm
D [4, 3] = 37.10 µm
Sauter Mean (D[3,2]) = 2.12 µm
Specific Surface Area = 2.8257 sq. m. / gm

Concentration = 0.009 %
d (0.1) = 0.49 µm
Span = 2.07

Obscuration = 20.78 %
d (0.9) = 73.41 µm
Standard Deviation = 25.88 µm
Mode = 0.00 µm
Density = 1.00 gm. / c.c.

Size (Lo) µm	Result In %	Size (Hi) µm	Result Below %
0.10	0.07	0.12	0.07
0.12	0.71	0.15	0.78
0.15	1.29	0.19	2.07
0.19	1.71	0.23	3.78
0.23	1.93	0.28	5.71
0.28	1.89	0.35	7.60
0.35	1.60	0.43	9.20
0.43	1.1[illegible]	0.53	10.30
0.53	0.55	0.66	10.85
0.66	0.14	0.81	11.00
0.81	0.00	1.00	11.00
1.00	0.00	1.23	11.00
1.23	0.00	1.51	11.00
1.51	0.00	1.86	11.00
1.86	0.06	2.30	11.05
2.30	0.37	2.83	11.42

Size (Lo) µm	Result In %	Size (Hi) µm	Result Below %
2.83	0.81	3.49	12.23
3.49	1.15	4.30	13.38
4.30	1.17	5.29	14.55
5.29	1.03	6.52	15.58
6.52	1.94	8.04	17.52
8.04	2.69	9.91	20.20
9.91	3.08	12.21	23.28
12.21	4.16	15.04	27.45
15.04	4.90	18.54	32.35
18.54	5.55	22.84	37.91
22.84	5.79	28.15	43.69
28.15	5.86	34.69	49.55
34.69	6.44	42.75	55.99
42.75	8.57	52.68	64.55
52.68	12.98	64.92	77.54
64.92	22.46	80.00	100.00

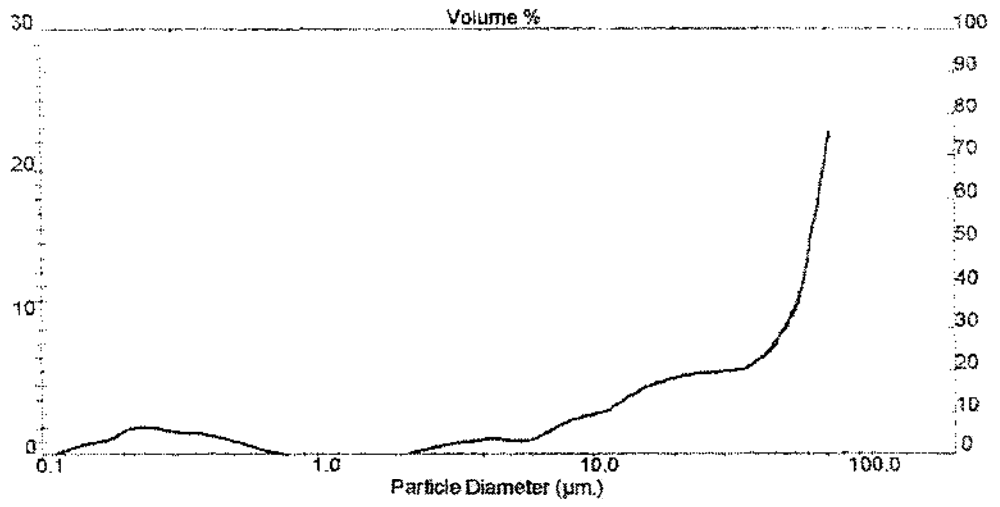

Fig. 4.3 PSD of lactalbumin determined using Mastersizer

The results obtained by the two methods were found to be within the same order (Table 4.1).

Table 4.1 Comparison of PSD of lactalbumin obtained from the Mastersizer and microscopic examination

(a) Results in volume per cent

Particle size (μm)	Microscope	Mastersizer
0-5	5.30	13.76
5-10	9.90	15.60
10-25	48.40	45.64
>25	36.40	25.00

(b) Results in number per cent

Particle size (μm)	Microscope	Mastersizer
0-5	91.00	95.10
5-10	6.36	3.90
10-25	2.44	0.92
>25	0.20	0.06

Since the higher reading limit of the Mastersizer is 80 μm, any particle larger than that is not measured correctly. However, no particle larger than 80 μm was encountered during microscopic examination of many (more than10) samples.

4.3 Behaviour of lactalbumin in suspension

4.3.1. Methods

The lactalbumin particles were soaked in the RO water for 4 or 6 hours and analyzed for particle size distribution using the Mastersizer. Samples were also observed under microscope. The results from both analyses were compared with those of freshly suspended lactalbumin particles. The mean values of three replications were used to analyze the results. The particles were soaked for a further extended period and the suspension analyzed for PSD after 48 and 72 hours.

In a separate experiment, a few of the lactalbumin particles were held in the suspension on a microscopic slide and each of them was observed for any change in size or shape with time after 1,2, 4, and 6 hours. This experiment was particularly aimed at checking the possibility of swelling of the particles under the condition of soaking. Mean values of three replicates were considered for the study.

A suspension of lactalbumin particles with concentration of 2.5 g/l was pumped using two different rotary positive displacement pumps with different types of rotors. The first unit had twin rotors with 8 flower petal shaped blades (model 10-20 G, Johnson Pump (UK) Ltd.); the second system had twin lobe rotor (as described in Chapter 3.3.3). For the latter, pumping was carried out under 100 kPa pressure and 3.0 m/s or 0.75 m/s flow through the membrane tube. For this pump, samples were drawn after 15, 30, 60, 90, 120, 150 and 180 minutes and analyzed for PSD using the Mastersizer. For the 8 blade rotor pump, pumping was done at 100 kPa and 3.0 m/s through the 2.5 mm membrane tube. The sample was drawn only after 60 minutes for analysis of PSD. The results were compared with PSD of fresh lactalbumin suspension that was not pumped. The rotor speed of the pump was measured using a non-contact type tachometer (Isspro, model R1620A, Instrument Sales and Services Inc., Oregon, USA) with a reading range of 50-25000 rpm and an accuracy of ± 1 rpm for 50-9999 rpm and ± 10 for 10000-25000 rpm. This was done for approximation of the maximum rate of shear assumed to be responsible for the particle break-up.

4.3.2 Results and discussion

4.3.2.1 Soaking of lactalbumin

Lactalbumin particles when suspended in the RO water mostly settled immediately. However, the fine particles remained in the suspension for a long time (nearly 2 hours). The suspension held undisturbed for 2 hours, 4 hours, and 6 hours, formed clusters of the particles (observed under microscope as shown in Fig. 4.4). However, there was no change in PSD of lactalbumin by Mastersizer analysis indicating that the clusters were not strongly bonded and presumably the aggregates were disrupted by pump circulation in the Mastersizer. Further soaking up to 48 to 72 hours resulted in the formation of an elastically compressible gel revealing the tendency of lactalbumin to soften when

soaked. This agrees with the high level of water absorption by lactalbumin (85 to 175 g water/100g lactalbumin) reported by Short *et al.* (1978).

The individual particles held in suspension on the microscope slide after 2, 4 and 6 hours showed no significant change in size or shape indicating no swelling occurred.

Fig. 4.4 Clusters formed by lactalbumin particles suspended in water (after 4 hrs. of soaking)

4.3.2.2 Effect of pumping on lactalbumin particles

The results of the performance of the two different pumps with respect to the PSD are shown in Table 4.2 and in Fig. 4.5. Both pumps had an effect on the PSD of the lactalbumin due to breakage of the particles. However, the lobe pump had less effect, which was mainly confined to larger particles (above about 73 μm) as seen in Fig. 4.5. The smaller size range (0.1 to 25 μm) in particular, which is expected to play a greater role in fouling the membrane during CFMF of lactalbumin was not significantly affected. Thus for practical purposes the effect of the lobe pump on the PSD of lactalbumin can be considered negligible. In contrast, the effect of the 8 blade rotor pump, in a short time period of 60 minutes was very significant over the entire size range of the lactalbumin, although the greatest effect was again on the large particles.

Thus out of the two pumps available, the lobe pump was suitable for the CFMF experiments.

Table 4.2 Effect of pumping on PSD of lactalbumin

Operating pressure = 100 kPa

Time (min)	Velocity = 0.75 m/s				Velocity = 3 m/s			
	$d_{0.1}$ (μm)	$d_{0.5}$ (μm)	$d_{0.9}$ (μm)	d_{sauter} (μm)	$d_{0.1}$ (μm)	$d_{0.5}$ (μm)	$d_{0.9}$ (μm)	d_{sauter} (μm)
Lobe pump								
0	0.49	35.24	73.41	2.12	0.49	35.24	73.41	2.12
15	0.45	30.94	72.50	2.00	0.46	33.36	73.26	2.03
30	0.42	28.39	71.80	1.89	0.44	31.13	72.95	1.96
60	0.42	27.65	71.72	1.86	0.42	29.93	72.91	1.87
90	0.49	27.25	70.98	2.06	0.42	29.53	72.69	1.86
120	0.40	24.10	70.15	1.78	0.4	26.24	72.03	1.77
150	0.39	22.54	69.64	1.71	0.4	24.83	71.49	1.75
180	0.39	22.54	70.38	1.73	0.39	24.24	71.22	1.73
8 blade rotor pump								
0					4.81	43.51	74.35	2.46
60					0.31	22.85	59.7	1.5

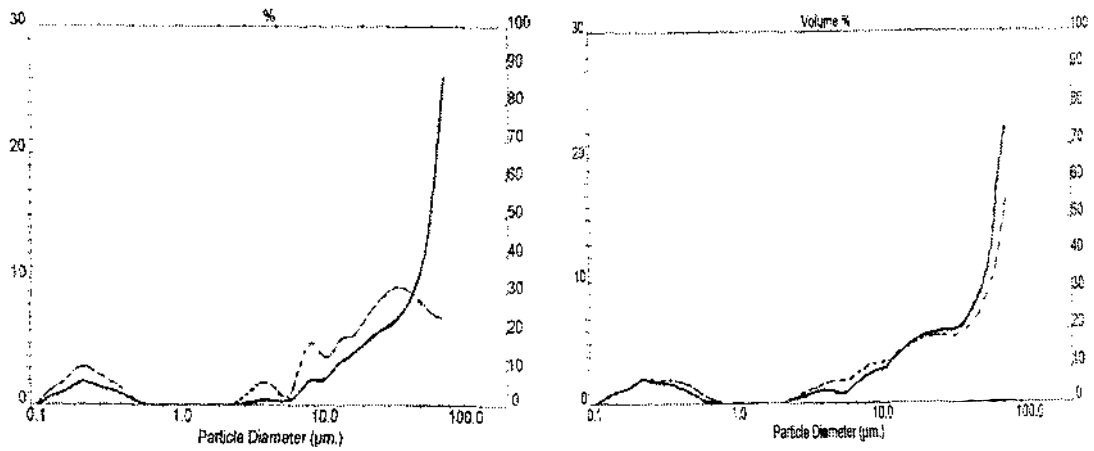

(a) (b)

Fig. 4.5 Effect of pumping at 100 kPa and 3.0 m/s on the PSD of lactalbumin, (a) 60 minutes of pumping with 8 blade rotor pump, (b) 180 minutes of pumping with lobe pump

To understand the mechanism of particle break-up during pumping, it was assumed that the shear stress was the major cause for the particle size reduction. Maximum shear stress in a rotary pump occurs in the clearance between the rotor and the pump housing. The maximum shear rate (γ_{max}) in this region, assuming no fluid back-flow in the clearance, and that the clearance is smaller than the boundary layer thickness, can be approximated by (Hoare *et al.* 1982):

$$\gamma_{max} = \pi N D / \delta \qquad (4.1)$$

where,

$\pi N D$ = angular velocity of the rotor tip
N = speed of rotor (rps)
D = diameter of rotor (m)
δ = clearance between rotor and housing (m)

At the conditions 100 kPa operating pressure and 3.0 m/s flow velocity, the values of γ_{max} for the lobe pump and the 8 blade rotor pump were 12696 and 16781 s^{-1} respectively. γ_{max} for 100 kPa operating pressure and 0.75 m/s flow velocity in the case of the lobe pump was 8672 s^{-1}. The greater shear rate in the case of the 8 blade rotor pump could be responsible for the greater particle size reduction compared to that of the lobe pump at the same operating condition. But for the lobe pump, there was no significant difference in the type and level of the particle break-up at the two different flow velocities (Table 4.2) despite of a significant difference in γ_{max}. This suggests that either the particle break-up was affected by the shear rate only above certain level (12700 s^{-1} in this case), or the shear rate did not play a major role in particle break-up.

As noted, the major effect of pumping occurred in the size range of above about 73 μm for the lobe unit. Given the clearance between the rotor and the housing was 0.12 mm (120 μm) for both the units suggests that the major mechanism of particle break-up was possibly impact and grinding of particles with and between the rotor and housing. The levels of impact as well as grinding depend on the shape and number of rotor blades. This could be the reason for the difference in the extent of break-up caused by different pumps in this study. Hoare *et al.* (1982) observed greater particle break-up with increasing shear rate during pumping of soya protein precipitates using peristaltic, mono and gear pumps (γ_{max} = 70, 1500 and 2600 s^{-1} respectively). However, the level of break-up in mono and gear pumps was equivalent to the break-up at 32900-82200 s^{-1} in

a Couette flow device. They considered the particle-wall and particle-rotor impact in the pumps as a probable reason for this difference. The results of the present study also indicate the dominant role of the physical impact between particles and pump components on the particle break-up during pumping.

To provide a comparison between the results of the present study and the study by Hoare *et al.* (1982), the change in $d_{0.9}$ of lactalbumin is plotted against number of passes through the pump (estimated from the flow rate and quantity of the feed) in Fig. 4.6. Ratio of $d_{0.9}$ to the initial $d_{0.9}$ (i.e. $d_{0.9}$ n/$d_{0.9}$) is plotted against number of passes for both the studies in Fig. 4.7.

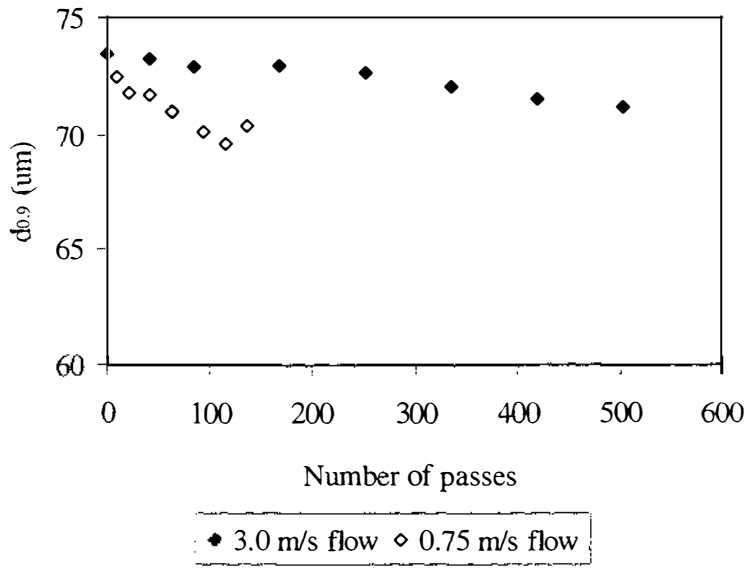

Fig. 4.6 Change in $d_{0.9}$ of lactalbumin with number of passes through the lobe pump at 100 kPa pressure, 0.75 and 3.0 m/s flow velocity conditions, 2.5 g/l C_{feed}

Compared to the soya protein precipitates when pumped by the positive displacement pumps, lactalbumin particles suffered a minor and slow break-up despite the much greater shear rates in the case of the lobe pump (Fig. 4.7). This could be due to the difference in the firmness of the fresh soya protein precipitates and dried precipitates of lactalbumin, and the difference in the type of positive displacement pumps used. Although, the number of passes made by a feed particle through the pump was different at the two flow velocities for the same operational time the size reduction was similar.

This could be due to the longer residence time of a particle in the gap between the rotor and the housing during a pass at the lower velocity.

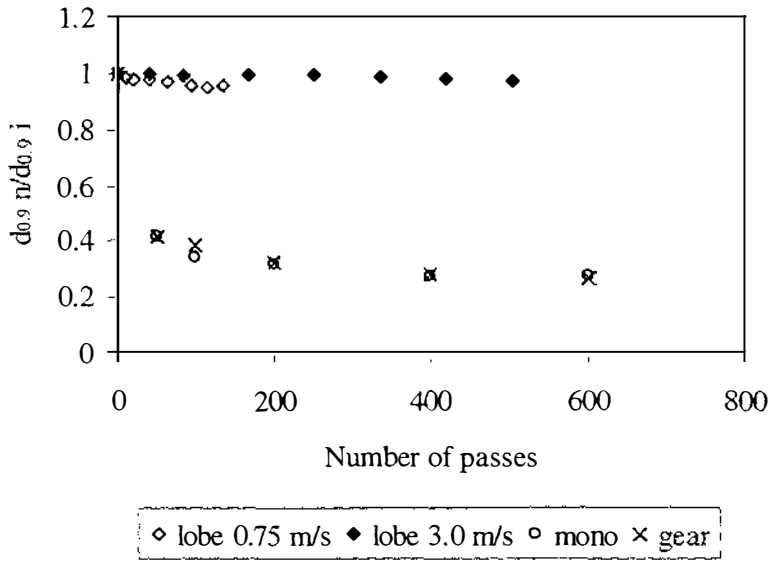

Fig. 4.7 Comparison of the results of present study (lactalbumin particles pumped by lobe pump) with the results reported by Hoare et al. (1982), (soya precipitates pumped by mono and gear pumps)

4.4 Porosity of the particle bed

4.4.1 Methods

An experimental set-up as shown in the Fig. 4.8 was used for this study. This comprised a glass tube with 5.62 mm inner diameter with a 0.2 μm pore sizeWhatmanfilter paper fitted at one end, a three way valve, a pressure gauge, connecting rubber pipes and a high pressure water supply. The filter was secured in place with help of a PVC holder and screws.

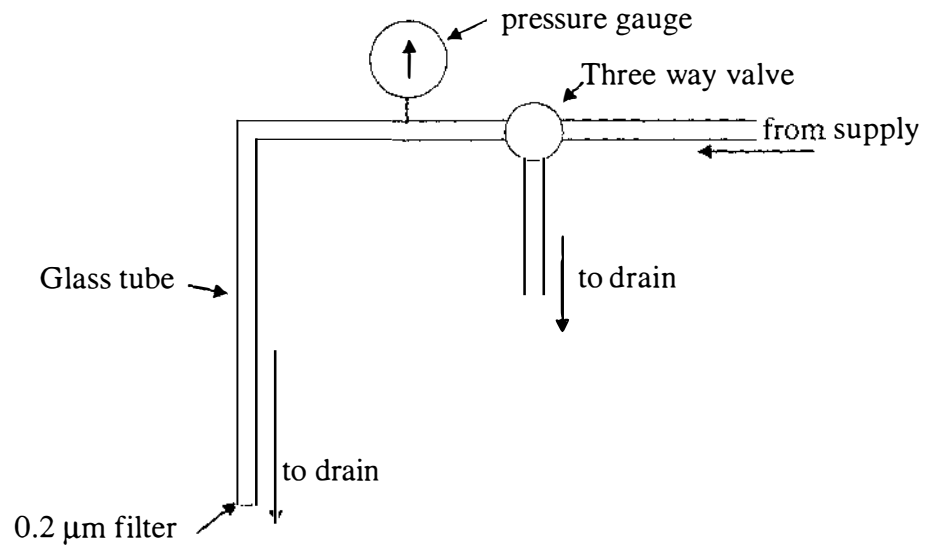

Fig. 4.8 Schematic of the experimental set-up for estimation of porosity

A known mass of lactalbumin was placed on the filter, 0.5 ml of water was added and allowed to mix with the lactalbumin. Once the column of powder settled, its height was measured using a vernier caliper. Then the tube was fully filled with water and pressure was applied from the top using the high pressure water supply. The height of the lactalbumin column was measured at pressures of 20, 50 and 100 kPa (adjusted using the three way valve). The bulk density (ρ_b) of the lactalbumin column was calculated from the measured height and used for estimating the porosity (ε) as follows:

$$\varepsilon = 1 - \frac{\rho_b}{\rho_p} \qquad (4.2)$$

The effect of adding different masses of lactalbumin to the glass tube on the apparent porosity was investigated. This was done to ensure that the lactalbumin column height did not become too high, so the applied pressure acted only on the bottom of the tube and not also on the wall of the tube. The average value of the porosity from three replications was considered. The PSD of lactalbumin exposed to the pressure was measured using the Malvern Mastersizer to check for any change in particle size due to application of the pressure.

To check the validity of the experimental method, non-compressible spherical glass particles (BDH chemicals Ltd., UK) of 100 μm mean diameter with reasonably narrow PSD (as measured by Malvern Mastersizer) were used as a standard.

4.4.2 Results and Discussion

The glass spheres used as model particles were found to be of uniform size with a narrow size distribution ($d_{0.1}$ = 91 μm, $d_{0.5}$ = 108 μm, and $d_{0.9}$ = 139 μm). The shape of the glass particles as observed under the microscope was perfectly spherical (Fig. 4.9).

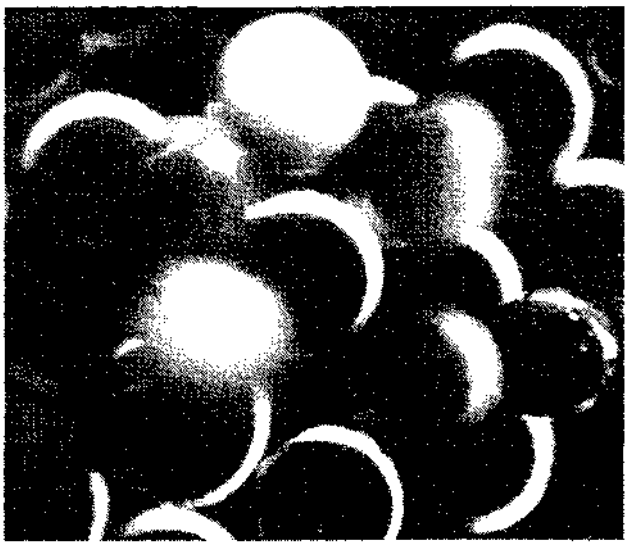

Fig. 4.9 Glass spheres under 100 x magnification

The results of the porosity determination for the glass spheres are shown in Table 4.3. These values are typical of the range reported for randomly packed rigid and uniform spheres (chapter 2.7.3.2) and there was no significant effect of the applied pressure on the porosity.

Table 4.3 Porosity of glass spheres under different applied pressures

Applied pressure (kPa)	Porosity
0	0.40
20	0.38
50	0.38
100	0.38

Based on the preliminary experiments to decide the appropriate amount of lactalbumin to be taken for accurate porosity estimation, bed porosities under 100 kPa pressure for different masses are shown in Fig. 4.10. Porosity dropped with decrease in mass indicating the wall effect (Perry 1963) for taller columns at higher mass. The porosity did not drop below 0.065 g. Therefore, 0.065 g was chosen as the mass of lactalbumin for this study.

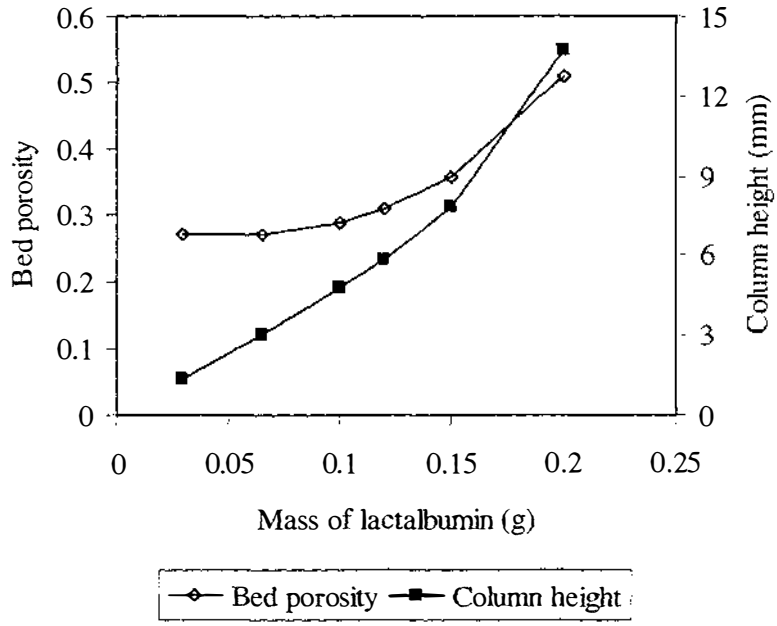

Fig. 4.10 Change in bed porosity at 100 kPa applied pressure with change in mass of lactalbumin

The determined values of porosity of the lactalbumin particles are shown in Table 4.4. The porosity was very high with no applied pressure but was dramatically reduced to 0.29 on application of a pressure of only 20 kPa. However, a further increase in applied pressure did not result into a further significant drop in the porosity. Removal of the external pressure did not reverse the bed height or porosity. The lactalbumin exposed to applied pressure conditions did not show any change in the PSD (data not shown).

Table 4.4 Porosity of lactalbumin particles under different applied pressures (standard condition i.e. 0.065g lactalbumin)

Applied pressure (kPa)	Porosity
0	0.60 ± 0.02
20	0.29 ± 0.02
50	0.29 ± 0.02
100	0.27 ± 0.00

The lower porosity of the lactalbumin compared to the uniform size glass spheres was due to the wide PSD of lactalbumin. The drop in porosity with application of the pressure could mainly be due to rearrangement of the bed to give denser packing. The change in porosity due to application of pressure was irreversible. Thus elastic compression of the cake under pressure did not occur. The insignificant effect of further increase in the pressure on the porosity and PSD also indicated that there was no significant compression or break up of the particles. That suggested very compact lactalbumin cakes with a porosity lower than 0.3 can be expected to form on the membrane surface during CFMF experiments even at low operating pressure.

4.5 Overall discussion

The irregular shape and wide PSD, plus the tendency to absorb moisture and to soften when soaked in water are the salient features of lactalbumin. Therefore, the CFMF of lactalbumin particles is expected to be interesting as most of the CFMF studies reported in the literature generally involve regular sized, shaped, rigid model particles. The action of the lobe pump appears to be reasonably gentle on the lactalbumin and hence the effect of pumping by this pump on lactalbumin during CFMF studies should be negligible. Lactalbumin is also expected to form very compact cakes on the membrane surface as well as foul the membrane internally (theoretically, if the membrane pore size is larger than 0.1 μm).

5. CFMF OF LACTALBUMIN UNDER CONSTANT TMP MODE

5.1 Introduction

The performance of the ceramic tubular membranes during CFMF of lactalbumin particles under constant TMP mode with permeate recycle is discussed in this chapter. The variables investigated were: (1) time of filtration, (2) TMP, (3) CFV, (4) C_{feed}, (5) feed particle size (6) membrane pore size, and (7) module design.

The content of this chapter is grouped into three parts: (1) general methods and confirmatory experiments, (2) the effects of operating parameters and process development based on these effects, and (3) the effects of feed properties and membrane configuration on process performance. An overall discussion follows each part.

5.2 General methods

All experiments in this study, unless otherwise mentioned, were carried out in triplicate and the results averaged. In this section, the general procedures employed in all runs are introduced. Specific procedures employed for each investigation are described in the appropriate section.

5.2.1 Running the experiment

The required operating conditions were set during RO water circulation, and the pure water flux (J_w) was measured. The RO water was then drained from the system and replaced by freshly prepared lactalbumin suspension with the desired concentration. The rig was then operated under the set conditions with the permeate outlet connected to the feed tank to recycle permeate. At pre-determined time intervals the permeate flux (J) was measured gravimetrically and recorded. Each experimental run was continued until a nominal steady-state value (no change for 10 min) of the permeate flux (J_{ss}) was obtained. The temperature of the feed suspension was maintained constant during the filtration run at 18 $^{\circ}$C for all experiments by the tubular heat exchanger (Fig. 3.1).

5.2.2 Estimation of different resistances to the flux

Permeate flux values measured at different stages of the filtration process were used to estimate different resistances to permeate flux, by applying Darcy's law (eq. 2.4) and the resistances in series model (eq. 2.5).

R_m was estimated from J_w before starting the actual filtration:

$$R_m = \frac{\Delta P}{\eta \cdot J_w} \qquad (5.1)$$

At pre-determined time intervals the instantaneous flux (J(t)) and at the end of the filtration period, the steady state flux (J_{ss}) were measured to estimate R_f:

$$R_f = \frac{\Delta P}{\eta \cdot J} - R_m \qquad (5.2)$$

where,

J = J(t) or J_{ss} as appropriate

At the end of each experiment, the cake formed on the membrane surface was recovered as described later in section 5.2.3. Then pure water flux ($J_{w,if}$) was measured under the operating conditions used during the filtration run. Based on this value of $J_{w,if}$, resistances due to internal (R_{if}) and surface fouling (R_{sf}) were estimated.

$$R_{if} = \frac{\Delta P}{\eta \cdot (J_{w,if})} \qquad (5.3)$$

$$R_{sf} = R_f - R_{if} \qquad (5.4)$$

Since the cake was removed only at the end of the run, it was possible to divide R_f into its surface and internal fouling components only at this time.

5.2.3 Collection and analysis of the cake

To better understand the fouling mechanism, cakes deposited on the membrane surface during different experimental runs were collected and their mass, height or thickness, and particle size distribution (PSD) determined. The cake deposited on the membrane surface was removed manually using a polyethylene rod with 2 mm diameter to physically push cake out of each lumen coupled with RO water flushing. The cake mass was estimated using the standard gravimetric method in duplicate and the average value

considered. The samples of cake suspension were analysed for PSD using the Malvern Mastersizer as described in section 3.1.3.

Estimation of the height of the cake

Due to the small diameter of the membrane lumen (2.5 mm), direct observation of the cake height deposited on the membrane surface was not feasible without a facility like NMR micro-imaging (Wandelt *et al.* 1992). Therefore, an indirect method for cake height estimation was developed. In this method, the cake was first recovered as a slurry in water and then the cake height was reconstructed on a 0.2 μm pore size Watman filter paper using dead-end filtration (Fig. 4.8). The following procedure was used:

1. Take 2 ml of the cake suspension in the glass tube and fill the rest of the tube with water
2. Apply a pressure equal to TMP used in the CFMF run from top of the tube using a high pressure water supply for the same time period as that of the CFMF run (i.e. the time required to achieve steady-state)
3. Measure the height of the cake with vernier callipers
4. Estimate the actual cake height on the membrane surface as follows:

$$\text{Actual cake height} = \frac{\text{cake mass per unit area on membrane} \times \text{cake height in tube}}{\text{cake mass per unit area in the tube}} \qquad (5.5)$$

The apparent actual cake porosity was then calculated using eq. 2.9.

The results obtained by this method were confirmed by an alternative cake reconstruction method using a vacuum flask. In this method, the pressure difference across the filter was created by applying vacuum on the permeate side of filter. The following procedure was used:

1. Arrange the flask with two circular filters (0.2 μm Whatman filter paper) laid on one another, the top filter with a 5 mm wide pre-cut strip. Two parallel cuts are made, 5 mm apart, running from the periphery across the central filtration area ending about 2 mm away from the opposite edge of the filter to form the strip. Thus the strip

remained in place, attached to the rest of the filter from one end, maintaining the overall circular shape of the top filter.

2. Take the required volume of the slurry on the filter to obtain the same ratio of cake mass to filter area to reconstruct exactly the same cake height as that expected in CFMF experiment
3. Start the vacuum pump and operate at the pre-set desired TMP for the same time as the total time of the CFMF run
4. Detached the strip from the top filter with the cake on it to measure the cake height at 10 different places on the stripe under 400x magnification using a standard light microscope. Calculate the average height.

The filter paper with a pre-cut strip was used to avoid any compression of the cake that would occur if the strip were cut after cake deposition. The method, although clearly liable to damage or disruption of the cake, proved reasonably simple and effective to use. However, because of the inherent uncertainties involved, this method was used only to confirm the results of the glass tube method and not for further calculations.

5.3 Confirmatory experiments

In this set of experiments the extent of lactalbumin permeation through the membrane, the reversibility of internal and surface membrane fouling, and the significance of concentration polarisation during CFMF of lactalbumin were checked.

5.3.1 Checking for the presence of lactalbumin in the permeate

5.3.1.1 Introduction

This study was carried out to investigate the possibility of lactalbumin passing through the membrane into the permeate. As some lactalbumin particles in the feed were smaller than the nominal pore sizes (0.2 and 1.0 μm) of the membranes chosen for CFMF experiments (Fig. 4.3), there was a possibility of these particles passing through the membrane.

5.3.1.2 Methods

Permeates from the runs at 100 kPa TMP and 0.75 m/s CFV using both the 1.0 μm and 0.2 μm pore size membranes on the multi-channel module were analysed for their protein content using a standard Kjeldahl method. The multiplication factor of 6.38 was used to calculate protein content from the total nitrogen content estimated (Short *et al.* 1978). Permeate samples for this analysis were drawn at 1, 30, and 60 minutes of filtration time.

5.3.1.3 Results and discussion

The results of this study are shown in Table 5.1. The apparent protein content of all permeate samples was very low compared to the protein content of the feed (i.e. 2.5 to 3.0 % of lactalbumin concentration in feed). But considering the feed (4.2 l/min) and average permeate flow rates (for first 60 min, approximately 0.2 l/min), the amount of lactalbumin passing through the membrane (average 0.0139 g/min) is negligible compared to the amount of lactalbumin processed (10.5 g/min) per unit time. If this detected presence of protein in the permeate was only due to the small lactalbumin particles passing through the membrane, the protein concentration should drop with time due to the retention of these particles by the cake formed on the membrane surface. However, no major change in the apparent protein content of permeate with time was seen. Considering that lactalbumin is insoluble in water (Robinson *et al.* 1976) and since only total nitrogen was determined by the method used, this suggests another possibility, namely permeation of the soluble nitrogen, which is less than 0.2 % in lactalbumin (Robinson *et al.* 1976). In either case, the lack of a significant difference between the nitrogen permeation levels for the two different membrane pore sizes suggests the similar properties of the cakes formed on the two different pore size membranes that later governed the filtration process. Since the level of nitrogen detected was negligible, any marked passage of lactalbumin into permeate was considered to be not significant to further investigation.

Table 5.1 Permeation of lactalbumin through the membrane

TMP = 100 kPa
CFV = 0.75 m/s
C_{feed} = 2.5 g/l
membrane module = multi-channel

Time of filtration (min)	Protein content of the permeate (g/l)	
	0.2 μm membrane	1.0 μm membrane
1	0.073 ± 0.004	0.080 ± 0.003
30	0.066 ± 0.003	0.063 ± 0.005
60	0.065 ± 0.003	0.069 ± 0.003

5.3.2 Checking the reversibility of the membrane fouling

5.3.2.1 Introduction

As discussed in 2.2.2, membrane fouling is often not easily reversible. This study aimed to evaluate the reversibility of internal and surface fouling.

5.3.2.2 Methods

To check the reversibility of internal fouling under the influence of surface flushing, at the end of filtration runs at 100 kPa TMP and 3.0 m/s CFV, the total fouling and the internal fouling were estimated as described in 5.2.2 (i.e. with cake removal). Then RO water was circulated at 5.0 m/s CFV and no applied pressure conditions for 60 minutes. J_w under the filtration run conditions was measured and R_{if} for the washed membrane calculated from eq. 5.3 and compared to the initial value.

The reversibility of the surface fouling examined in another experiment at 100 kPa TMP and 3.0 m/s CFV. First the total fouling at steady state was estimated, then RO water was circulated under 5.0 m/s CFV and no applied pressure conditions (without first removing the cake). J_w under the filtration run conditions was measured every 30 minutes and R_{if} and R_f calculated. Water circulation continued until a steady state J_w was achieved.

5.3.2.3 Results and discussion

There was no change in the resistance to the flux (R_f = 1.9 x 10^{11} /m) due to water circulation at high CFV after the manual removal of the surface fouling. This indicated the internal fouling was firmly trapped within the membrane. The possibility of removing this material by backflushing was not investigated as it was outside the scope of this study.

When the surface fouling was not removed, R_f decreased with time of water circulation at high crossflow until it reached a steady-state value as shown in Table 5.2. This R_f at the steady-state equalled the internal fouling resistance determined in the first experiment. This indicated that the surface fouling was completely reversible and the cake was fully removed by the procedure used. Based on these results, from this point onwards the internal fouling resistance and surface fouling resistance are referred to as irreversible fouling resistance (R_{ir}) and reversible fouling resistance (R_{re}), respectively. This study also revealed the highly adhesive nature of the lactalbumin cake based on the long time (about 60 min) required to completely wash off the cake. The observed cake erosion under water circulation was due the change in the force balance on the deposited particles as a result of change in the operating parameters. The increase in CFV increased the force away from the membrane and the decrease in TMP reduced the force towards the membrane (eq. 2.22 and eq. 2.23).

Table 5.2 Change in R_f with time due to erosion of surface fouling

TMP = 100 kPa
CFV = 3.0 m/s (deposition), 5.0 m/s (erosion)
C_{feed} = 2.5 g/l
membrane module = multi-channel

Time of RO water circulation (min)	R_f (/m)	R_m (/m)
0	17 x 10^{11}	1.9 x 10^{11}
30	6.2 x 10^{11}	
60	1.9 x 10^{11}	
90	1.9 x 10^{11}	

The conclusions drawn here are with an assumption that only the surface fouling was removed, and the surface fouling was completely removed when the cake was manually recovered.

This can be verified by microscopic observation of the membrane surface after removal of the cake. But that would require breaking the membrane due to the type of the module design. Considering this limitation as well as the fact that any residual surface deposit will not significantly contribute to the fouling, further experiment was not planned.

5.3.3 Checking the significance of concentration polarisation

5.3.3.1 Introduction

This experiment was aimed at studying the change in resistance to the flux due to the replacement of the feed with water at the steady state to check the significance of concentration polarisation. The present study, as well as the most of the investigations of fouling during CFMF of particulate suspensions reported in the literature, has neglected concentration polarisation. Although this approach appears logical considering that the hydrodynamic resistance to flux offered by a concentrated layer of the particles in the feed stream would be much lower compared to that offered by the deposited cake, confirmation of this is required. Further, in contrast, Ousman and Bennasar (1995) have reported very high levels of concentration polarisation (R_{cp} reported to be 18 to 46 % of R_t) at the steady-state during CFMF of starch suspensions under varying experimental conditions. Therefore, there is a need to investigate the significance of the concentration polarisation in CFMF of particulate suspensions.

5.3.3.2 Methods

A CFMF run was carried out at 100 kPa TMP and 3.0 m/s CFV using feed at 2.5 g/l C_{feed}. On reaching the steady-state (J_{ss}), the feed was replaced with RO water with an aim of removing lactalbumin particles not deposited including the concentration polarisation layer from the system. Water coming out of the return line for the first 10 seconds was drained to ensure the complete removal of the layer. Then water was circulated under the same operating conditions of the filtration run (to maintain the same force balance and hence avoid the cake erosion) and a steady-state J_w was achieved. After 10 min of steady-state J_w, water was replaced with the feed suspension

and again run until a steady-state (J_{ss}) obtained. The feed was once again replaced with RO water after 10 min of steady-state and a steady-state J_w was obtained.

5.3.3.3 Results and discussion

Change in the permeate flux and R_t with time for the experiment are shown in Fig. 5.1.

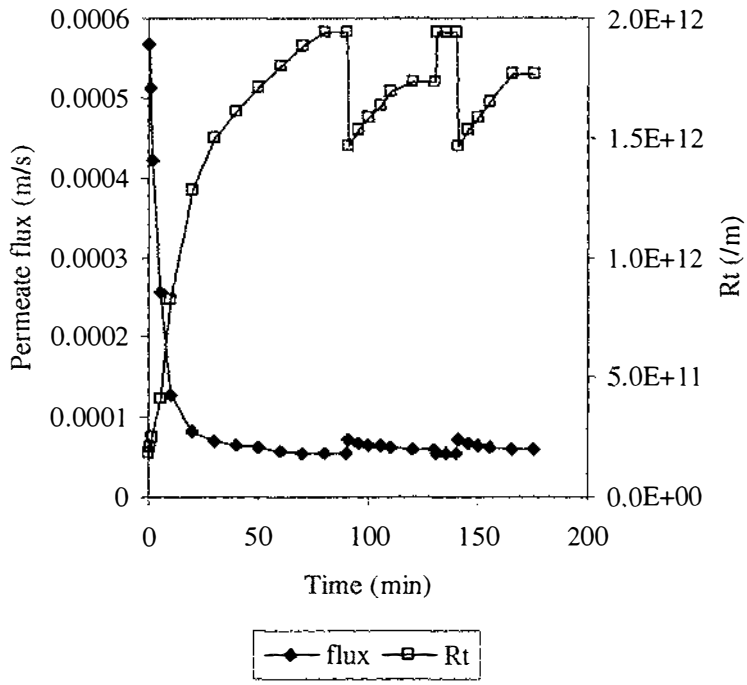

Fig. 5.1 Effect of replacing feed with RO water on the flux and R_t at 100 kPa, 3.0 m/s and 2.5 g/l C_{feed}

With replacement of the feed by RO water, the flux instantly increased by about 20 % but then slowly decreased with time and reached the steady-state in 25 to 30 min. R_t was about 8.75 % lower with RO water circulation (1.77×10^{12} /m) compared to that in the case of operation with the feed (1.94×10^{12} /m). This could be due to the removal of the polarisation layer. If so, R_{cp} contributed 8.75 % of R_t. Ousman and Bennasar (1995) estimated R_f and R_{cp} during CFMF of starch suspension by measuring the pure water flux after rinsing the membrane in three de-ionised water baths at the end of the run to eliminate traces of solution and polarisation layer. They reported the proportion of R_{cp} to be 18 to 46 % of R_t at different combinations of CFV, TMP, C_{feed} and membrane pore size. For conditions close to those used here, they reported R_{cp} to be 19 % of R_t at 100 kPa, and 1.8 m/s for 15 g/l feed using a 0.2 μm pore size membrane. These levels of R_{cp}

are much greater than that observed in the present study. However, the method used by Ousman and Bennasar (1995) raises doubts about the reliability of reported results. It is very likely that during rinsing of the membrane the loosely attached top cake layer was also removed and therefore, R_{cp} was overestimated. Similarly in the present study when feed was replaced by water, it is likely the top mobile cake layer (Mackley and Sherman 1992, Wakeman 1994) was no longer replaced by newly depositing particles and hence the R_{cp} was overestimated. This suggests R_{cp} is not easily separated from the R_{sf} and can not be estimated reliably, but the overall effect of concentration polarisation is limited in the case of CFMF of the particulate suspensions. Most studies neglected R_{cp} for CFMF of particulate suspensions while applying the resistance in series model (Persson and Nilsson 1991, Dharmappa *et al.* 1992, Chang *et al.* 1995, Piron *et al.* 1995, Altmann and Ripperger 1997) and the present study confirms this approach to be appropriate. Makley and Sherman (1992) and Wakeman (1994) observed but did not explain the rolling of top cake layer particles even under steady-state conditions during the cake visualisation study on the polyethylene particles. The possible reasons for the cake mobility are discussed later (see Chapter 6).

The immediate increase in the flux on replacement of the feed with water and subsequent slow drop to a steady-state could be due to the rapid removal of the mobile top layer some particles of which remained in the system and deposited later during the water circulation. Another possibility is that as a result of the removal of the top layer, the new top layer also became mobile and allowed increased penetration of the particles into the cake or the membrane. Live in situ observation of the cake surface may be required to resolve this issue.

5.3.4 Overall discussion

Estimations of R_f, R_{re} and R_{ir} as well as cake properties – height, mass, porosity and PSD are the main tools besides the measurement of permeate flux, selected in the present study to further understand the process of CFMF of particulate suspensions. With the exception of the report from Ousman and Bennasar (1995), there has been a trend in literature to neglect concentration polarisation i.e. to consider it as a part of surface fouling during the studies on the CFMF of particulate suspensions. Although this approach is reasonable, the present study (Section 5.3.3) appears the first to clearly

demonstrate that the effect of concentration polarisation is limited in the case of the CFMF of particles. The findings of this study contradict to the findings of Ousman and Bennasar (1995), but their methods to distinguish between surface fouling and concentration polarisation must be questioned. This study also revealed that operating with water on a fouled membrane under the same process conditions slightly reduces surface fouling due to unavailability of particles to replace the mobile particles in the top layer but a major cake erosion is not possible. This is because the force balance remains unchanged.

The CFMF membranes allowed permeation of negligible amounts of lactalbumin during operation. The retained lactalbumin particles fouled the membrane both internally as well as externally. The external fouling was found to be fully reversible but the internal fouling was not reversible by surface flushing. Backflushing may be able to remove the internal fouling to some extent but this possibility was not investigated. The full reversibility of the surface fouling confirmed the completeness of the cake removal by physical means.

Many reports dealing with CFMF of particulate suspensions involve the estimation of cake height. Methods reported to measure the cake height can be broadly classified into two groups: (1) post-mortem measurement, and (2) live observation of the cake during the filtration process using intrusive or non-intrusive devices. Riesmeier *et al.* (1987) made a first attempt of the post-mortem estimation of cake height during CFMF of bacterial cells. They analysed parts of the cakes along with membrane for protein content and used the results to estimate cells per unit volume of the cake. Then they assumed the cells to be spherical and cake porosity to be 0.33 to calculate the cake height. They reported cake heights in the range of 0.3 to 40 µm under varying experimental conditions. Although Riesmeier *et al.* (1989) later used scanning electron micrographs during CFMF of yeast and bacterial cells to validate this method (the results of the comparison are not reported), the method is certainly very complex with a high potential for experimental error. Cake heights between 0.5 and 40 µm were determined during this study. Fordham and Ladva (1989) also reported the post-mortem measurement of bentonite cakes. Altmann and Ripperger (1997) recently used electron microscopy to study the deposition pattern of diatomaceous earth and silica particles with respect to the particle size. The application of post-mortem observation is however

limited to those membrane modules where the cake and the membrane surface are available for observation i.e. flat sheets. However, most commercial interest in CFMF centres on the use of tubular (especially ceramic) modules.

Live measurement or observation of the cake has the advantage of continuous monitoring of the cake deposition. Hodgson *et al.* (1993) observed cake growth from the permeate side using a light microscope with SLR camera focused through a hole in the membrane supporting plate. This was possible as the membranes used became transparent when wet. Mackley and Sherman (1992) made in situ observations of cake deposition on a flat surface filter using a 15 x magnification video camera mounted nearly normal to the cake surface. They analysed the deposition mechanism using slow motion replays and still frames obtained every 1/50 second. However, the low magnification limited the smallest observable particle to above 100 μm. They used 125-180 μm polyethylene particles for their study. Wakeman (1994) used a high speed video camera with zoom lens to observe the cake deposition during CFMF of micron size particles (calcite and anatase with a mean size of 0.5 to 25 μm) using a flat sheet module. Fibre optics was used to illuminate the module. Schluep and Widmer (1996) and Altmann and Ripperger (1997) used laser distance sensors to monitor the cake height in the flat sheet module during CFMF of yeast and diatomaceous earth and silica particles, respectively. These optical devices though sophisticated, are also limited to specially designed flat sheet membrane modules. A notable exception for this limitation is the use of NMR micro-imaging for cake height monitoring in a hollow fibre module (0.93 mm inner diameter) during CFMF of 0.7 μm mean size bentonite particles reported by Wandelt *et al.* (1992). The NMR imaging set-up with a resolution of 10 - 20 μm was aligned with the cross-section of the hollow fibre to observe the cake as it developed. Cake heights of about 30 - 120 μm were measured during the study. The major drawback of this method is that because it can not measure the height all along the cake surface, it ignores the variation in the cake height along the membrane tube.

Thus there was a need to develop a method of cake height estimation which would be simple, but still effective and applicable irrespective of the type of the membrane and module used. Although the methods developed in the present study meet these requirements, they do involve reconstruction of cake under dead-end mode and

therefore, ignore the possible effect of CFV on the cake packing. Under crossflow the particle deposition is expected to be selective in contrast to random under dead-end mode. Although the cake of 125-180 μm polyethylene particles is reported to pack more tightly under crossflow compared to that under dead-end filtration (Mackley and Sherman 1992), the level of CFV is not found to significantly affect the packing of the yeast cell cake (Riesmeier *et al.* 1989). Analysis of the cake heights estimated using the developed methods, and their comparison with other reports is necessary to reveal the actual level of significance of the crossflow in the cake height estimation (see Section 5.4.5).

5.4 Effect of operating parameters

5.4.1 Effect of time of filtration

The effect of time of filtration on the permeate flux and the nature of membrane fouling caused by lactalbumin particles are investigated in this study.

5.4.1.1 Methods

Filtration runs at 100 kPa TMP, 0.75 m/s CFV, and 2.5 g/l C_{feed} were carried out for 2, 5, 10, 30, 60, and 140 minutes using a 1.0 μm pore size membrane on the multi-channel module. Permeate fluxes, different resistances to the flux and cake properties were determined for all experiments as described in Section 5.2.

5.4.1.2 Results

Effect on the permeate flux

Permeate flux (J) and R_f are plotted against time for the experiment done at 100 kPa TMP and 0.75 m/s CFV in Fig. 5.2. After an initial sharp decline, the flux gradually dropped to its steady-state value. The measured flux values were highly reproducible (e.g. values J (5 min) and J_{ss} for three replications were 2.19×10^{-4}, 2.18×10^{-4} and 2.18×10^{-4}, and 2.77×10^{-5}, 2.77×10^{-5} and 2.77×10^{-5} m/s, respectively).

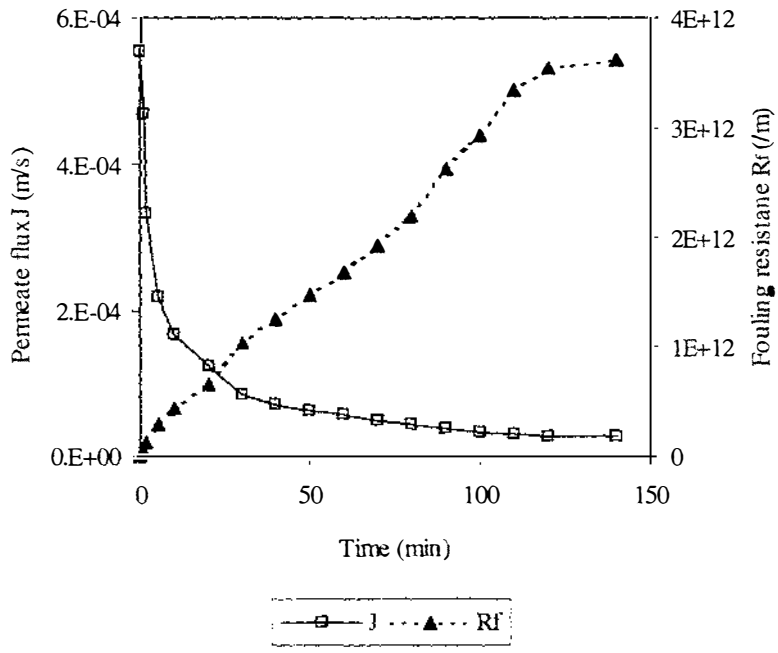

Fig. 5.2 Permeate flux versus Time at 100 kPa TMP and 0.75 m/s CFV at 2.5 g/l C_{feed} using a 1.0 μm pore size membrane

Effect on membrane fouling

As shown in Fig. 5.2, R_f increased steadily with time of filtration and reached a steady-state value. Table A1.1 (Appendix 1) shows the values of the permeate flux and the various resistances to the flux at different filtration times. Fig. 5.3 shows the change in R_{re} and R_{ir} with time. R_{re} which was initially lower than R_{ir}, equalled the R_{ir} value within 5 minutes of filtration and then linearly increased with time and became the main contributor to R_f. R_{ir} dominated initially for about the first 3 to 4 minutes, and a small and gradual increase in R_{ir} was then observed up to about 30 min. After that, there was no significant increase in R_{ir}.

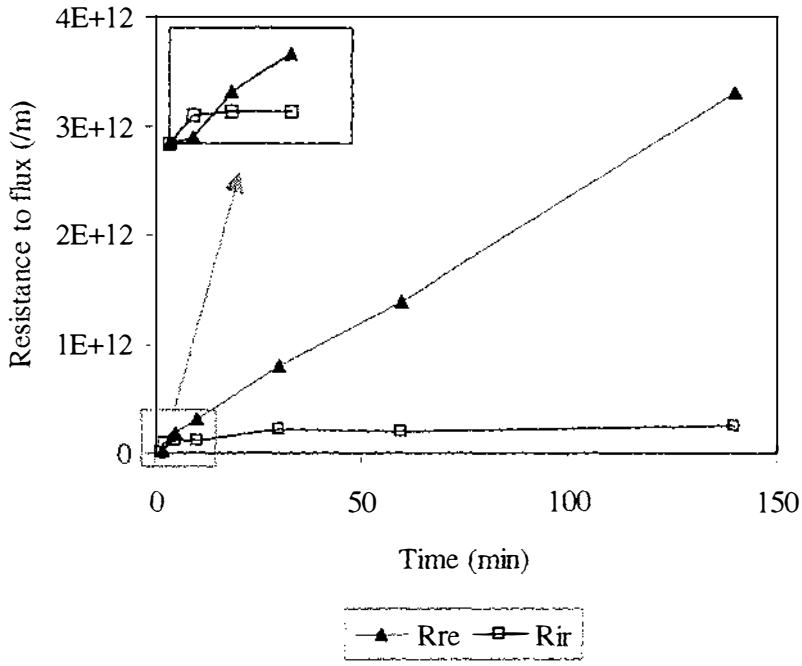

Fig. 5.3 Change in R_{ir} and R_{re} with time of filtration at 100 kPa TMP, 0.75 CFV, 2.5 g/l C_{feed} using 1.0 μm membrane pore size

Effect on the cake properties

Fig 5.4 shows the change in permeate flux with increasing deposition of cake mass. The flux dropped linearly with an increase in cake mass under the operating conditions. An off line point on the y-axis in the figure represents J_w. Table A1.2 in Appendix 1 shows the values of the mass, height, and porosity of the cake formed on the membrane surface at different stages of filtration. A plot of cake mass against time of filtration under the operating conditions is shown in Fig. 5.5 and the effect of time on the cake height and porosity is shown in Fig. 5.6. The level of reproducibility of cake mass and height, and hence of the porosity are demonstrated in these figures by including the results of all three replications. These values were reasonably reproducible. There was a good agreement (within about ±2 %) between the cake heights estimated by the two different methods (Table A1.2 in Appendix 1). Initially, the cake height increased sharply with

time and then gradually reached a steady-state at about 60 min. Continued deposition of mass up to 140 min caused a drop in porosity as well as flux.

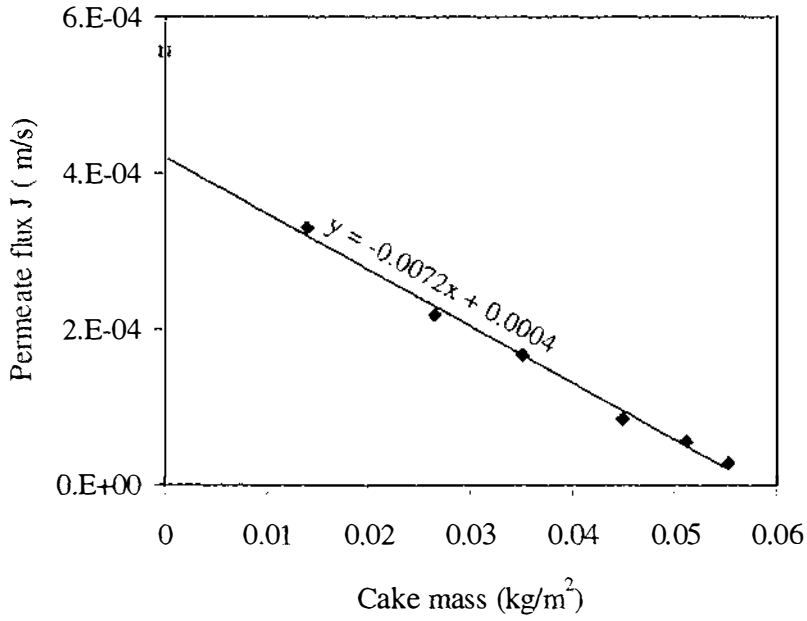

Fig. 5.4 Cake mass versus permeate flux during the filtration at 100 kPa TMP and 0.75 m/sCFV, 2.5 g/l C_{feed} and 1.0 μm membrane pore size

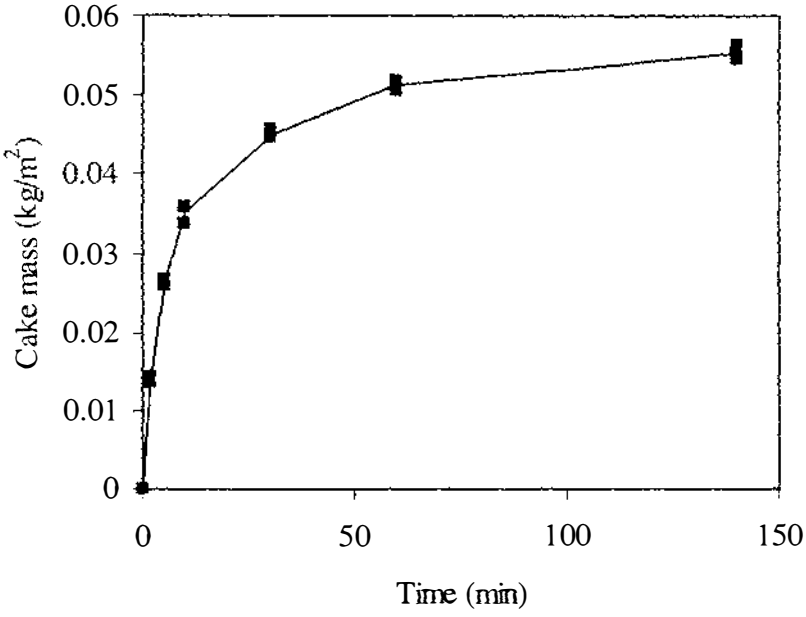

Fig. 5.5 Cake mass build up with time of filtration at 100 kPa TMP, 0.75 m/s CFV, 2.5 g/l C_{feed} using 1.0 μm pore size membrane

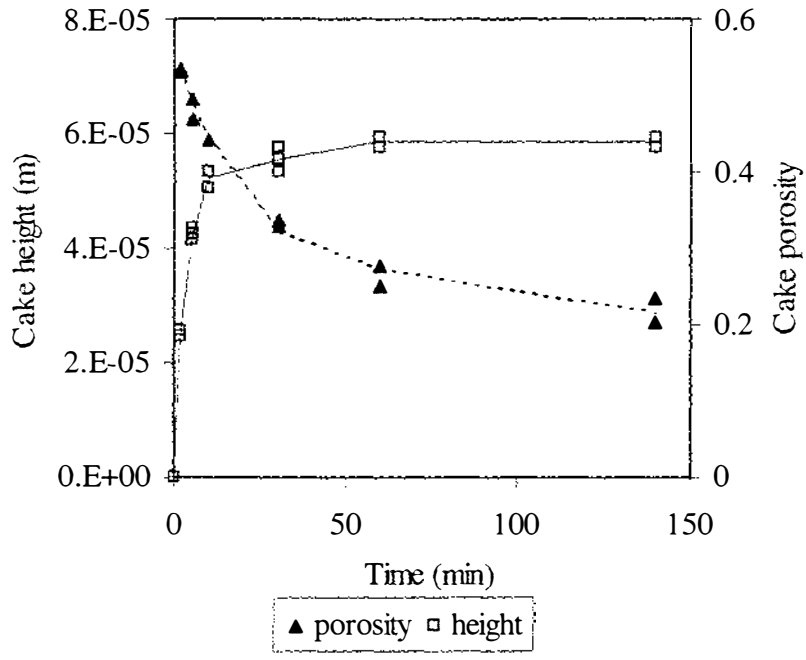

Fig. 5.6 Change in the cake height and porosity with time at 100 kPa TMP, 0.75 m/s CFV, 2.5 g/l C_{feed} using 1.0 μm pore size membrane

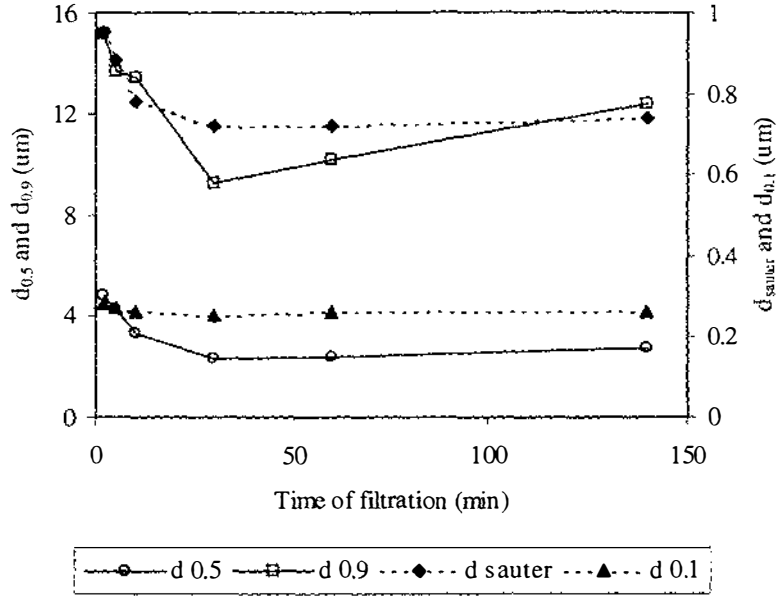

Fig 5.7 Change in the cake PSD with time at 100 kPa TMP, 0.75 m/s CFV, 2.5 g/l C_{feed} using 1.0 μm membrane

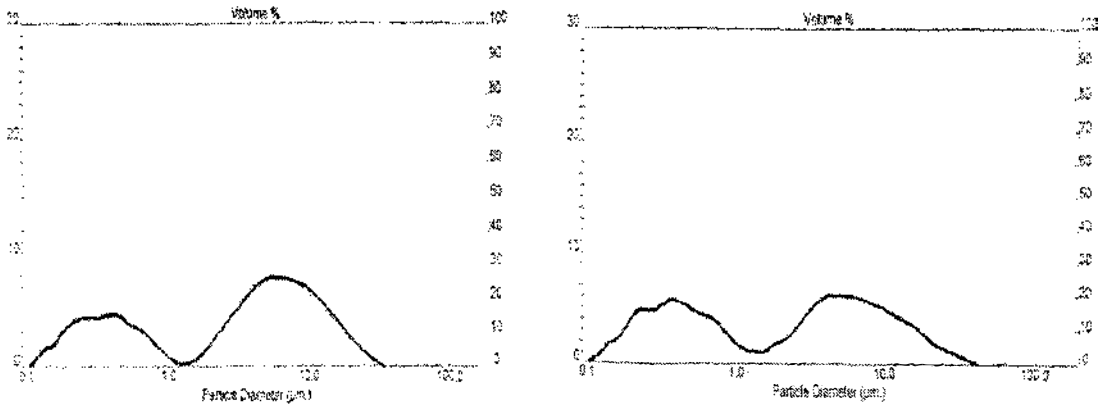

(a) (b)

Fig 5.8 Cake PSD at (a) 2 min, and (b) 140 min, of filtration at 100 kPa TMP, 0.75 m/s CFV, 2.5 C_{feed} using 1.0 μm pore size membrane

Change in the cake PSD with time of filtration is shown in Fig. 5.7 and detailed results of the analysis of the cake for its PSD obtained by Malvern Mastersizer at 2 min and 140 min of fltration are shown in Fig. 5.8. Full data on d_{sauter}, $d_{0.1}$, $d_{0.5}$, and $d_{0.9}$ at different time are listed in Table A1.2 in Appendix 1. All values – d_{sauter}, $d_{0.1}$, $d_{0.5}$, and $d_{0.9}$ decreased with time up to 30 min. After that there was no significant change in these values. An increase in $d_{0.9}$ beyond 30 min was observed, however, the reproducibility of this parameter at 140 min was relatively poor ($d_{0.9}$ = 13.30, 10.62, and 13.21 μm). Whilst the reproducibility for all other reported values was much better. The particles deposited in the cake under the operating conditions were grouped into two size ranges: one in the range of 0.1 – 2 μm, and the other in the range of >2 – about 30 μm (Fig. 5.8). With increasing filtration time the proportion of particles in the larger size range became smaller. Thus, with time the fraction of smaller particles in the size range of < 2 μm increased and the fraction of particles larger than 2 μm decreased.

Jang (1987) studied the effect of time of filtration on the cake PSD during CFMF of kaolin clay suspension at 90 kPa TMP and 3.0 m/s CFV (Fig. 2.13). The permeate flux in that study reached its steady-state at 100 min. To provide a comparison between the results of the present study and the results reported by Jang (1987), the change in the proportion of the small particles i.e. $d_p \leq d_{0.1}$ of feed (≤1.5 μm for kaolin clay and ≤0.47 μm for

lactalbumin) in the cake with time is shown in Fig. 5.9. The change in the 'foulant layer concentration' (the term is not clearly defined in the report) with time for kaolin clay suspension is also plotted against time of filtration in Fig. 5.9. During both studies the proportion of small particles in the cake continued to increase with time throughout the run. In the case of lactalbumin, the proportion of small particles increased at a greater rate for first 10 min but beyond 30 min the rate of increase was greater in the case of clay suspension. There was no noticeable change in the reported concentration of foulant layer beyond 20 min during CFMF of kaolin clay suspension, whereas there was a continual increase in cake mass all throughout 140 min of filtration during CFMF of lactalbumin (Fig. 5.5).

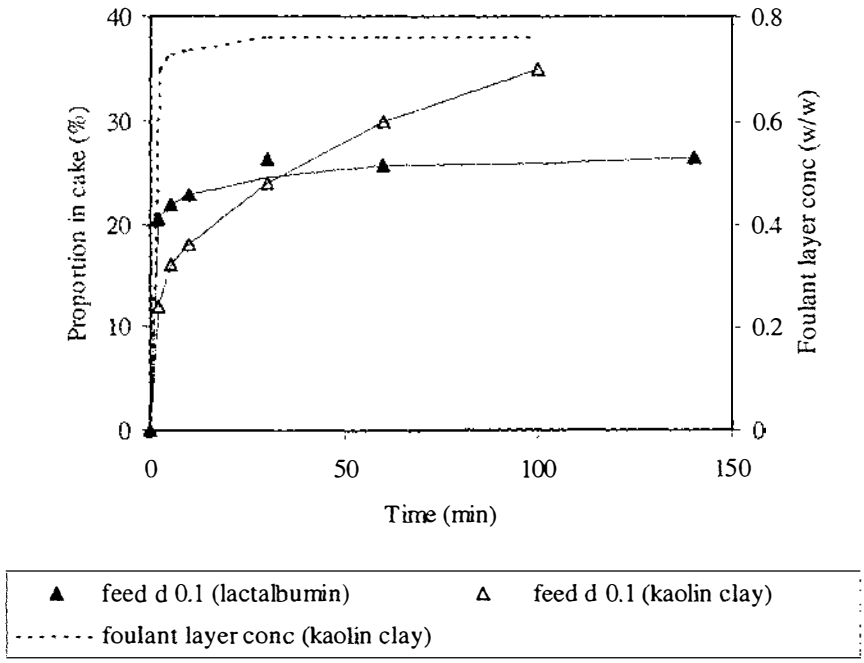

Fig. 5.9 Change in the proportion of small particles ($\leq d_{0.1}$ of feed) in the cake-comparison of the results of CFMF of kaolin clay (Jang 1987) and lactalbumin (present study)

5.4.1.3 Discussion

The observed trend of flux with respect to time (Fig. 5.2) is typical of the behaviour of membrane filtration under crossflow mode as discussed earlier in 2.7.2.1. The observed

change in R_{re} and R_{ir} with time (Fig. 5.3) reveals the pattern of progression from internal to surface fouling. Initially, with the clean membrane, penetration of smaller particles into the membrane pores was very high which resulted in dominant internal fouling. However, the drag force towards the membrane surface was also high due to high flux. Thus the largest particles found in the cake are also expected to have deposited during initial period of filtration. The observed change in cake PSD with time confirms this (e.g. $d_{0.9}$ at 2 min and 140 min were 15.15 and 12.37 μm, respectively). The surface deposition of large particles would modify the rejection properties of the membrane. Therefore, after initial short period of dominant internal fouling, the cake can be expected to govern the rest of the filtration process. This first hypothesise based on the observed concentration levels of lactalbumin in the permeate in section 5.3, is well supported by the presence of particles smaller than the nominal membrane pore size in the cake. The gradual and small increase in R_{ir} between 5 and 30 min suggested that a few of the small particles still managed to penetrate into the membrane pores through the deposited cake during that period. However, the steady, linear increase in R_{re} with time indicated that most of the depositing particles were retained by the cake. The behaviour of R_{re} and R_{ir} with respect to the time is similar to that reported by Visvanathan and BenAïm (1989) for the CFMF of silica suspensions. They observed internal fouling to be less than 10 % of the total fouling even though the average size of the feed particles (12 nm) was much smaller than the pore size (0.2 μm) and attributed this to the pore bridging. They did not measure the change in internal and surface fouling with time, but used standard blocking (SBM) and cake filtration (CFM) models to explain their results. Due to lower TMP (4.85 and 8.78 kPa) employed in this study, the fouling rates were very low. They showed the SBM was applicable for period of 5 to 20 min, suggesting internal fouling including pore bridging period and demonstrated the applicability of CFM thereafter, suggesting cake formation. However, neither model explained (fitted to) the results obtained for the first 5 min. Compared to the study by Visvanathan and BenAïm (1989) the feed PSD and pore size-particle size relation, and the key operating conditions were different in the study of CFMF of lactalbumin. Given that no model appears applicable across the whole filtration time, actual measurement of changes in R_{re}, R_{ir} and cake properties with time were therefore chosen as tools of study rather than predicting changes in type of fouling using models like SBM and CFM.

The straight line representing the apparent relationship of flux and cake mass when extended (Fig 5.4), predicted a flux of 0.00042 m/s at the beginning of the cake deposition. This suggests that flux rapidly reduced from J_w (0.000553 m/s) to 0.00042 m/s due to internal fouling before cake deposition started. This value is lower than flux at 1 min (0.000469 m/s) indicating that the first significant cake deposition took place only after one min of filtration. This agreed well with the initial changes in internal and surface fouling observed in this study (Fig. 5.3). Thus information on change in cake mass with time in the later stage of filtration could be used to estimate the initial fouling behaviour.

The continuation of drop in flux after the stabilization of cake height has also been commonly reported by other workers in the case of the CFMF of particulate suspensions (Jang 1987, Mackley and Sherman 1992, Schluep and Widmer 1996, Altmann and Ripperger 1997, Tien *et al.* 1997). This, as explained first by Dharmappa *et al.* (1992), is due to the penetration of fines into the cake during the later part of the filtration resulting in denser packing of the cake and increased cake resistance. Estimation of both the cake mass as well as height in the present study allowed the estimation of cake porosity. The drop in cake porosity with time observed during the present study has for the first time demonstrated this hypothesised behaviour. Significantly that behaviour was further confirmed by the observed increase in the proportion of small particles in the cake during later part (60 to 140 min) of filtration (Fig. 5.9).

The analysis of cake PSD revealed that with progress in the filtration, smaller and smaller particles were deposited on the membrane surface. This observation agrees with the observations of the cake made by Jang (1987) and also supports the findings of Altmann and Ripperger (1997). Jang (1987) measured changes in the concentration of different particle sizes in the cake of kaolin clay particles with time of filtration. That study revealed that the concentration of large particles remained constant ($\leq$ 2.5 μm) or decreased ($>$ 2.5 μm) and the concentration of small particles ($\leq$ 1.5 μm) increased beyond 50 min (Fig. 2.13). Almann and Ripperger (1997) using electron microscopy showed that the particle size reduced towards the top of the cake during CFMF of diatomaceous earth. This can be

attributed to the decreasing forces toward the membrane surface due to drop in flux.There was a greater increase in the proportion of small particles in the clay cake compared to that in the lactalbumin cake despite no change in the clay cake layer concentration after 30 min. This suggested that large kaolin clay particles were probably removed and replaced by depositing small clay particles during this period due to the decrease in forces toward the membrane surface with time. That this did not happen to an appreciable level in the case of lactalbumin probably indicating a greater adhesiveness of the lactalbumin cake compared to that of the kaolin clay cake. Therefore, the proportion of small particles,during the later part of CFMF of lactalbumin,did not increase as markedly as in the case of kaolin clay cake. An estimate of the adhesiveness of the cake can be made with help of the cake erosion study, which has been done for lactalbumin in the present study (section 5.3.2), but not in the case of kaolin clay by Jang (1987). Therefore, it is difficult to check the relative adhesiveness of the two materials.

The increase in $d_{0.9}$ after 30 min (Fig. 5.7) is very likely to be due to the inconsistency in data at 140 min. Due to retention of fines by the cake, nearly 30 % (vol. basis) of the cake particles at 2 min were smaller than the nominal membrane pore size (1 μm). This increased with time and reached above 40 % at the steady state. Of course some pores would be smaller than nominal pore size of the membrane and so would retain smaller particles.

5.4.2 Effect of TMP

Studies on the effect of TMP on the permeate flux (J), J_{ss}, fouling (reversible and irreversible) of the membrane and properties of the cake formed on the membrane surface are reported in this part.

5.4.2.1 Methods

The experiments for this study used the multi-channel module. TMP levels of 20, 50, 100, 150, and 200 kPa were used for the 1.0 μm pore size membrane, and 20, 50, 100, and 200 kPa for the 0.2 μm pore size membrane. The experiments were done at 0.75 m/s and 3.0 m/s CFV, and at 2.5 g/l C_{feed}. However, the effect of TMP on different resistances to the flux and on the cake properties were studied only at 20, 50, and 100 kPa TMP.

5.4.2.2 Results

Effect on permeate flux and steady-state flux

The change in permeate flux with time of filtration at different TMP is shown in Fig. 5.10. The effect of TMP on J_{ss} is shown Fig. 5.11. Similar results were obtained for both pore size membranes (Table A1.3 and Table A1.4 in Appendix 1).

J_w and initial product fluxes were higher at higher TMP. J_{ss} increased with increasing TMP up to 100 kPa, but above 100 kPa there was no significant change in J_{ss}. This trend was observed with both the membrane pore sizes studied. Thus 100 kPa was the optimum TMP level with respect to J_{ss} under the experimental conditions.

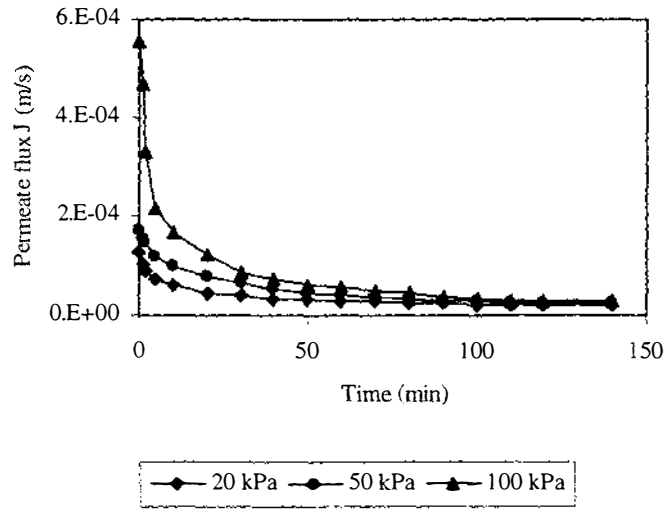

(a)

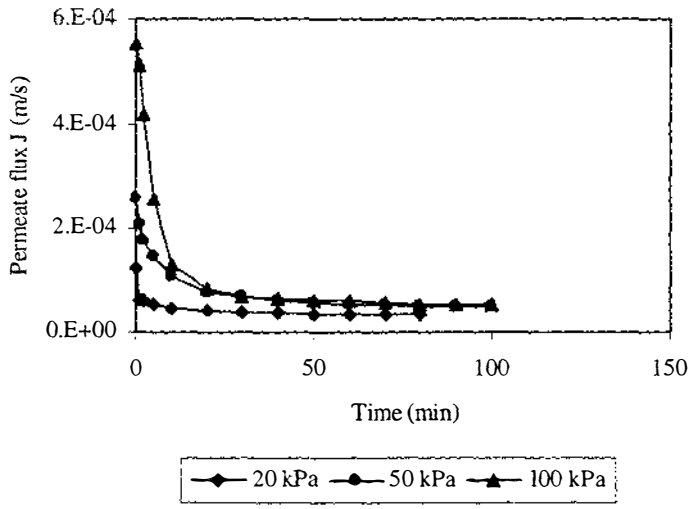

(b)

Fig. 5.10 Effect of TMP on the flux at (a) 0.75 m/s CFV and (b) 3.0 m/s, 2.5 g/l C_{feed} on a 1.0 μm pore size membrane

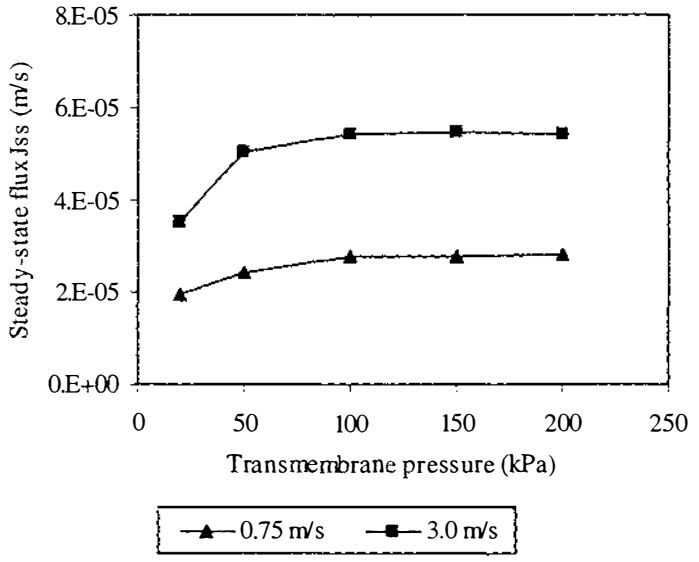

Fig. 5.11 Effect of the TMP on J_{ss} at 0.75 and 3.0 m/s CFVs, 2.5 g/l C_{feed} on a 1.0 μm pore size membrane

Effect on membrane fouling

The effect of TMP on R_f, R_{re} and R_{ir} is shown in Fig. 5.12 and Fig. 5.13. The effect of TMP on the proportion of R_{ir} is shown in Fig. 5.14. Similar results were obtained for the two membrane pore sizes. The values of different resistances to the flux at different TMP for both membranes are given in Table A1.3 and Table A1.4 in Appendix 1.

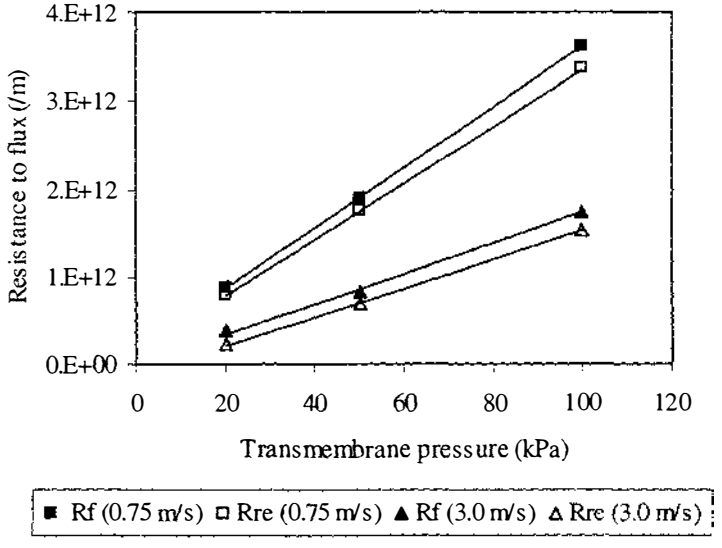

Fig. 5.12 Change in the R_f and R_{re} with change in TMP at 0.75 and 3.0 m/s CFVs, 2.5 g/l C_{feed} on a 1.0 μm pore size membrane

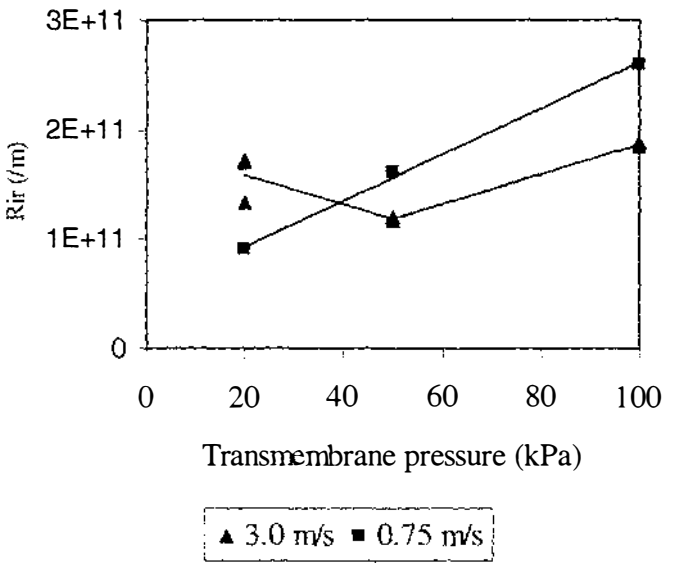

Fig. 5.13 Change in the R_{ir} with change in TMP at 0.75 and 3.0 m/s CFV, 2.5 g/l C_{feed} on a 1.0 μm pore size membrane

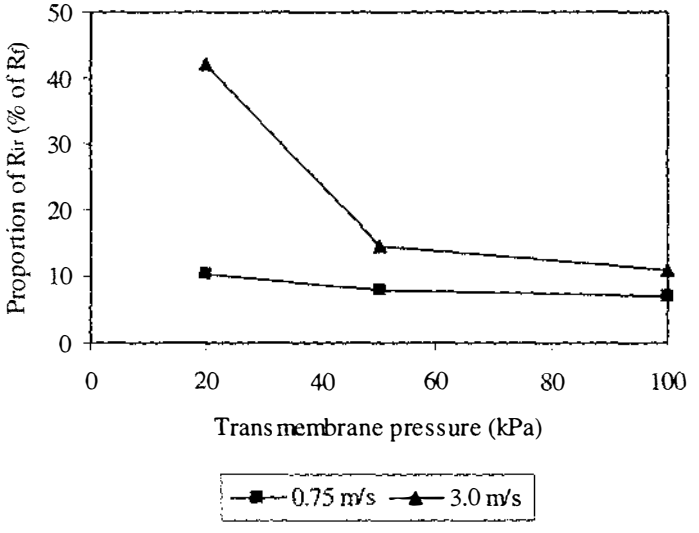

Fig. 5.14 Change in the proportion of R_{ir} with change in TMP at 0.75 and 3.0 m/s CFV, 2.5 g/l C_{feed} on a 1.0 μm pore size membrane

Generally all three resistances, R_f, R_{re} and R_{ir} increased linearly with an increase in the TMP. The reversible fouling was the major contributor to the total fouling. Although R_{ir} generally increased with the increase in TMP, the proportion of the R_{ir} contributing to the total R_f decreased. A notable exception was that R_{ir} decreased with increase in TMP from 20 kPa to 50 kPa at 3.0 m/s CFV. This was observed with both membrane pore

sizes used for the study. Actual R_{ir} values for three replications shown in Fig. 5.13 indicated that this effect was significant (many data points are superimposed).

Effect on the cake properties

The effect of TMP on the cake mass and porosity is shown in Fig. 5.15. The cakes formed at 3.0 m/s CFV were too thin to estimate the cake mass at 20 kPa TMP or the cake height at any TMP level with the methods used. The cake at 20 kPa and 3.0 m/s, when reconstructed on the flat filter using the vacuum flask, did not cover the filter area completely, and many uncovered patches on the filter were observed. The values of the cake mass, height, porosity and PSD values for 1 and 0.2 μm membranes are given in Table A1.5 and Table A1.6,respectively, in Appendix 1.

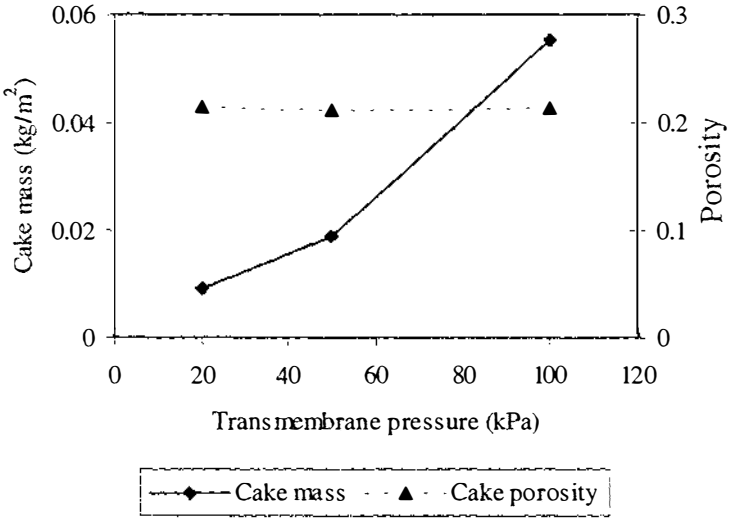

Fig 5.15 Effect of TMP on the cake mass and porosity 0.75 m/s CFV, 2.5 g/l C_{feed} using 1.0 μm pore size membrane

The cake mass and the cake height increased with an increase in TMP. The increase in the cake height was linear with the increase in cake mass, indicating the cake porosity was independent of TMP. The effect of TMP on the cake PSD is shown in Fig. 5.16 at 0.75 and 3.0 m/s CFV for the 1.0 μm pore size membrane.

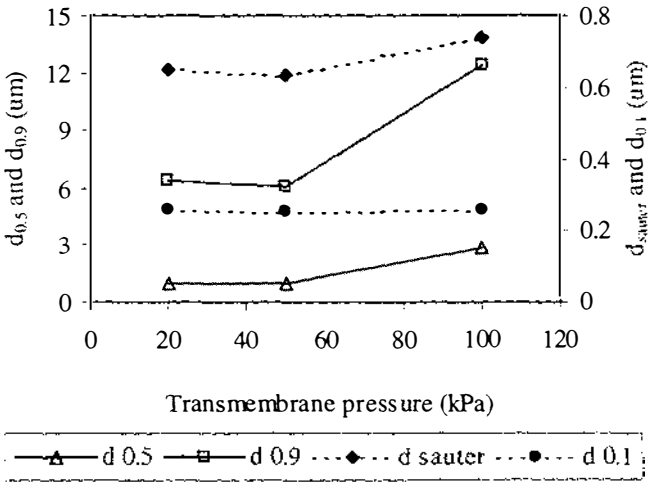

(a)

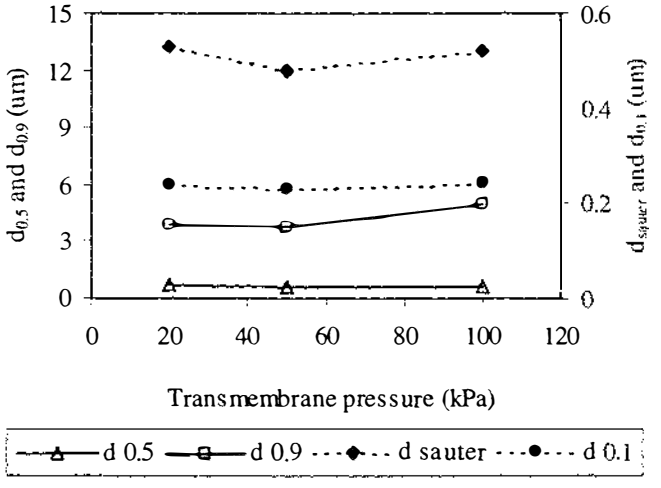

(b)

Fig. 5.16 Effect of TMP on the PSD of the cake at (a) 0.75 m/s and (b) 3.0 m/s CFV, 2.5 g/l C_{feed}, using 1.0 μm pore size membrane

Increasing the TMP from 20 kPa to 50 kPa did not significantly change the cake PSD. An overall increase in the cake PSD (d_{sauter}, $d_{0.5}$, and $d_{0.9}$) was observed with the increase in the TMP from 50 to 100 kPa. at 0.75 m/s CFV. However, at 3.0 m/s CFV only $d_{0.9}$ value showed a noticeable increase from 50 to 100 kPa TMP and the relative change was much less than at 0.75 m/s. The cake PSD span became wider from 50 to 100 kPa TMP at both the CFVs. Similar behaviour was observed with both the membrane pore sizes-1.0 μm and 0.2 μm (Table A1.5 and Table A1.6).

5.4.2.3 Discussion

A higher initial flux but faster decline in the flux was observed at higher TMP during this study (Fig. 5.10). This behaviour is common and has also been reported by Persson *et al.* (1993), Tarleton and Wakeman (1994), and Russotti *et al.* (1995) during the CFMF of different particulate suspensions. This behaviour is due to the higher driving force towards the membrane at higher TMP as explained by Darcy's law (eq. 2.4). The observed trend of J_{ss} with respect to TMP is similar to that reported by Matsumoto *et al.* (1988), Riesmeier *et al.* (1989) and Taddei *et al.* (1990). Matsumoto *et al.* (1988) during CFMF of 30 g/l yeast suspension using a 1.6 μm pore size alumina tubular membrane observed a limiting flux at around 80 to 100 kPa in the studied range of 20 to 100 kPa. Riesmeier *et al.* (1989) also reported the optimum TMP to be 80 kPa for CFMF of yeast cells using a 0.2 μm pore size membrane in the studied range of 0 to 150 kPa. Taddei *et al.* (1990) observed no further increase in flux beyond 600 kPa (TMP levels studied – 200, 600 and 1000 kPa) during yeast cell harvesting from a broth also using 0.2 μm pore size membrane. Flux increases with increase in TMP up to the optimum TMP value due to an increase in driving force toward the membrane and then reaches its limiting value. This is as a result of the equilibrium between increase in flux force and increased fouling as explained by these workers. Given that the mechanism limiting J_{ss} beyond the optimum TMP is well known and operation above the optimum TMP is of little interest, resistances to flux and cake properties were not analysed for runs above 100 kPa in the present study.

The three reports mentioned above that showed a similar trend of no change in J_{ss} above the optimum TMP involved yeast cells presumably in the same size range of 1 to 8 μm,

and yet the optimum TMP value reported by Taddei *et al.* (1990) was very different. The details of the experimental conditions for these studies are shown in Table 5.3 to provide a better analysis on the possible cause of the difference. The major difference in the experimental conditions between the work of Taddei *et al.* (1990) and the other two studies is in the range of TMP examined, feed pH and possibly in the C_{feed}. Besides the studied range of TMP, C_{feed} is known to have effect on the value of optimum TMP for example, Matsumoto *et al.* (1988) observed lower optimum TMP with higher C_{feed}. However, Taddei *et al.* (1990) did not state C_{feed} they used. The effect of pH on the optimum TMP is not reported.

Table 5.3 Comparison of the experimental conditions used in different studies on CFMF of yeast cells

Parameter	Matsumoto et al. (1988)	Resmeier et al. (1989)	Taddei et al. (1990)
Temperature	30 °C	30 °C	25 °C
pH	normal water pH	5.8	3.2
Feed components	yeast, Nacl, water	yeast, yeast extract, peptone, glucose, water	yeast, apple juice, hydrolysed starch, thiamine, water
C_{feed}	30 g/l	1.6 % (v/v)	not reported
TMP range / levels studied (kPa)	20 to 100	0 to 150	200, 600, 1000
membrane	1.6 μm	0.2 μm	0.2 μm

Different studies in the literature involving different feed materials reported different optimum TMP in a wide range of 0.1 kPa to 600 kPa for the CFF of particulate suspensions. Different studies involve different feed at different concentration, under different operating conditions using different membrane configurations. Therefore, it is very difficult to compare the values of optimum TMP reported in different studies.

The overall linear increase in fouling by lactalbumin with increasing TMP in the studied range further clarified the effect of TMP on the driving force towards the membrane. Riesmeier *et al.* (1989) also observed a linear increase in the cake layer resistance with increasing TMP in the range of 0 to 150 kPa. Considering the similarity in the trends of J_{ss} and R_{re} with respect to TMP between their and the present study, R_{re} in the present study can also be expected to increase linearly beyond the optimum TMP (100 kPa). The dominance of the reversible fouling and the presence of particles smaller than

membrane pore size in the cake, even at 3.0 m/s CFV suggest that the cake governed the filtration process for most conditions. The overall increase in the irreversible fouling with increase in TMP observed in this study, as reported and explained by Visvanathan and Ben Aïm (1989), can be attributed to greater penetration of smaller particles at higher TMP. The effect of TMP on R_{ir} observed at 3.0 m/s CFV in the range of 20 to 50 kPa could be due to better penetration of smaller particles into the membrane pores through a very thin cake formed at this low TMP and high CFV condition. Another possible reason is less effective pore blocking by smaller particles deposited under this condition which allowed more internal fouling of the membrane. The low cake deposition at 20 kPa TMP and 3.0 m/s CFV in this study which did not cover the entire filter area when reconstructed using the vacuum flask suggests that the cake also did not cover the entire membrane surface during the CFMF operation. This supports the former but the latter is disproved as the cake PSD at 20 kPa and 50 kPa are not significantly different at 3.0 m/s CFV.

Very little has been reported on the effect of TMP on the cake properties. The increase in the cake mass and hence cake height is due to increased driving force toward the membrane at higher TMP. Wakeman (1994) also observed an increase in cake height directly proportional to the TMP during CFMF of calcite and anatase suspensions. Riesmeier *et al.* (1989) reported a drop in the specific cake resistance with increase in TMP up to 0.7 bar (70 kPa) which they attributed to the smaller size deposition at lower TMP due to lower flux. However, they observed an increase in the specific cake resistance above 0.7 bar, which they proposed was due to the compression of the particles. That there was no significant effect of TMP on the cake porosity in the present study (Fig. 5.15) indicated no significant consolidation or compression or compaction of the cake in the studied range of TMP. This was expected based on the results of study on bed porosity of lactalbumin in 4.4. Though the cake PSD was different for different TMP, this showed no significant effect on cake packing. However, there was a significant effect of the TMP on the cake PSD in the range of 50-100 kPa (Fig. 5.16). The overall increase in the particle size with TMP in this range was due to higher drag force towards the membrane at higher TMP. Increasing TMP from 20 to 50 kPa increased the flux and hence the flux force F_f also increased. However, this did not change the forces toward the membrane enough to cause any change in cake PSD. This could be due to another force acting towards the membrane, namely the adhesive force

F_c which is discussed later (see Chapter 6). The particle classification effect of TMP was less significant at higher CFV due to greater forces away from the membrane. Further, it is interesting to note that the largest particles in the cakes formed under the studied conditions (Fig. 5.16) were much smaller than the largest particles in the feed i.e.80 μm (Fig. 4.3). In fact, they were even smaller than the average particle size (i.e. $d_{0.5}$ which is ~35 μm) of the feed. Further, there was a difference in the PSD of cakes formed at the two levels of CFV (0.75 and 3.0 m/s). Both these indicated selective particle deposition under the effect of the crossflow. The effect of CFV was studied further in detail (see Section 5.4.3).

In summary, 100 kPa was found to be the optimum value with respect to the flux in the studied range of TMP and therefore, should be used for rest of the study. The observed trend with respect to R_{ir} in the low range of TMP at high CFV is different from the behaviour reported in literature but can be explained based on the basic membrane theory. This is attributed to the better penetration of small particles through a very thin cake that was insufficient to cover the entire filtration area. Though the effect of TMP on the porosity and PSD of the cake observed in this study can be explained by the existing theory, is not reported before. Significantly, it has demonstrated that a particle classification effect can be attributed to TMP.

5.4.3 Effect of CFV

The effects of CFV on the permeate and steady-state fluxes, membrane fouling, and cake properties are discussed in this Section.

5.4.3.1 Methods

Experiments were performed on both the multi-channel and single-channel modules. Membranes of 0.2 μm and 1.0 μm pore size were used in the multi-channel module and of 0.2 μm and 0.8 μm pore size in the single-channel module. CFV levels of 0.375, 0.75, 1.1, 1.5, 3.0, and 4.5 m/s were used at 100 kPa TMP and 2.5 g/l C_{feed}. Information on R_{re} and R_{ir}, and different cake properties was limited to the filtration runs done on the multi-channel module. To check the applicability of the wall shear stress model

(Chapter 2.6.5), the wall shear stress (τ_w) at different CFV was calculated as (Holdich *et al.* 1995):

$$\tau_w = \frac{\Delta P \cdot d}{4L} \qquad (5.6)$$

where,

ΔP = pressure drop along the membrane (Pa)
d = diameter of the membrane tube (m)
L = length of the membrane tube (m)

5.4.3.2 Results

Effect on permeate flux and steady-state flux

Flux profiles at different CFV are shown in Fig. 5.17. The values of J_{ss} and time required to obtain the same at different CFV for all membranes are given in Table A1.7 in Appendix 1. The rate of flux decline slightly increased with increase in CFV, particularly at 3.0 and 4.5 m/s. However, the difference was slight and difficult to identify on a linear plot. The log-linear plot (Fig. 5.17) showed the decreases in rate of flux decline more clearly. The time required to reach J_{ss} for the 1.0 μm membrane is plotted against CFV in Fig. 5.18.

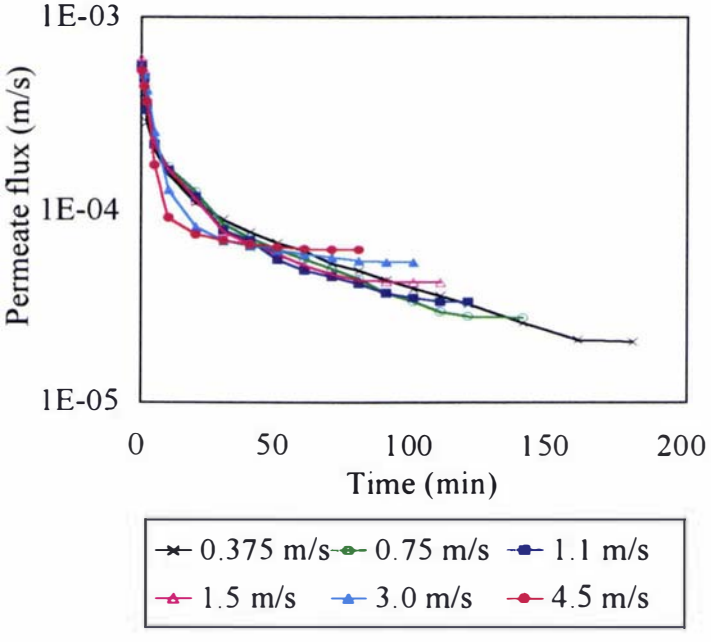

Fig. 5.17 Permeate flux versus Time at different CFV, at 100 kPa TMP and 2.5 g/l C_{feed} using 1.0 μm membrane

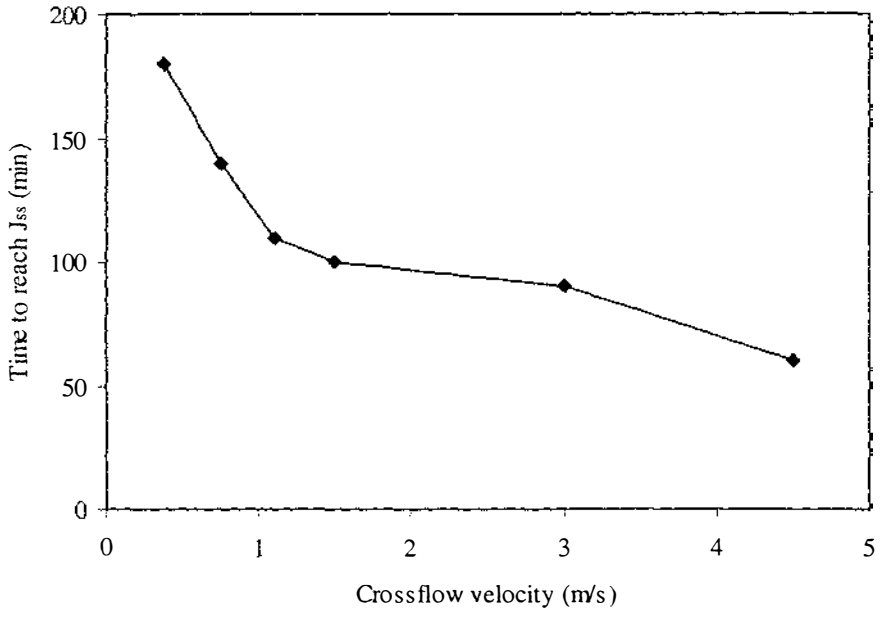

Fig. 5.18 Effect of CFV on the time required to reach J_{ss} at 100 kPa TMP, 2.5 g/l C_{feed} using 1.0 μm membrane

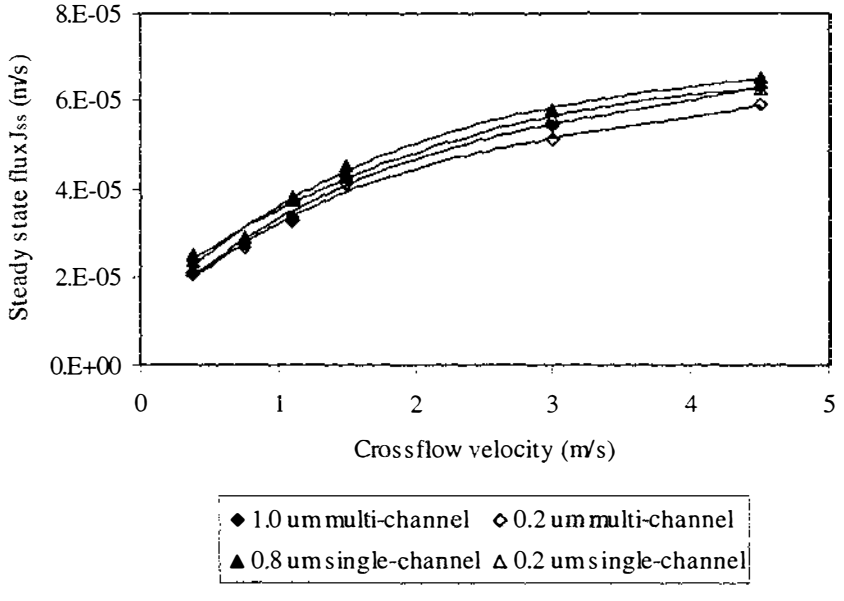

Fig. 5.19 Effect of CFV on J_{ss} at 100 kPa TMP and 2.5 g/l C_{feed}

The effect of CFV on J_{ss} for all four membranes used is shown in Fig. 5.19. The higher the CFV, the higher was J_{ss} and the lesser the time required to obtain J_{ss}. To check the applicability of the wall shear stress model (Holdich *et al.* 1995) J_{ss} is plotted against τ_w

in Fig. 5.20. Error bars in the figure show the variation in τ_w due to pressure fluctuation during the operation. J_{ss} increased with the increase in τ_w. The increase was linear up to about 2 m/s CFV if the line passed through the origin and otherwise up to 3.0 m/s.

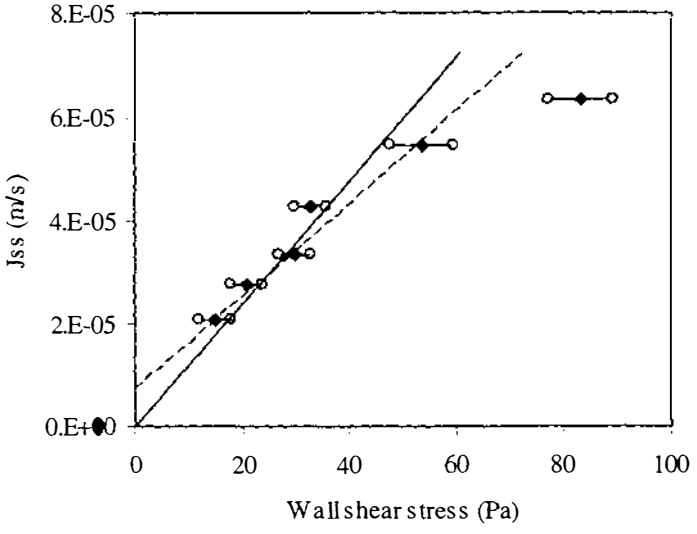

Fig. 5.20 Effect of wall shear stress on J_{ss} 100 kPa TMP, 2.5 g/l C_{feed}, using a 1.0 μm membrane

Pressure difference between inlet and outlet of the module, used here for calculation of τ_w, is due to the friction within the membrane tubes and also due to entrance and exit effects resulting from tube diameter change. There is no reported method for analysing the end effects under the situation as in the present study, where the feed flows from a single tube feed line to a multi-channel membrane. Using the method reported by Perry (1963) for a simple situation of single tube to single tube, three different possible approaches were checked to estimate these effects. These are reported in Appendix 1. As none exactly described the real situation, they have been ignored in Fig. 5.20 and in the subsequent discussion.

Effect on membrane fouling

Different resistances to the flux at different CFV for the two membrane modules are shown in Table A1.8 and Table A1.9, respectively, in Appendix 1. These resistances for the 1.0 μm membrane are plotted against CFV in Fig. 5.21, with the effect of CFV on R_{ir} for replicate runs being shown in Fig. 5.22.

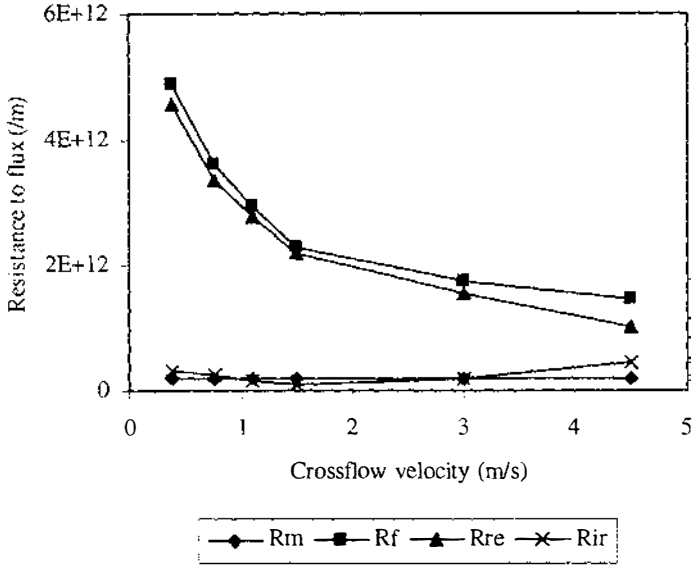

Fig. 5.21 Effect of CFV on different resistances to the flux at 100 kPa TMP, 2.5 g/l C_{feed}, using a 1.0 μm membrane

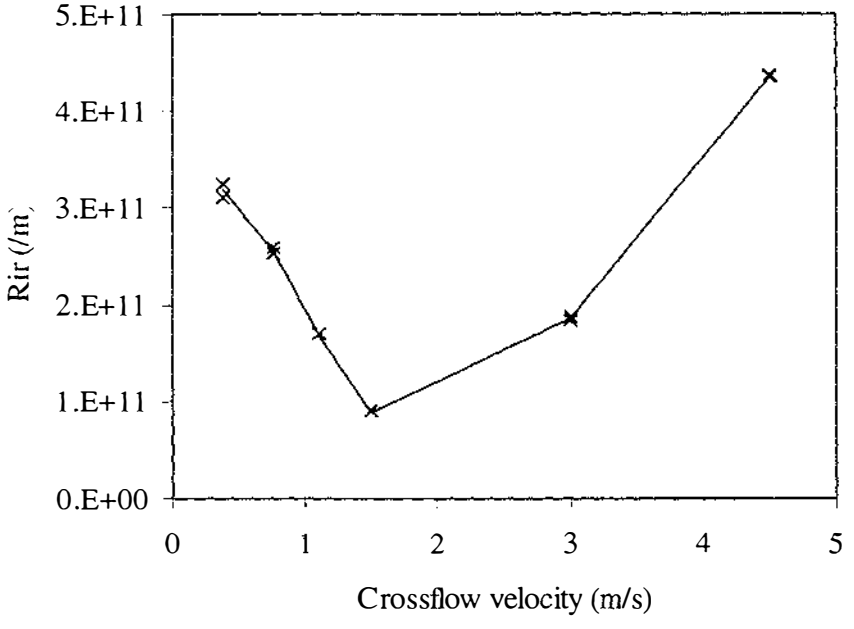

Fig. 5.22 Effect of CFV on R_{ir} at 100 kPa TMP, 2.5 g/l C_{feed}, using a 1.0 μm membrane

The change in proportion of R_{ir} and R_{re} with CFV is shown in Fig. 5.23. It is important to note that similar behaviour was observed with 0.2 μm membrane (Table A1.8).

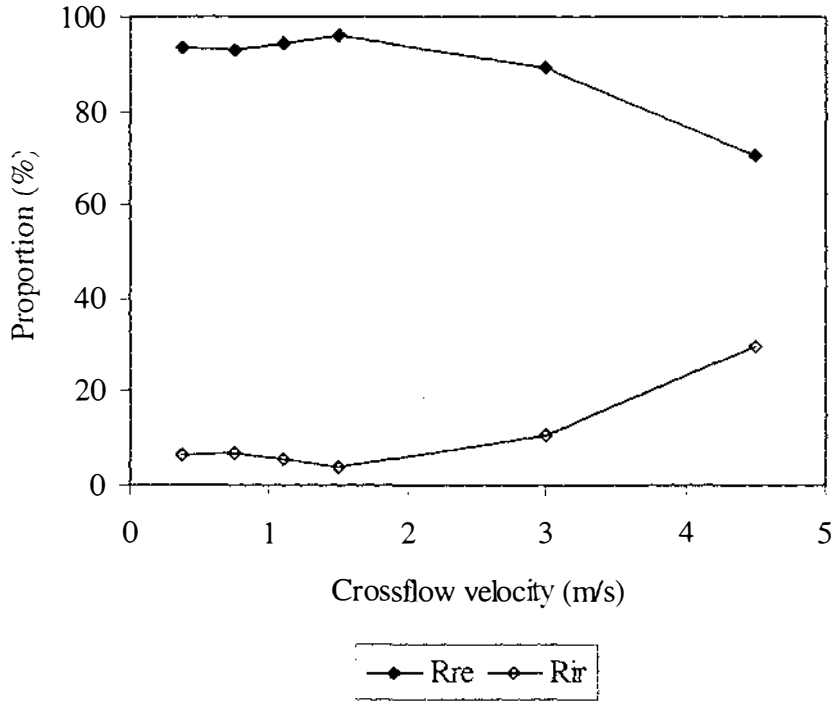

Fig. 5.23 Change in the proportion of R_{ir} and R_{re} with change in CFV at 100 kPa TMP, 2.5 g/l C_{feed}, using a 1.0 μm membrane

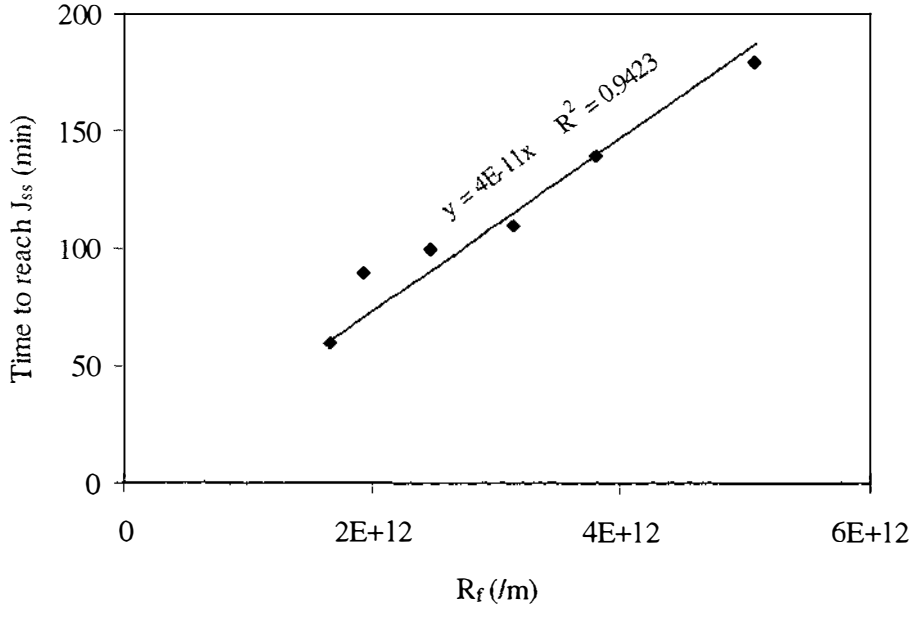

Fig. 5.24 Time to reach steady-state versus R_f at 100 kPa TMP, 2.5 g/l C_{feed}, using a 1.0 μm membrane

R_m remained uniform throughout the experiments, whilst R_f and R_{re} decreased with an increase in CFV. R_{ir} decreased from 0.375 to 1.5 m/s and beyond that increased with an increase in CFV. The proportion of R_{ir} also increased and the proportion of R_{re} decreased with increase in CFV beyond 1.5 m/s. However, R_{re} was the major contributor to the R_f at all CFV levels. A straight line assumed to be passing through the origin could be obtained when R_f was plotted against time to obtain J_{ss} as shown in Fig. 5.24.

Effect on the cake properties

The estimated values of mass, height and porosity of the cake at different CFV and 100 kPa TMP for 1.0 and 0.2 μm multi-channel membranes are given in Table A1.10 in Appendix 1. Very similar trends were obtained for both membranes. Because of a very small cake build-up, cake heights at 3.0 and 4.5 m/s and cake mass at 4.5 m/s could not be estimated. The cake mass is plotted against CFV in Fig. 5.25, and the effects of CFV on cake height and porosity are shown in Fig. 5.26. Overall, the cake porosity did not change significantly with CFV.

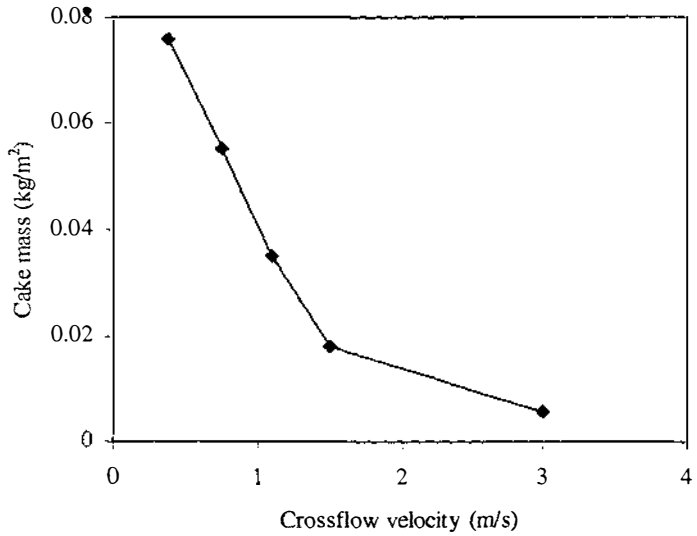

Fig. 5.25 Effect of CFV on the cake mass at 100 kPa TMP, 2.5 g/l C_{feed}, using a 1.0 μm membrane

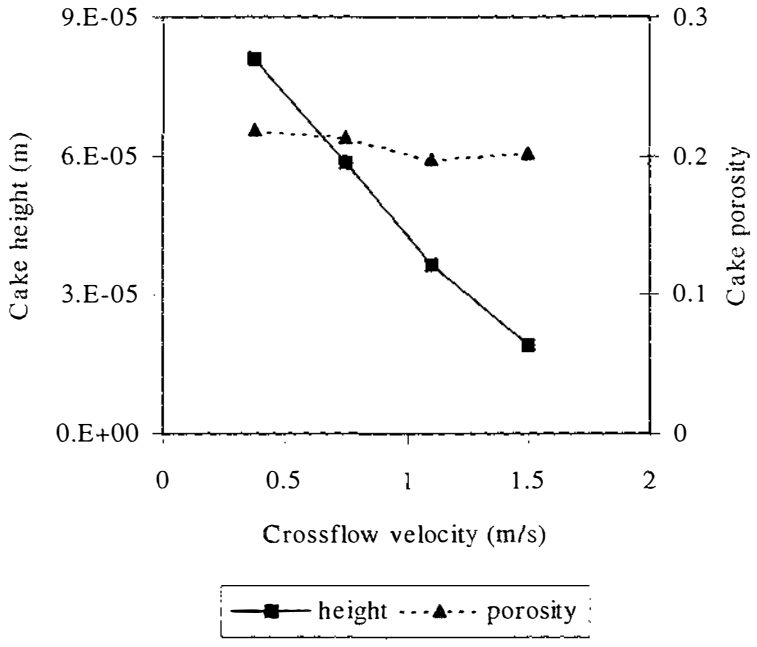

Fig. 5.26 Effect of CFV on the cake height and porosity at 100 kPa TMP and 2.5 g/l C_{feed}, using a 1.0 μm membrane

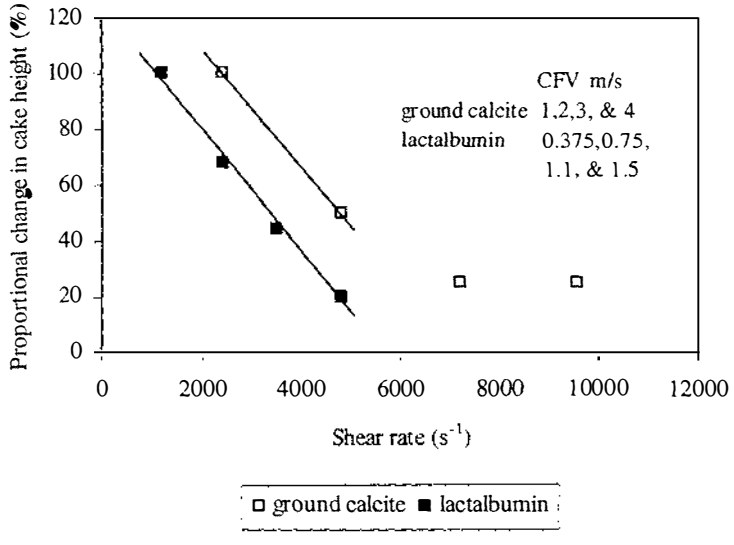

Fig. 5.27 Comparison of proportional change in cake height with shear rate during CFMF of lactalbumin and ground calcite (data drawn from Wakeman 1994)

the effect of CFV on the cake height for ground calcite was determined by Wakeman (1994). To provide a comparison between two studies, the proportional changes in cake height with shear rate for lactalbumin in the present study and in that for ground calcite (Wakeman 1994) are shown in Fig. 5.27. The rates of decline in cake height with

increasing CFV or shear rates were similar in the range where lactalbumin data were available for comparison (i.e. 0-1.5 m/s or 0-4800 s^{-1}).

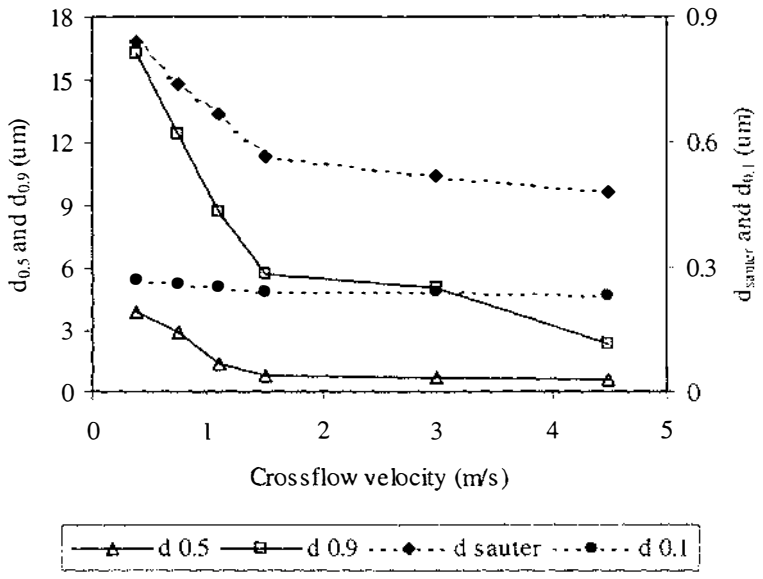

Fig. 5.28 Effect of CFV on the cake PSD at100 kPa TMP, 2.5 g/l C_{feed}, for a 1.0 μm membrane

The cake PSD values at different CFV for both the membranes tested are given in Table A1.10 in Appendix 1 and shown in Fig. 5.28 for the 1.0 μm membrane. Again very similar trends were obtained for both membranes. Clearly, very marked changes were observed: the cake comprised smaller particles at higher CFV. All values- d_{sauter}, $d_{0.1}$, $d_{0.5}$ and $d_{0.9}$ decreased with an increase in the CFV, with this classification effect being greatest up to 1.5 m/s.

5.4.3.3 Discussion

The increase in J_{ss} with increase in the CFV (Fig. 5.19) is due to the thinner cake formation as a result of the higher forces carrying particles away from the membrane under higher CFV. The observed changes in R_{re} (Fig. 5.21) and cake mass (Fig. 5.25) with CFV further confirmed this basic membrane theory. Mackley and Sherman (1992) during CFMF of polyethylene particles, and Wakeman (1994) during CFMF of calcite and anatase particles, also observed thinner cake formation at higher CFV. The observed effect of CFV on the time required to reach J_{ss} (Fig. 5.18), neglecting the minor difference in the rate of fouling at different CFV, can be explained by the force

balance mechanism (Chapter 2.6.3). Under constant TMP operation at constant CFV, the forces on the particles acting toward the membrane surface decrease with time due to membrane fouling. Depending on the level of CFV, the forces toward the membrane and away from the membrane reach an equilibrium at a certain level of fouling where J_{ss} is obtained. Thus, at higher CFV, there is less membrane fouling at steady state and therefore, less time required to reach this condition. The time to reach J_{ss} changed almost linearly with change in R_f in the present study (Fig. 5.24) suggesting it could be possible to estimate the time required to reach the steady state at any CFV level in the studied range. However, the observed effect of CFV on time to reach J_{ss} is contradictory to the report of a longer time being required to reach J_{ss} at higher CFV during CFMF of 2.7 μm mean size ground calcite (Wakeman and Tarleton 1991). No explanation was given for this observed trend that can not be explained by force balance mechanism or other basic membrane theory. In contrast, Wakeman (1994) using a similar feed material (ground calcite, mean size 2.6 μm) observed that less time was required to reach the steady-state cake height at higher CFV. Based on the flux profile reported by Wakeman (1994), the time required to reach J_{ss} did not appear to be different at different CFV. However, the J_{ss} trend with respect to CFV was similar to that obtained for lactalbumin in the present study.

The wall shear stress or shear rate model has been successfully applied in the case of magnesium hydroxide slurries (Holdich *et al.* 1995) and polystyrene latex particles (Chang *et al.* 1995). It appeared applicable in the present study only up to about 2 m/s (denoted by solid line in Fig. 5.20). The applicability of the model could be extended to 3.0 m/s by not considering the point of origin (denoted by dashed line in Fig. 5.20), as done by Chang *et al.* (1995) and for some experiments by Holdich *et al.* (1995). Above that CFV, J_{ss} was lower than that predicted by the model. This can be attributed to the higher proportion of internal fouling at high CFV (Fig. 5.23), since the wall shear stress model is based solely on the change in the surface fouling with changing wall shear stress. Holdich et al. (1995) also observed that the wall shear stress model did not apply for magnesium hydroxide slurry containing fine particles (d 0.1 $\leq$ 1 μm) which substantially fouled the membrane (0.5 μm pore size) internally, resulting in severely reduced fluxes. Although the pressure losses due to entrance and exit effects are ignored

in this study (Section 5.4.3.2), the results of this study are in good agreement with the fouling resistance data and thus provide an explanation for the observed phenomena.

Since reversible fouling was the major contributor to fouling in the present work, the total fouling also decreased with increase in CFV. However, the increase in irreversible fouling with increasing CFV observed beyond 1.5 m/s is not reported before. Based on the results of the effect of CFV on the cake PSD (Fig. 5.28), this effect can be attributed to the size classification effect of CFV. Deposition of smaller particles at higher CFV resulted in less effective pore blocking and greater pore penetration. Although, the information about the R_{re} and R_{ir} is not available for single channel membranes, considering the similarity in the flux and total fouling profile (Table A1.7, Table A1.8 and Table A1.9, also see Section 5.5.4), a similar trend for these membranes is expected.

The actual cake heights reported in the study by Wakeman (1994) for ground calcite particles (mean size 2.6 μm) were 0.5 - 2 mm, compared to only 19 – 81 μm estimated in the present study. This could be due to the differences in the TMP (273 and 100 kPa respectively), in the shear rates (*e.g.* for CFV = 1 m/s, 2400 and 3200 s^{-1} respectively) as a result of different module dimensions, the feed PSD which determines the proportions of internal and surface fouling, in and the cake PSD which determines the specific resistance and hence the cake height at steady-state. However, the rates of the decrease in the steady-state cake height with increasing CFV or shear rate were similar for the two studies in the range of 0 – 2 m/s where data from both the studies were available for comparison (Fig. 5.27). The observed insignificant effect of CFV on the cake porosity was somewhat surprising given the significant change in cake PSD with CFV. It suggests the PSD in the observed size range does not have any marked effect on the cake packing, although the true effect of CFV on cake packing could not be measured in this study as the reconstruction of cake height was under dead-end mode (Section 5.2.3). However, as discussed in Section 5.3.4, Resmeier *et al.* (1989) also observed no marked effect of CFV on the specific cake resistance during CFMF of yeast cells (in 1-8 μm size range). CFMF has been reported to produce a cake with higher specific resistance than that in the dead-end MF (Mackley and Sherman 1992), the level of CFV may not have any significant effect on the cake packing.

The observed effect of the CFV on the cake PSD (Fig. 5.28) is similar to the crossflow particle size classification reported by Fischer and Raasch (1986), Lu and Ju (1989), Foley *et al.* (1992), and Wakeman (1994). The marked extent of the selective particle deposition can be realised by comparing the PSD of cakes at different CFV with the PSD of the feed (Fig. 4.4). At all CFV levels, 90 percent of the deposited particles were smaller than 18 μm, which is about half of the average size ($d_{0.5}$) of the feed particles (i.e. 35 μm). At and above 1.5 m/s, at least 50 % of the deposited particles were smaller than the membrane pore size of 1.0 μm. However, the selective deposition in the case of the CFMF of lactalbumin particles did not lead to a dramatic change in J_{ss} with change in CFV as reported by some workers (Fischer and Raasch 1985, Lu and Ju 1989, Wakeman and Tarleton 1991, Mackley and Sherman 1992, Tarleton and Wakeman 1994[a], and Wakeman 1994).

While some of the studies mentioned above involving widely size distributed particulate feed have reported drops in flux with increasing CFV, the others have observed the common trend of an increase in flux with increasing CFV. Among those reporting a drop in flux with CFV, the report by Mackley and Sherman (1992) dealt with large (125-180 μm) polyethylene particles and the other reports involved CFMF of unground (1- ~30 μm) calcite particles with very low concentration of small particles (only 5-10 % particles were 1-2 μm in size). The trend observed in these cases can be attributed to higher resistance offered by thinner cakes comprising smaller particles at higher CFV. In the studies reporting an increase in flux with CFV, the feed comprised widely size distributed particles with the smallest in the sub-micron size range. These include lactalbumin in the present study with $d_{0.1} = 0.47$ μm, ground calcite with $d_{0.1} = 0.77$ μm, (Wakeman and Tarleton 1991 and Wakeman 1994), and magnesium hydroxide, type A, $d_{0.1} \cong 1$μm and type B, $d_{0.1} < 1$ μm (Holdich *et al.* 1995). The possible explanation is that during CFMF of such feed materials, the maximum cake packing through filling of inter-particle voids by fines is reached at steady-state, irrespective of the level of CFV (Fig. 5.25). Thus cake porosity does not change with CFV. According to the Carman-Kozeny eq. (eq. 2.6 and eq. 2.8), particle diameter and cake height, in addition to cake porosity (which play a more significant role) determine the cake resistance (R_c). For the cakes with a wide size distribution, the smallest particles offer a maximum resistance to flux, and the cake layers containing these smallest particles mainly determine the R_c

(Altmann and Ripperger 1997). The size classification effect of CFV on the smallest particles is not marked when they are in the submicron range. For example, in the present study $d_{0.1}$ of the cake dropped only by ~10 % (0.27 to 0.24 μm) compared to a ~80 % drop in $d_{0.5}$ (3.84 to 0.77 μm) and a ~60 % drop in $d_{0.9}$ (16.29 to 5.68 μm) with an increase in CFV from 0.375 to 1.5 m/s. Compared to the 10 % drop in the diameter of the small particles, the cake height dropped by ~75 % (81 to 19 μm) across this CFV range. According to the Carman-Kozeny equation, a drop of 10 % in the particle diameter would increase R_c by only ~20 % but a 75 % drop in cake height would decrease R_c by 75 %. Thus, the change in cake height is more significant compared to the change in particle size with CFV in determining R_c when the smallest particles are in the submicron range and the porosity can be assumed constant.

In summary, the results of the present study provide a possible explanation to the contradictory reports on the effect of CFV on J_{ss} for particulate feeds with wide size distribution, and thus improve the understanding about the significance of the particle size in CFMF process. The early attainment of the steady state at higher CFV is not reported before but can be explained by the force balance mechanism. Increase in internal fouling with increase in CFV observed above 1.5 m/s in this study is also not reported before and not expected based on the basic membrane theory. This is attributed to the selective deposition under the effect of CFV. This suggests a possibility of operating at an optimum CFV to obtain minimal internal fouling. Further experiments were therefore carried out to explore this possibility (see Section 5.4.4).

5.4.4 Process development based on the effect of operating parameters

Based on the results of the previous studies on the effect of operating parameters on CFMF of lactalbumin particles, a process was designed with the aim of providing a high permeate flux and low internal fouling. Such conditions would mean lower capital, operating and cleaning costs.

5.4.4.1 Methods

The following observations from the study on the effect of the operating parameters were considered for the process development:

(1) the particles in the cake on the membrane surface have strong adhesion,
(2) the largest particles in the cake deposit during the initial period of filtration and govern the rest of the filtration process,
(3) 100 kPa is the optimum TMP level with respect to the permeate flux, and
(4) the highest steady-state flux is obtained at 4.5 m/s but the lowest internal fouling is obtained at 1.5 m/s in the studied range of CFV.

Combined CFV runs at 100 kPa TMP and 2.5 g/l C_{feed} using a 1.0 μm pore size membrane were carried out. CFMF was started at 100 kPa TMP and 1.5 m/s CFV to deposit large particles on the membrane surface with minimum pore penetration of the fines. Filtration was continued under this condition for 10 min to obtain a tightly packed cake with strong adhesion. Then CFV was stepped up to 4.5 m/s to obtain a high flux regime. Permeate flux was measured at regular time intervals, and different resistances to the flux and the cake mass were estimated at 10, 30 and 160 min.

The increase in CFV to 4.5 m/s was expected to cause some erosion of the deposited cake as well as further deposition of particles. To understand the deposition mechanism at 100 kPa and 4.5 m/s conditions, the flux profile for the run at these conditions was studied. To understand the erosion mechanisms, in a separate run the cake deposited at 100 kPa and 1.5 m/s for 10 min was eroded by flushing RO water at 100 kPa and 4.5 m/s conditions and the flux recorded at varying time intervals. Average results of two replications for this run were considered.

5.4.4.2 Results

The flux profile from the point of change in CFV for this experiment, which combines erosion and deposition (4.5 m/s combined) is shown in Fig. 5.29. Flux profiles for the pure

deposition runs at constant CFV (1.5 m/s and 4.5 m/s) and for the pure erosion of the cake (deposited under 1.5 m/s for 10 min) at 4.5 m/s are also shown in the figure for comparison. Values of R_f, R_{re}, R_{ir} and cake mass at 10, 30 and 160 min for these experiments are given in Table 5.4. Permeate flux from the point of change in CFV is plotted against time on log-log scale in Fig. 5.30. The starting point was taken as 0.1 min rather than 0 min to avoid situation log (0).

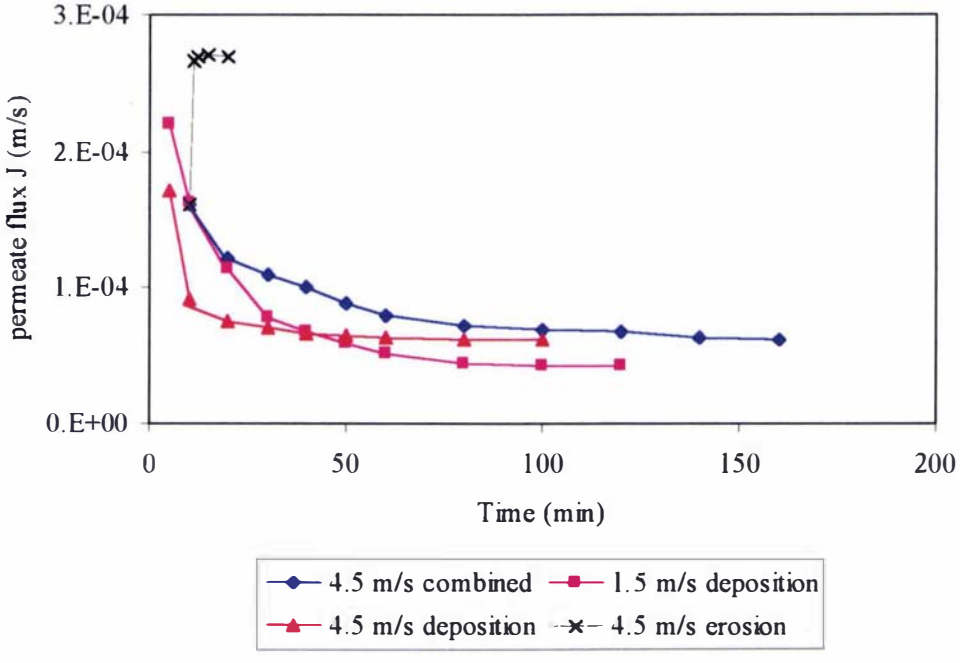

Fig 5.29 Different runs representing deposition, erosion and a combination of the two, at 100 kPa TMP, using 1.0 μm membrane

Table 5.4 Comparison of filtration resistances and cake mass for the combined CFV run with constant CFV runs at 1.5 and 4.5 m/s

TMP = 100 kPa
membrane = 1.0 μm multi-channel

CFV (m/s)	J (m/s)	R_f (/m)	R_{re} (/m)	R_{ir} (/m)	Cake mass (kg/m^2)
1.5 (at steady state)	4.25×10^{-5}	2.3×10^{12}	2.2×10^{12}	8.9×10^{10}	0.0182
4.5 (at steady state)	6.33×10^{-5}	1.5×10^{12}	1.0×10^{12}	4.4×10^{11}	----
1.5/4.5 at 10 min	1.62×10^{-4}	4.7×10^{11}	3.9×10^{11}	8.0×10^{10}	0.0086
30 min	1.09×10^{-4}	8.6×10^{11}	7.6×10^{11}	9.9×10^{10}	0.0015
160 min	6.22×10^{-5}	1.5×10^{12}	1.4×10^{12}	1.1×10^{11}	0.0016

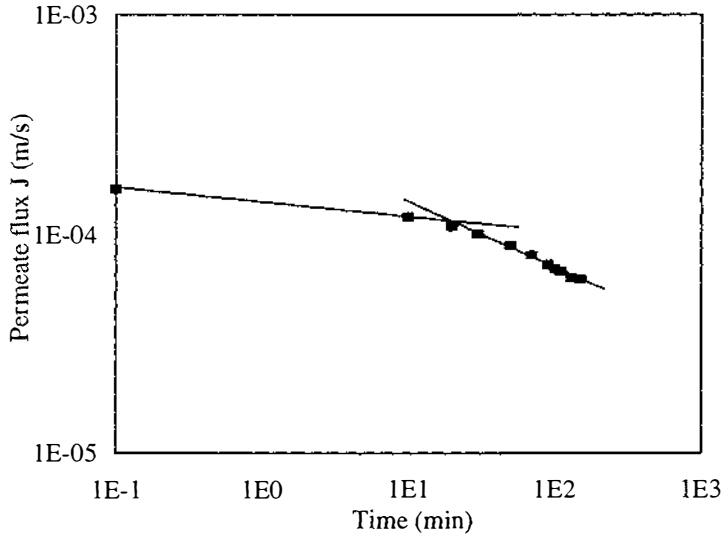

Fig. 5.30 Change in flux with time from the point of change in CFV from 1.5 to 4.5 m/s at 100 kpa TMP and 2.5 g/l $_{Cfeed}$ using 1.0 μm membrane

The permeate flux for the combined CFV run declined with time and at 160 min it was similar to J_{ss} for the 100 kPa – 4.5 m/s deposition run. However, the rate of flux decline for the combined CFV run from the point of CFV change was significantly lower than that of both deposition runs (i.e. constant CFV runs at 1.5 and 4.5 m/s at 100 kPa TMP). Therefore, the system could be operated at a higher flux for a longer time compared to these constant CFV runs. During pure erosion of the cake deposited at 100 kPa - 1.5 m/s for 10 min, only about 2/3 of the surface fouling could be removed (R_{re} decreased from 3.9 x 10^{11} to 1.2 x 10^{11} /m). Most of this removal took place during the first min and there was no significant change in flux after 5 min. When flux was plotted against time on the log-log scale for the operation at 4.5 m/s in the combined CFV run, the rate of flux decline appeared to have increased after first 20 min from the point of CFV change. All R_f, R_{re}, and R_{ir} increased with time. The cake mass dropped with time for first 20 min from the point of CFV change and then slightly increased during rest of the run. At 160 min, R_f was similar to that of 100 kPa – 4.5 m/s run at steady state. However, R_{ir} was much lower for the combined CFV run and close to that of a 100 kPa –1.5 m/s run at steady-state.

Correspondingly the R_{re} for the combined run was much higher than that for the constant CFV run at 4.5 m/s.

Curve fits were obtained for flux versus time for the processes of deposition, erosion and a combination of the two at 100 kPa - 4.5 m/s conditions using the logistic model. The curves are characterized by equation:

$$y = \frac{a}{1 + b\, e^{-cx}} \qquad (5.7)$$

Where,
(1) for deposition,
a = 0.03502, b = -0.906, c = 0.0365,
standard error s = 2.6×10^{-5}, correlation coefficient r = 0.9914
(2) for erosion,
a = 0.00027, b = 0.658, c = 3.8614,
s = 7.1×10^{-7}, r = 0.9999

(3) for combined process,
a = 0.04168, b = -0.618, c = 0.0182,
s = 3.1×10^{-6}, r = 0.9958

The slope (dy/dx) of the curve gives the rate of the change in flux at any time.

For the logistic curve (Sneddon 1976):

$$\frac{dy}{dx} = \frac{a\, c\, b\, e^{-cx}}{(1+b\, e^{-cx})^2} \qquad (5.8)$$

Assuming that the studied process (the combined run) can be expressed as the two basic components deposition and erosion, the sum of the rate of deposition and rate of erosion at 100 kPa - 4.5 m/s should give the rate of the 4.5 m/s CFV part of the developed process.

$$\therefore dy_{deposition}/dx + dy_{erosion}/dx = dy_{combined}/dx \qquad (5.9)$$

The prediction of process rate based on this model is compared with actual process rate of the 4.5 m/s part of the developed process in Fig. 5.31. The rate was over predicted during

about first 30 min and then slightly under predicted for rest of the process by the model. To make the small under prediction of the rate look obvious, the process rates are plotted on log scale.

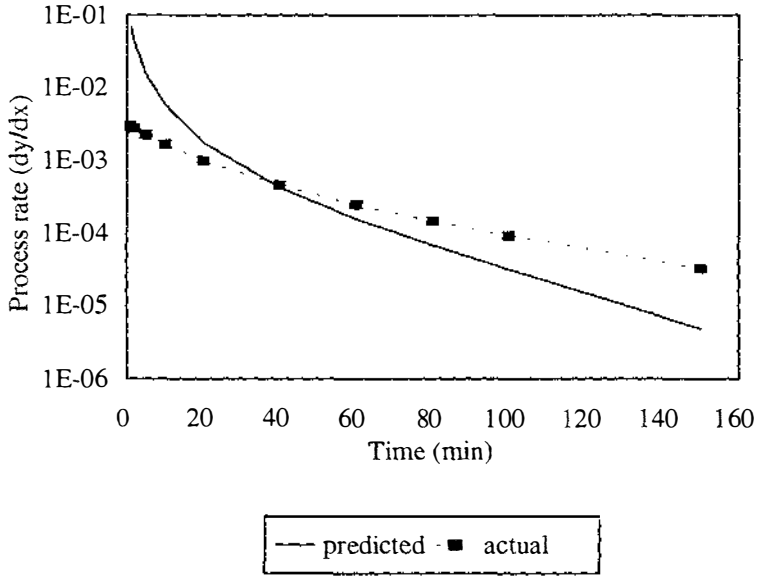

Fig 5.31 comparison of predicted rate and actual process rate of the developed process from the point of change in CFV

5.4.4.3 Discussion

During the combined CFV runs, the lower rate of flux decline and therefore the higher operating fluxes obtained after changing the velocity can be attributed to changes to the properties of the cake deposited during first 10 min. The observed change in cake mass with time, as well as the plot of flux versus time on log-log scale suggests that most of the erosion took place during the first 20 min after changing CFV. Erosion during the combined CFV run took place at a slower rate compared to the pure erosion run due to simultaneous deposition and cake compaction. The cake compaction was evident from the increase in R_{re} despite the decrease in the cake mass with time (Table 5.4). The cake compaction further illustrates the effects of time on cake packing as seen in 5.4.1 (Fig. 5.6), as well as the effect of higher CFV on the size of deposited particles (Fig. 5.28 in 5.4.3) and possibly on cake packing. Smaller particles deposited at the higher CFV reduced the cake permeability by forming a 'tighter' cake on the top of existing cake and/or by penetrating

into the existing cake. Considering the observed increase in R_{ir} with time and simultaneous cake erosion, the latter is more plausible particularly during first 20 min. At the end of first 20 min at higher CFV, only about one sixth of the cake mass deposited during the 10 min of low CFV operation remained on the membrane surface. As observed by Mackley and Sherman (1992) and Wakeman (1994) during cake visualization studies, the top one or two layers of cake are mobile or semi mobile. The bottom layer is stationary as a result of better particle-particle and/or membrane-particle attachment. The integrity of the strongly attached bottom cake layer after the erosion appears to play a vital role in preventing any significant pore penetration of fines during the rest of the filtration process. However, the small particles continue to deposit at a low rate at high CFV and were mostly retained by the cake during rest of the filtration. During this stage, the depositing particles may or may not have formed a separate top layer with higher resistance. Live observation of fouling during this experiment, had it been possible,would have provided more insight.

The attempt to model the process based on pure erosion and deposition had a limited success. High level of over prediction of the process rate indicates over-prediction of deposition, or in other words, under-prediction of erosion during first 30 min. There are many possible reasons for the over prediction of the process rate. Firstly, the 100 kPa – 4.5 m/s run is considered as a pure deposition. However, the deposition during that run began with a clean membrane condition and hence a higher degree of pore penetration can be expected. In the case of the combined CFV run, the deposition at 100 kPa - 4.5 m/s began on the fouled membrane with 10 min of cake deposition at 100 kPa – 1.5 m/s conditions. Therefore, the initial fouling rates are expected to be lower than that with clean membrane. Secondly, the presence of larger particles (being eroded simultaneously from the cake during first 10 min from change of CFV) near the cake surface might have inhibited deposition through particle-particle interaction. Thirdly, the large particles, under high shear force at 4.5 m/s, might have produced a scouring effect and enhanced the erosion process. Again live observation of membrane fouling would have provided more information. A slight under-prediction of the process rate after about 40 min is due to underestimation of deposition since erosion is not expected during this period (Fig. 5.30). Again different deposition rates are possibly due to the different surface conditions during

pure deposition at 100 kPa – 4.5 m/s, and the actual process. The cake formed in the former was thin and tightly packed and hence allowed no significant cake penetration of small particles for long time. Therefore, the deposition rate slowed quickly and approached zero. Whereas, the cake formed in the latter even after erosion was thicker (Table 5.4) and with more voids due to larger particle sizes (since the major deposition took place at lower CFV) and hence deposition continued at higher rates and for longer time.

5.4.4.4 Further scope

Since the attempt to run the CFMF process at high flux and low internal fouling was successful for lactalbumin suspension, there is a scope to further develop this process and apply it for any widely size distributed particulate suspension. However, values of the operating parameters may vary with feed properties. This process is obviously applicable to adhesive material, but for less or non-adhesive material a thicker initial build up may help. Due to a very small internal fouling, there is scope to couple this process with backflushing to form a sequential chain of process and backflushing, and obtain a longer and more efficient operation between cleanings at industrial scale. This is because backflushing is known to remove surface deposits very efficiently but is less effective on internal fouling (Van Veen 1996).

5.4.4.5 Conclusions

The developed process could be successfully used to obtain higher fluxes and lower internal fouling for CFMF of lactalbumin particles. This provides a base for further development of this process or similar process es for different particulate suspensions. There is scope to combine the developed process with backflushing to apply it at industrial scale.

5.4.5 Overall discussion

Much work is found in the literature on the effects of the process parameters on the CFMF of particulate suspensions. Surprisingly there is still some confusing or contradictory information regarding the effects of basic process parameters. For example, there are contradictory reports concerning the effect of CFV on J_{ss} as well as on the time required to obtain the same. Often adequate justifications are not provided for the reported results. A straight comparison of the results is not possible since there are no uniform standard operating or feed conditions adopted in these reports. Further, all parameters required for the analysis are not estimated in any individual report. Therefore, the reliable interpretation of the reported results and their application to other feed and operating conditions has become difficult. As noted earlier (Chapter 2.8), the feed materials used in different reports do not always represent the feed in the actual CFMF processes. The present study is the first to attempt the estimation of all key parameters for a given stream under defined operating conditions. Analysis of the cake for all of: mass, height, porosity, and PSD, together with division of membrane fouling into internal and surface fouling, has not been reported before for a given feed. This work has therefore provided the opportunity for elucidating the effect of process parameters and hence providing a more complete picture of CFMF of particulate suspensions. This has resolved the controversy over the effect of CFV on the J_{ss} as well as the time required to obtain the same for particulate feed systems with wide size distribution. The wide PSD of lactalbumin, the chosen feed material for this study, has also played a very important role in further development of the understanding about the CFMF of the particulate suspensions.

Further and importantly, detailed study on the effects of the process parameters has enabled the process development giving higher permeate fluxes and lower internal fouling. The developed process will be useful mainly for feeds with wide PSD. This process is reported for the first time and has a potential to become commercial if successfully coupled with backflushing. There is scope for further study in this area.

The cake heights estimated in this study, as discussed in Section 5.3.4, do not include the effect of CFV on the cake packing due to the methods used for the estimation. Although the presence of the crossflow is significant, the level of the crossflow is not significant in determining the level of cake packing (Riesmeier *et al.* 1989). The presence of crossflow is significant for cake packing because the particle deposition is expected to be selective under crossflow, as the particle rolls on the cake surface and finds a suitable place to deposit, but random under the dead-end mode (Mackley and Sherman 1992). However, due to the wide PSD of the cake in the present study, the particle deposition under dead-end mode during the reconstruction of the cake has not been completely random. This is because the large particles, due to greater flux force F_f and gravitational force F_g acting on them, deposited first followed by the deposition of small particles that also filled the inter-particle voids. This is evident from the estimated low levels of cake porosity (~0.2). Cake height values from 0.3 μm to several mm during CFMF of particles have been reported in the literature (as discussed in Section 5.3.4). Cake height can be affected by operating conditions, feed concentration and PSD, and the membrane and flow channel configuration. Therefore, wherever the experimental conditions are similar, cake heights in the similar range can be expected. The estimated cake heights (10 - 81 μm) in the present study are in the same order as that measured by Riesmeier *et al.* (1989) and Wandelt *et al.* (1992) using sophisticated technique like scanning electron micrography and NMR micro-imaging. Riesmeier *et al.* (1989) during CFMF of yeast and bacterial cells using a tubular module (0.2 μm pore size, 5.5 mm inner diameter) reported cake heights between 0.5 and 40 μm. TMP and CFV were varied in the range 0 – 150 kPa and 0.5 – 5.0 m/s, respectively, in this study. Considering the similarities in the operating conditions, feed PSD (both feeds involved submicron size particles) as well as membrane configuration (both studies involved small clearance tubular module) between the study by Riesmeier *et al.* (1989) and the present study, similar cake height values can be expected and were obtained. Wandelt *et al.* (1992) during CFMF of 0.7 μm mean size bentonite particles using a hollow fibre module (0.01 μm pore size, 0.93 mm inner diameter) measured cake heights of about 30 - 120 μm using NMR micro-imaging technique. Although the operating conditions for this study are not known, the feed PSD and membrane configuration are again similar to that in the present study and measured cake heights are also similar. The observed low porosity of

~0.2 and the estimated cake heights that are comparable with the cake heights measured using sophisticated techniques under similar experimental conditions support the validity of the methods of cake height estimation used in the present study.

The very low levels of cake porosity (~0.2) observed in this study are due to inter-particle voids effectively filled by small particles which is a result of the wide PSD of the feed particles. The results of cake porosity suggest that only the presence of TMP and not the level of TMP is significant for the level of cake packing. The cake PSD also did not significantly affect the cake packing. Although there was a big difference between the PSD of cakes obtained during the study and the feed PSD, the porosity values of the feed particle bed (Table 4.5) and the reconstructed cakes were not widely different. However, a significant effect of time of filtration on porosity suggests that time for which pressure is applied is significant for cake packing. Another significant observation with respect to cake packing is that irrespective of the level of TMP or CFV, cake porosity reached a similar low value of about 0.2 at the steady-state in the range of these parameters (where the information on porosity was available). Under constant porosity situation, R_{re} will depend only on cake mass and diameter of deposited particles. Thus with known cake mass and PSD, J_{ss} can possibly be estimated using the resistance in series model (Section 2.6.1.4).

Fischer and Raasch (1986) first proposed that the size of the depositing particle is decided by the net resultant force acting on feed particles arising from the total forces towards the membrane surface and total forces away from the membrane. This is the basis of the flowing cake model (Section 2.6.3) and is evident in the change in cake PSD with time, TMP and CFV observed in the present study. However, for lactalbumin particles, in addition to flux and shear forces, adhesive forces are also expected to play a significant role. The possibility of describing the observed behaviour of lactalbumin particles during CFMF study by developing a mathematical model based on the resistance in series and flowing cake theories should be explored (see Chapter 6).

5.5 Effect of feed properties and of membrane and module characteristics

5.5.1 Effect of feed concentration

The effect of the C_{feed} on J_{ss}, fouling of the membrane and cake properties is discussed in this part of the Chapter.

5.5.1.1 Methods

Initially three levels of C_{feed} – 0.625 g/l, 2.5 g/l and 5.0 g/l were studied at 100 kPa TMP and 0.75 m/s and 3.0 m/s CFV. Only the multi-channel module with 1.0 μm membrane was used for this study. The upper value of the C_{feed} used for this study was limited by the difficulty in maintaining the lactalbumin particles in suspension at higher concentrations. To confirm the trends observed with respect to J_{ss}, a C_{feed} level of 3.5 g/l was later investigated at both CFV (only J_{ss} was measured at 3.5 g/l, and membrane fouling or cake properties were not studied). Considering the agreement between the results of the two methods of cake height estimation, from here onward only glass tube method was used.

5.5.1.2 Results

Effect on the steady-state flux

Values of J_{ss} at different C_{feed} are listed in Table A1.11 and plotted in Fig. 5.32. J_{ss} decreased with increase in C_{feed} from 0.625 g/l to 2.5 g/l but did not change significantly with increase from 2.5 g/l to 5.0 g/l at both 0.75 m/s and 3.0 m/s CFVs. The latter trend was confirmed by measuring J_{ss} at 3.5 g/l and plotting on the curve.

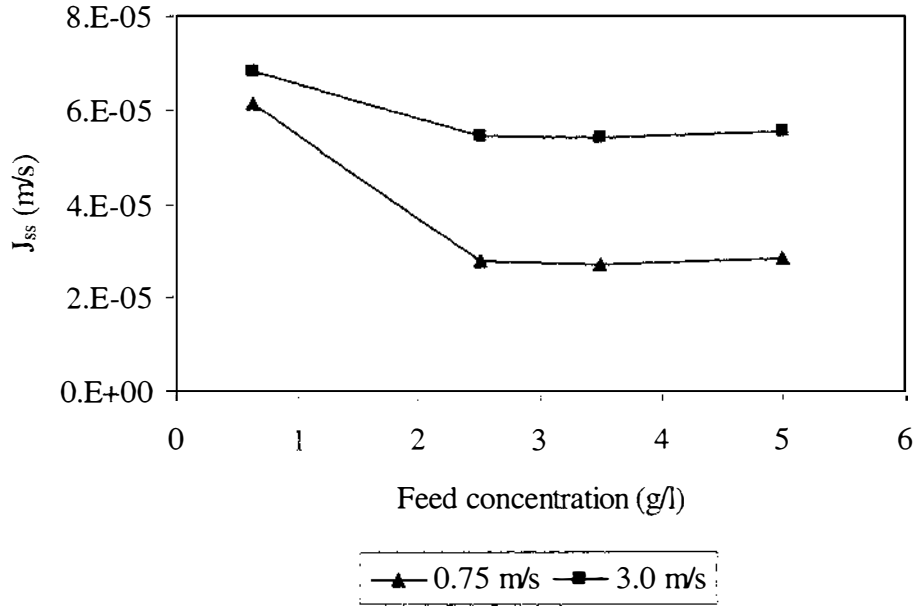

Fig. 5.32 J_{ss} versus C_{feed} at 100 kPa TMP, 0.75 m/s and 3.0 m/s CFVs, and 1.0 μm membrane pore size

Effect on membrane fouling

The values of the different resistances to the permeate flux at different C_{feed} are listed in Table A1.11 and plotted in Fig. 5.33. R_m remained almost unchanged all through out the experimental runs as observed also during the previous studies on the effects of operating parameters (part 5.4 in this Chapter). R_f, R_{re} and R_{ir} increased with increase in C_{feed} from 0.625 to 2.5 g/l and remained unchanged with increase from 2.5 g/l to 5.0 g/l. R_{re} was the main contributor to R_f for all levels of C_{feed}.

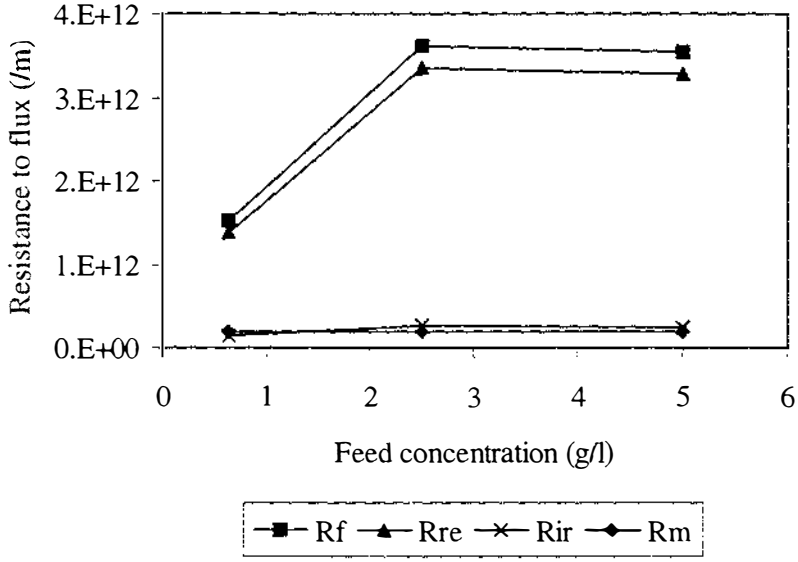

(a)

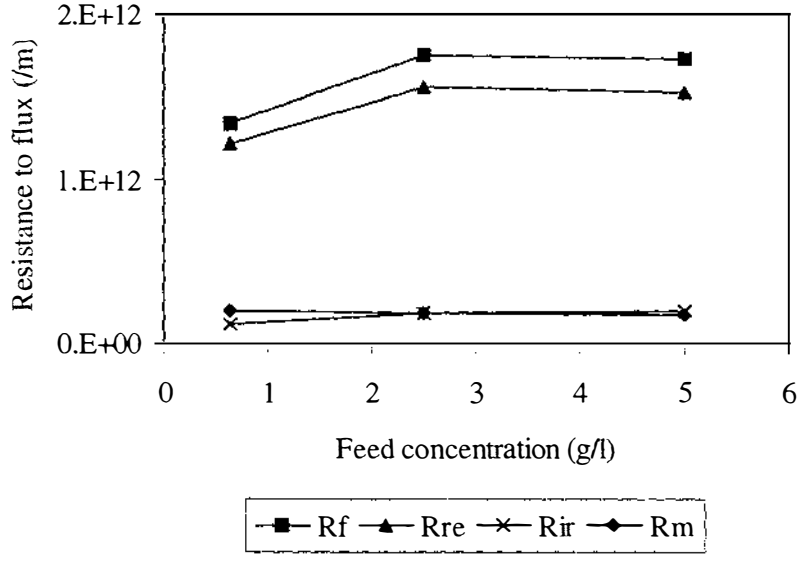

(b)

Fig. 5.33 Effect of C_{feed} on the membrane fouling at (a) 0.75 m/s, and (b) 3.0 m/s CFV, 100 kPa TMP, using 1.0 μm membrane pore size

Effect on the cake properties

Table A1.12 shows the values of the cake properties: mass, height, porosity and PSD at different C_{feed}. The cakes formed during the experimental runs at 3.0 m/s CFV were not thick enough to reliably estimate the cake height and porosity. The plot of cake mass against C_{feed} is shown in Fig. 5.34. Cake height and porosity are plotted against C_{feed} in Fig. 5.35. There was an increase in mass and height of the cake with increase in C_{feed} from 0.625 g/l to 2.5 g/l. The increase in the cake mass was higher at 0.75 m/s CFV compared to the increase at 3.0 m/s CFV. There was no significant change in the mass and height with change in C_{feed} from 2.5 g/l to 5.0 g/l. The porosity of the cake (for 0.75 m/s) did not change significantly with any change in C_{feed} in the studied range.

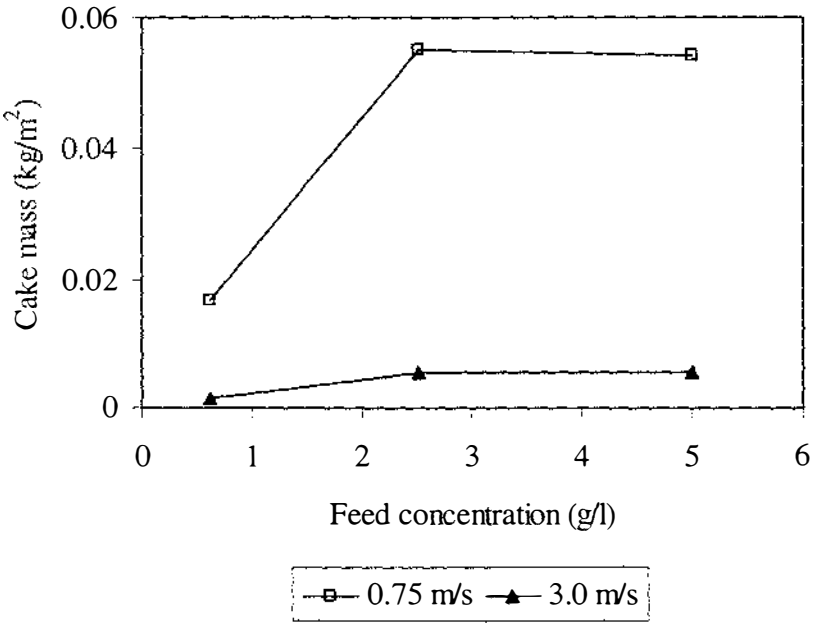

Fig. 5.34 Cake mass versus feed concentration at 100 kPa TMP, 0.75 m/s and 3.0 m/sCFV, and 1.0 μm membrane pore size

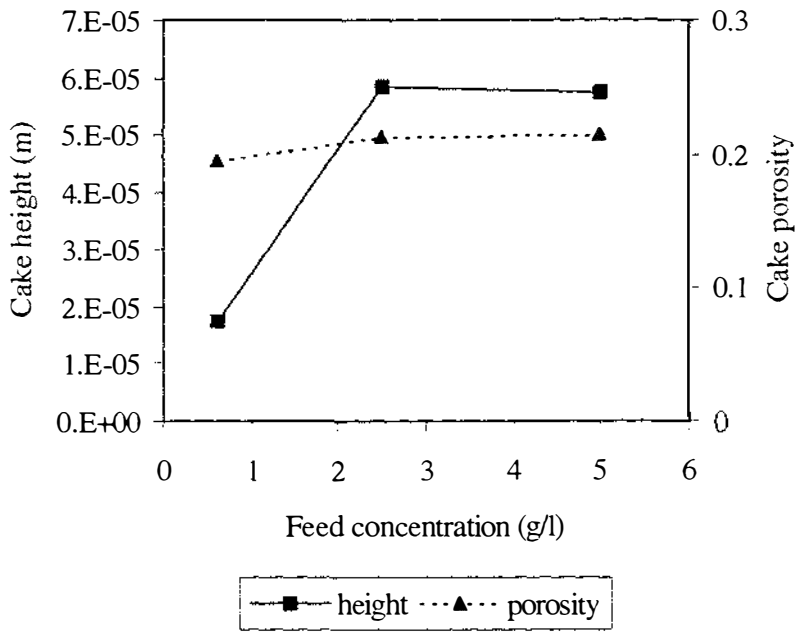

Fig. 5.35 Effect of C_{feed} on cake height and porosity at 100 kPa TMP, 0.75 m/s CFV, and 1.0 μm membrane pore size

The values of d_{sauter}, $d_{0.1}$, $d_{0.5}$, and $d_{0.9}$ of the cakes are plotted against C_{feed} in Fig. 5.36. At 0.75 m/s CFV, d_{sauter}, $d_{0.1}$ and $d_{0.9}$ values decreased with increase in C_{feed} from 0.625 g/l to 2.5 g/l. Beyond 2.5 g/l there was no significant change in d_{sauter} and $d_{0.1}$ values with a change in C_{feed}. However, $d_{0.9}$ value increased with increase in C_{feed} from 2.5 g/l to 5.0 g/l. The $d_{0.5}$ value slightly decreased with increasing C_{feed} in the entire range of C_{feed}. The overall effect of C_{feed} at 0.75 m/s was very little and there was no significant effect of C_{feed} on the cake PSD at 3.0 m/s CFV.

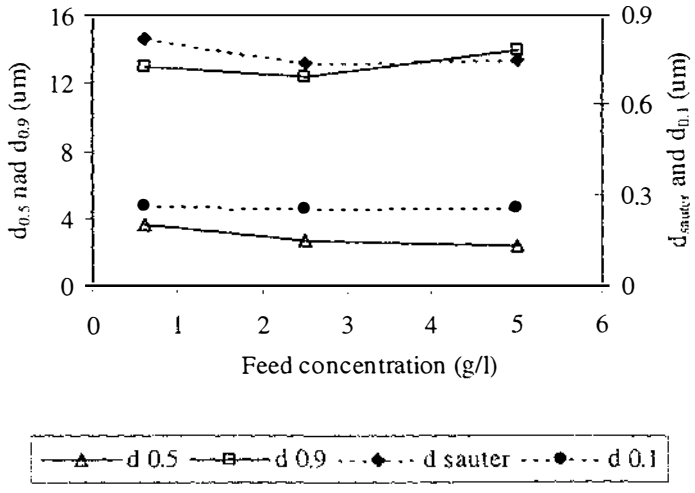

(a)

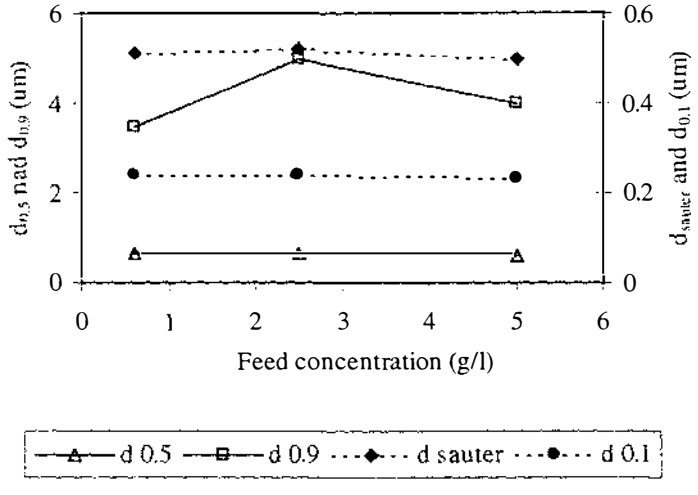

(b)

Fig. 5.36 Effect of C_{feed} on the cake PSD at (a) 0.75 m/s and (b) 3.0 m/s CFV, 100 kPa TMP, using 1.0 μm pore size membrane

5.5.1.3 Discussion

The drop in J_{ss} with an increase in C_{feed} resulted mainly from the increased surface fouling. The increase in both reversible and irreversible fouling with an increase in C_{feed} reflected availability of more particles to foul the membrane at higher C_{feed}. However, beyond 2.5 g/l further availability of the particles did not foul the membrane any further. A trend of this type has not been reported before, although Wakeman and co-workers

have reported some unexpected effects of C_{feed}. Wakeman and Tarleton (1991), Tarleton and Wakeman (1994[a]), and Wakeman (1994) observed the expected trend of decrease in flux with increasing C_{feed} in the range of 0.033-2.0 % v/v and 0.0001-0.018 solid volume fraction, respectively, for small size particles (anatase, mean size 0.5 μm and ground calcite, mean size 2.6 μm). However, they observed a negligible effect of C_{feed} on long term and steady-state fluxes for large particles (unground calcite, mean size 25 μm and china clay, mean size 4.4 μm) in the entire studied range of C_{feed} (0.033-2.0 % v/v). In contrast, under dead-end mode for these large particles they observed a drop in flux with increase in C_{feed}. They concluded that the observed trend for large particles under crossflow mode was solely due to the shear field generated at the membrane surface and its effect on the alignment and packing of the deposited particles. Riesmeier *et al.* (1989) noted an overall increase in the yeast cake resistance in the range 0 to 17.5 % v/v, but did not observe a significant change in cake resistance in the range of 2.5 to 7.5 % v/v of C_{feed}. Enough data are not reported in the 'no effect' zone (only one point reported in the range 2.5 to 7.5 % v/v) to draw a reliable conclusion. Further, their 'no effect' zone is in a higher range and the report deals with different feed material compared to the present study. Most of the reports on the effect of C_{feed} deal with a much wider range of concentrations than used in the present study. There are many possible reasons for no significant effect of C_{feed} on J_{ss} above 2.5 g/l in the case of lactalbumin particles. Firstly, a steady-state net resultant force may be reached around 2.5 g/l and therefore, further increase in availability of the particles at higher concentration does not increase the steady-state fouling. Secondly, the hindering of the particle movement towards the membrane surface by other particles is increased at higher C_{feed}. Thirdly, it is possible that the increased number of hard large particles increases the scouring effect on the cake, and the cake heights therefore reaches an equilibrium at higher C_{feed} above 2.5 g/l. The overall identical cake properties of runs at 2.5 and 5.0 g/l supports the first. But the third reason may explain the insignificant effect of C_{feed} on flux for large particles (calcite and china clay) found in some reports. The changes observed in cake PSD (Fig. 5.36) were negligible and hence are not thought to be of any significance.

5.5.2 Effect of feed PSD

As noted above, scouring by large particles may positively influence the filtration process. Equally, a large proportion of fines may promote cake and pore blockage, decreasing the permeate flux. To further elucidate the mechanism involved, the effect of varying feed PSD on the flux profile (J), J_{ss}, membrane fouling and cake properties was studied.

5.5.2.1 Methods

The lactalbumin feed particles were separated into three size fractions: (1) > 53 – 80 μm, (2) 39 to 53 μm, and (3) < 39 μm by dry sieving. The sieving was carried out for 30 min using two stainless steel mesh sieves with apertures of 38 and 53 μm respectively (Endecott Ltd., London, England). The separated fractions were analysed once (no replication) for PSD using Malvern Mastersizer (Chapter 3.3.1). Two sets of CFMF experiments were conducted at 100 kPa TMP and 1.5 m/s CFV, using the 1.0 μm multi-channel membrane. In the first set of experiments the standard feed particles (Fig. 4.3) were used to prepare a 2.5 g/l feed suspension and J_{ss} was determined. At 110 min (after reaching the steady-state), further standard feed particles were added to the feed at a concentration of 10 % of the original C_{feed} (i.e. 0.25 g/l added). In the second experiment of this set, only particles > 53 μm (fraction 1) were used to increase C_{feed} by 10 % at 110 min. In the second set of experiments, feed particles of < 39 μm (fraction 3) were used to make the 2.5 g/l feed suspension and CFMF was carried out until steady-state. Then, batches of either the largest (fraction 1) or intermediate (fraction 2) particles were added to give an increase in C_{feed} of 0.25 g/l at a time at 110 min. Any change in J due to addition of particles at steady-state was observed for in these experiments. The cakes from these experiments were then analysed for mass at the steady-state in duplicate and the results averaged. Where J_{ss} differed from the J_{ss} of the standard feed, the cake was also analysed for PSD at the steady-state in duplicate and results averaged. The cake height at the steady-state for feed < 39 μm (fraction 3) was also estimated in duplicate. The cake mass, height and PSD for the standard feed were obtained from the experiments reported in Section 5.4.3.

5.5.2.2 Results

The dry sieving produced reasonably distinct groups of feed particles which are shown in Fig. 5.37. The fraction 3 (< 39 μm) comprised particles in the range of 0.1 to ~ 40 μm ($d_{0.1}$ = 0.46 μm, $d_{0.5}$ = 20.27 μm, $d_{0.9}$ = 35.34 μm). The largest fraction (fraction 1) had particles in the range ~ 50 to 80 μm ($d_{0.1}$ = 58.31 μm, $d_{0.5}$ = 72.19 μm, $d_{0.9}$ = 78.46 μm). However, the intermediate fraction (fraction 2) was relatively less accurately separated. The particles in this fraction ranged from ~ 20 to 80 μm, with $d_{0.1}$ = 41.74 μm, $d_{0.5}$ = 62.46 μm, and $d_{0.9}$ = 76.64 μm. Thus, although fraction 2 was clearly distinct from fraction 3, there was considerable overlap with fraction 1.

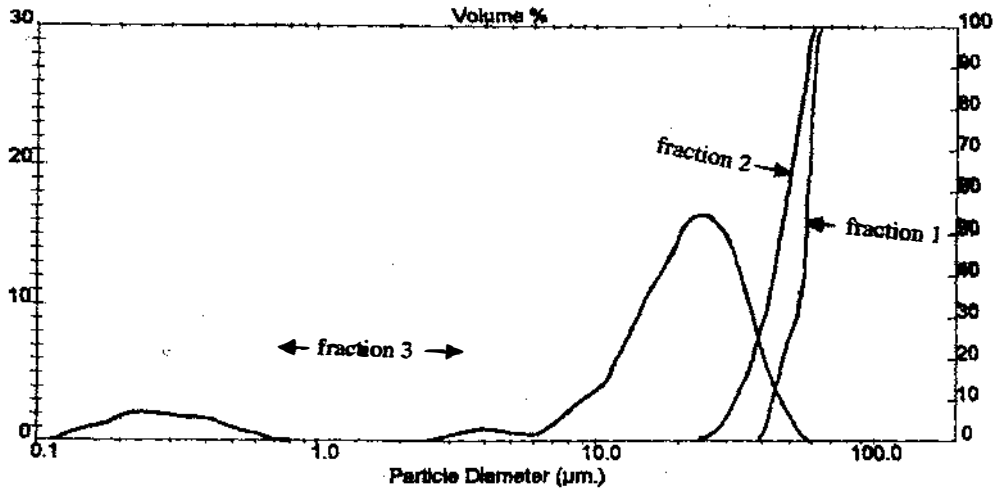

Fig. 5.37 PSD of the three feed fractions (1) >53 μm, (2) 39-53 μm, and (3) < 39 μm used in the study

The flux profiles of the CFMF experiments are shown in Fig. 5.38. J_{ss} was slightly lower for fraction 3 (3.94×10^{-5} m/s) compared to the standard feed (4.25×10^{-5} m/s). Addition of the standard feed particles at the steady-state into a standard feed suspension had no effect on flux as expected (as observed in 5.5.1). However, addition of large particles (fraction 1) caused temporary increase in flux, although the flux quickly returned to the original level. For the feed < 39 μm, addition of both intermediate (fraction 2) and large particles (fraction1) increased J_{ss} to 4.15×10^{-5} and 4.20×10^{-5} m/s, respectively. Although the changes in flux were relatively small (flux improved by ~ 6 %), the effects were reproducible. Further addition of large particles beyond 10 % of original C_{feed} had no effect on flux (data not shown).

The values of J_{ss}, R_m, R_f, R_{re}, and R_{ir} are given in Table A1.13 in Appendix 1. R_m was uniform all throughout this study as expected. R_{re} for the feed < 39 μm was slightly higher (2.39 x 10^{12} /m) than that of the standard feed (2.2 x 10^{12} /m). Although, there was a difference in R_{ir} for these two feed systems (8.99 x 10^{10} and 9.75 x 10^{10} /m respectively), considering that the contribution of R_{ir} to R_f is very small compared to that of R_{re} this had a very little significance. Addition of particle at the steady-state had no effect on R_{ir}.

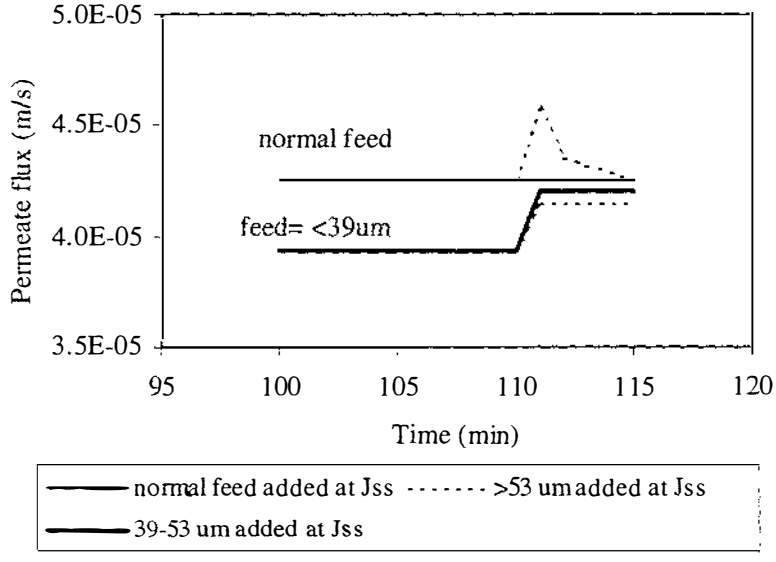

Fig. 5.38 Effect of feed PSD on J and J_{ss} at 100 kPa TMP, 1.5 m/s CFV, using 1.0 μm membrane

The results of the study on the cake properties are given in Table A1.14 in Appendix 1 and the cake mass and PSD for different runs are shown in Fig. 5.39 and Fig. 5.40, respectively. There was no marked difference in the cake mass or height at the steady-state between the feed < 39 μm (mass = 0.017869 kg/m^2, height = 1.9 x 10^{-5} m) and the standard feed (mass = 0.018188 kg/m^2, height = 1.9 x 10^{-5} m). Note also that no marked change in cake mass due to addition of the particles at steady-state was observed. The only marked difference in the PSD between the cakes formed using the feed <39 μm and the standard feed was that the particles > 39 μm, as expected, were present only in the cake formed with the standard particles (detailed PSD not shown). However, there was no effect of the addition of the particles at the steady-state on cake PSD.

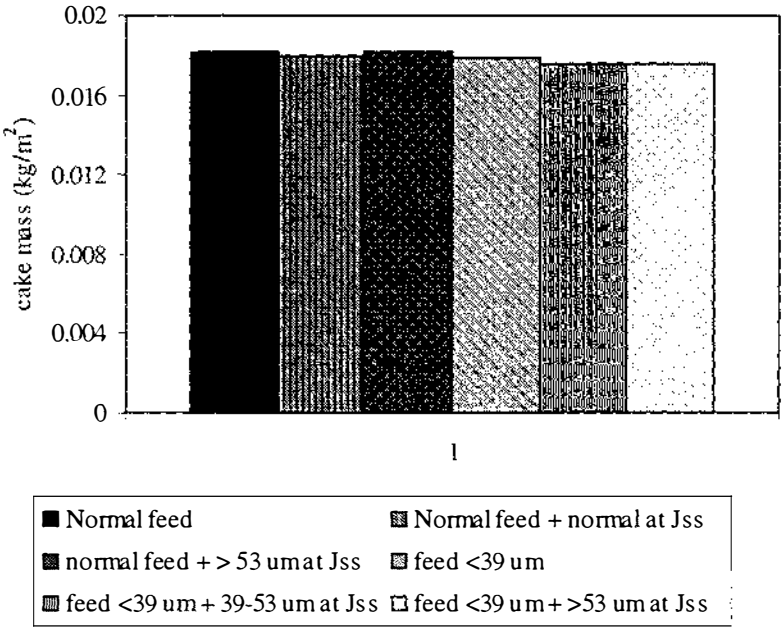

Fig. 5.39 Effect of feed PSD on cake mass for different CFMF runs at 100 kPa TMP, and 1.5 m/s CFV using 1.0 µm membrane

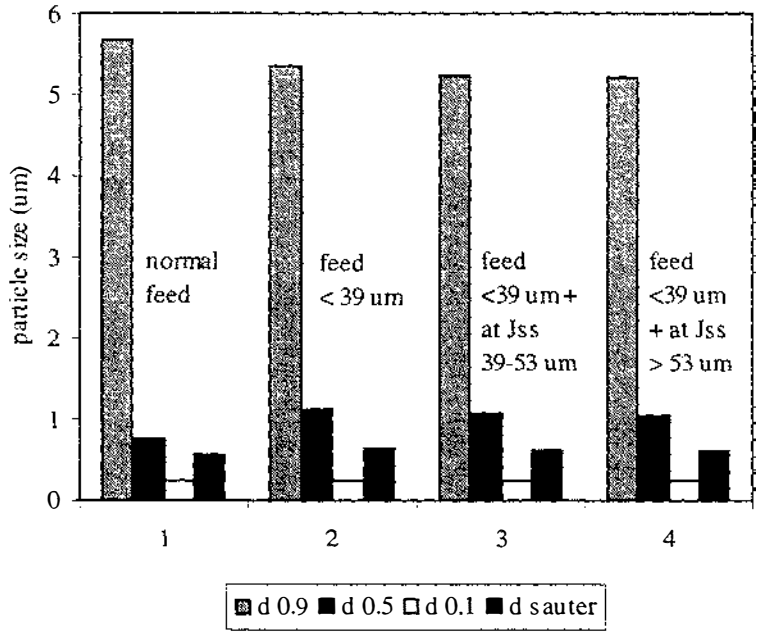

Fig. 5.40 Effect of feed PSD on cake PSD for different CFMF runs at 100 kPa TMP, and 1.5 m/s CFV using 1.0 µm membrane

5.5.2.3 Discussion

The higher fluxes with larger feed particles as observed in this study (Fig. 5.38) are also reported by Wakeman (1994). He reported an increase in both flux and cake thickness with an increase in particle size but did not specify the actual data. The cake porosity was not affected by the feed particle size as there was no marked difference in the cake mass and height for the two feed sizes in the present study. A slight difference in cake PSD for the two feed sizes also, as expected based on the results in 5.4.3 (Fig. 5.26) had no effect on cake porosity. The increase in flux with particle size therefore, can be attributed to the lower cake resistance offered by larger particles. Alternatively, it could be due to greater pore penetration by small particles. However, the contribution of R_{ir} to R_f was not marked in any run. Another possible explanation of the data is that for the same C_{feed} (W/V), a smaller particle feed contains a far greater number of particles compared to the large particle feed. However, as no effect of C_{feed} on J_{ss} above 2.5 g/l was demonstrated in Section 5.5.1, this effect does not appear important. That no change in flux on further addition of standard size feed particles at the steady-state was also in agreement with the results of the effect of C_{feed} on J_{ss} noted in Section 5.5.1.

An improvement in J_{ss} due to introduction of larger feed particles during CFMF has not been reported before. This increase in flux on addition of large particles is very likely to be due to scouring effect of large particles on the cake surface where the partial removal of surface fouling occurs as result of increase in local shear at the cake surface. The concept of improving UF fluxes through increasing local shear by introducing particulate material is not new (Bixler and Rappe 1970). The particle enhancement of flux was successfully used to improve the ability of UF to concentrate proteins and up to 35 % flux improvement was reported (Devereux and Hoare 1986, and Heng Meng and Glatz 1990). In contrast, in the case of CFMF, the scouring particles were thought to possibly have the disadvantage of pushing smaller particles onto the membrane surface (Dekker and Boom 1995). This is disproved by the present study, although clearly the improvement in flux in the present study is not as great as that reported for UF despite of the scouring particles being close to the conventional size range of ~100 µm. In the case of feed containing standard size particles, an increase in the large feed particles at the steady-state had only a temporary effect on flux. This suggests that there may be an equilibrium achieved with respect to scouring effect by large particles

already present in the feed. In contrast, for feed containing small particles, introduction of large particles induces the scouring action and hence, the increase in J_{ss} was permanent. Overall the results further support the hypothesis that the top layers of the cake are mobile, by Mackley and Sherman (1992) and Wakeman (1994).

The change in the surface fouling and hence in J_{ss} due to introduction of the large particles although reproducible, was small and presumably therefore any marked change in cake mass, height or PSD was not detected. The small difference in cake PSD for small particle feed and large particle feed was only in the large cake particle size fraction. The small size fraction of the cake that is expected to contribute most towards the cake resistance was not different for the two feed systems.

There was no great improvement in flux observed due to the addition of large particles in the present study and therefore similar experiments at other levels of CFV were not planned. The level 1.5 m/s was chosen as it was a central value in the entire range of CFV (0.375 – 4.5 m/s) studied in Section 5.4.3. However, varying CFV might affect the level of scouring effect of the large particles and there is a scope to further explore the effect of CFV on the improvement in the flux due to addition of large particles.

5.5.3 Effect of membrane pore size

5.5.3.1 Methods

Three different membrane pore sizes were used in this study - 1.0 μm, 0.8 μm and 0.2 μm. 1.0 μm and 0.2 μm pore size membranes were used in the multi-channel module and 0.8 μm and 0.2 μm pore size membranes in the single-channel module. Information on the effect of pore size on the membrane fouling and cake properties is limited to multi-channel module only.

5.5.3.2 Results

Effect on pure water and steady-state fluxes

The average values of J_w for different membrane pore sizes are given in Table 5.8. Detailed data can be found in Table A1.15 in Appendix 1. In the case of the multi-channel membrane module, 1.0 μm pore size membrane had higher J_w compared to that of 0.2 μm pore size membrane. Similarly in the case of the single-channel membrane module, 0.8 μm pore size membrane gave higher J_w compared to 0.2 μm pore size membrane.

Table 5.5 Average pure water flux for four different membranes

TMP = 100 kPa
CFV = 0.375 m/s to 4.5 m/s

Module	Multi-channel module		Single-channel module	
Pore size	0.2 μm	1.0 μm	0.2 μm	0.8 μm
Average J_w (m/s)	4.09×10^{-4}	5.59×10^{-4}	7.41×10^{-4}	3.43×10^{-3}

To understand the difference in J_w for different pore size membranes of the same type of module, two possibilities: (1) same porosity (total open pore area per unit membrane area), and (2) same pore density (number of pores per unit membrane area) were considered. If both the membranes in each module had the same porosity, then the difference in J_w for the two different pore size membranes would be solely due to the difference in the diameter of the flow channel. Assuming laminar flow through the straight pore channels, Poiseuille's equation for laminar flow in straight tube can be used to correlate flux with the pore diameter (Geankoplis 1993) as:

$$-\frac{\Delta P}{L} = \frac{32\eta v}{D^2} \qquad (5.10)$$

where,

ΔP = pressure drop i.e. TMP (Pa)
L = length of the pore channel (m)
η = fluid viscosity (Pa.s)
v = flow velocity i.e. flux (m/s)
D = pore diameter (m)

Thus, at a given experimental (operating and feed) condition the flux should be proportional to the square of the pore size. Therefore, for the membranes with the same total open pore area per unit membrane area the ratio of flux to the square of the pore size should be the same. However, this was not the case with either of the modules. The ratio J_w/D^2 for 0.2 and 1.0 μm (multi-channel) were 1.0 x 10^{10} and 5.6 x 10^8 respectively, whereas for 0.2 and 0.8 μm (single-channel) were 1.9 x 10^{10} and 5.4 x 10^9 respectively. Thus in the case of both the modules, larger pore size membranes had less porosity. If the pore density was the same for both the pore size membranes, the membrane porosity and therefore, the flux would be directly proportional to the membrane pore size. Therefore, the 1.0 μm multi-channel membrane should have about 5 times greater J_w than that of the 0.2 μm multi-channel membrane and the 0.8 μm single-channel membrane should have four times greater J_w than that of the 0.2 single-channel membrane. Considering the J_w values in Table 5.5 this is certainly not true for multi-channel membranes but it is approximately true for single-channel membranes.

Although, the time required to reach the steady-state during different runs was not significantly affected by the pore size of the membrane, there was a very small difference in the value of J_{ss} for different pore size membranes mainly at higher CFV (Fig. 5.17).

Effect on membrane fouling

Different resistances to the flux for 0.2 μm and 1.0 μm pore size membranes at different CFV are shown in Fig. 5.41. R_m was higher with 0.2 μm pore size membrane (average 2.65 x 10^{11} /m) than that with 1.0 μm pore size membrane (average 1.94 x 10^{11} /m). The R_f, R_{re} and R_{ir} were also slightly higher with 0.2 μm pore size membrane than that with 1.0 μm pore size membrane under the same operating conditions but the differences were very small. Similarly, there was no maked difference between the fouling of the two membranes at different TMP (Table A1.3 and Table A1.4 in Appendix 1).

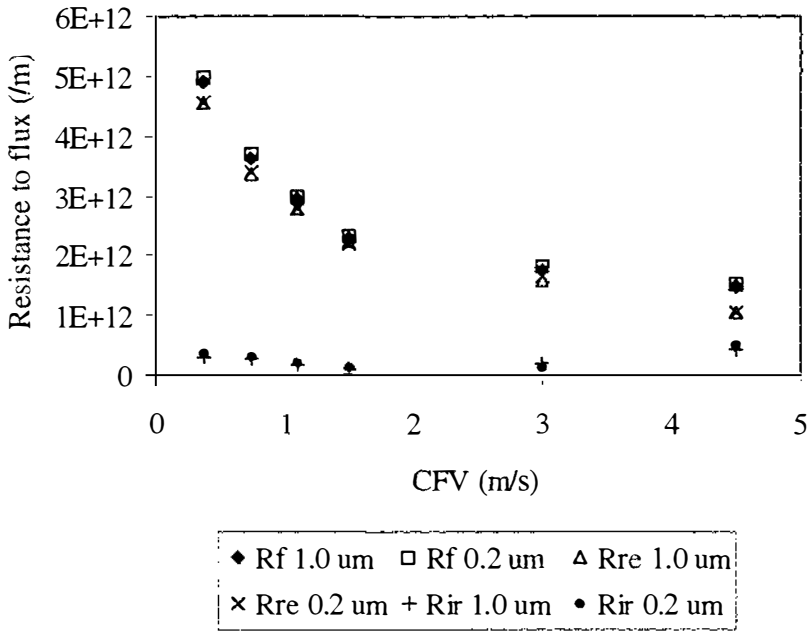

Fig. 5.41 Different resistances to flux at different CFV for different pore size membranes of multi-channel module

Effect on the cake properties

There was no significant difference in the mass, height and porosity of the cakes formed on the two different pore size membranes under the same operating conditions (Table A1.5, Table A1.6 and Table A1.10 in Appendix 1). However, the cake formed on the 0.2 μm pore size membrane comprised slightly smaller particles as compared to the cakes formed on the 1.0 μm pore size membrane. The difference in the cake PSD for the two membranes is shown in Fig. 5.42. The overall particle size was smaller for the cakes formed on the 0.2 μm pore size membrane than that on the 1.0 μm pore size membrane. A similar trend was observed when TMP was varied keeping the CFV constant (Table A1.5 and Table A1.6). However, the difference in cake PSD was also very small for the two pore sizes of the membrane.

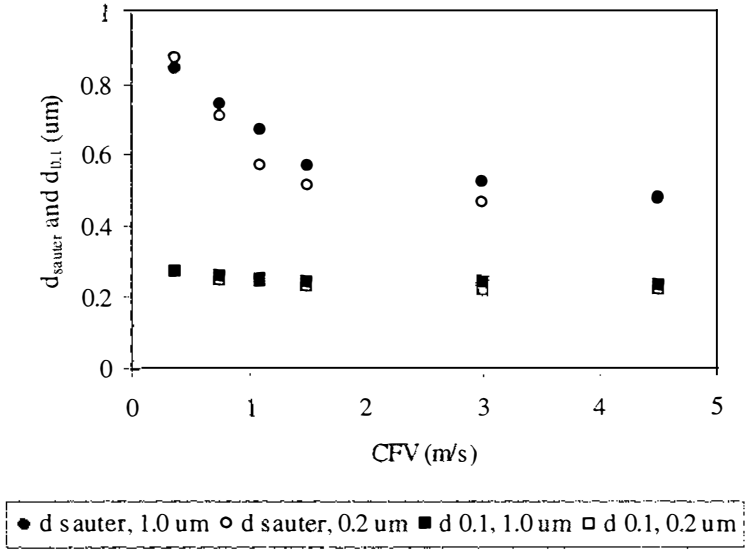

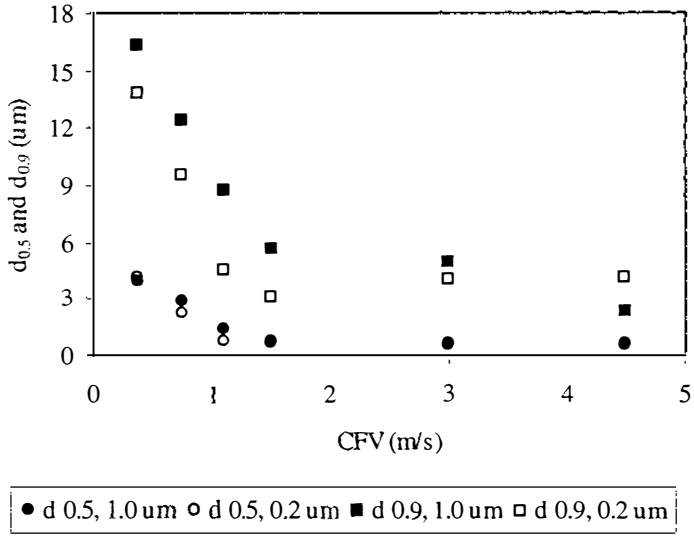

Fig. 5.42 Effect of membrane pore size on cake PSD for the multi-channel module

5.5.3.3 Discussion

The only marked difference between the performances of the membranes was in the resistance offered by the membrane itself. A greater membrane resistance was offered by smaller pore size membrane than that by the larger pore size membrane. This was due to the smaller diameter pore-channels. The analysis on the difference in the J_w for different membranes suggested that the 0.2 μm multi-channel membrane had a greater

porosity as well as pore density compared to than the 1.0 μm multi-channel membrane. Whereas, the 0.2 μm single-channel had a greater porosity and a similar pore density compared to that of the 0.8 μm single-channel membrane. However, this was with an assumption of a perfectly mono dispersed pore size distribution in all cases. Appropriate tests (Mulder 1991) should be carried out to correctly estimate the pore density, pore size distribution and porosity of the membranes. The differences in J_{ss}, levels of internal and surface fouling, or the cake PSD were very small. Therefore, it can be concluded that the significance of the membrane in the studied range of pore size was very little as compared to that of the secondary membrane (cake layer) formed on the surface that governed most of the filtration process.

5.5.4 Effect of module design

As discussed in Chapter 3, two different membrane modules were used for the study. The modules were different in number of tubes and tube diameter but same in length and material of the membrane. For the same dimensions of the modules, the multi-channel module offers greater filtration area, whereas the single-channel module has the advantage of the larger bore. Study on the membrane module design was limited by unavailability of data related to the reversible fouling, irreversible fouling and the properties of the cake in case of the single-channel module.

5.5.4.1 Results

Effect on pure water flux and steady-state flux

The J_w values for different membranes used in the two different membrane modules can be seen in Table 5.5. The single-channel module offered higher J_w than the multi-channel module. The difference was greater with larger pore size membranes. However, no significant difference in J_{ss} was observed (Fig. 5.19).

Effect on membrane fouling

R_m was higher in the case of multi-channel module, but there was no significant effect of the module design on J_{ss} or membrane fouling (Table A1.8 and Table A1.9 in Appendix 1).

5.5.4.2 Discussion

The difference in J_w between the two membrane modules can be attributed to the difference in the design. Again eq. 5.10 can be used to explain the difference in the J_w for the same (or similar) pore size membranes of different modules. Assuming the same porosity, and pore size distribution the measured J_w can be correlated to the length of the pore channels (L). Permeate through the central lumen in the multi-channel module had to travel on a longer and a more tortuous path to reach the permeate outlet compared to the shorter and relatively a straight path in the case of the single-channel module. Differences in porosity and pore size distribution of membranes are also important but unknown factors.

5.5.5 Overall discussion

The lack of a significant effect of the membrane pore size or type of membrane module on the process performance during this study indicates that in the case of CFMF of lactalbumin particles, the key factor was the cake properties. In all the experimental runs, after initial short period of time, the filtration was governed by the cake formed on the membrane surface. The properties of the cake were not affected significantly by the type of the membrane modules studied. The studied range of the membrane pore size (0.2 to 1.0 μm) was not wide enough to cause any major difference in the type of membrane fouling.

Importantly some new effects of feed properties on the process performance were observed during this study. The observed absence of an effect of C_{feed} on J_{ss} beyond a certain level (2.5 g/l in the present study) has not been reported before and is attributed to the force balance mechanism. Different studies on the effect of feed properties reported so far are carried out in a uniform or a narrow size distribution. In the case of

the reports by Wakeman and co-workers, the effect of C_{feed} was studied for large and small feed particles separately. The feed in the present study comprised particles in a wide size range from very small to large (0.1 – 80 μm) which is commonly the case in actual CFMF processes. The observed ~6% increase in J_{ss} on the addition of large lactalbumin particles has disproved the suggestion by Dekker and Boom (1995) that scouring particles are disadvantageous in CFMF. However, the improvement in flux was small compared to that for UF (up to 35%) reported by Devereux and Hoare (1986) and Heng Meng and Glatz (1990). The large particles are thought to be improving the flux through the scouring action or by chipping off of the deposited particles. The live observation of the actual process may confirm the exact mechanism of flux improvement. The results indicate the effect of the large particles may vary for different feed and at different CFV and this also can be further explored. However, for further study, selection of both membrane pore size and material has to be carefully done to avoid any possible adverse effect of large scouring particles on fouling of or damage to the membrane as reported by Dekker and Boom (1995) and Fane (1984). The continuous removal and re-deposition of particles under the possible scouring effect indicates large particles as a cause for the mobility of the cake layers as observed by Mackley and Sherman (1992) and Wakeman (1994). The mobility of the cake layers is further discussed later in Chapter 6.

6. DEVELOPMENT AND APPLICATION OF MATHEMATICAL MODEL

6.1 Introduction

In this Chapter, the evaluation and further development of mathematical models to explain the experimental results obtained during CFMF of lactalbumin is presented. Several mathematical models for CFMF of particulate suspensions based on different theories are found in the literature. These were discussed in Chapter 2.6.

6.2 Resistance in series model

According to the resistance in series model as discussed earlier in Chapter 2.6.1.4, the total resistance to the flux can be broken into resistances due to the membrane, internal fouling, and surface fouling, providing concentration polarisation is neglected for CFMF of particulate suspensions as discussed earlier (Chapter 5.3.3):

$$R_t = R_m + R_{if} + R_{sf} \qquad (6.1)$$

The resistance due to the surface deposit R_{sf} (or cake resistance R_c) can be estimated using the Carman-Kozeny equation (eq. 2.6 which is reported again here as eq. 6.2):

$$R_c = \frac{180 \cdot (1-\varepsilon)^2 \cdot h}{d_p^2 \cdot \varepsilon^3} \quad \text{for mono dispersed particles} \qquad (6.2)$$

where,

R_c = cake resistance (/m)
d_p = particle diameter (m)
ε = cake porosity
h = height of the cake (m)

The cake height can be estimated if porosity and mass of the cake are known (eq. 2.9 reported here as eq. 6.3):

$$h = \frac{m}{\rho_p \cdot (1-\varepsilon)} \qquad (6.3)$$

where,

m = mass per unit area of cake (kg/m^2)
ρ_p = particle density (kg/m^3)

6.2.1 Evaluation of appropriate d_p for the estimation of cake resistance

The cake resistance R_c at the steady-state was estimated based on the cake mass, porosity and PSD using eq. 6.2 and eq. 6.3. A constant porosity of 0.2 was considered. R_c was then compared to R_{re} calculated from the J_{ss} for those constant TMP runs for which cake porosity data were available (Table A1.5, Table A1.10, Table A1.11, and Table A1.14) with the assumption that $R_c = R_{re}$ (i.e. neglecting concentration polarisation). Since eq. 6.2 is for uniform size particles and the cakes in the present study comprised widely size distributed particles, the use of an effective d_p was necessary. The sauter mean diameter (d_{sauter}) is that particle having the same surface-to-volume ratio as the entire particle sample and represents the entire sample better than the ordinary mean particle diameter (Masters 1976). This mean diameter value is commonly used to represent different particle systems that are widely size distributed. Altmann and Ripperger (1997) also used d_{sauter} of a certain cake layer as the effective d_p to estimate R_c during CFMF of the diatomaceous earth particles. Therefore, cake d_{sauter} was used as d_p in eq. 6.2.

6.2.1.1 Results

The calculated R_c values based on d_{sauter} are plotted against R_{re} values of corresponding runs in Fig. 6.1. Clearly R_c values were very low compared to the experimental R_{re} values. This implies that either another resistance contributes to the flux decline or d_{sauter} is a poor parameter to use in the calculations. The only additional resistance contributing to R_{re} is R_{cp} which can not be so significant as found earlier (Chapter 5.3.3). Therefore, the results suggest that d_{sauter} is not truly representative of cake d_p for estimation of R_c. Rather, the effective d_p must be smaller than d_{sauter}.

Different levels of particle size smaller than d_{sauter} namely $d_{0.1}$, $d_{0.2}$, $d_{0.23}$, $d_{0.24}$, $d_{0.25}$, $d_{0.3}$ were evaluated as d_p to calculate R_c. These values were obtained from the cake PSD analyses done using Malvern Mastersizer. Regression analyses between the resultant R_c and the corresponding R_{re} values were carried out for each of these particle sizes to find the most appropriate particle size as d_p. The results are shown in Table 6.1 and from these $d_{0.24}$ was selected to best represent d_p. Estimated R_c values with an assumption $d_p = d_{0.24}$ are plotted against corresponding R_{re} in Fig. 6.2.

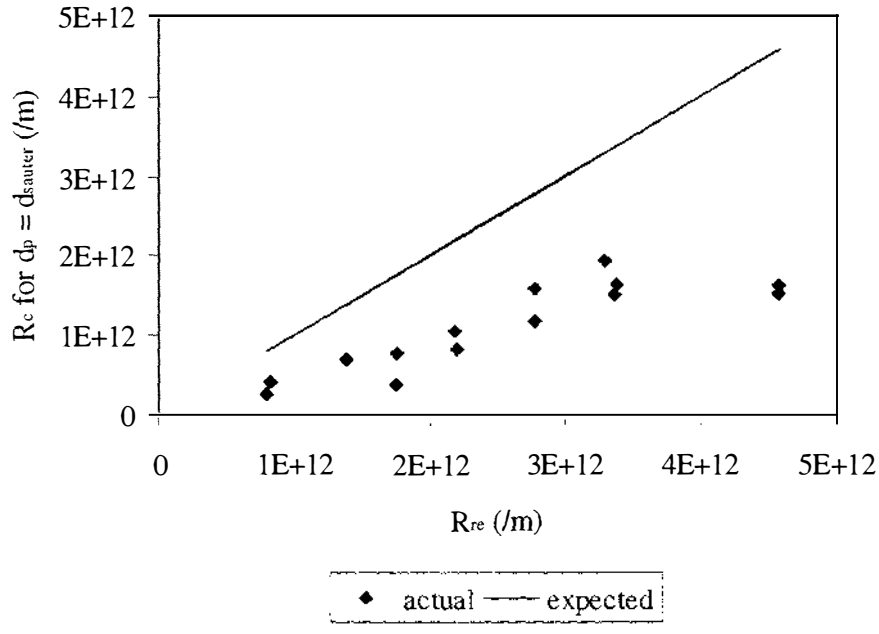

Fig. 6.1 R_c with an assumption that $d_p = d_{sauter}$, versus R_{re} at different CFV, TMP, and C_{feed} using 1.0 and 0.2 μm pore size membranes

Table 6.1 Results of the regression analyses for R_c Vs R_{re} for different parameters considered as d_p

selected parameter as d_p	slope	R^2
$d_{0.1}$	3.31	0.92
$d_{0.2}$	1.41	0.93
$d_{0.23}$	1.13	0.90
$d_{0.24}$	1.04	0.90
$d_{0.25}$	0.95	0.92
$d_{0.3}$	0.64	0.71

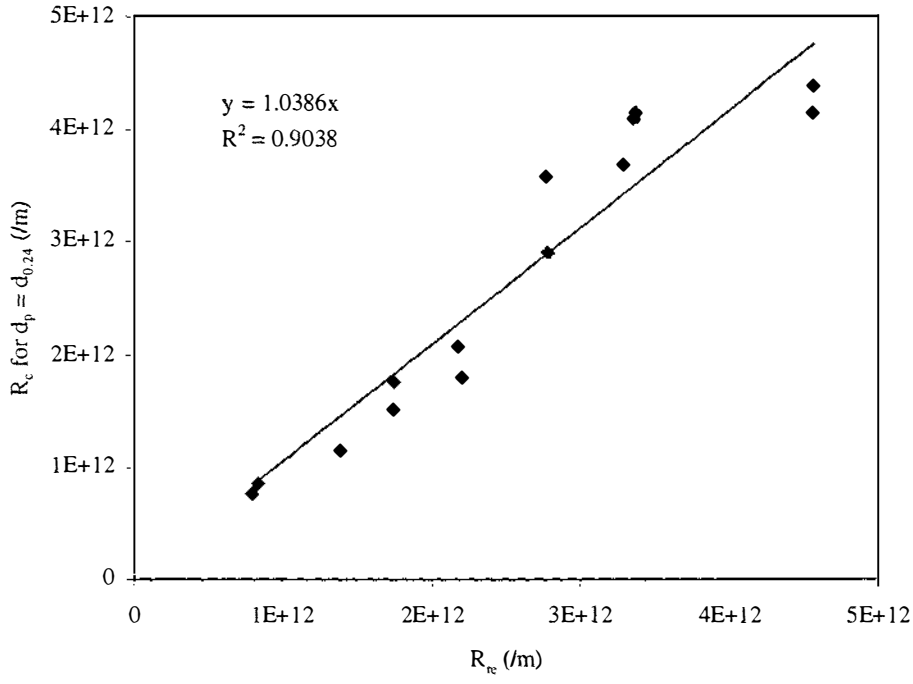

Fig. 6.2 R_{re} versus R_c calculated for $d_p = d_{0.24}$, at different CFV, TMP, and C_{feed} using 1.0 and 0.2 μm membranes

Although $d_{0.24}$ proved a good estimate of d_p, it does not represent the whole cake PSD which varied with operating parameters. The change in the size distribution as a result of different operating regimes should be taken into account to obtain the truly effective d_p for different runs. Considering that the smaller particles are the main contributor to R_c, an attempt was made to include the difference in cake PSD over the small size range of particles together with that for the overall range. The parameter $d_{0.1}$ was chosen to represent the small size range and d_{sauter} was the selected mean value to represent the whole cake PSD. Based on preliminary calculations, a relationship was established as follows:

$$d_p = d_{0.1} + (d_{sauter} - d_{0.1}) \times 0.44 \qquad (6.4)$$

The number 0.44 in eq. 6.4 is an empirical constant that gives the best fit. R_c values based on this model are plotted against the corresponding R_{re} values in Fig. 6.3. The slope improved with this assumption compared to that for $d_p = d_{0.24}$ but at the cost of R^2 which is another important measure of performance. The calculation of d_p is also more complicated in this case.

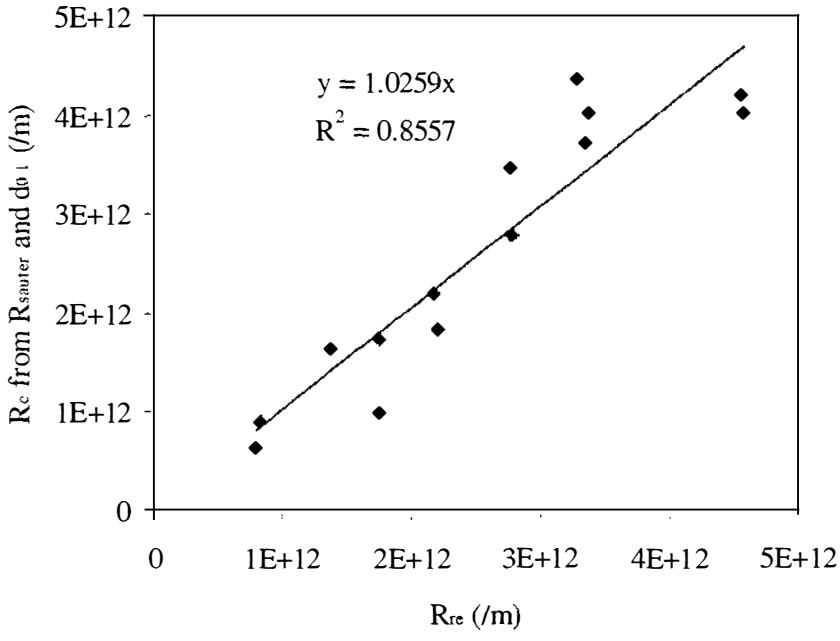

Fig. 6.3 R_{re} versus R_c calculated for $d_p = d_{0.1} + (d_{sauter} - d_{0.1}) \times 0.44$, at different CFV, TMP, and C_{feed} using 1.0 and 0.2 μm membranes

A further attempt was made to include the difference in the entire range of the cake PSD in a similar way by replacing d_{sauter} with $d_{0.9}$ in eq. 6.1 and using an appropriate empirical constant. In this case, when a constant value of 0.02 was used, a good slope (1.055) but with a very poor R^2 (0.48) resulted. Thus, the attempt to include the larger size range in the calculation of R_c was not successful.

6.2.1.2 Discussion

Based on this analysis it is clear that the small particles in the cake play a major role in offering resistance to the flux. Altmann and Ripperger (1997) also successfully estimated R_c using the cake PSD for CFMF of widely size distributed diatomaceous earth (about <1 to 35 μm). They used d_{sauter} of the particles deposited at a 'certain height' of the layer. However, the exact level of the height is not specified as well nor is the reason for the selection of that 'certain height' explained in the report. In comparison, the approach in this study is clearly defined. However, both studies have assumed a constant porosity, whereas in reality the porosity may vary over the cake thickness. The results based on $d_p = d_{0.24}$ and eq. 6.4 are not markedly different. The

assumption $d_p = d_{0.24}$ is simpler and has a better linear fitting (determined by comparing the R^2 values) but slightly poorer matching with the expected trend (slope =1) compared to the latter. However, the latter is more generalised and better represents the whole size range. Regardless, with information on the level of R_{ir}, the flux at any time (J(t)) or J_{ss} during CFMF of particulate suspensions can be estimated using the resistance in series model if the cake mass, porosity and PSD are known. This is a second attempt (after the first by Altmann and Ripperger 1997) to estimate the R_c for widely size distributed cakes and use it to estimate permeate flux applying the resistance in series model. There is a need to further generalise this model to any experimental conditions. Fischer and Raasch (1985), Jang (1987) and Lu and Ju (1989) measured the actual cake PSD during their studies on the CFMF of particulate suspension. However, none of these studies reported the complete information required to check the applicability of the developed relationships between cake PSD and permeate flux.

6.3 Application of force balance mechanism

The flowing cake and surface transport theory using the concept of the single-particle model is considered (Chapter 2.6.3). The experimental results obtained during CFMF of the lactalbumin particles in the constant TMP mode are used to check the applicability of the developed model.

6.3.1 Forces acting on a particle

The various forces acting on each lactalbumin particle can be analysed and depending upon the direction and value of the net resultant force, a particle is presumed to remain either in the feed stream or to deposit and remain on the membrane surface.

A perfectly spherical particle with diameter d_p is assumed to be at the membrane surface to develop the force balance mechanism. Fig. 6.4 shows the forces assumed to be acting on the particle at the membrane surface.

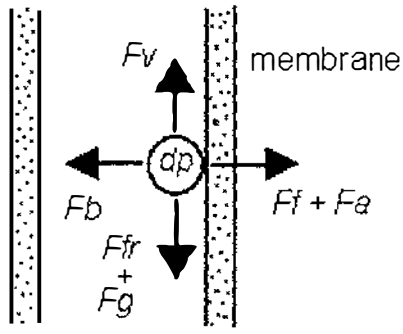

Fig. 6.4 Different forces acting on a spherical particle with diameter d_p at the membrane surface

F_v and F_f are drag forces due to the crossflow velocity and permeate flux respectively. F_b is the back diffusion force caused by either the Brownian diffusion or shear-induced diffusion or the inertial lift (Chapter 2.6.2). F_g is the gravitational force due to the weight of the particle. F_a and F_{fr} are adhesive and friction forces, respectively. As discussed in Chapter 2.6.3, the drag forces F_v and F_f can be estimated using Stoke's equation. F_f can be estimated using eq. 2.23 which is reintroduced here as eq. 6.5.

$$F_f = 3 \cdot \pi \cdot \eta \cdot d_p \cdot J \qquad (6.5)$$

where,

η = feed viscosity (Pa.s)
J = permeate flux (m/s)

If it is assumed that the actual force is 2.11 times the force calculated using the Stokes law (Rubin 1977, Altmann and Ripperger 1997) when applied for the estimation of F_v gives:

$$F_v = 2.11 \cdot 3 \cdot \pi \cdot \eta \cdot d_p \cdot v(z = d_p/2) \qquad (6.6)$$

where,

$v(z = d_p/2)$ = undistributed velocity at position $z = d_p/2$

Since wall shear stress τ_w can be expressed as (Davis 1996)

$$\tau_w = (dv/dy) \cdot \eta \qquad (6.7)$$

Therefore, τ_w at the position $z = d_p/2$ will be

$$\tau_w = \frac{v(z = d_p/2)}{d_p/2} \cdot \eta \qquad (6.8)$$

$$\therefore\ v\,(z = d_p/2) = \frac{\tau_w \cdot d_p}{2 \cdot \eta} \qquad (6.9)$$

Replacing $v\,(z = d_p/2)$ with its value from eq. 6.9, eq. 6.6 can be rewritten as

$$F_v = 3.165 \cdot \pi \cdot \tau_w \cdot d_p^{\,2} \qquad (6.10)$$

where,

τ_w = shear stress (Pa)

As stated earlier (Chapter 5.4.3) τ_w can be calculated as (Holdich *et al.*, 1995):

$$\tau_w = \frac{\Delta p \cdot d}{4L} \qquad (6.11)$$

where,

Δp = pressure drop along the membrane (Pa)
d = diameter of the membrane tube (m)
L = length of the membrane tube (m)

As discussed in Chapter 2.6.3, F_b can also be calculated from Stoke's equation.

$$F_b = 3 \cdot \pi \cdot \eta \cdot d_p \cdot V_b \qquad (6.12)$$

where,

V_b = back diffusion velocity (m/s)

When F_b is due to the inertial lift, it can be estimated based on eq. 2.27 and eq. 2.20 (reintroduced here as eq. 6.12 and eq. 6.13)

$$V_l = \frac{b \cdot \rho \cdot \gamma^2 \cdot r_p^{\,3}}{16 \cdot \eta} \qquad (6.13)$$

where,

b = dimensionless function of dimensionless distance from the wall
ρ = fluid density (kg/m^3)
V_l = inertial lift velocity (m/s)
r_p = particle radius (m)
γ = shear rate (s^{-1})

$$F_b = F_l = 3 \cdot \pi \cdot \eta \cdot d_p \cdot [0.577 \cdot \rho \cdot \gamma^2 \cdot (d_p/2)^3 / 16 \cdot \eta] \qquad (6.14)$$

since for a tube,

$$\gamma = \frac{4 \cdot V_{av.}}{r} \qquad (6.15)$$

where,

$V_{av.}$ = average crossflow velocity (m/s)
r = radius of the tube (m)

Putting the value of γ from eq. 6.15 in eq. 6.14,

$$F_l = \frac{0.216 \cdot \pi \cdot d_p^4 \cdot \rho \cdot V_{av.}^2}{r^2} \qquad (6.16)$$

Alternatively, the lift force, according to the theoretical and experimental analysis of Rubin (1977) which was used by Altmann and Ripperger (1997), can be calculated as follows:

$$F_l = 0.761 \cdot \frac{\tau_w^{1.5} \cdot d_p^3 \cdot \rho^{0.5}}{\eta} \qquad (6.17)$$

When F_b is due to the shear-induced diffusion, eq. 2.17 (reintroduced as eq. 6.18) and eq. 6.12 can be used to estimate F_b

$$V_s = \frac{V_{av} \cdot d_p^2}{20\, r^2} \qquad (6.18)$$

where,

V_s = shear-induced velocity (m/s)

$$\therefore F_b = F_s = 3 \cdot \pi \cdot \eta \cdot d_p \cdot [V_{av.} \cdot d_p^2 / 20 \cdot r^2] \qquad (6.19)$$

$$\therefore F_s = \frac{0.15 \cdot \pi \cdot \eta \cdot V_{av.} \cdot d_p^3}{r^2} \qquad (6.20)$$

When F_b is due to the Brownian diffusion, eq. 2.13 (reintroduced as eq. 6.21) and eq. 6.12 can be used to estimate F_b

$$V_{br} = \frac{k \cdot T}{3\pi \cdot \eta \cdot r \cdot d_p} \qquad (6.21)$$

where,

V_{br} = Brownian diffusion motion (m/s)

k = Boltzmann's constant (1.38×10^{-6} g cm^2/ s^2 °K)

T = absolute temperature (°K)

$$\therefore F_b = F_{br} = 3 \cdot \pi \cdot \eta \cdot d_p \cdot [\, k \cdot T / 3 \cdot \pi \cdot \eta \cdot r \cdot d_p \,] \qquad (6.22)$$

The adhesive forces are caused by Van der Waals forces and by electrostatic interactions. Neglecting the electrostatic interactions, the adhesive forces can be

estimated by calculating the Van der Waals force between two spheres as follows (Visser 1978, Altmann and Ripperger 1997):

$$F_a = F_{vdW} = \frac{\eta\varpi \cdot d_p}{32 \cdot \pi \cdot a^2} \qquad (6.23)$$

where,

$\eta\varpi$ = Lifschitz-Van der Waals constant (10^{-20} J)

a = adhesive distance between two spheres

The friction force F_{fr} is caused by the action of the forces acting towards the membrane surface (i.e. F_f and F_a).

$$F_{fr} = \mu \cdot (F_f + F_a) \qquad (6.24)$$

where,

μ = friction coefficient

The gravitational force due to the weight of the spherical particle F_g can be calculated using eq. 2.28 (reintroduced as eq. 6.25):

$$F_g = \pi/6 \cdot d_p^3 \cdot (\rho_p - \rho_f) \cdot g \qquad (6.25)$$

where,

ρ_p = particle density (kg/m^3)

ρ_f = feed density (kg/m^3)

g = gravitational acceleration (9.81 m/s^2)

6.3.2 Vectorial addition of the forces

If F_1 and F_2 are the two forces acting perpendicular to each other and F_3 is the net resultant force ($F_{resultant}$) acting at angle θ,

Then,

$$F_3 = F_{resultant} = (F_1^2 + F_2^2)^{1/2} \qquad (6.26)$$

and

$$(F_2/F_1) = \tan\theta \qquad (6.27)$$

Applying eq. 6.27 to the situation shown in Fig. 6.1 gives

$$\frac{F_v - (F_{fr} + F_g)}{(F_f + F_a) - F_b} = \tan\theta \qquad (6.28)$$

where,

θ = angle of repose for a particle

6.3.3 Determination of the largest particle in the cake

For a system where the feed contains a wide range of the particle size, a situation as shown in Fig. 6.5 will occur.

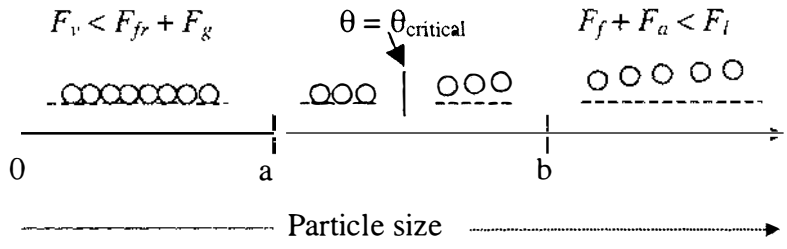

Fig. 6.5 Classification of the particle size range based on magnitudes of different forces acting on the particles

For any particular set of operating conditions of CFMF, in the range of the particle size present in the feed stream, there will be a size of particle for which $F_v = F_{fr} + F_g$. Similarly, there will be a size of particle for which $F_f + F_a = F_l$. These two particle sizes are denoted by 'a' and 'b' in Fig. 6.5, respectively. In the particle size range below 'a', $F_v < F_{fr} + F_g$ and $F_f + F_a > F_l$. Therefore, the value of tan θ given by eq. 6.28 will be negative and the particle will definitely stay on the membrane surface. In the range above 'b', there will be $F_v > F_{fr} + F_g$ and $F_f + F_a < F_l$. Therefore, the value of tan θ will again be negative but the particle definitely will not stay on the membrane surface. In the range between 'a' and 'b', $F_v > F_{fr} + F_g$ and $F_f + F_a > F_l$. The value of tan θ will be positive and $0° < \theta < 90°$. Under this situation, the particle may or may not stay on the membrane surface depending on the angle of repose θ. There is a critical value of the angle of repose i.e. $\theta_{critical}$. If $\theta > \theta_{critical}$, the particle will not stay on the membrane but will do so if $\theta \leq \theta_{critical}$. Therefore, the largest particle size that stays on the membrane will have $\theta = \theta_{critical}$. The value of $\theta_{critical}$ depends mainly on the material and the shape of the particle as well as nature of the deposition surface. Depending on the geometry of the deposition surface, $\theta_{critical}$ will or will not depend on the size of the particle. For a surface of the membrane with pores much smaller than the largest depositing particles, and a feed with spherical particles of the same material, the value of $\theta_{critical}$ will be constant under different operating conditions of CFMF (Lu and Ju 1989, Belfort *et al.* 1994).

6.3.4 Analysis of CFMF results

It was assumed that the largest particle that can go into the cake for any experimental run under constant TMP would settle on the membrane at the beginning of the filtration run. This is because of the highest value of F_f due to the highest flux in the beginning of the filtration (where J = J_w). This assumption is well supported by the results of the effect of the time of filtration on the cake PSD (Chapter 5.3.1). Therefore, the conditions at the beginning of each of filtration run were considered for estimating the largest particle that could go into the cake. Filtration runs carried out under constant TMP mode were considered. The minimum value of 'a' (0.5 nm) in eq. 6.23, and maximum value of 'μ' (1.0) in eq. 6.24 were assumed (Visser 1978). For the runs at 50 kPa TMP and 0.75 m/s CFV, the values of $d_{0.9}$ from the cake PSD were taken as the largest size of the deposited particle and the value of $\theta_{critical}$ for each run was determined. Ideally, the $d_{1.0}$ of the cake deposited should be considered as the largest deposited size. However, $d_{1.0}$ being the upper most level of the size range, the experimental error and run to run variation were more pronounced compared to that at the next lower level i.e. $d_{0.9}$, and hence, $d_{0.9}$ was preferred over $d_{1.0}$. A common value of $\theta_{critical}$ was considered to determine the largest particle size for all of the constant TMP runs at different TMP, CFV, C_{feed} and membrane pore sizes. No correction of the Stoke's law due to C_{feed} was made as the studied levels of C_{feed} were low. The curves representing correction factor versus C_{feed} for diatomaceous earth reported by Altmann and Ripperger (1997) were adopted for lactalbumin for this purpose (Fig. 2.14). Calculations were done for all the three assumptions - $F_b = F_l$, $F_b = F_s$ and $F_b = F_{br}$ to determine the suitable back transport mechanism. F_l was calculated using eq. 6.16. Later, to check the applicability of the semi-empirical formula (Altmann and Ripperger 1997), F_l was estimated using eq. 6.17, and $\theta_{critical}$ as well as the largest d_p values were calculated in a similar way.

6.3.5 Results and discussion

Based on the force balance obtained at 50 kPa TMP and 0.75 m/s CFV, the obtained common value of $\theta_{critical}$ is shown in Table 6.2. The plot of the calculated values of largest d_p (based on $\theta_{critical}$ when $F_b = F_l$) against the measured values of $d_{0.9}$ is shown in

Fig. 6.6. The calculated values of different forces considered to be acting on the particle at 50 kPa TMP and 0.75 m/s CFV, are given in Table A3.1 in Appendix 3. The calculated largest d_p with the assumptions $F_b = F_l$ as well as $F_b = F_s$ for different constant TMP runs and corresponding measured $d_{0.9}$ values are given in Table A3.2 in Appendix 3.

Table 6.2 $\theta_{critical}$ for operating condition 50 kPa TMP and 0.75 m/s

C_{feed} = 2.5 g/l
Membrane module = multi-channel

Membrane pore size	$\theta_{critical}$ (degree)		Average $\theta_{critical}$
(μm)	when $F_b = F_l$	when $F_b = F_s$	(degree)
1.0	65.0	65.0	64.9
0.2	64.8	64.8	

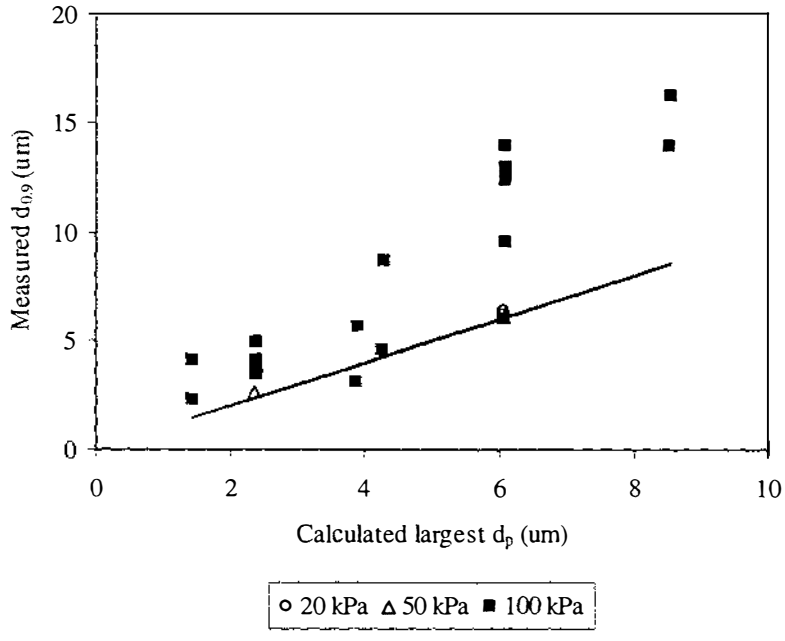

Fig. 6.6 Calculated largest d_p at $\theta_{critical}$ = 64.9° versus measured $d_{0.9}$ of cakes obtained for constant TMP runs

The values of F_{br} as expected were too small to cause any impact on the force balance for the particle size range studied. Although, the obtained values of F_l and F_s were larger than that of F_{br}, they were still significantly smaller than the values of the other

major forces - F_f, F_v, F_a and F_{fr}. Therefore, despite F_l being larger than F_s, the calculated $\theta_{critical}$ (Table 6.1) and largest d_p values were not significantly affected by the type of back diffusion mechanism considered. Thus, the force balance was mainly decided by F_f, F_v, and F_a. Experimental $d_{0.9}$ for cakes formed during runs at TMPs 20 kPa and 50 kPa agreed with the calculated values of largest d_p. However, the calculated values of largest d_p for runs at 100 kPa TMP were far smaller than the experimental $d_{0.9}$ values. That means the largest particles actually found in the cakes formed at 100 kPa TMP were far bigger than the estimated values based on this model. This indicated that the forces acting normal to the membrane surface were actually higher than the calculated. For a rigid particle, TMP is expected to affect only F_f through the change in the permeate flux and this effect is included in the calculations. That suggests the other force normal to the membrane surface, F_a may also be dependent on TMP. This could be due to the elastic deformation of the lactalbumin particles caused by the applied pressure. Since, the level of elastic deformation of particles depends on the level of applied force, this could explain why the experimental values at 100 kPa TMP did not fit on the line. The agreement of experimental values at 20 kPa with the model was probably due to less significant difference in the deformation at 20 and 50 kPa.

A very high F_l (5.5×10^{-10} N) was obtained when estimated using eq. 6.17, the semi-empirical formula used by Altmann and Ripperger (1997), compared to that obtained when eq. 6.16 was used (3.4×10^{-13} N). Eq. 6.17 gave a higher $\theta_{critical}$ of 70° at 50 kPa and 0.75 m/s conditions compared to 64.9° obtained using eq. 6.16 (Table 6.2). However, the trend of calculated largest d_p with respect to the measured $d_{0.9}$ was very similar as that reported in Fig. 6.6 (data not reported). The details on how the semi-empirical formula (eq. 6.17) was derived are not known, hence, the difference in the resultant F_l can not be explained. However, considering the similarity in the resultant d_p versus $d_{0.9}$ plot, it can be concluded that eq. 6.17 despite being semi-empirical, can also be successfully used in force balance analysis.

During the study on the characterisation of lactalbumin particles, any elastic deformation of the particles was not noticed (Chapter 4.4). However, the observed gel formation and softening of lactalbumin particles under prolonged soaking in water (Chapter 4.3), could be of significance in explaining the assumed effect of pressure on

elastic deformation. That means the change in the rigidity of the lactalbumin particles which depended on the time of soaking, during the filtration, were probably too small to observe during the studies on the estimation of cake height and porosity (Chapter 4 and Chapter 5).

6.3.6 Extension of the model to accommodate the particle deformation

Changes were made in the model to accommodate the effect of elastic deformation of the lactalbumin particles under the applied pressure conditions. Changes were made to the theoretical assumptions in the developed model and the force balance was recalculated to estimate the largest d_p values for each experimental run.

6.3.6.1 Model development

The spherical particle at the membrane surface was assumed to be undergoing elastic deformation due to the applied pressure as shown in Fig. 6.7.

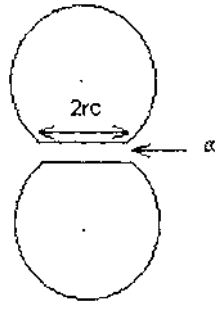

Fig. 6.7 Elastic deformation of lactalbumin particle under applied pressure

According to the theoretical analyses by Visser (1978), F_a acting on the compressible sphere for the situation shown in Fig. 6.7 is the sum of the adhesive force between the two spheres and the adhesive force between two flat surfaces. This can be obtained as:

$$F_a = \frac{\eta\varpi \cdot d_p}{32 \cdot \pi \cdot a^2} + \frac{\eta\varpi}{8 \cdot \pi^2 \cdot a^3} \cdot \pi r_c^2 \qquad (6.29)$$

where,

r_c = radius of the contact area (m)
(as shown in Fig. 6.7)

Radius r_c is given by (Visser, 1978):

$$r_c = [\, 3/8 \cdot d_p \cdot F \cdot \{ (1-\sigma_1^2)/E_1 + (1-\sigma_2^2)/E_2 \}]^{1/3} \qquad (6.30)$$

where,

σ_1, σ_2 = Poisson's ratio of materials
E_1, E_2 = Elastic deformation moduli of materials (Pa)
F = Force causing deformation (N)

Since it is assumed that the adhesive force is inter-particle, and elastic deformation due to applied pressure, $\sigma_1 = \sigma_2 = \sigma$ and $E_1 = E_2 = E$, and $F = F_f$.

Considering $\sigma = 0.5$ for an elastic material,

$$r_c = [\, 0.5625 \cdot d_p \cdot F_f/E]^{1/3} \qquad (6.31)$$

To calculate F_a based on the above assumption (in 6.5.1), a value of the elastic deformation moduli (E) for lactalbumin soaked in water for 1 - 3 hours (time range used for filtration runs) is required. The value of E for wet lactalbumin or for other similar material softened by wetting is not known. Therefore, based on the discussion about the probable level of rigidity of lactalbumin(6.3.5), values of E in the wide range of 1×10^5 to 1×10^8 Pa were used for calculation. This range covers soft to semi hard material (Perry and Green 1984). For each value of E, different values of $\theta_{critical}$ in the whole range of 1° - 89° were taken to calculate the largest d_p for different constant TMP runs using the modified model equation. Regression analysis between the calculated largest d_p and measured $d_{0.9}$ values for all constant TMP runs for different combinations of $\theta_{critical}$ and E was used to obtain the best estimates of $\theta_{critical}$ and E. Since it was established that the type of back diffusion mechanism (shear-induced diffusion or inertial lift) chosen had no significant effect on the results, this time only $F_b = F_l$ was considered for the calculations.

6.3.6.2 Results and discussion

The detailed results of the regression analysis are shown in Appendix 3. The regression results of d_p versus $d_{0.9}$ only for the best suited $\theta_{critical}$ for each of the four levels of E are picked from these detailed results and reported in Table 6.3. Calculated values of the largest d_p for the best suited values of $\theta_{critical}$ for all levels of E are given in Table A3.3

in Appendix 3. Among the four most suitable combinations, one each for four different levels of E shown in Table 6.3, the combination $\theta_{critical}$ = 17° and E = 1 x 10^6 Pa gave the best linear fit with the slope of the line very close to unity. Thus, these were the best suited values of $\theta_{critical}$ and E. The calculated largest d_p at $\theta_{critical}$ = 17° and E = 1 x 10^6 Pa are plotted against the measured values of $d_{0.9}$ in Fig. 6.8.

Table 6.3 Regression analysis between calculated largest d_p at the best suited level of $\theta_{critical}$ for each level of E

E (Pa) – corresponding best suited $\theta_{critical}$ (°)	Regression out put	
	slope	R^2
1 x 10^8 – 73	1.04	0.755
1 x 10^7 - 65	1.01	0.859
1 x 10^6 - 17	1.01	0.887
1 x 10^5 - < 0.001	N.A	N.A

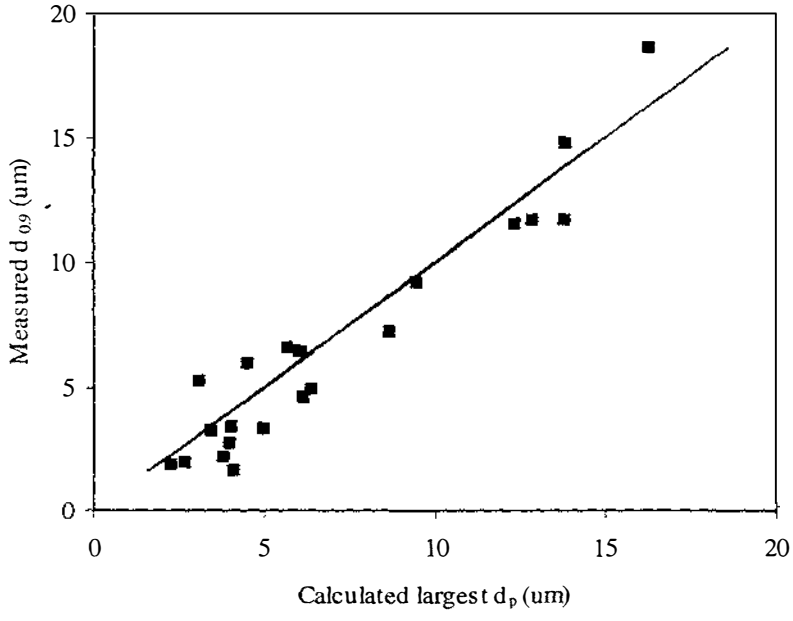

Fig. 6.8 Largest d_p estimated when E = 1 x 10^6 Pa and $\theta_{critical}$ = 17° versus $d_{0.9}$ of cakes obtained from constant TMP runs

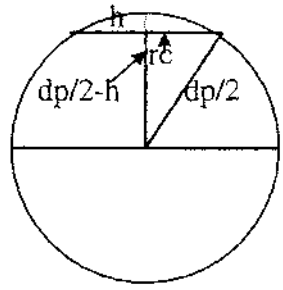

Fig. 6.9 Elastic deformation 'h' of a spherical particle under applied pressure

Based on the value of r_c, the linear deformation of a spherical particle as shown in Fig. 6.9 can be calculated as follows:

$$(d_p/2-h)^2 = (d_p/2)^2 - (r_c)^2 \qquad (6.32)$$
$$\therefore (d_p/2-h) = [(d_p/2)^2 - (r_c)^2]^{1/2}$$

For the largest particle (d_p = 16.29 μm) deposited at 100 kPa TMP - 0.375 m/s CFV

$$(16.29/2 - h) = [(16.29)^2 - (0.11)^2]^{1/2} = 8.1443$$
$$\therefore h = 7.43 \times 10^{-4} \text{ μm} = 0.743 \text{ nm}$$

It is obvious that this level of elastic deformation of a single lactalbumin particle soaked in water could not be detected without high magnification. An Atomic Force Microscope or other similar equipment can be used after developing and standardising the correct procedure for this purpose (Instruction manual, nanoscope [Atomic Force Microscope], Digital Instruments). Due to unavailability of such an instrument, detection the elastic deformation of lactalbumin particles could not be done during the present study. However, there is a scope to advance this study in that area.

Although F_f is not a major force keeping the particle at the membrane surface compared to other forces F_a and F_{fr}, it plays an important role in deciding the size range of the particles that can stay on the membrane surface at any stage of the filtration run. This is because F_f changes with time due to the continuous drop in flux under constant TMP mode.

From the force balance, with increased time of filtration the size of the largest particle that stays on the membrane surface also changes. As the cake grows the largest size of

the particle that can deposit on the cake decreases. Hence, the cake should comprise layers of different particle sizes, with the size of particles becoming smaller from bottom to top. That does not mean that only larger particles are deposited in the early part of the run. This is well supported by the findings in the present study (Fig. 5.7 and Fig. 5.8) as well as in the other studies where the cake was observed or the cake PSD was measured (Jang 1987, and Altmann and Ripperger 1997). However, the smaller particles that settle later, can contribute to the previous layer(s) by penetrating into the inter-particular voids and packing the layer(s) more densely. Ideally, the forces at the steady-state should be balanced and hence, no further deposition or removal of particles should take place. However, the results in the present study (Chapter 5.6.2) as well as the cake observations reported by Mackley and Sherman (1992) and Wakeman (1994) suggest that the top cake layer is mobile. The particles have been observed to continuously deposit, roll along the cake surface and leave. This could be due to the difference in the local force balance and the overall force balance at the entire membrane surface. This could also be due to the scouring effect of large particles as suggested by the results in the present study (Chapter 5.6.2). The model also explains the size classification effects as a result of shift in the force balance towards (change in TMP or flux), as well as away from (change in CFV), the membrane surface, as observed in the present study as well as other studies (Fischer and Raasch 1986, Jang 1987, Lu and Ju 1989, Foley *et al.* 1992, and Altmann and Ripperger 1997). That suggests the possibility of predicting the operating conditions for depositing certain size range of particles or predicting the cake PSD under the given operating conditions. These possibilities should be explored. This can be done more conveniently under constant flux operation. The validity of the assumption that the lactalbumin particles are compressible as well as the estimated value of E can also be checked from the accuracy of such predictions. This is carried out later (see Chapter 7.7). Unfortunately detailed studies on or models for the CFF of compressible particles are not found in the literature. Therefore, the developed model at present is limited to this study only. At present it is not possible to check its validity for various compressible particles or to compare its performance with other similar models. Further work is necessary in that direction.

7. CFMF OF LACTALBUMIN UNDER CONSTANT FLUX MODE

7.1 Introduction

The information revealed by the study on CFMF of lactalbumin particles under the constant TMP mode (Chapter 5) clearly enhanced understanding of the process and the results of this study could be explained by the resistance in series and force balance mechanisms (Chapter 6). However, the information obtained through the conventional constant TMP mode of operation is limited by the changing conditions due to changing flux with time. Alternatively, in the constant flux mode TMP becomes a dependent variable. It offers better control over the flow of material since the flow towards the membrane is constant throughout the run. Another important aspect of constant flux is the concept of critical flux as hypothesised by Field *et al.* (1995), and therefore, the possibility of operating without membrane fouling. This study was carried out with an aim of exploring these aspects of constant flux mode to obtain further information on the performance of the CFMF of lactalbumin particles.

7.2 Experimental set-up

The schematic diagram of the experimental set-up used for constant flux operation is shown in Fig. 7.1. The experimental set up used for constant TMP operation (Fig. 3.1) was modified such that the permeate outlet was connected to a peristaltic pump. The flow from the peristaltic pump was taken to the balance for flux measurement or diverted to the feed tank.

The feed side pressure, CFV, and the filtration temperature were set to the desired level as for constant TMP mode (Section 3.2.2). To change the flux, the speed of the peristaltic pump was adjusted.

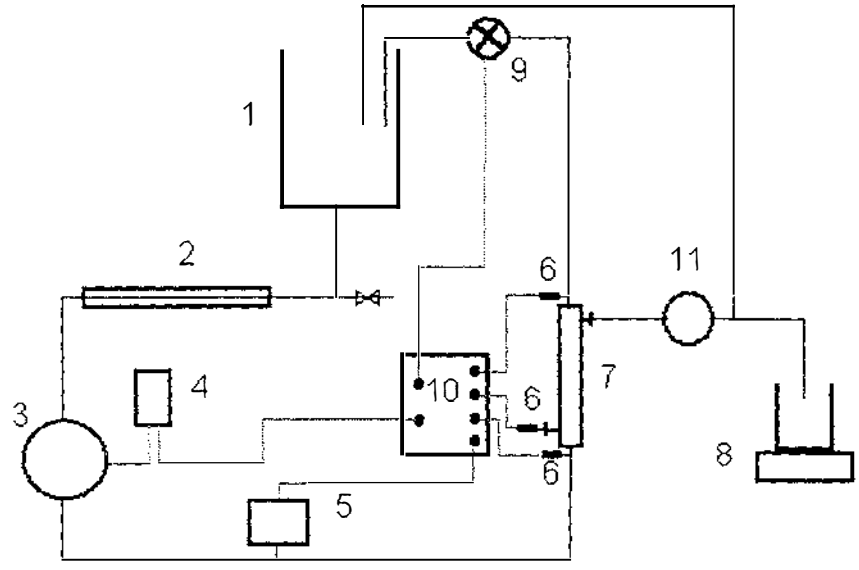

Fig. 7.1 Schematic of the experimental set-up for constant flux operation-
(1) jacketed feed tank, (2) heat exchanger, (3) rotary pump,
(4) frequency inverter, (5) magnetic flowmeter,
(6) pressure transducers each on inlet side, outlet side and
permeate side of the membrane module, (7) membrane module,
(8) weighing scale (9) electro-pneumatic valve and (10) control panel
(11) peristaltic pump

7.3 Running the experiment

J_w with the clean membrane was measured in constant TMP mode using RO water under the pressure and CFV conditions of the constant flux run. The feed suspension prepared as described earlier wasplaced in the balance tank and circulation started at a set feed side pressure, CFV and filtration temperature. The desired flux was then set by operating the peristaltic pump at predetermined speed. The permeate flux was measured as described earlier. The permeate was recycled to maintain C_{feed} and TMP was recorded at certain intervals throughout the experiment.

7.4 Determination of critical flux

7.4.1 Methods

Experimental runs were carried out at 0.375, 0.75, 1.1, 1.5, 3.0, and 4.5 m/s CFV at 100 kPa feed side pressure, 18 °C filtration temperature and 2.5 g/l C_{feed}. Both the membrane modules and all three membrane pore sizes were used in this study. J_{ss} at

corresponding CFV from the 100 kPa constant TMP runs was used as an initial estimate of J_{cr} value under the constant flux mode. Each run was started at a constant flux value well below J_{ss} ($< 0.5J_{ss}$) and maintained for 20 min to observe any increase in the TMP due to membrane fouling. If there was no change in TMP in 20 min, the constant flux was stepped up to the next level. This was continued until membrane fouling commenced, as indicated by a continual increase in TMP. The lowest value of the constant flux at which TMP began to increase due to fouling was recorded as J_{cr}. Based on measured TMP values, R_t was calculated using Darcy's law as described in Chapter 5.2.2.

7.4.2 Results

The plot of R_t versus time for the run at 4.5 m/s CFV is shown in Fig. 7.2. On stepping up the flux, R_t increased but remained constant until the next step up in the flux. However, once the constant flux was stepped up to J_{cr}, R_t increased with time without any further increase in flux. This was typical of the behaviour observed for all constant flux runs.

J_{cr} at different CFV for different membranes are given in Table A2.1 in Appendix 2. These values are plotted against CFV in Fig. 7.3. J_{ss} values at different CFV at 100 kPa TMP and J_{cr} values at different CFV for 1.0 μm pore size membrane are shown together in Fig. 7.4 for comparison. For other membranes, J_{ss} values can be obtained from Table A1.4 and Table A1.5 in Appendix 1 for comparison with J_{cr}. J_{cr} increased with increase in CFV. The trend was very similar to that of J_{ss} with CFV (Fig. 5.19). The values of J_{cr} were very close to the J_{ss} values under the same operating conditions. J_{cr} generally were slightly (~0.2 to 6 %) lower than corresponding J_{ss} values for different membranes used. Overall, J_{cr} values were slightly lower for 0.2 μm membrane compared to 1.0 μm (or 0.8 μm in the case of single-channel module).

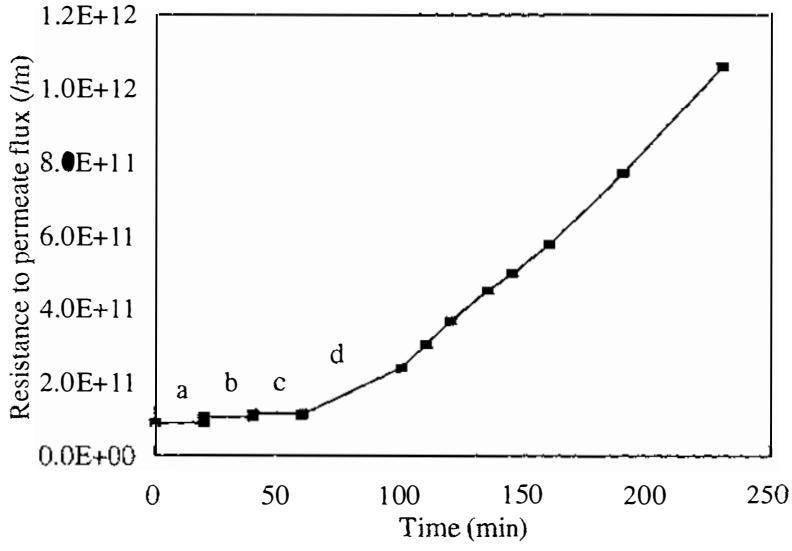

Fig. 7.2 Change in R_t with time at 4.5 m/s CFV, 100 kPa feed side pressure, 2.5 g/l C_{feed} at fluxes (a) 4.7 x 10^{-5}, (b) 5.9 x 10^{-5}, (c) 6.4 x 10^{-5}, and (d) 6.6 x 10^{-5} m/s

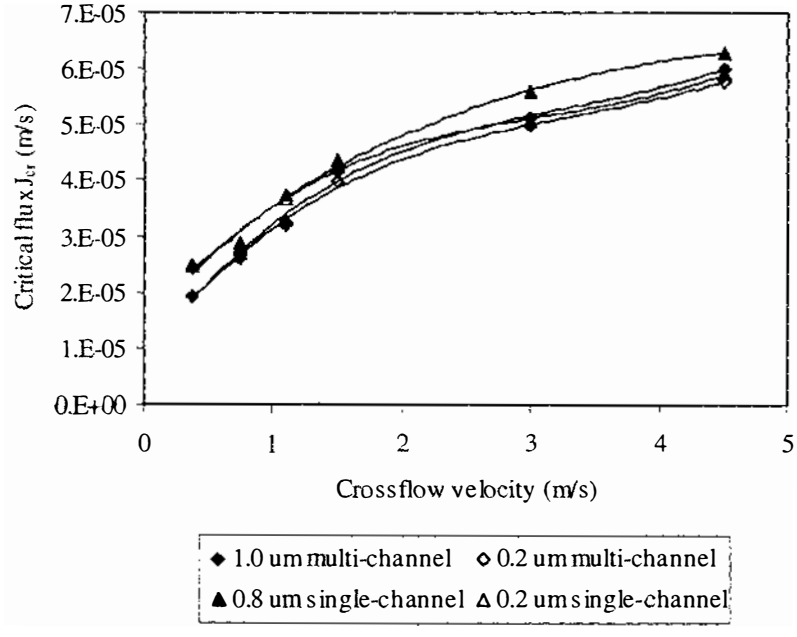

Fig. 7.3 Effect of CFV on J_{cr} at 100 kPa feed side pressure, and 2.5 g/l C_{feed}

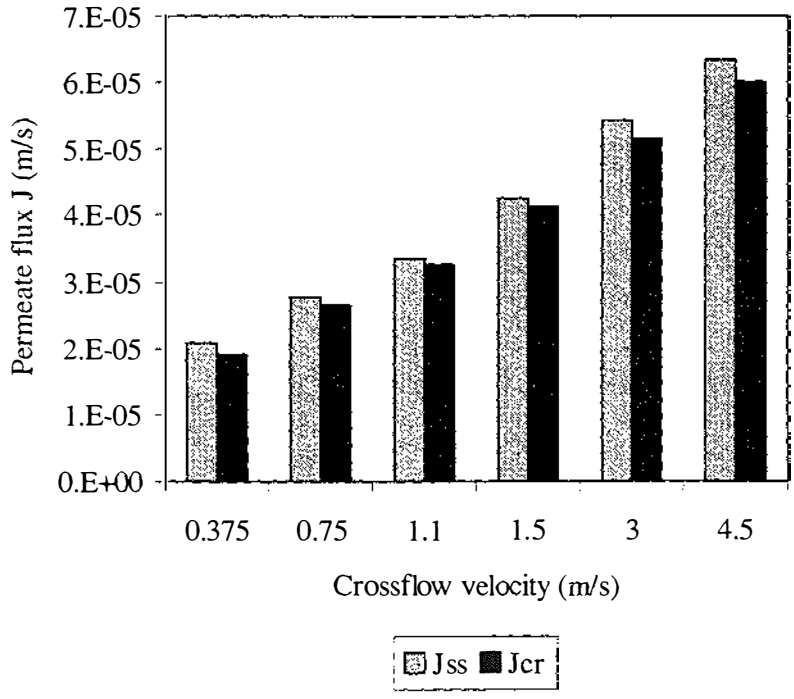

Fig. 7.4 Comparison of J_{ss} and J_{cr} at different CFV for 1.0 μm pore size membrane

7.4.3 Discussion

There are not many reports on the constant flux filtration of particulate suspensions. Further, in the literature, there is also a natural tendency to focus the results and discussion only on the changes at J_{cr}, as that is the part of major interest. However, a step incrase in R_t with step-up in flux at $J < J_{cr}$ as seen here, was also observed by Kwon *et al.* (1996) during constant flux CFMF of mono-dispersed polystyrene latex particles. In their work, based on the reported time versus TMP plot for the conditions of 0.3 m/s CFV and 10 mg/l C_{feed}, with 0.46 μm particle size and 0.2 μm pore size; R_t increased up to 7.2 x 10^{-8} m^{-1} with step change in flux below J_{cr}. This may not be due to the membrane fouling because R_t did not increase with time at $J < J_{cr}$. Therefore, further experiments were carried out later to investigate the absence of fouling at $J < J_{cr}$ (see Section 7.5).

Considering the force balance, at $J = J_{cr}$, the net resultant force on a feed particle is expected to be just strong enough to cause its deposition on or into the membrane. Once fouling commences, it continues during further filtration and causes an increase in R_t with time. Due to a greater drag force towards the retentate outlet at higher CFV, the

fouling only occurred at a higher permeate flux, and so, J_{cr} increased with CFV. Kwon *et al.* (1996) observed a linear increase in J_{cr} with CFV in the range of 0.1 to 0.35 m/s. The J_{cr} trend with respect to CFV in the lower range of 0.375 to ~1.1 m/s which is nearly linear (Fig. 7.3), suggests the possibility of a linear increase in J_{cr} with CFV in the range of 0.1 to 0.35 m/s in the present study too. However, due to the different ranges of CFV used in the two studies, a direct comparison between the two is not possible. Once again as in the case of J_{ss} (Fig. 5.19), the difference in J_{cr} for different pore size membranes was not marked. Kwon *et al.* (1996) also reported no significant effect of membrane pore size (in the range 0.1 to 0.65 μm) on J_{cr} during CFMF of mono sized (0.816 and 3.2 μm) polystyrene latex particles. However, only surface deposition would have taken place, unlike in the present study with lactalbumin as, the particle sizes were always greater than the pore size range in their study.

Importantly, as at $J = J_{cr}$ the net resultant force is just enough to cause the particle deposition, only the smallest particles are expected to deposit at J_{cr} when the feed particles are widely size distributed. Therefore, when some of the feed particles are smaller than the membrane pore size, as in the case of the present study, at constant $J \cong J_{cr}$ the membrane is expected to severely foul from inside. Interestingly, this may lead to a totally different type of membrane fouling than that observed under constant TMP mode where the surface fouling dominated (Chapter 5).Furtherexperiments were carried out later to study the fouling under constant flux (see Section 7.6).

7.5 Further investigation of the absence of fouling at $J < J_{cr}$

7.5.1 Methods

To investigate the absence of fouling at $J < J_{cr}$ further runs were conducted at 0.75 and 3.0 m/s CFV using the 1.0 μm multi-channel membrane. The flux was increased from a low value to a value just less than J_{cr} and held for 30 minutes. The flux was then reduced to the original low value. Then the flux was increased to J_{cr} and held for 30 minutes and then again reduced to the original low value. The TMP values were recorded and R_t was calculated.

7.5.2 Results and discussion

The results of this study are given in Table A2.2 in Appendix 2. The plots of the R_t versus time for the runs at 0.75 and 3.0 m/s CFV are shown in Fig. 7.5.

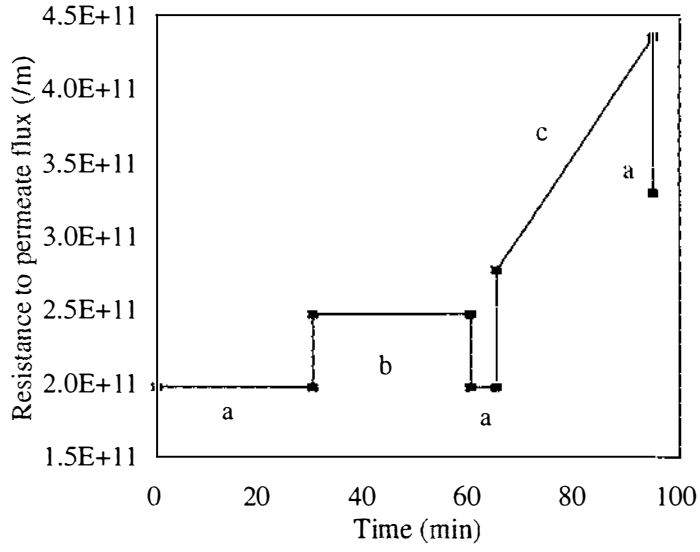

(i)

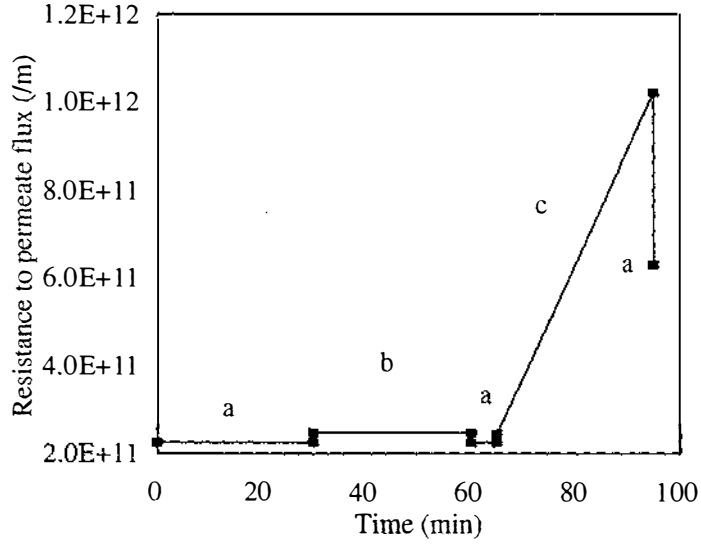

(ii)

Fig. 7.5 Reversibility of change in R_t with change in the flux at and below J_{cr} at (i) 0.75 m/s CFV where flux a = 1.6, b = 2.6, and c = 2.7, x 10^{-5} m/s and (ii) 3.0 m/s CFV, where flux a = 4.7, b = 5.1, and c = 5.2, x 10^{-5} m/s, 100 kPa feed side pressure and 2.5 g/l C_{feed} using a 1.0 μm pore size membrane

The increase in R_t due to stepping up the flux at $J < J_{cr}$ was relatively small as well as fully and instantly reversible. But the increase in R_t with time at $J = J_{cr}$ was significant and not completely reversible.

As discussed earlier (Section 7.4.3), with increasing flux under the increased flux force F_f the smallest particles will deposit first. Since, the smallest particles in the present study are smaller (0.1 μm) than any of the membrane pore sizes (0.2, 0.8 and 1.0 μm) studied, this were expected to first cause internal fouling which is found earlier to be completely irreversible (Chapter 5.3.2). Therefore, the complete and instant reversibility of R_t at $J < J_{cr}$ confirmed the absence of membrane fouling. Considering the resistance in series model (Chapter 2.6.1.4), R_t is usually modelled as the sum of R_m, R_{ir}, R_{re}, and R_{cp}, where, R_{cp} is resistance due to concentration polarisation. When fouling is absent, R_t is due only to R_m and R_{cp}. R_m is taken as constant with change in flux or other parameter. However, R_{cp} can increase with increase in flux due to increased concentration polarisation. Increased F_f due to an increase in flux drives more particles towards the membrane surface and increases the concentration of the polarisation layer (Fig. 2.8). Hence the increase in R_t below J_{cr} is attributed to concentration polarisation. The present study is first to explain this phenomenon. The drop in R_t with reduction in the flux to the original low value after operating at J_{cr} indicated removal of a part of the fouling due to reduction in flux. This could be due to partial removal of the reversible surface fouling, that could have occurred in long run after the initial period of internal fouling, as a result of the drop in the drag force towards the membrane surface. This offers the possibility of the removing deposits by operating at below J_{cr}. This possibility is further explored later (see Section 7.8.2).

7.6 Fouling of the membrane

This study was aimed at understanding the mechanisms of the membrane fouling by lactalbumin particles under constant flux mode, and then comparing the fouling behaviour with that under constant TMP mode.

7.6.1 Methods

The experiments in this study were carried out at constant fluxes J = J_{ss} (obtained for 100 kPa constant TMP runs) at different CFV. The feed side pressure was kept 100 kPa, and each run was continued until the TMP became 100 kPa (i.e. permeate side pressure dropped to '0'). The conditions J = J_{ss} and feed side pressure = 100 kPa, and the continuation of run until TMP = 100 kPa were considered to obtain the same level of total fouling at the end of the run as that at the end of constant TMP (100 kPa) run at the corresponding CFV. This was to provide basis for comparison of fouling in the two modes of operation. Only the 1.0 μm multi-channel membrane was used in this study. Different resistances to the permeate flux were estimated as explained earlier in Chapter 5.2.2. The cakes deposited on the membrane surface, whenever thick enough, were recovered and analysed for their PSD using the Mastersizer. The cake was analysed for each set of experimental conditions only once in this case.

7.6.2 Results

The values of different resistances to the flux are shown in Table A2.3 in Appendix 2 and plotted in Fig. 7.6. There was a decrease in R_f and R_{re} with increase in CFV. The R_{ir} initially decreased with increase in CFV from 0.375 to 0.75 m/s, but beyond that increased with increasing CFV. At CFV ≤1.5 m/s, R_{re} was the main contributor to R_f, but at 4.5 m/s CFV, R_{ir} became dominant. The values of R_{re} and R_{ir} in constant TMP and constant flux modes are compared in Fig. 7.7. R_{ir} values under constant flux mode were greater than that in constant TMP mode. Since the values of R_f were same, the R_{re} was lower for constant flux runs than that for constant TMP runs.

The change in the proportion of R_{re} and R_{ir} with change in CFV is shown in Fig 7.8. The proportions of R_{re} and R_{ir} under constant TMP mode are also shown in Fig. 7.8 for comparison. In constant flux mode at CFV below 3.0 m/s, R_{ir} was lower than R_{re}. The proportions of the two were just equal at 3.0 m/s and R_{ir} was higher than R_{re} beyond 3.0 m/s.

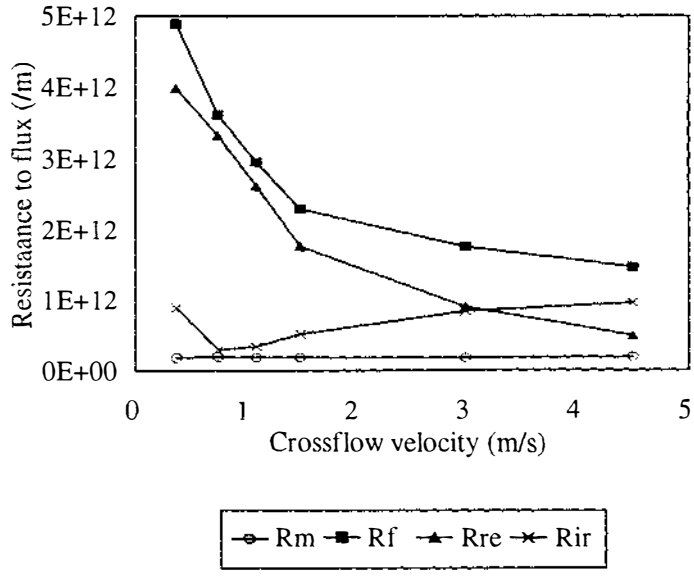

Fig. 7.6 Different resistances to the permeate flux at different CFV at flux $J = J_{ss}$, 100 kPa TMP, and 2.5 g/l C_{feed}, using 1.0 μm pore size membrane

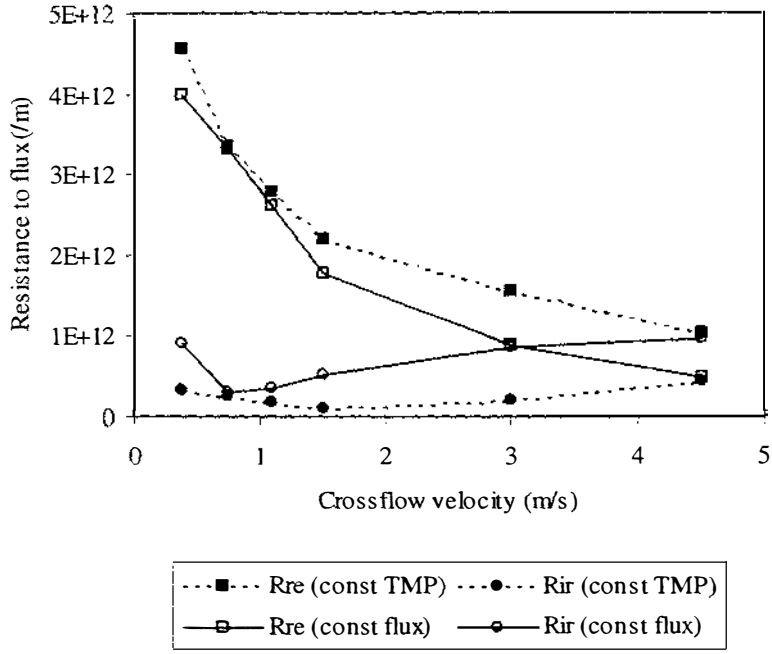

Fig. 7.7 Comparison of Rre and Rir under the two modes of operation 2.5 g/l C_{feed}, using 1.0 μm multi-channel membrane

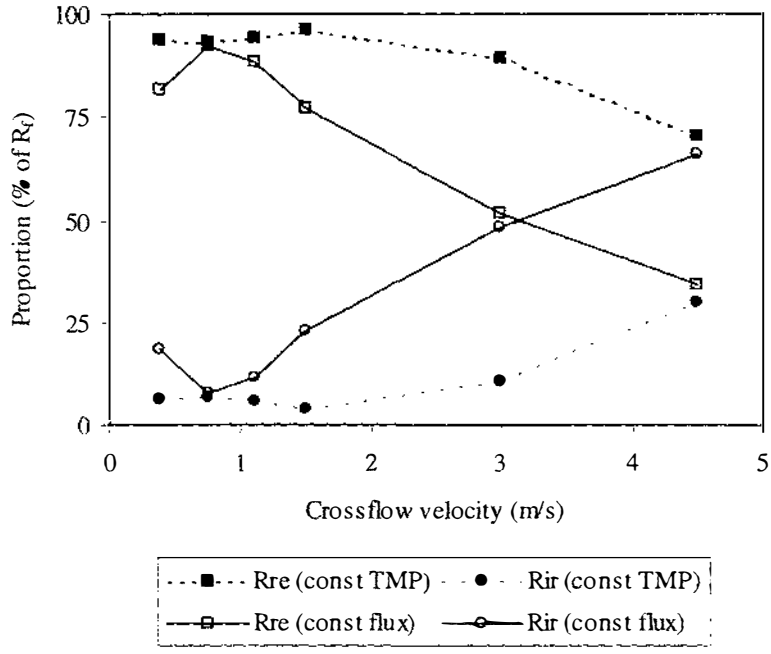

Fig. 7.8 Change in the proportion of R_{re} and R_{ir} with change in the CFV in constant flux mode at $J = J_{ss}$ and in constant TMP mode, at 100 kPa TMP, 2.5 g/l C_{feed}, using 1.0 μm multi-channel membrane

The cakes formed on the membrane surface during the experimental runs under constant flux mode were very thin, consequently, the mass and the height of the cakes could not be estimated. The cakes formed at 3.0 m/s and 4.5 m/s CFV were also too thin to recover effectively. Therefore, the PSD of cakes formed at these CFVs is not known. The available results are given in Table 7.1.

Table 7.1 Cake PSD at different CFV at flux $J = J_{ss}$

Module = multi-channel
Membrane pore size = 1.0 μm
Feed side pressure = 100 kPa
Feed concentration = 2.5 g/l

CFV (m/s)	d_{sauter} (μm)	$d_{0.1}$ (μm)	$d_{0.5}$ (μm)	$d_{0.9}$ (μm)
0.375	0.54	0.24	0.70	6.71
0.75	0.51	0.24	0.63	7.15
1.1	0.56	0.24	0.71	12.29
1.5	0.49	0.22	0.60	9.07

Overall, the cake PSD at different CFV under constant flux mode were similar. All values $d_{0.1}$, $d_{0.5}$, $d_{0.9}$ and d_{sauter} were smaller than these for constant TMP (100 kPa) runs at corresponding CFV. To illustrate this, the d_{sauter} values at different CFV for the two modes of operation are compared in Fig. 7.9.

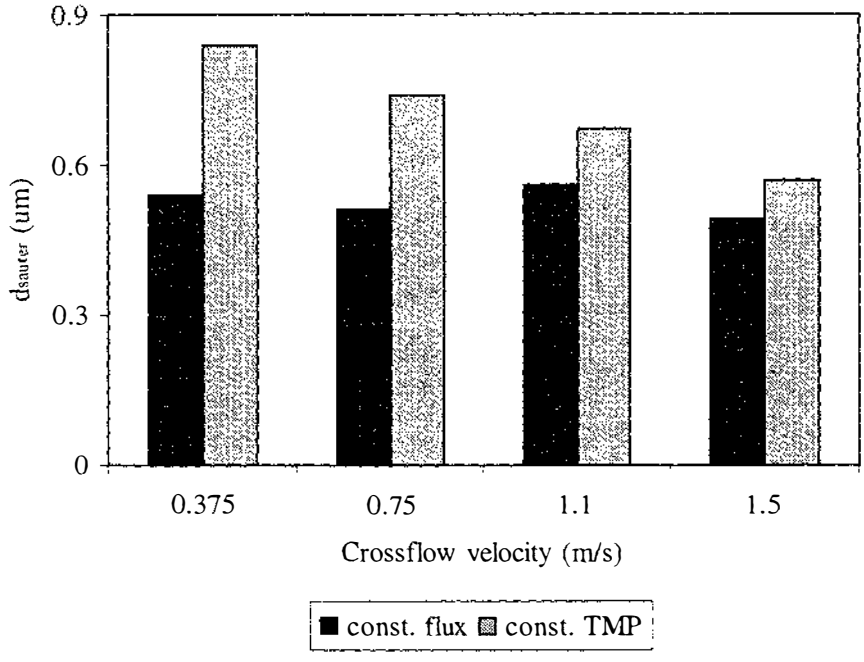

Fig. 7.9 Comparison of cake particle size under constant flux and constant TMP modes at different CFV, 2.5 g/l Cfeed using 1.0 μm pore size membrane

7.6.3 Discussion

Although the total fouling of the membrane was to the same level for any particular CFV under the two different modes of operation, the pattern and the proportions of the two types of fouling i.e. reversible and irreversible fouling were markedly different. This was due to the fact that the forces towards the membrane surface were low throughout the runs due to the low constant fluxes used. The key difference between the modes is that in the constant flux mode, besides the forces away from the membrane being constant (controlled by CFV), the forces towards the membrane surface also remained constant. The magnitude of these forces was similar to that at the steady-state in constant TMP mode since the constant flux was equal to J_{ss}. This caused deposition of relatively smaller particles under constant flux mode. This agrees with the observed

cake PSD in this study (Table 7.1, Fig. 7.9). The smaller particles would be expected to penetrate the pores to a greater extent. The greater level of internal fouling compared to that in constant TMP mode is consistent with this hypothesis.

The similar cake PSD at different CFV (Table 7.1) suggests similar level of force balance. Considering the fact that J_{cr} at any CFV was very close to J_{ss}, under the condition $J = J_{ss}$, the force balance would be similar to that at J_{cr} and hence, similar to each other. This further suggests the scope of obtaining desired level of particle size classification by adjusting the relative magnitude of the forces acting on the particles. The developed force balance model (Chapter 6) can be used for this purpose. To avoid any experimental error in cake PSD measurement due to very thin cake depositions as obtained under the present experimental conditions, higher constant flux conditions where thicker cakes can be deposited should be used to explore this possibility. Further experiments were conducted in this area (see the following Section).

7.7 Size separation using the developed force balance model

The possibility of separating a certain size range of the feed particles by adjusting the force balance using the developed model was explored in this part. Constant flux was a better mode of operation for this due to a constant driving force toward the membrane surface as earlier suggested in Chapter 6.3.6.2 and discussed in Section 7.1.

7.7.1 Methods

This study was done in two parts. In the first part, cake $d_{0.9}$ values for constant flux 3.49 x 10^{-4} m/s at 0.75, 1.1, and 1.5 m/s CFV were calculated using the model. Experiments were done at these CFVs and constant flux at 2.5 g/l C_{feed} using 1.0 μm multi-channel membrane. Filtration was continued until TMP = 100 kPa. Cake was then recovered and analysed for PSD. The experimental $d_{0.9}$ values were compared with the calculated ones. In the second part, constant flux values to obtain $d_{0.9}$ = 4.0 μm at 0.75, 1.1, and 1.5 m/s CFV were calculated with help of the model. Experiments were done at these levels of constant flux and CFVs in the same way as described above. Again the experimental

$d_{0.9}$ values were compared with the calculated one i.e. 4.0 μm. Two replications of the experiments for both the parts were done and results averaged.

7.7.2 Results and discussion

The results of this study are shown in Table 7.2. The actual $d_{0.9}$ values were reasonably close to the calculated values for all the experiments (difference $\leq \pm$ 0.3 μm) and the results were reproducible (variation $\leq \pm$ 0.31 μm).

Table 7.2 Comparison of estimated and measured $d_{0.9}$ for different runs

Membrane pore size = 1.0 μm
Membrane module = multi-channel

CFV (m/s)	Constant flux (m/s)	$d_{0.9}$ (μm) estimated	measured
0.75	3.49×10^{-4}	8.49	8.19 (8.22, 8.16)
1.1	3.49×10^{-4}	5.35	5.51 (5.52, 5.50)
1.5	3.49×10^{-4}	4.73	4.67 (4.82, 4.51)
0.75	6.33×10^{-5}	4.0	4.11 (4.06, 4.15)
1.1	1.99×10^{-4}	4.0	4.25 (4.3, 4.2)
1.5	2.54×10^{-4}	4.0	4.13 (4.14, 4.12)

A reasonably good level of agreement between calculated values and experimental data suggested that it was possible to obtain a deposition of specified size range by adjusting the force balance without using different membrane pore sizes. The results of this study provide a scope to further explore the possibility of applying controlled size classification to separate different feed particle sizes or different feed components based on their sizes at commercial level. The results have further supported the validity of the model developed in Chapter 6.

7.8 Combining the two modes of operation

7.8.1 Constant flux - constant TMP operation

Methods

To further develop understanding of the behaviour of the particles during CFMF, a set of experiments was carried out in a constant flux - constant TMP combined mode. Here the filtration was done in constant flux mode at $J = J_{ss}$ until the TMP reached 100 kPa. Then the mode of operation was changed to constant TMP at 100 kPa and filtration was continued until steady state was achieved.

These experiments were carried out at 0.75 and 3.0 m/s CFV at 100 kPa feed side pressure and 2.5 g/l C_{feed} using 1.0 μm pore size membrane on the multi-channel module. Two replications of each experiment were done and the results averaged.

Results and discussion

J_{ss} values under the constant flux - constant TMP mode are shown in Table A2.4 along with the original values of J_{ss} under constant TMP mode in Appendix 2. Changes in J and R_t with time of filtration are shown in the Fig. 7.10 for the runs at 3.0 and 0.75 m/s CFV. R_{re} and R_{ir} values at the end of constant flux run and constant flux – constant TMP run at 3.0 and 0.75 m/s CFV are compared in Table 7.3. Under constant flux - constant TMP mode, J_{ss} values were lower (by ~16 and ~28 % at 0.75 and 3.0 m/s, respectively) than that in case of the constant TMP mode. R_{re} was not significantly different but R_{ir} and therefore R_f were higher in the case of combined runs compared to constant flux runs. Flux declined at much slower rate during combined mode compared to the constant TMP mode.

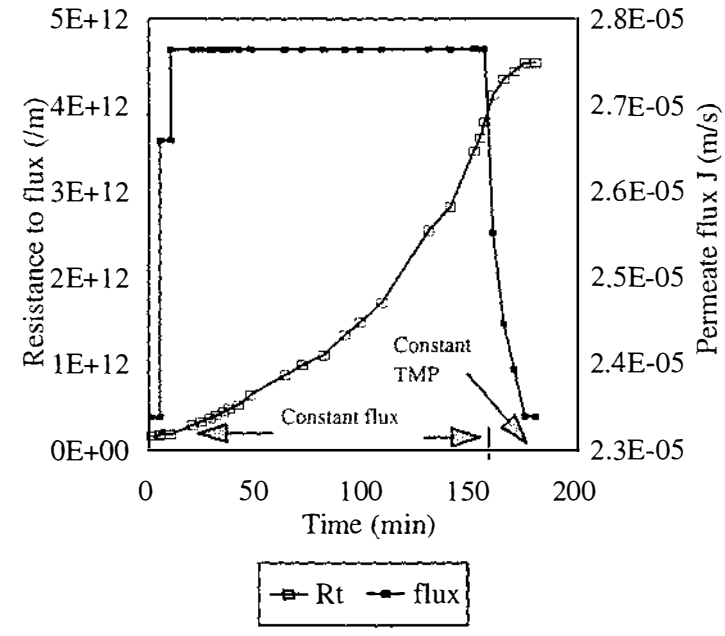

(a)

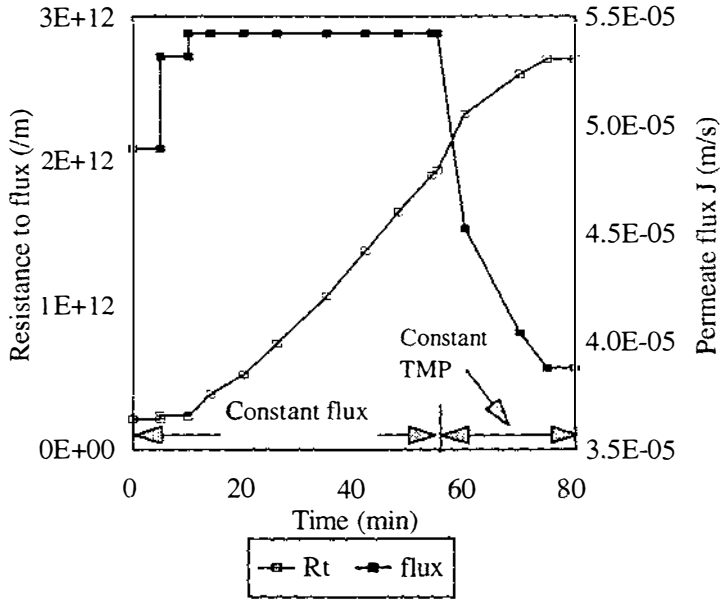

(b)

Fig. 7.10 Change in permeate flux and resistance to permeate flux with time for a constant flux - constant TMP run at (a) 0.75 and (b) 3.0 m/s CFV

Table 7.3 Change in resistance to flux during constant flux – constant TMP runs

Module = multi-channel
Membrane = 1.0 μm pore size
C_{feed} = 2.5 g/l

Type of run	R_f (/m)	R_{re} (/m)	R_{ir} (/m)
0.75 m/s CFV			
constant flux run	3.61×10^{12}	3.31×10^{12}	0.29×10^{12}
combined run	4.30×10^{12}	3.34×10^{12}	0.96×10^{12}
3.0 m/s CFV			
constant flux run	1.75×10^{12}	0.90×10^{12}	0.85×10^{12}
combined run	2.45×10^{12}	1.00×10^{12}	1.45×10^{12}

Since the total fouling at the end of constant flux run (when TMP = 100 kPa) was the same as that of the constant TMP run, J was not expected to drop further during the constant TMP part of the combined run. However, J dropped considerably during this period and reached the steady-state at a lower flux. This was clearly due to the further internal fouling of the membrane during the constant TMP period as shown by the marked increase in R_{ir} during this period (Table 7.3). It appears that during the constant TMP period, small particles continued to penetrate through the relatively thinner cakes, formed during the low constant flux part, into the membrane pores.

7.8.2 Constant TMP - constant flux operation

Methods

Another set of experiments was carried out in a constant TMP - constant flux combined mode. The sole aim of operating under this mode was to check the possibility of removing the surface deposition by changing the force balance through operating at low flux. First the filtration was carried out in constant TMP mode at 100 kPa TMP and continued until J_{ss} was obtained. Then the mode of operation was changed to constant flux. The constant flux was maintained exactly half of J_{ss}. The filtration was continued until a steady-state TMP was obtained. These experiments were carried out at 0.75 and

3.0 m/s CFV and 2.5 g/l C_{feed} using the 1.0 μm multi-channel membrane. Two replications of each experiment were done and the results averaged.

Results and discussion

Change in J and R_t with time for 0.75 and 3.0 m/s CFV runs are shown in the Fig. 7.11. R_f, R_{re} and R_{ir} for these combined runs are compared with that for constant flux runs where $J = J_{ss}$ in Table 7.4. The detailed results of this study are provided in Table A2.5 in Appendix 2. The change in R_t with time during constant flux part of these experiments and during the erosion of cake deposited under constant TMP 100 kPa – 1.5 m/s CFV conditions by water flushing at 4.5 m/s CFV (Chapter 5.4.4), are shown together in Fig. 7.12.

Table 7.4 Change in resistance to flux during constant TMP – constant flux runs

Module = multi-channel
Membrane = 1.0 μm pore size
C_{feed} = 2.5 g/l

Type of run	R_f (/m)	R_{re} (/m)	R_{ir} (/m)
0.75 m/s CFV			
constant TMP run	3.61×10^{12}	3.36×10^{12}	0.25×10^{12}
combined run	2.70×10^{12}	2.45×10^{12}	0.25×10^{12}
3.0 m/s CFV			
constant TMP run	1.75×10^{12}	1.56×10^{12}	0.19×10^{12}
combined run	1.10×10^{12}	0.90×10^{12}	0.20×10^{12}

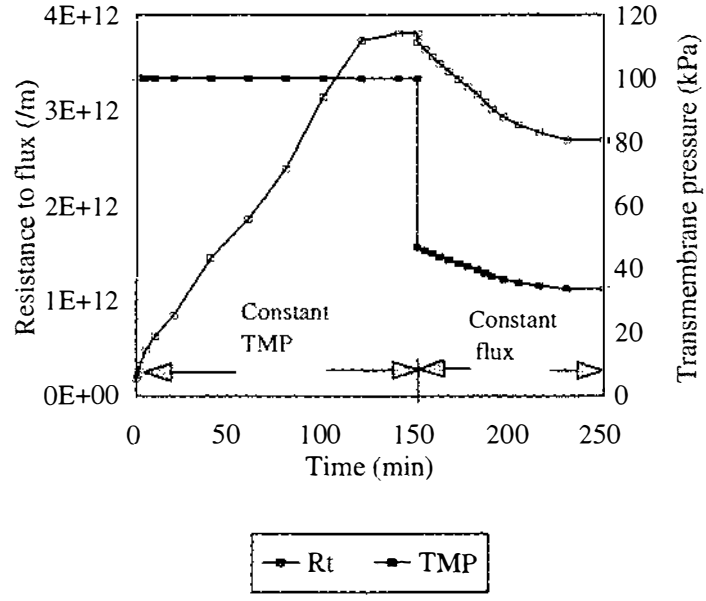

(a)

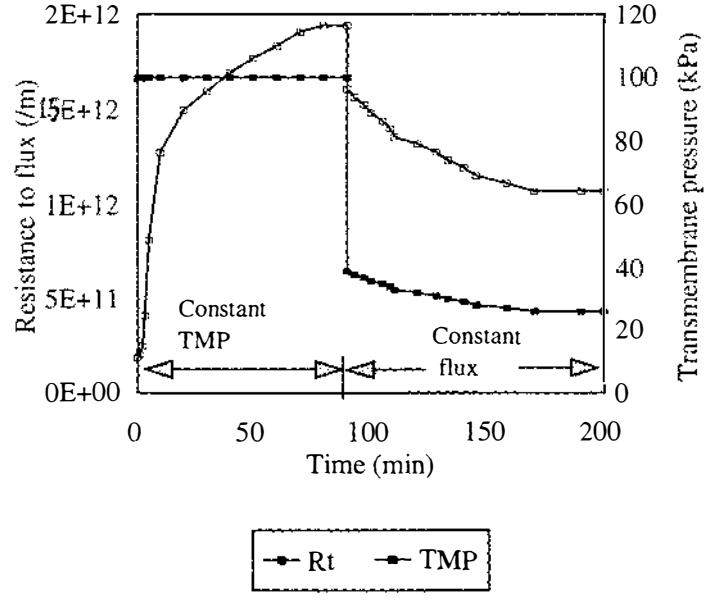

(b)

Fig. 7.11 Change in R_t and TMP with time for a constant TMP - constant flux run at (a) 0.75 and (b) 3.0 m/s CFV

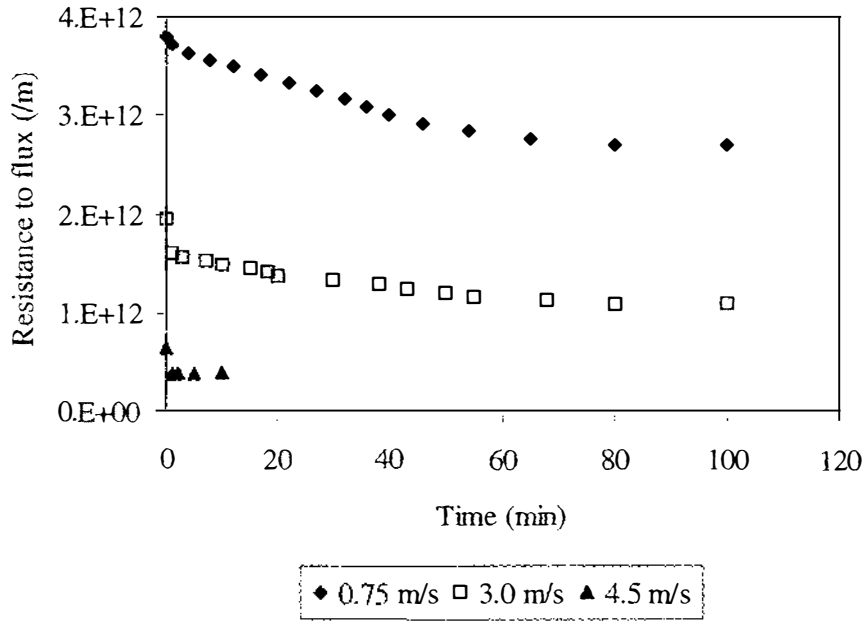

Fig. 7.12 Cake erosion at 0.75 and 3.0 m/s in constant flux mode and at 4.5 m/s in constant TMP mode on 1.0 μm multi-channel membrane

Only a partial removal of the deposited cake was possible with this method. The removal was faster during first few seconds at 3.0 m/s compared to that at 0.75 m/s CFV. This was obviously due to the higher shear force at higher CFV. However, a complete removal was not achieved suggesting an irreversible attachment of the particles due to high adhesive forces. Altmann and Ripperger (1997) also reported irreversible attachment of the diatomaceous earth and spherical silica particles. They reduced the fluxes by decreasing TMP. They also attributed this to the strong influence of the adhesive forces acting on the particles. No difference in R_{ir} between pure constant TMP run and combined run suggests that internal fouling as expected was not affected during constant flux part of the combined run. Only surface fouling was reduced.

Since the constant flux was half of the J_{cr}, any significant fouling during constant flux part of the run can be ruled out. Therefore, this part of the run represents pure cake erosion. So, all three processes shown in Fig. 7.12 are pure erosion processes. However, they represent erosion of cakes deposited under different operating conditions and hence, with totally different properties – mass, height, PSD, and porosity. Further, erosion at 0.75 m/s and 3.0 m/s is in presence of feed particles whereas erosion at 4.5 m/s is achieved by flushing the water. Therefore, they do not provide a scope for a

straight comparison of the processes or mathematical modelling of erosion kinetics. But it is obvious from the rates of these processes that at higher CFV, erosion during first few seconds is very high compared to at a low CFV. The quicker drop in erosion rate at higher CFV compared to low CFV could be due to difference in the cake eroded or due to a simultaneous effect of high CFV on cake packing. The *in situ* observation of the erosion process might tell somethingmore about that and there is scope to further study the erosion kinetics of particulate feed systems during CFMF.

Reducing the flux below J_{cr}, particularly at high CFV as done in this study, may provide an alternative to stopping or reversing the permeate flow periodically (backflushing), at industrial scale operations. This is because here the permeate flow does not completely stop and hence other synchronised process(es) are less affected, and special equipment for reversing permeate flow is not required. This process technique may be more useful for feeds with less adhesive solids. Further work can be carried out to check the applicability of this method for reduction of fouling and thereby improving the efficiency of CFMF process.

7.9 Overall discussion

The constant flux mode provides an advantage of operating under a constant force balance. This provides an opportunity to study the process of CFMF of lactalbumin particles from a different angle and to further develop understanding about the process.

The concept of critical flux as hypothesised by Field *et at.* (1995) is apparently very attractive as it offers operation totally without fouling. But for the present study, J_{cr} was close to J_{ss} which means, for the operation without fouling the system is to be run at flux below J_{ss}. At industrial scale, the operating flux has to be even lower to accommodate fluctuations in operating parameters and be certain about no fouling. Running at such a low flux may mean uneconomic operation. Operating at even slightly above J_{cr} results in severe internal membrane fouling, more significantly so at higher CFV, and when the feed has components smaller than membrane pore size. Only those systems where J_{cr} are reasonably high and all the fouling components in the feed are significantly larger than the membrane pore size will benefit significantly from operating below critical flux.

This study has indicated that any change in resistance to flux due to change in constant flux below J_{cr} is due to concentration polarisation. This issue has not been focused at before.

Operating under constant flux just above J_{cr} followed by constant TMP operation caused worst membrane fouling as the pore penetration of small particles continued through the cake for a long time and therefore, is not a desirable way of operation. But constant TMP operation followed by very low constant flux operation offered a scope to reduce surface fouling by reducing flux force F_f toward the membrane. Benkahla *et al.* (1995) however, observed no change in cake resistance when they reduced F_f by reducing TMP from 400 kPa to ~ 25 kPa during CFMF of $CaCO_3$ suspension at 3.5 m/s using a 0.2 μm multi-channel tubular ceramic membrane. They attributed this effect to very tight cake packing under high TMP. The results of the study in Section 7.8, combined with results of study on process development based on the effect of the operating parameters in Chapter 5.4.4 reveal that for a feed system containing components smaller than membrane pore size, operating at low flux with a clean membrane is not desirable. On the other hand initially operating at high flux can in fact help preventing internal fouling if there are feed components larger than membrane pore size. Since it is not feasible to operate at high constant flux for long time, constant flux is not the preferred mode of operation. However, constant flux mode does offer the prospect of controlling the size classification by adjusting the force balance through adjusting constant flux and CFV.

8. CONCLUSIONS AND SUGGESTIONS FOR FUTURE WORK

CFMF is emerging as a very important separation process with many applications in different industries including the dairy and other food industries. Many of the applications involve CFMF of particulate suspensions. As a result of this, a considerable amount of work has been reported on CFMF of particulate suspensions. However, the reports often deal with uniform sized and/or shaped rigid model particles that are very different from the particles involved in actual filtration. Further, these reports often contain contradictory and unexplained results. Most of the reports dealing especially with the mathematical modeling of CFMF of particles use flat sheet modules for simplicity of calculation. In contrast, nowadays ceramic tubular modules are more commonly used for the actual filtration of particles in the food industry and other similar fields. Compared to the approach commonly found in the literature, the approach in the present work is more realistic as it involved CFMF of lactalbumin particles, which are more like the feed particles found in the actual filtration than model particles, and used the ceramic tubular modules.

The selection of lactalbumin as a feed material, however, necessitated its characterization prior to the actual CFMF experiments. The characterization of lactalbumin helped in determining the experimental set-up and conditions as well as in predicting some of its behaviour during CFMF. The use of lactalbumin as feed particles coupled with estimation of all the important parameters: internal and external fouling, and cake mass, height, porosity and PSD during the study provided an almost complete picture of the process. This led to the observation of some unpredicted effects of the experimental conditions, confirmed or disproved different hypotheses suggested in the literature, and helped explain some of the contradictory results reported in the literature.

The developed methods for cake height and porosity estimation are simple and can be used irrespective of the membrane module used for the filtration. The results obtained using these methods are of the same order as those obtained using sophisticated techniques like scanning electron microscopy and NMR micro-imaging under similar feed and other experimental conditions (Riesmeier *et al.* 1989, Wandelt *et al.* 1992).

The present study in the constant TMP mode revealed that at a very low TMP and a high CFV, the deposited cake mass can be so small that it does not cover the entire membrane area, leaving patches of the surface exposed to the fine particles for pore penetration. The observed increase in the internal fouling with decrease in TMP from 50 to 20 kPa at 3.0 m/s is attributed to this effect and has not been reported before. Similarly, an increase in internal fouling with an increase in CFV observed in the range of 1.5 to 4.5 m/s at 100 kPa, which was due to the selective deposition effect of crossflow, has not been reported before. Although the size classification effect of CFV is commonly reported (Fischer and Raasch 1985, Lu and Ju 1989, Wakeman and Tarleton 1991, Mackley and Sherman 1992, Foley *et al.* 1992 etc.), the present study is the first to demonstrate the size classification effect of TMP, through measurement of cake PSD. The present study is the first to clearly demonstrate the penetration of fine particles in the cake during the later part of filtration, first hypothesized by Dharmappa *et al.* (1992), through the estimated cake porosity and measured cake PSD. The existence of an optimum TMP (100 kPa in the experimental conditions used) was confirmed in this work. The contradictory effects of CFV on J_{ss} for feed with wide PSD reported in the literature (Fischer and Raasch 1985, Lu and Ju 1989, Wakeman and Tarleton 1991, Mackley and Sherman 1992, Wakeman 1994, Holdich *et al.* 1995) are explained for the first time in the present work. The difference in the reported effect is attributed to the presence of submicron particles in some of the feeds used in the studies. Similarly, the present study explained the effect of CFV on the time required to obtain the steady-state, that is contradictorily reported and not explained in literature (Wakeman and Tarleton 1991, Wakeman 1994).

The observed trend of J_{ss} with respect to C_{feed}, i.e. no further decrease in J_{ss} above 2.5 g/l, is attributed to a steady-state net resultant force achieved at that C_{feed}. The observed increase in J_{ss} by ~6 % on addition of large lactalbumin particles at the steady-state is due to the scouring or other similar (chipping of the cake surface) action of the large particles. This effect has been observed in the case of CFMF for the first time. Although the increase in flux is not as great as the ~35 % increase reported for CFUF (Heng Meng and Glatz 1990), this disproved the hypothesis of Rappuoli and Unutmaz (1995) that the scouring particles have the disadvantage of pushing particles into the membrane during CFMF. The increase

in J_{ss} on addition of large particles thus suggests the scouring action of large particles as one of the possible mechanisms for the unexplained mobility of the top cake layer(s) even at the steady-state reported by Mackley and Sherman (1992) during CFF of 125 – 180 μm polyethylene particles. Another possible reason for the cake mobility could be the difference between the overall and the local force balance along the cake surface. However, there is a need to check the beneficial effect of large particles for CFMF of different particulate feed materials. There is also scope to extend this study to explore the possibility of achieving a greater improvement in the flux by introduction of large particles. Further work in this area is therefore suggested.

The deposited cake governed most of the filtration during constant TMP runs and therefore, there was no marked effect of membrane pore size or module design on the process performance.

Operation in constant flux mode can offer better control over the flow of material compared to that in constant TMP mode as the flow toward the membrane is constant throughout the run. This mode can also offer the possibility of operation without membrane fouling if flux is maintained below a critical level (Field *et al.* 1995). This area is relatively new and less explored, and therefore, there are only a few reports on constant flux CFMF of particulate suspensions. Experiments were done in this mode with the aim of utilizing the above benefits to widen the base of information and thereby further enhancing understanding of the process.

The study in the constant flux mode at 100 kPa feed side pressure revealed that J_{cr} (below which no membrane fouling occurred) was only slightly less than J_{ss} of the constant TMP (100 kPa) run at the corresponding CFV. This study for the first time clearly revealed that the increase in R_t with step up of flux below J_{cr} observed in this study and also during CFMF of polystyrene latex particles (Kwon *et al.* 1996) is not due to membrane fouling and can be attributed to concentration polarization. Operation at constant flux just above J_{cr} resulted in very high internal fouling particularly at high CFV due to the net resultant force on the particles at around J_{cr} being just enough to cause the deposition of fine particles only

that foul the membrane internally. The level of internal fouling was much lower in constant TMP mode because large particles deposited under high initial flux force F_f blocked the pores and minimized pore penetration by fine particles. Thus, only those systems where J_{cr} are reasonably high and all the foulants are significantly larger than membrane pore size can actually benefit from operating below J_{cr}. Combining the two modes of operation by operating in constant TMP mode after initial low constant flux mode caused the worst membrane fouling. The fines during constant TMP mode continued to penetrate through a very thin cake formed during the low constant flux operation. However, operating in constant flux (well below J_{cr}) mode after steady-state fouling in constant TMP mode had some benefit as some erosion of cake took place at low constant flux under lower F_f. There is scope for further study and mathematically model the cake erosion resulting from a shift in force balance for the deposited particles. This may enhance the understanding of behaviour like scouring action and cake mobility and may also help in developing methods for in process fouling reversal.

All the results in this study could be explained by the force balance mechanism. The inter-particle adhesive forces were found to be very strong, whereas, the type of back diffusion considered (inertial lift or shear-induced diffusion) had no significant effect on the resultant force balance as lift or back diffusion forces were not very strong. In this study, the force balance model was extended to include the compressibility of the particles. This has extended the potential applicability of the model to food and other compressible particles. However, the actual compressibility of lactalbumin particles could not be measured due to the unavailability of instruments and methods for measuring a very small compression that was a few nanometers. Further work may be done to develop a method of estimating the compressibility of lactalbumin particles using an instrument like the atomic force microscope. One drawback of the force balance model is that the cake resistance and height are not determined.

To overcome this limitation the resistance in series model was used in addition to the force balance model. The present study is the first to demonstrate that the concentration polarization resistance R_{cp} and top cake layer resistance are very difficult to distinguish but

the combined effect of is very limited, and hence, the most common approach of neglecting R_{cp} during the estimation of cake resistance R_c is appropriate. Use of the Carman-Kozeny equation for estimation of R_c was originally for the cakes comprising uniform size particles. However, recently Altmann and Ripperger (1997) used this equation to estimate R_c for cake comprising widely size distributed particles of diatomaceous earth. For this they used d_{sauter} of a certain layer of the cake. But the term 'certain layer' is not defined. Compared to that, in the present study $d_{0.24}$ as well as a d_p value based on the combined effect of d_{sauter} and $d_{0.1}$ of the cake are used to estimate R_c of widely size distributed cakes of lactalbumin particles which is certainly a more logical approach. Thus, the present study has made an important contribution in extending the applicability of the resistance in series model to the widely size distributed cakes. However, the present model is a semi-empirical equation and there is scope to further develop and generalize this model.

While water flushing can reverse surface fouling, internal fouling is completely irreversible and requires chemical cleaning of the membrane to restore the membrane performance. The process developed based on the observed effects of operating parameters on the CFMF of lactalbumin enabled operation at a low internal fouling (R_{ir} = 1.1 x 10^{11} m^{-1} at 160 min of operation) and high flux (> 6.33 x 10^{-5} m/s, the highest J_{ss} observed in the studied range of CFV) for a long time (160 min). This has demonstrated the possibility of improving the process performance by varying the operating conditions during the filtration. This kind of process has not been reported before. If coupled with backflushing, forming a sequential chain of processing and backflushing, the process can be applied at a commercial level for a long high efficiency performance without intermittent cleanings. Further work is required in the area to explore this possibility.

NOMENCLATURE

A	membrane surface area	m^2
a	adhesive distance between two spheres	m
CFV	crossflow velocity	m/s
C_{feed}	feed concentration	g/l
d	diameter of the membrane tube	m
d_p	particle diameter	m
d_{sauter}	sauter mean diameter	m
$d_{0.1}$ $d_{0.5}$ $d_{0.9}$ $d_{1.0}$	represents the size levels below which 10, 50, 90 and 100 % particles are sized, respectively	m
E	elastic deformation moduli	Pa
F_v	force due to crossflow velocity	N
F_f	force due to premeate flux	N
F_b	back diffusion force	N
F_{br}	brownian diffusion force	N
F_s	shear diffusion force	N
F_l	inertial lift force	N
F_a	adhesive force	N
F_{vdW}	Van der Waals force	N
F_{fr}	friction force	N
F_g	gravitational force	N
g	gravitational acceleration	(9.81 m/s^2)
h	height of the cake	m
J	permeate flux	m/s
J_w	pure water flux	m/s
J_{ss}	steady-state flux	m/s
J_{cr}	critical flux	m/s
k	Boltzmann's constant	
L	length of the membrane tube	m
m	mass per unit area of cake	kg/m^2
R_t	total resistance to the permeate flux	m^{-1}
R_m	membrane resistance	m^{-1}
R_f	fouling resistance	m^{-1}
R_{cp}	resistance due to concentration polarization	m^{-1}
R_c	cake resistance	m^{-1}
R_{re}	reversible resistance	m^{-1}
R_{ir}	irreversible resistance	m^{-1}
r	clearance of crossflow channel (radius of tube)	m
r_c	radius of the contact area	m
r_p	particle radius	m
T	absolute temperature	°K
TMP	transmembrane pressure difference	Pa
V_b	back diffusion velocity	m/s
V_{br}	brownian diffusion velocity	m/s
V_s	shear-induced velocity	m/s
V_l	inertial lift velocity	m/s

V_{av}	average crossflow velocity	m/s
α	specific cake resistance	
η	feed viscocity	Pa.s
ρ	fluid density	kg/m^3
ρ_p	particle density	kg/m^3
ε	cake porosity (or void fraction)	
γ	shear rate	s^{-1}
τ_w	shear stress	Pa
$\eta\varpi$	Lifschitz-Van der Waals constant	$(10^{-20}$ J)
μ	friction coefficient	
θ	angle of repose	deg.
$\theta_{critical}$	critical angle of repose	deg.

REFERENCES

Aimar,P., Howell,J.A., and Turner,M. (1989): Effects of Concentration Boundary Layer Development on the Flux Limitations in Ultrafiltration. *Chem. Eng. Res. Des.*, **67**, 255-261.

Akhtar,S., Hawes,C., Dudley,L., Reed,I., and Startford, P. (1995): Coatings Reduce the Fouling of Microfiltration Membranes. *J. Membr. Sci.*, **107**, 209-218.

Altena,F.W., and Belfort,G. (1984): Lateral Migration of Spherical Particles in Porous Flow Channels: Application to Membrane Filtration. *Chem. Eng. Sci.*, **39**(3), 343-355.

Altmann,J., and Ripperger, S. (1997): Particle Deposition and Layer Formation at the Crossflow Microfiltration. *J.Membr.Sci.*,**124**, 119-128.

Anon (1993): Fine Filters. *Dairy Field*, **176**(6): 59.

Bartlett,M., Bird,M.R., and Howell,J.A. (1995): An Experimental Study for the Development of a Qualitative Membrane Cleaning Model. *J. Membr. Sci.*, **105**, 147-157.

Belfort,G., Davis,R.H., and Zydney,A.L. (1994): Review: The Behaviour of Suspensions and Macromolecular Solutions in Crossflow Microfiltration. *J. Membr. Sci.*, **96**, 1-58.

Bell,D.J., Hoare,M., and Dunnill,P. (1983): The Formation of Protein Precipitates and Their Centrifugal Recovery. *Advances in Biochemical Engg./ Biotechnol.*, **26**,2-72.

Bellusi,A. (1990): Cross-flow Microfiltration. *Industries-Alimentaires-et-Agricoles*, **107**(10): 1084 -1086 (*Cited in Dairy Sci. Abstr.*, 1992, 054-03976).

Ben Amar,R., Gupta,B.B., and Jaffrin,M.Y. (1990): Apple Juice Clarification Using Mineral Membranes : Fouling Control by Backwashing and Pulsating Flow. *J. Food Sci.*, **55**, 1620.

Benkahla,Y.K., Ould-Dris,A., Jaffrin,M.Y., and Si-Hassen,D. (1995): Cake Growth Mechanism in Crossflow Microfiltration of Mineral Suspensions. *J. Membr. Sci.*, **98**, 107-117.

Bentham,A.C., Ireton,M.J., Hoare,M. and Dunnill,P. (1988): Protein Precipitate Recovery Using Microporous Membranes. *Biotechnol. Bioengg.*, **31**, 984-994.

Bixler,H.J., and Rappe,G.C. (1970): Ultrafiltration Process. US Patent 3,541,006 (*Cited in* Fan,A.G. (1984): Ultrafiltration of Suspensions. *J. Membr. Sci.*, **20**, 249-259.).

Blanpain,P., Hermia,J., and Lenoel,M. (1993): Mechanisms Governing Permeate Flux and Protein Rejection in the Microfiltration of Beer with a Cyclopore Membrane. *J. Membr. Sci.*, **84**, 37-51.

Bouton,Y., and Grappin,R. (1995): Comparison of the Final Quality of a Swiss-type Cheese Made from Raw or Microfiltered Milk. *Lait*, **75**, 31-44.

Bowen,W.R., and Gan,Q. (1991): Properties of Microfiltration Membranes: Flux Loss During Constant Pressure Permeation of Bovine Serum Albumin. *Biotechnol. Bioengg.*, **38**, 688-696.

Bowen,W.R., and Hall,N.J. (1995): Properties of Microfiltration Membranes: Mechanisms of Flux Loss in the Recovery of an Enzyme. *Biotechnol. Bioengg.*, **46**, 28-35.

Bowen,W.R., Kingdon,R.S., and Sabuni,H.A.M. (1989): Electrically Enhanced Separation Processes: the Basis of In Situ Intermittent Electrolytic Membrane Cleaning (IIEMC) and In Situ Electrolytic Membrane Restoration (IEMR). *J. Membr. Sci.*, **40**, 219-229.

Buffham,B.A., and Cumming,I.W. (1995): Prevention of Particle Deposition in Crossflow Microfiltration. *Trans. I. Chem. E.*, **73** (A), 445-454.

Chan,M.Y.Y., Hoare,M., and Dunnill,P. (1986): The Kinetics of Protein Precipitation by Different Reagents. *Biotechnol. Bioengg.*, **28**, 387-393.

Chang,D-J, Hsu,F-G, and Hwang,S-J (1995): Steady-state Permeate Flux of Cross-flow Microfiltration. *J. Membr. Sci.*, **98**, 97-106.

Chen, J.P., and Wang C.H. (1991): Microfiltration Affinity Purification of Lactoferrin and Immunoglobulin G from Cheese Whey. *J. Food Sci.*, **56** (3), 701-713.

Cheryan,M. (1986): Ultrafiltration Handbook. Pub. Technomic, Lancaster,PA.

Cheryan,M. (1991): Membranes in Food Processing. Effective Industrial Membrane Processes- Benefits and Opportunities, Elsevier Science Publishers Ltd, England, 157-180.

Cheryan,M. (1992): Membrane Technology in Food and Bioprocessing. Advances in Food Engineering,Ed., Singh,R.P., and Wirakartakusumah,M.A., CRC Press, London,165-179.

Daufin,G., Merin,U., Labbe,J.P., Quemerais,A., and Kerherve,F.L. (1991): Cleaning of Inorganic Membranes After Whey and Milk Ultrafiltration. *Biotechnol.Bioengg.*, **38**, 82-89.

Daufin,G., Michel,F., Labbe,J.P., Quemerais,A., and Grangeon,A. (1993): Ultrafiltration of Defatted Whey: Improving Performance by Limiting Membrane Fouling. *J. Dairy Res.*, **60**, 79-88.

Daufin,G., Michel,F., Labbe,J.P., Quemerais,A., Grangeon,A. (1994): Optimizing Clarified Whey : Influence of pH. *J. Dairy Res.*, **61**(3), 355-363.

Dekker,M. and Boom,R. (1995): Improving Membrane Filtration Processes, *Tibtech*, **13**, 129-131.

Davies,W.L. (1939): The Chemistry of Milk. Second Ed., Chapman & Hall Pub.,London, 279.

Davis,R.H. (1996[a]): Definitions. Membrane Handbook, Ed. Ho,W.S.W., and Sirkar,K.K., Chapman & Hall Pub., New York, London, 457-460.

Davis,R.H. (1996[b]): Theory for Crossflow Microfiltration. Membrane Handbook, Ed. Ho,W.S.W., and Sirkar,K.K., Chapman & Hall pub., New York, 480-505.

Davis,R.H.. and Sherwood,J.D. (1990): A Similarity solution for Steady-state Cross-flow Microfiltration, *Chem. Eng. Sci.*, **45**, 3203-3209.

Davis,R.H., and Leighton,D.T. (1987): Shear-induced Transport of a Particle Layer Along a Porous Wall. *Chem. Eng. Sci.*, **42**(2), 275-281.

Devereux,N., Hoare,M., and Dunnill,P. (1986): Membrane Separation of Protein Precipitates: Unstirred Batch Studies. *Biotechnol. Bioengg.*, **28**, 88-96.

Devereux,N. and Hoare,M. (1986): Membrane Separation of Protein Precipitates: Studies with Cross Flow in Hollow Fibers. *Biotechnol. Bioengg.*, **28**, 422-431.

Dharmappa,H.B., Verink,J., Ben Aim,R., Yamamoto,K. and Vigneswaran,S. (1992): A Comprehensive Model for Cross-flow Filtration Incorporating Polydispersity of the Influent. *J. Membr. Sci.*, **65**, 173-185.

Drew,D.A., Schonberg,J.A., and Belfort,G. (1991): Lateral Inertial Migration of a Small Sphere in Fast Laminar Flow Through a Mambrane Duct. *Chem. Engg. Sci.*, **46** (12), 3219-3224.

Dullien,F.A.L. (1979): Porous Media- Fluid Transport and Pore Structure. Academic Press Pub., N.Y., London, Toronto, Sydney, San Francisco, 131-137.

Eckstein,E.C., Bailey,P.G., and Shapiro, A.H. (1977): Self-Diffusion of Particles in Shear Flow of a Suspension. *J. Fluid Mech.*, **79**, 191-208 (*Cited in* Belfort,G., Davis,R.H., and Zydney,A.L. (1994): Review: The Behaviour of Suspensions and Macromolecular Solutions in Crossflow Microfiltration. *J. Membr. Sci.*, **96**, 1-58).

Evans,E.W. (1984): Uses of Milk Proteins in Formulated Foods. *Dev. Food Proteins*, **1**, 131-169.

Fan,A.G. (1984): Ultrafiltration of Suspensions. *J. Membr. Sci.*, **20**, 249-259.

Fauquant, J., Maubois, J.L., and Pierre, A. (1988): Microfiltration of Milk Using a Mineral Membrane. *Technique-Laitiere-and-Marketing*, **1028**, 21-23 (*Cited in Dairy Sci. Abstr.*, 1988 05-04400).

Field,R.W., Wu,D., Howell,J.A., and Gupta,B.B. (1995): Critical Flux Concept for Microfiltration Fouling. *J. Membr. Sci.*, **100**, 259-272.

Finnigan,S.M., and Howell,J.A. (1989): The Effect of Pulsatile Flow on Ultrafiltration Fluxes on a Baffled Tubular Membrane Sustem. *Chem. Eng. Res. Des.*, 278-282.

Fischer,E., and Raasch,J. (1985): Cross-flow Filtration. *Ger. Chem. Eng.*, **8**, 211-216.

Fischer,E., and Raasch,J. (1986): Model Tests of the Particle Deposition at the Filter Medium in Cross-Flow Filtration. *World Filtration Congress* (4th: 1986: Ostend, Belgium), Pub. Filtration Society, London, Antwesp, Belgium, 11.11-11.17.

Foley,G. (1994): Membrane Fouling in Crossflow Filtration: Implications for Measurement of the Steady State Specific Cake Resistance. *Biotechnol. Tech.*, **8** (10), 743-746.

Foley,G., MacLoughlin,P.F., and Malone,D.M. (1992): Preferential Deposition of Smaller Cells During Cross-flow Microfiltration of a Yeast Suspension.
Biotechnol.Techniques, **6** (2), 115-120.

Fordham,E.J., and Ladva,H.K.J. (1989): Cross-flow Filtration of Bentonite Suspensions. *Physicochem. Hydrodyn.*, **11**, 411 (*Cited in* Wakeman,R.J. (1994): Visualisation of Cake Formation in Crossflow Microfiltration. *Trans. I. Chem. E.*, **72** (A), 530-540.).

Foust,A.S., Wenzel,L.A., Clump,C.W., Maus,L., and Andersen,L.B. (1980): Principles of Unit Operations. Sec. Ed., John Wiley & Sons Pub., New York, 711-713.

Gan,Q., Field,R.W., Bird,M.R., England,R., Howell,J.A., McKechnie,M.T., and O'Shaughnesy,C.L. (1997): Beer Clarification by Cross-flow Microfiltration: Fouling Mechanism and Flux Enhancement. *Trans. I.Chem. E.*, **75**(A), 3-7.

Gatenholm,P., Fell,C.J., and Fane,A.G. (1988): Influence of the Membrane Structure on the Composition of the Deposit-Layer During Processing of Microbial Suspensions. *Desalination*, **70**, 363-378.

Geankoplis,C.J. (1993): Transport Processes and Unit Operations, Pub. PTR Prentice-Hall,Inc., A Simon & Schuster Co., Englewood Cliffs, New Jersey, USA.

Gekas,V. and Hallström,B. (1990): Microfiltration Membranes, Cross-Flow Transport Mechanisms and Fouling Studies. *Desalinatn*, **77**, 195-218.

Gesan,G., Merin,U., Daufin,G., and Maugas,J.J. (1993): Performance of Industrial Cross-flow Microfiltration Plant for Clarifying Rennet Whey. *Netherlands-Milk-Dairy.J.*, **47** (3-4), 121-135.

Gesan,G., Daufin,G., and Merin,U. (1994): Whey Crossflow Microfiltration Using an M14 Carbosep Membrane: Influence of Initial Hydraulic Resistance. *Lait*, **74**, 267-279.

Glatz,C.E. (1990): Precipitation. Separation Processes in Biotechnology, Ed. Asenjo,J.A., Pub. Marcel Dekker, New York., 329-358.

Goren,S.L. (1979): The Hydrodynamic Force Resisting the Approach of a Sphere to a Plane Permeable Wall. *J. Colloid Interface Sci.*, **69**, 78-85 (*Cited in* Belfort,G., Davis,R.H., and Zydney,A.L. (1994): Review: The Behaviour of Suspensions and Macromolecular Solutions in Crossflow Microfiltration. *J. Membr. Sci.*, **96**, 1-58).

Green,G., and Belfort,G. (1980): Fouling of Ultrafiltration Membranes : Lateral Migration and the Particle Trajectory Model. *Desaln.*, **35**, 129-147 (*Cited in* Belfort,G., Davis,R.H., and Zydney,A.L. (1994): Review: The Behaviour of Suspensions and Macromolecular Solutions in Crossflow Microfiltration. *J. Membr. Sci.*, **96**, 1-58).

Gupta, B.B., Blanpain,P., and Jaffrin,M.Y. (1992): Permeate Flux Enhancement by Pressure and Flow Pulsations in Microfiltration with Mineral Membranes, *J. Membr. Sci.*, **70**, 257-266.

Gutman,R.G. (1987): Membrane Filtration : The Technology of Pressure-Driven Crossflow Processes. Pub. Adam Hilger, Bristol.

Hanemaaijer,J.H., Robbertsen,T., Boomgaard, T., and Gunnink,J.W. (1989): Fouling of Ultrafiltration Membranes. The Role of Protein Adsorption and Salt Precipitation. *J.Membr. Sci.*, **40**, 199-217.

Hawks,S.E., Phillips,L.G., Rasmwssen,R.R., Barbam,D.M., and Kinsella,J.E. (1993): Effects of Processing Treatment and Cheese-making Parameters on Foaming Properties of Whey Protein Isolates. *J. Dairy Sci.*, **76** (9), 2468-2477.

Heng Meng,H., and Glatz,C.E. (1990): Biotechnol. Prog., 6, 129-134 (*Cited in* Rappuoli,R., and Unutmaz,D. (1995): Improving Membrane Filtration Processes, *Tibtech*, **13**, 129-131.

Hermia,J. (1982): Constant Pressure Blocking Filtration Laws- Application to Power-Law Non-Newtonian Fluids. *Trans.I.Chem. Engineers*, **60**, 183-187.

Hlavacek,M., and Bouchet,F. (1993): Constant Flowrate Blocking Laws and an Example of their Application to Dead-EndMicrofiltration of Protein Solutions. *J. Membr. Sci.*, **82**, 285-295.

Hoare,M.(1982): Protein precipitation and Precipitate Ageing Part I : Salting-out and Ageing of Casein Precipitates. *Trans. I.Chem. Ers.*, **60**, 79-87.

Hoare,M., Narendranathan,J.J., Flint, J.R., Waddington,D.H., Bell, D., and Dunnill,P.(1982): Disruption of Protein Precipitates During Shear in Couette Flow and in Pumps. *Ind. Eng. Chem. Fundam.*, **21**, 402-406.

Hoare,M., and Dunnill,P. (1984): Precipitation of Food Proteins and Their Recovery by Centrifuging and Ultrafiltration. *J. Chem. Tech. Biotechnol.*,**34** (B), 199-205.

Hodgson,P.H., Pillay,V.L., and Fane,A.G. (1993): Visual Studies of Crossflow Microfiltration with Inorganic Membranes: Resistance of Biomass and Particulate Cakes, *Proc. 6th World Filtration Congress*, 607-610 (*Cited in* Wakeman,R.J. (1994): Visualisation of Cake Formation in Crossflow Microfiltration. *Trans. I. Chem. E.*, **72** (A), 530-540.).

Holdich,R.G., Cumming,I.W., and Ismail,B. (1995): The Variation of Crossflow Filtration Rate with Wall Shear Stress and the Effect of Deposit Thickness.*Trans.I.Chem. Engineers*, **73** (A), 20-26.

Hwang,K-J., Liu,H-C., and Lu,W-M. (1998): Local Properties of Cake in Cross-flow Microfiltration of Submicron Particles. *J. Membr. Sci.*, **138**, 181-192.

Jang,C.D. (1987): Effect of Different Operating Parameters and Pretreatment in Cross-flow Microfiltration, Thesis for M. Engg., Asian Ist. Technol., Thailand (*Cited in* Dharmappa,H.B., Verink,J., Ben Aim,R., Yamamoto,K. and Vigneswaran,S. (1992): A Comprehensive Model for Cross-flow Filtration Incorporating Polydispersity of the Influent. *J. Membr. Sci.*, **65**, 173-185).

Jensen,J., and Larsen,P.H. (1993): Method for Obtaining High Quality Protein Products from Whey. PCT-International -Patent-Application, 1993, WO 93121781 AI, 9 (*Cited in Dairy Sci. Abstr.*, 1994, 056-03014).

Kawakatsu,T., Nakao,S and Kimura,S (1993): Effects of Size and Compressibility of Suspended Particles and Surface Pore Size of Membrane on Flux in Crossflow Filtration. *J. Membr. Sci.*, **81**, 173-190.

Kelly,P.M., Horton,B.S., and Burling,H. (1993): Partial Demineralization of Whey by Nanofiltration. New Applications of Membrane Processes, *Int. Dairy Fed. Special Issue* no.**9201**, 130-140.

Kelly,S.T., Opong,W.S., and Zydney,A.L. (1993): The Influence of Protein Aggregates on the Fouling of Microfiltration Membranes During Stirred Cell Filtration. *J. Membr. Sci.*,**80**, 175-187.

Kuwata,T., Pham,A.M., Ma, C.Y., and Nakai,S. (1985): Elimination of β-lactglobulin from Whey to Simulate Human Milk Protein. *J. Food Sci.*, **50**, 605-609.

Kwon,D.Y., Vigneswaran,S., Ngo,H.H., Ben Aim,R., Fane,A.G., Shin,H.S. (1996): Experimental Study on Critical Flux in Crossflow Microfiltration. *Proc. Int. Membr. Sci. Technol. Conference, Sydney, Australia*, **2**, 59-61.

Laimay,F. (1991): A New Process for Continuous Washing of Casein - a Search for Total Improvement. *Process-Rennes*, **1058**, 51-52 (*Cited in Dairy Sci. Abstr.*, 1993, 055-04266).

Le,M.S. (1987): Recovery of Beer From Tank Bottoms with Membranes. *J. Chem. Tech. Biotechnol.*, **37**, 59-66.

Le Berre,O., and Daufin,G. (1994): Fouling and Selectivity of Membranes During Separation of β-casein. *J. Membr. Sci.*, **88**, 263-277.

Leighton,D., and Acrivos,A. (1987): The Shear-induced Migration of Particles in Concentrated Suspensions. *J. Fluid Mech.*, **181**, 415-430 (*Cited in* Belfort,G., Davis,R.H., and Zydney,A.L. (1994): Review: The Behaviour of Suspensions and Macromolecular Solutions in Crossflow Microfiltration. *J. Membr. Sci.*, **96**, 1-58).

Levesley,J.A. and Bellhouse,B.J. (1993): Particulate Separation Using Inertial Lift Forces. *Chem. Engg. Sci.*, **48** (21), 3657-3669.

Loh,D.W. (1990): Lactic Acid Casein from Microfiltered Skim Milk. *XXIIV Int. Dairy Cong.*, **Vol. II**, 452 (*Cited in* Dairy Sci. Abstr., 1991, 053-04279).

Lu,W.-M., and Ju,S.-C. (1989): Selective Particle Deposition in Crossflow Filtration. *Sep. Sci. Technol.*, **24** (7 & 8), 517-540.

Mackley,M.R., and Sherman,N.E. (1992): Cross-Flow Cake Filtration Mechanisms and Kinetics. *Chem. Engg. Sci.*, **47** (12), 3067-3084.

Mackley,M.R., and Sherman,N.E. (1993): Cake Filtration Mechanism in Steady and Unsteady Flows. *J. Membr. Sci.*, **77**, 113-121.

Mallubhotla,H., Nunes,E., and Belfort,G. (1995): Microfiltration of Yeast Suspensions with Self-cleaning Spiral Vortices: Possibilities for a New Membrane Module Design. *Biotechnol. Bioengg.*, **48**, 375-385.

Marshall,A.D., Munro,P.A., and Trägårdh,G. (1993): The Effect of Protein Fouling in Microfiltration and Ultrafiltration on Premeate Flux, Protein retention and Selectivity: A Literature Review. *Desalinatn*, **91**, 65-108.

Masters,K. (1976): Spray Drying, an Introduction to Principles, Operational Practice and Applications, Pub. George Godwin Litd., London. 42.

Matsumoto,K., Katsuyama,S., and Ohya,H. (1987): Separation of Yeast by Crossflow Filtration with Backwashing. *J. Fermn. Technol.*, **65**, 77-83.

Matsumoto,K., Kawahara,M., and Ohya,H. (1988): Cross-Flow Filtration of Yeast by Microporous Ceramic Membrane with Backwashing. *J.Ferment.Technol.*, **66**(2), 199-205.

Maubois,J.L., Pierre,A., Fauquant,J., and Piot,M. (1987): Industrial Frctionation of Main Whey Proteins. *Int. Dairy Fed. Bull.*, **212**, 154-159.

Maubois,J.L., and Ollivier,G. (1993): Milk Protein Fractionation. *Int. Dairy Fed. Sp. Issue* **No. 9201**, 15-22.

McDonogh,R.M., Bauser,H., Stroh,N., and Chmiel,H. (1990): Concentration Polarisation and Adsorption Effects in Cross-Flow Ultrafiltration of Proteins. *Desalination*, **79**, 217-231.

Meireles,M., Aimar,P., and Sanchez,V. (1991): Albumin Denaturation During Ultrafiltration: Effects of Operating Conditions and Consequences on Membrane Fouling. *Biotechnol. Bioengg.*, **38**, 528-534.

Merin,U., and Daufin,G. (1990): Crossflow Microfiltration in the Dairy Industry: State-of-the-Art. *Lait*, **70**, 281-291.

Merin,U., Gordin,S., and Tanny,G.B. (1983): Microfiltration of Cheese Brine. *J. Dairy Res.*, **50**, 503-509.

Michaels,S.L. (1989): Crossflow Microfilters: The Ins and Outs. *Chem. Engg.*, Jan., 84-91.

Mir,L., Michaels,S.L., and Goel,V. (1996): Crossflow Microfiltration: Applications, Design, and Cost. in Membrane Handbook, Ed. Winston Ho,W.S. and Sirkar,K.K., Pub. Chapman & Hall, New York. 571-594.

Mucchetti,G., and Taglietti,P. (1993): Microbiological Stabilization of Whey by Cross Flow Microfiltration. *Lait*, **73**, 79-84.

Mulder,M. (1991): Basic Principles of Membrane Technology. Kluwer Academic Pub. Dordrecht.

Mueller,J., and Davis,R.H. (1996): Protein Fouling of Surface-Modified Polymeric Microfiltration Membranes. *J. Membr. Sci.*, **116**, 47-60.

Murkes,J., and Carlsson,C-G. (1988): Crossflow Filtration, Theory and Practice. John Wiley and Sons Pub., Chichester, 18-21.

Olesen,N., and Jensen,F. (1989): Microfiltration. The Influence of Operation Parameters in the Process. *Milchwissenschaft*, **44**(8), 476-479.

O'Neill,M.E. (1968): A Sphere in Contact with a Plane Wall in Slow Linear Shear Flow. *Chem. Eng. Sci.*, **23**, 1293-1297.

Ousman,M., and Bennasar,M. (1995): Determination of Various Hydraulic Resistances During Cross-flow Filtration of a Starch Grain Suspension Through Inorganic Membranes. *J. Membr. Sci.*, **105**, 1-21.

Paddilla-Zakour,O., and McLellan,M.R. (1993): Optimization and Modeling of Apple Juice Cross-flow Microfiltration with a Ceramic Membrane. *J.Food Sci.*, **58**(2), 369-374.

Parnham,C.S., and Davis,R.H. (1995): Protein Recovery from Cell Debris Using Rotary and Tangential Crossflow Microfiltration. *Biotechnol. Bioeng.*, **47**, 155-164.

Pedersen,P.J. (1993): Microfiltration for the Reduction of Bacteria in Milk and Brine.*Int. Dairy Fed. Special Issue* **No. 9201**,33-50.

Perrot,N., Trichard,J.M., Trrystram,G., and Decloux,M. (1996): Automatic Control of the Crossflow Microfiltration Process using Fuzzy Logic. *J. Membr. Sci.*, **116**, 93-105.

Perry,J.H. (1963): Chemical Engineers' Handbook. Pub. McGraw-Hill Book Co., New York.

Persson,K.M. and Nilsson,J.L. (1991): Fouling Resistance Models in MF and UF. *Desalinatn.*, **80**, 123-138.

Persson,K.M., Trägårdh,G., and Dejmek,P. (1993[a]): Fouling Behaviour of Silica on Four Different Microfiltration Membranes. *J. Membr. Sci.*, **76**, 51-60.

Persson,K.M., Capannelli,G., Bottino,A., and Trägårdh,G. (1993[b]): Porosity and Protein Adsorption of Four Polymeric Microfiltration Membranes. *J. Membr. Sci.*, **76**, 61-71.

Pierre,A., Fauquant,J., Graet,Y., Piot,M., Maubois,J.L. (1992): Preparation of Native Phosphocaseinate Using Membrane Microfiltration. *Lait-Layon*, **72**(5), 461-474.

Piot,M., Vachot,J.C., Veaux,M., Maubois,J.L., and Brinkman,G.E. (1987): Separation and Bacterial Purification of Raw Whole Milk Using Crossflow Microfiltration Membranes. *Technique-Laitiere-and-Marketing*, **1016**, 42-46.

Piron,E., Rene,F., and Latrille,E. (1995): A Crossflow Microfiltration Model Based on Integration of the Mass Transport Equation. *J. Membr. Sci.*, **108**, 57-70.

Pouliot,M., Pouliot,Y, Britten,M., and Ross,N. (1994): Effects of pH and Ionic Environment on the Permeability and Rejective Properties of an Alumina Microfiltration Membrane for Whey Proteins. *J. Membr. Sci.*, **95**, 125-134.

Rautenbach,R., and Albrecht,R. (1989): Membrane Processes. John Wiley & Sons Ltd., Wiltshire, England.

Redkar,S.G., and Davis,R.H. (1993): Crossflow Microfiltration of Yeast Suspensions in Tubular Filters. *Biotechnol. Prog.*, **9**, 625-634.

Riesmeier,B., Kroner,K.H., and Kula,M.R. (1987): Studies on Secondary Layer Formation and its Characterization During Cross-flow Filtration of Microbial Cells. *J. Membr. Sci.*, **34**, 245-266.

Riesmeier,B., Kroner,K.H., and Kula,M.-R. (1989): Tangential Filtration of Microbial Suspensions: Filtration Resistances and Model Development. *J. Biotechnol.*, **12**, 153-172.

Robinson,B.P., Short,J.L., and Marshall,K.R. (1976): Traditional Lactalbumin Manufacture, Properties and Uses. *N. Z. J. Dairy Sci. Technol.*, **11**, 114-126.

Rubin,G. (1977): Widerstands-und Aufrtriebsbeiwerte von Ruhenden Kugelfórmingen Prtiklen in Stationären, Wandnahen Laminaren Grenzschichten, Dissertation, TH Karlsruhe (*Cited in* Altmann,J., and Ripperger, S. (1997): Particle Deposition and Layer Formation at the Crossflow Microfiltration. *J.Membr.Sci.*,**124**, 119-128.).

Russotti,G., Osawa,A.E., Sitrin,R.D., Buckland,B.C., Adams,W.R., and Lee,S.S. (1995): Pilot-Scale Harvest of Recombinant Yeast Employing Microfiltration: a Case Study. *J. Biotechnol.*, **42**, 235-246.

Saksena,S., and Zydney,A.L. (1993): Effect of Solution pH and Ionic Strength on the Separation of Albumin from Immunoglobulins (IgG) by Selective Filtration. *Biotechnol. Bioengg.*, **43**, 960-968.

Schluep,T. and Widmer,F. (1996): Initial Transient Effects During Cross Flow Microfiltration of Yeast Suspensions. *J. Membr. Sci.*, **115**, 133-145.

Schmitz,P., Houi,D., and Wandelt,B. (1992): Hydrodynamic Aspects of Crossflow Microfiltration. Analysis of Particle Deposition at the Membrane Surface. *J. Membr. Sci.*, **71**, 29-40.

Schmitz,P., Wandelt,B., Houi,D., and Hildenbrand,M. (1993): Particle Aggregation at the Membrane Surface in Crossflow Microfiltration. *J. Membr. Sci.*,**84**, 171-183.

Schuck,P., Piot,M., Mejean,S., Fauquant,J., Brule,G., and Maubois,J.L. (1994): Dehydration of an Ultra-clean Milk and Micellar Casein Enriched Milk. *Lait*, **74**, 47-63.

Schulz,G., and Rippperger,S. (1989): Concentration Polarization in Crossflow Microfiltration. *J. Membr. Sci.*, **40**, 173-187.

Sethi,S., and Wiesner,M.R. (1997): Modelling of Transient Permeate Flux in Cross-flow Membrane Filtration Incorporating Multiple Particle Transport Mechanism. *J. Membr. Sci.*, **136**, 191-205.

Sherwood,J.D. (1988): The Force on a Sphere Pulled Away From a Permeabe Half-Space. *Physicochem. Hydrodyn.*, **10**, 3-12 (*Cited in* Sethi,S., and Wiesner,M.R. (1997): Modeling of Transient Permeate Flux in Cross-flow Membrane Filtration Incorporating Multiple Particle Transport Mechanism. *J. Membr. Sci.*, **136**, 191-205).

Short,J.L., Cooper,H.R., and Doughty,R.K. (1978): The Effect of Manufacturing Variables on Lactalbumin for Use in High Protein Biscuits. *N. Z . J. Dairy Sci. Technol.*, **13**, 43-48.

Short,J.L., and Skelton, R. (1991): Crossflow Microfiltration in the Food Industry. in Effective Industrial Membrane Processes- Benefits and Opportunities, Elsevier Science Pub. Ltd., England, 181-189.

Sneddon,I.N. (1976): Encyclopaedic Dictionary of Mathematics for Engineers and Applied Scientists, Pergamon Press, Oxford.

Solberg,S. (1991): Microfiltration of Milk for Cheese Making. Tesing of Bactocatch. *Meiriposten*, **80**(22), 603-605 (*Cited in Dairy Sci. Abstr.*, 1993, 055-07084).

Surel,O., and Famelart,M.H. (1995): Ability of Ceramic Membranes to Reject Lipids of Dairy Products. *Aus. J. Dairy Technol.*, **50**, 36-39.

Taddei,C., Aimer,P., Howell,J.A., Scott,J.A. (1990): Yeast Cell Harvesting from Cider Using Microfiltration. *J. Chem. Tech. Biotechnol.*, **47**, 365-376.

Tanny,G.B., Hauk,D., and Merin,U. (1982): Biotechnical Applications of Pleated Crossflow Microfiltration Module. *Desalinatn.*, **41**, 299-312.

Tarleton,E.S. and Wakeman,R.J. (1993): Understanding Flux Decline in Crossflow Microfiltration: Part I- Effects of Particle and pore size. *Trans. I. Chem. E.*,**71** (A), 399-410.

Tarleton,E.S., and Wakeman,R.J. (1994[a]): Understanding Flux Decline in Crossflow Microfiltration: Part II - Effects of Process parameters. *Trans. I. Chem. E.*, **72** (A), 431-440.

Tarleton,E.S., and Wakeman,R.J. (1994[b]): Understanding Flux Decline in Crossflow Microfiltration: Part III - Effects of Membrane Morphology. *Trans. I.Chem. E.*, **72** (A), 521-529.

Tien,C., Bai,R., and Ramarao,B.V. (1997): Analysis of Cake Growth in Cake Filtration: Effect of Fine Particle Retention. *AI Ch E J.*, **43**(1), 33-44.

Timmer,J.M.K., Van der Hoarst,H.C., and Labbé,J.-P. (1997): Cross-flow Microfiltration of β-lactoglobulin Solutions and the Influence of Silicates on the Flow Resistance. *J. Membr. Sci.*, **136**, 41-56.

Trägårdh,G. (1989): Membrane Cleaning. *Desalinatn.*, **71**, 325-335.

Turker,M. and Hubble,J. (1987): Membrane Fouling in a Constant Flux Ultrafiltration Cell, *J. Membr. Sci.*, **34**, 267-281.

Uchida,Y., Simatani,M., Matsune,I., Nishizaki,S., Koutake,M. (1992): Process for the Manufacture of a Milk Fraction with a High α-lactalbumin Content, and Production Obtained by the Implementation of this Process. French-Patent-Application 1992 FR 2669 810 AI (*Cited in Dairy Sci. Abstr.*, 1992, 054-06990).

Uchida,Y., Simatani,M., Matsune,I., Nishizaki,S., Koutake,M. (1993): Process for the Preparation of a Fraction with a High Content of α-lactalbumin from Whey and Nutritional Compositions Containing this Fraction. French-Patent-Application 1993 FR 2 687 901 AI (*Cited in Dairy Sci. Abstr.*, 1994, 056-00155).

Valming,G. (1988): Development of Bacteria-Free Milk by Microfiltration. Nordisk-Mejeriindustri, 15(3), 167 (*Cited in Dairy Sci. Abstr.*, 1988, 050-05508).

Van der Horst,H.C. (1995): Fouling of Organic Membranes During Processing of Dairy Liquids. *Int. Dairy. Fed. Special issue* **No. 9504**, 36-52.

Van der Horst,H.C., and Piersma,I. (1993): Cross-flow Microfiltration of Skim Milk. *Proceedings of Int. Cong. Milk '93*, Hedenberg, Germany.

Van Der Horst,H.C., and Hanemaaijer,J.H. (1990): Cross-Flow Microfiltration in the Food Industry. State of Art. *Desalinatn.*, **77**, 235-258.

Van Veen,G. (1996): The Influence of Surface Flushing on the Performance of the Crossflow Microfiltration of Yeast in Whey. *Post Graduate Project Report*, Dept. Process & Environ. Technol., Massey Uni., New Zealand.

Visser,J. (1978): Colloid and Other Forces in Particle Adhesion and Particle Removal. *Proceedings of 'Deposition and Filtration of Particles from Gases and Liquids'* - a Symposium Held at Loughborough Uni., England. Pub. Soc. Chem. Ind., London. 121-141.

Visvanathan,C., and Ben Aïm,R. (1989): Studies on Colloidal Membrane Fouling Mechanisms in Crossflow Microfiltration. *J. Membr. Sci.*, **45**, 3-15.

Wakeman,R.J. (1994): Visualisation of Cake Formation in Crossflow Microfiltration. *Trans. I. Chem. E.*, **72** (A), 530-540.

Wakeman,R.J. and Tarleton,E.S. (1991): Colloidal Fouling of Microfiltration Membranes during the treatment of Aqueous Feed Streams. *Desalinatn*, **83**, 35-52.

Wandelt,B., Schmitz,P., and Houi,D. (1992): Investigation of Transient Phenomena in Cross-flow Microfiltration of Colloidal Suspensions Using NMR Microimaging, *Proc 6th World Filtration Congress*, 601-606 (*Cited in* Wakeman,R.J. (1994): Visualisation of Cake Formation in Crossflow Microfiltration. *Trans. I. Chem. E.*, **72** (A), 530-540).

Wenten,I.G. (1995): Mechanisms and Control of Fouling in Crossflow Microfiltration. *Filtration and Separation*, **32**(3), 252-253.

Woychick,J.H. (1992): Preparation of Simulated Human Milk Protein by Low Temperature Microfiltration. U.S-Patent 1992 US 5 169,666 (*Cited in Dairy Sci. Abstr.*, 1993, 055-02069).

Xu-Jiang,Y., Dodds,J., Leclerc,D., and Lenoel,M. (1995): A Technique for the Study of the Fouling of Microfiltration Membranes Using Two Membranes in Series. *J. Membr. Sci.*, **105**, 23-30.

Zoon,P., Straatsma,J., and Allersma,D. (1991): Concentration of Cheese Brine by Evaporation, and its Effect on Cheese Quality. *Voedingsmiddelen technologie*, **24**, 11-16 (*Cited in Dairy Sci. Abstr.*, 1992, 054-06347).

Zoon,P., and Hup,G. (1993): Process for Preparation of Raw Milk Cheese. European-Patent-Application 1993 EP 0546 641 AI (*Cited in Dairy Sci. Abstr.*, 1993, 055-07987).

Zydney,A.L., and Colton, C.K. (1986): A Concentration Polarization Model for the Filtrate Flux in Cross-flow Microfiltration of Particulate Suspensions. *Chem. Eng. Commun.*, **47**, 1-21 (*Cited in* Belfort,G., Davis,R.H., and Zydney,A.L. (1994): Review: The Behaviour of Suspensions and Macromolecular Solutions in Crossflow Microfiltration. *J. Membr. Sci.*, **96**, 1-58).

Zydney,A.L. (1998): Protein Separations Using Membrane Filtration : New Opportunities for Whey Fractionation. *Int. Dairy J.*, **1**, 1-8.

APPENDIX 1

CFMF OF LACTALBUMIN UNDER CONSTANT TMP MODE

APPENDIX 2

CFMF OF LACTALBUMIN UNDER CONSTANT FLUX MODE

APPENDIX 3

MATHEMATICAL MODELLING

These appendices are in form of Excel files located in the floppy disc provided herewith.

File names : APPENDIX 1. xl

APPENDIX 2. xl

APPENDIX 3. xl